IN-34
63381

NASA Contractor Report 198476

Surface Tension Driven Convection Experiment (STDCE)

S. Ostrach and Y. Kamotani
Case Western Reserve University
Cleveland, Ohio

June 1996

Prepared for
Lewis Research Center
Under Contract NAS3-25937

National Aeronautics and
Space Administration

ABSTRACT

This document reports the results obtained from the Surface Tension Driven Convection Experiment (STDCE) conducted aboard the USML-1 Spacelab in 1992. The experiments used 10 cSt silicone oil placed in an open circular container that was 10 cm wide and 5 cm deep. Thermocapillary flow was induced by using either a cylindrical heater placed along the container centerline or by a CO_2 laser. The tests were conducted under various power settings, laser beam diameters, and free surface shapes. Thermistors located at various positions in the test section recorded the temperature of the fluid, heater, walls, and air. An infrared imager was used to measure the free surface temperature. The flow field was studied by flow visualization and the data was analyzed by a PTV technique. The results from the flow visualization and the temperature measurements are compared with the numerical analysis that was conducted in conjunction with the experiment. The compared results include the experimental and numerical velocity vector plots, the streamline plots, the fluid temperature, and the surface temperature distribution.

ACKNOWLEDGMENTS

We wish to express our appreciation to many people, especially the NASA Lewis Research Center engineering and operations teams, who contributed to make the STDCE a successful and important experiment. Special thanks to Dr. Eugene Trinh who, as a payload specialist aboard the USML-1, conducted the STDCE tests tirelessly and expertly for many hours. We also thank Mr. Matthew Roussel who, as a graduate assistant at the Department of Mechanical and Aerospace Engineering, Case Western Reserve University, compiled the data presented in this report for his M.S. thesis. We also gratefully acknowledge the financial support of the Microgravity Science and Applications Division at NASA Headquarters for this experiment.

TABLE OF CONTENTS

NOMENCLATURE

Ar = aspect ratio = H/R

Ca = capillary number

c_p = specific heat of fluid

D = container diameter

D_H = heating zone diameter for CF case and rod diameter for CT case

H = container depth

Hr = relative heater size (heater ratio) = D_H/D

k = thermal conductivity of fluid

Ma = Marangoni number = $\sigma_T \Delta T R/\mu\alpha$

Pr = Prandtl number = ν/α

R = container radius

Ra = radiation parameter = $\varepsilon\sigma^{\circ} T_a^3 H/k$

(r,z) = coordinate system defined in Fig. 1

S = surface deformation parameter = $\sigma_T \Delta T/\sigma(1/Pr)$

t = time

T = temperature

T_a = ambient temperature

T_c = side wall temperature

T_h = heater temperature for CT case and center temperature for CF case

(u,v) = velocity components

α = thermal diffusivity

ΔT = net temperature variation along free surface

ε = emissivity of fluid free surface

θ = dimensionless temperature = $(T - T_c)/\Delta T$

μ = fluid dynamic viscosity

ν = fluid kinematic viscosity

ρ = fluid density

σ = surface tension

σ^{o} = Stefan-Bolzmann constant

σ_T = temperature coefficient of surface tension

CHAPTER I. INTRODUCTION

In a microgravity environment surface tension becomes a dominant force and can generate significant fluid flows. Thermocapillary flow is caused by a heat-induced surface tension variation along a liquid free surface. The heat and mass transfer associated with the flow are important in various engineering applications in microgravity[1]. For that reason experimental and numerical work has been conducted in the past on steady and transient thermocapillary flows. However, the detailed nature and extent of such flows under a variety of test conditions remain to be clarified. The lack of knowledge is associated with certain experimental limitations encountered in a terrestrial environment. Buoyancy effects overshadow thermocapillarity unless a very small system (~ a few mm or smaller) is used. Gravity affects the shape and motion of liquid free surfaces. Moreover, only a small number of liquids are suitable to conduct thermocapillary flow experiments because of the requirement that surface tension be very insensitive to surface contamination. These factors make it quite difficult to cover wide ranges of parameters experimentally on the ground. Many numerical analyses of steady thermocapillary flows have been conducted (e.g. Fu and Ostrach[2], Zebib et al.[3], Carpenter and Homsy[4], Kamotani and Platt[5]), however most of their results are yet to be validated experimentally.

An important aspect of thermocapillary flow is that it undergoes a transition to an oscillatory flow when certain conditions are reached. The transition phenomenon was originally discovered by Schwabe et al.[6] and Chun and Wuest[7] more than 15 years ago. Despite the fact that many experimental and theoretical studies have been conducted subsequently, the transition and the parameters to characterize the transition are not yet fully understood mainly because of the lack of experimental data over wide conditions and no numerical analysis has yet predicted the transition accurately. For thermocapillary flow in an open container if the deformation of the free surface is assumed to be negligible, then the only parameter representing the convection within the fluid is the Maragoni number (Ma). Therefore, in many studies the transition from thermocapillary steady flow to oscillatory thermocapillary flow is characterized by the critical Maragoni number (Ma_{cr}). However, Kamotani et al.[8,9] and Ostrach et al.[10] showed experimentally that the Ma_{cr} alone does not specify the transition to oscillatory flow, and that the free surface deformation plays an important role in the oscillation mechanism. As a result, they introduced a surface deformation parameter that represents the effect of the deformable free surface. To resolve the role of the deformable free surface in the oscillation mechanism it is necessary to conduct experiments in a microgravity environment where a wider range of conditions can be covered.

For those reasons experiments on thermocapillary flows were conducted in a microgravity environment. In these experiments the test fluid was placed in an open cylindrical container. Steady thermocapillary flows under two heating modes were to be investigated, as well as, the onset for oscillatory flow conditions. The experiments, designated the Surface Tension Driven Convection Experiment (STDCE), took place aboard the First US Microgravity Laboratory (USML-1) Spacelab on the Space Shuttle Columbia (STS-50) which was launched on June 25 and landed on July 9, 1992. The hardware performed well generally and we were able to conduct more tests than originally planned. From the successful experiments a large amount of data was obtained. Ostrach, Kamotani, and Pline[11,12,13,14,15] analyzed the data and reported many important results from the experiments. The present document is the final report for the STDCE project and contains the data that was obtained along with the results of the numerical analysis that was conducted in complement with the experimental tests.

The STDCE project was managed by the following personnel:

Principal Investigator:	Simon Ostrach
Co-Investigator:	Yasuhiro Kamotani
	Department of Mechanical and Aerospace Engineering Case Western Reserve University
Project Manager:	Thomas Jacobson
Project Scientists:	Robert Thompson and Alexander Pline
	NASA Lewis Research Center

CHAPTER II. TEST APPARATUS

The important considerations behind the design of the STDCE are discussed by Kamotani and Ostrach[16]. The development of the flight hardware is described by Pline et al.[17] and the hardware performance during the flight is reported by Pline et al.[18] The experiment used 10 cSt silicone oil as the test fluid. The relevant properties of the fluid are given in Table 1. The fluid was placed in a circular container 10 cm wide and 5 cm in depth. There were two modes of heating (see Fig. 1): a CO_2 laser was the first mode and designated the constant heat flux (CF) configuration, and a 1.11 cm cylindrical heater was the second mode, placed at the center of the container and designated the constant temperature (CT) configuration. During the CF tests the 1.11 cm heating rod was withdrawn.

The diameter of the laser beam during the CF tests was varied from 0.5 cm to 3.0 cm, and the beam had an axisymmetric Gaussian profile. The beam diameter is defined herein based on the location where the flux falls to e^{-2} of its maximum value. The laser beam diameter was set for 5, 10, or 30 mm at the flat free surface location. When the surface was curved or convex the laser beam diameter would then expand or shrink respectively. For the 5 mm cases there was a 0.35 mm change in beam diameter per 25.4 mm axial distance, and for the 30 mm cases there was a 1.6 mm change per 25.4 mm distance. The 10 mm beam was nearly parallel and therefore the diameter was the same at every level. These changes were taken into account in computing the actual beam diameters at the free surface. The mean absorption length of the CO_2 laser (10.6 μm wavelength) was measured to be 0.060 mm,[17] as a result most of the laser beam was absorbed within 0.2% of the fluid depth.

The side wall of the circular container was made of 5 mm thick copper. The side wall was kept at uniform temperature by using copper tubing wrapped around the container allowing cooling water to flow through the tube. The cooling water was stored in a large reservoir. The bottom of the container was made of 8 mm average thickness Plexiglas.

There were a variety of free surface shapes that were used for both the CF and CT tests (see Figs. 2-4). In all cases the liquid surface was anchored at the top edge of the side wall. Unlike in the CF configuration, where only one parameter (i.e. the total fluid volume in the container) controls the free surface shape, the shape in the CT configuration is also affected by the height of the heater if the fluid surface is anchored at the edge of the heater, so more different shapes were tested in the CT configuration. The shapes in Figs. 2 and 3 are the originally specified shapes and those in Fig. 4 are additional shapes which were created mainly to study the effect of the meniscus shape near the heater on the flows. Figs. 2-4 show the relative volume of each shape, the total volume corresponding to the flat surface being unity. The fluid was kept in a reservoir and pumped into or out of the container through a hole located at the bottom. The calibrated counter on the experiment panel showed the total volume in the test chamber. The free surface shape was also checked from the flow visualization video after the flight. The surface shape was set within ± 1 mm of the prescribed location. To ensure that the fluid would not overflow, the top of the container had a sharp edge to anchor the fluid for all tests.

The overall arrangement for the experiments is sketched in Fig. 5. Two main diagnostic tools were used: flow visualization and thermography. Flow visualization was employed to study the velocity fields, and the thermography was used for surface temperature measurements.

For flow visualization, 50-60 μm alumina particles were mixed into the fluid and a cross-section of the flow field was illuminated using a 1 mm sheet of light from a 200 milliwatt near-infrared laser diode. The particle motions were then tracked and recorded using a CCD camera located underneath the container. Because of the copper side wall of the test chamber, a Plexiglas bottom was used as a viewport, as a result the image was distorted ('keystone' effect) but the distortion was corrected in the data reduction process. The videos were then analyzed after the mission had ended, and a Particle Tracking Velocimetry (PTV) technique was used to determine the velocity vectors at various points in the flow field. This technique is explained by Wernet and Pline.[19] The velocity vectors were determined at various points in the flow. The errors in the velocity magnitude and direction measurements are estimated to be 1.8 % and 1°, respectively, in the high velocity region and 18 % and 10° in the relatively low velocity region of the flows[19].

The thermographs were taken of the free surface by an infrared imager. The infrared imaging system used in the STDCE is described by Pline and Butcher.[20] The operating wavelength was 8-14 μm and the mean absorption length of the fluid in that range was measured to be 0.012 mm. As will be discussed later, the thermal boundary layer thickness along the free surface can become comparable to the above absorption length in certain relatively small areas but along most of the free surface the boundary layer is thicker than the absorption length, so the infrared data is considered to represent the surface temperature. The minimum detectable temperature difference was 0.15 °C and the spatial resolution was 1 mm.

The temperature of the bulk fluid was studied by thermistors. 9 probes were used to measure temperature at various locations in the fluid and in the container walls. In addition, one probe measured the ambient temperature above the fluid free surface and 6 thermistors monitored the temperature distribution along the heater length. Their positions designations are shown in Fig. 6. The top of the thermistor TCR #1 touched the free surface. The diameter of the thermistors in the fluid was 0.5 mm. The temperature data were taken once every 100 milliseconds during tests, digitized, and stored. They were downlinked during certain times to the POCC (Payload Operations Control Center) at NASA Marshal Space Flight Center where we monitored the experiment. The resolution of the digital data was 0.1 °C and the accuracy of thermistor sensors was ± 0.1 °C.

CHAPTER III. EXPERIMENTAL CONDITIONS

The important dimensionless parameters for steady thermocapillary flow in the present experimental configuration with a flat undeformable free surface and with negligible buoyancy are:

1) Ma (Marangoni number) = $\sigma_T \Delta T R / \mu \alpha$

2) Ar (aspect ratio) = H/R

3) Hr (relative heater size or heater ratio) = D_H/D

4) Pr (Prandtl number) = ν/α

In the CT tests ΔT is defined as the temperature difference between the heater and the side wall, while ΔT for the CF tests is defined as the temperature difference between the maximum fluid temperature, which will occur directly under the center of the laser beam, and the side wall. Since the total heat input, instead of ΔT, is measured in the CF tests, one could define a Ma based on the specified heat input, however in order to make comparisons between the CF and CT results convenient a Ma based on ΔT is used in both cases herein. As will be shown later, the IR imager cannot measure the free surface temperature at the center accurately in the CF tests, so ΔT's in those tests are calculated from the numerical analysis.

In the case of curved free surface tests an additional parameter is needed to specify the shape of the free surface. For given container and heater diameters, the surface shape can be specified either by the total fluid volume in the container or by the apparent contact angle between the free surface and the container side wall. In the case of the CT configuration it is useful to know also the height of the free surface at the heater surface.

Those values for each free surface shape used in STDCE are given in Figs. 2, 3, and 4. The free surface is always pinned at the top edge of the container side wall. In the CF configuration the free surface shape is a part of a spherical surface (Fig. 2). In the CT configuration the free surface shape is more complex due to the presence of the heater at the center and the shapes given in Figs. 3 and 4 are computed numerically. Although it is difficult to determine the free surface shape accurately from the flow visualization image due to various reflections, especially when the surface is highly curved, the computed shapes agree well with the observed shapes. Shapes 4 to 6 in Fig. 3 have 5 degree contact angle at the heater surface and the rest of the shapes in the CT configuration have various contact angles at the heater.

Another parameter represents the heat loss due to radiation from the free surface to the surroundings represented by the radiation parameter (Ra),

5) $Ra = \varepsilon\sigma^{o}T_a^{3}H/k$

The above expression is appropriate since the temperature difference between the free surface and the surroundings is much smaller than the average absolute temperature.

Thermocapillary flow is known to become oscillatory beyond a certain ΔT. From the above list of parameters only the Ma contains the temperature difference, therefore the critical condition for oscillatory flow would be represented by Ma_{cr} (critical Marangoni number). However, Kamotani et al.[8] and Ostrach et al.[10] have shown that the Ma_{cr} alone cannot specify the onset of oscillations. Based on their experimental and theoretical work of oscillatory flow they introduced a surface deformation parameter (S),

6) $S = (\sigma_T \Delta T/\sigma)(1/Pr)$

S represents the deformability of the free surface. It is based on the concept that in unsteady thermocapillary flow it takes a specific amount of time to deform the free surface, which causes a time delay between the flow at the surface and the return flow in the interior. This time-lag leads to the oscillations of the fluid.

In the STDCE, Ar was fixed at one. In the CT tests the heater diameter was fixed at 1.11 cm so that Hr was 0.111. In the CF tests Hr was set at 0.05, 0.1, and 0.3. The test conditions for all the tests are summarized in Table 2, in which the tests are arranged in the order they were performed. Several tests were performed in one series and they are assigned the same Run #. Each test is designated by its Run # and Test # in each run. The values of the Ma and Pr for each test are listed in Table 3. The pertinent physical properties of the test fluid are given in Table 1. Because of the temperature variation in the fluid the fluid properties, especially viscosity, are not constant. In Table 3, the viscosity is evaluated at both T_c and $1/2(T_h + T_c)$. As will be shown later, the fluid temperature over most of the flow field is near the side wall temperature (T_c) and, in the CF tests T_h is not known experimentally. However, many important features of the flow occur in the so-called hot corner region where the appropriate temperature is $1/2(T_h + T_c)$. For those reasons the dimensionless parameters are evaluated at both temperatures.

In summary, the ranges of the dimensionless parameters for STDCE were: $Ar = 1.0$, $50 \leq Pr \leq 100$, $1.7 \times 10^4 \leq Ma \leq 4.9 \times 10^5$ (viscosity evaluated at $1/2(T_h + T_c)$), and $Hr = 0.111$ for the CT cases and $0.049 \leq Hr \leq 0.316$ for the CF cases. The radiation parameter was fixed at about $Ra = 0.5$. The range of surface deformation parameter was $S \leq 0.004$. According to our ground based tests on oscillatory thermocapillary flows in small cylindrical containers in the CT configuration[9], the flow becomes oscillatory if Ma is larger than about 5×10^4 and S is larger than 0.007. Thus, only Ma went beyond the requirement for the onset of oscillations.

The pre-flight analysis and testing showed that at least one hour would be needed for a test to reach hydrodynamic and thermal equilibrium. Thus, two one-hour flat free surface tests, one each with a CT and CF configuration, were conducted with well defined initial conditions to study the development of flow with time and a steady state. In addition, various shorter 10 , 20, and 30 min. CF and CT tests were run to see if oscillatory flow would develop. No oscillatory flow was found but the shorter tests gave valuable information on steady velocity fields under various conditions, as will be discussed later.

CHAPTER IV. NUMERICAL ANALYSIS

The numerical program for flat free surface is based on the SIMPLER algorithm by Patankar[21]. The flow is assumed to be laminar, incompressible, and axisymmetric. The fluid properties are considered to be constant except for viscosity which varies with temperature in the analysis. The program analyzes both transient and steady states.

In the CT configuration the measured temperatures of heater and side wall are used as inputs. Both temperatures changed with time during the tests. In the CF case the measured values of laser power and side wall temperature, and the beam diameter are the inputs. The emissivity and the absorption length are also taken into account. In the present experiments, the radiation from the free surface is not negligible, so the radiation exchange among the surface elements and the surrounding air is included via view factors. The surface is assumed to be diffuse and gray. The coordinate system used in the analysis is defined in Fig. 1. The velocity components (u,v) are made dimensionless by $\sigma_T \Delta T/\mu$. The temperature T is non-dimensionalized as $\theta = (T - Tc)/\Delta T$, where Tc is the side wall temperature.

A non-uniform grid system is adopted with meshes graded toward the hot and cold walls and toward the free surface. In the CT cases due to the presence of a thin thermal boundary layer along the heater surface the free surface temperature varies very sharply near the heater. As a result the free surface velocity increases very sharply in that region and an accurate resolution of the surface velocity distribution near the heater is the most important requirement for the numerical grid. Based on the grid-dependency study by Kamotani et al.[11], the 58 x 51 (radial x axial) grid with the smallest mesh size of 0.0005 next to the heater is used both for the steady and transient CT computations. In the CF configuration there exists a very thin thermal boundary layer along the free surface in the region heated by the laser beam, so an accurate prediction of the surface temperature distribution near the heated region becomes important. Base on the study by Kamotani et al.[11], the 46 x 51 grid with the smallest axial mesh size next to the free surface of 0.001 is used for the CF transient and steady analysis.

The program for curved free surfaces is explained in Kamotani and Platt[5]. The computational domain with curved free surfaces is transformed into a rectangular domain by a coordinate transformation and the velocity and temperature fields are solved by a finite-difference scheme.

Based on the numerical analysis it can be shown that the capillary number ($Ca = \mu U/\sigma$, where U is the typical velocity along the surface) is at most 0.005 for the present tests so that the free surface shapes for both the transient and steady state analysis are assumed to be unchanged by the flow from the static shapes shown in Figs. 2 to 4.

CHAPTER V. RESULTS AND DISCUSSION

5.1 Overview

During the 14-day mission of the USML-1 Spacelab the STDCE hardware performed well generally. A total of 38 tests (20 CF and 18 CT tests) with flat or curved surfaces were conducted and over 10 hours of video and digital data were obtained. On day four of the mission the one-hour CF and CT tests were conducted. These tests were then followed by six CF shorter tests and four CT shorter tests respectively. The subsequent tests that were conducted are all shorter tests. The main shorter tests were conducted on days six and eight. Additional time became available to us on the tenth day, so three CT curved surface tests were conducted. Table 2 gives the start time and conditions for each test.

Since the two one-hour tests with flat free surfaces were the main tests in the STDCE, the results from those tests will be discussed first, followed by discussions on the shorter tests with flat surfaces, and finally the shorter tests with curved surfaces will be discussed. The test results are presented in Appendices. Refer to Table 4 to locate the results for a given test.

5.2 CF One-Hour Test

Before the test we made sure that the free surface was flat and no appreciable motion existed in the fluid through video downlink. The experimental results from the CF one-hour test are presented in Appendix A. The thermal conditions for the CF test are shown in Figs. A1 and A2. The beam diameter was 1.0 cm. The laser beam power remained nearly constant at 0.48 ± 0.02 W throughout (Fig. A1). However, the side wall temperature kept increasing and changed by 1.5 °C (15% of ΔT) after one hour (Fig. A2). Since in the CT one-hour test the side wall temperature did not change that much despite the fact that the heat input to the fluid was greater (1.2 W), as will be discussed later, the side wall temperature increase in the CF test was not because of the heat input from the laser beam. Considering the fact that the air temperature above the fluid also increased by the same rate as Fig. A2 shows, the increase is considered to be due to the ambient temperature increase due probably to an increase in thermal loading of the Shuttle avionics air system. In all other tests the side wall temperature remained relatively constant. The air temperature is assumed to represent the surrounding wall temperature in the calculation of the radiation loss from the free surface.

Fig. A3 shows the computed streamlines and isotherms at t (time after the start of heating) = 2 min. The streamline pattern agrees well with the observed pattern shown in Fig. A4 in terms of the overall flow structure and the location of the cell center. The experimental streamline pattern was obtained by averaging several video frames of the flow. The flow structure is unicellular (toroidal cell). The streamline pattern shows that the whole fluid was already in motion at this time and did not change appreciably after the first minute of testing. In comparison, in one-g the flow in this large system is confined to a thin region near the surface because of stratification. A bubble unexpectedly was present in the observed flow field. The bubble diameter was about 1 cm and it stayed along the bottom wall throughout the test. Since the bubble stayed in the region where the velocity was smallest, it did not affect the overall flow appreciably. The isotherms suggest that over most of the flow field the fluid temperature is basically equal to the initial temperature which was about 0.6 °C below the side wall temperature. The development of the temperature field is much slower than that of the velocity field because Pr is much larger than unity.

At t = 10 min. (Figs. A5 and A6) heat was spread only along the free surface and most of the fluid was still close to the initial temperature. The streamline pattern is almost identical to that at t = 2 min. Even at t = 30 min. (Fig. A7) a large portion of the fluid had a temperature below the side wall but convection was beginning to heat up the interior.

At t = 60 min. (Figs. A8 and A9), at the end of the test, most of the fluid had a temperature just above the side wall temperature and the temperature distribution was not yet close to the steady profile as discussed by Kamotani et al.[11] The main reason why the fluid temperature remained low compared to the side wall for that long time was the continuous increase of the latter temperature as discussed above.

The experimental and numerical velocity vectors are compared at 10, 20, and 60 minutes in Figs. A10-A12. Since the flow field reached a steady state very early in the experiment all the velocity vectors exhibit the same pattern. The velocity increases toward the heated region because thermocapillary driving force is largest there. The fluid moves very slowly over a large portion of the container. The experimental velocity vectors agree well with the numerical results except near the free surface in the heated region. Although the velocity is largest along the free surface in the heated region, as the numerical results show, it is very difficult to capture that experimentally because very few tracer particles were found in that region. Although we cannot validate the numerical analysis in the highest velocity region, note that it is not possible to predict the flow in other region accurately unless the highest velocity region is computed correctly, because the whole flow is mainly driven in that small region.

Fig. A13 shows the TCR#1-#3 and SHR#1-#3 thermistor readings (see Fig. 6 for the thermistor designation) and the numerical prediction. The figure shows good agreement between the data and the prediction. The fluid temperature increased at a nearly steady rate. The readings of the thermistors SHR#1-#3 are all close and the predicted temperature variations follow the data closely. According to the isotherms in Fig. A8 the thermal boundary layer thickness along the free surface is less than 1.5 mm near the center, so the SHR#1 thermistor, which was located at 2 mm from the surface, was just outside the boundary layer. The reading of TCR#3 thermistor seemed to be slightly too high (its reading should be below that of TCR#2 because the former is located below the latter, but it is nearly close to the reading of the probe at the free surface) but the difference between the data and the prediction is about 0.4 °C which is only 4.5% of ΔT.

The infrared imager data are compared with the predicted surface temperature distributions at t = 10 and 60 min. in Fig. A14. The infrared imager did not require in situ calibration but for a reason not yet fully understood its readings seemed to have shifted judging from a comparison of its measurement of the fluid initial temperature with that measured by the thermistors. It was calibrated before and after the flight but no drifting was found. For that reason instead of determining the absolute temperate of the free surface we computed the surface temperature increase above the initial temperature. Therefore, Fig. A14 shows the relative surface temperature distributions. The data and the prediction agree well but near the heated region the imager data was lower than the prediction because of the presence of a very thin thermal boundary layer there. Because of the thin boundary layer practically there is no accurate way to measure the surface temperature near the middle. The data at r/R = .5 agrees with the TCR#1 thermistor data.

5.3 CT One-Hour Test

The results for this test are presented in Appendix B. Figs. B1 and B2 show how the heater and side wall temperature varied during the one-hour period after the heating started. The power to the heater was boosted for the first 90 seconds to shorten the warm-up time of the heater. After the boost period the heater power was fixed at 1.2 W but the heater temperature increased gradually throughout the one-hour period. The side wall temperature variation was relatively small, about 0.6 °C increase after one hour. The increase was probably caused by the heater input. The readings of the two thermistors in the side wall were the same within the resolution of the data acquisition system (0.1 °C). As for the 6 thermistors in the heater shell ,4 of them, which are positioned in the top 2/3 of the heater length, read within 0.2 °C of each other but 2 thermistors near the heater bottom read about 0.5 °C below the above average probably due to the end loss.

Fig. B3 shows the computed streamlines and isotherms at t = 2 min., and the observed streamline pattern is shown in Fig. B4. The observed pattern agrees well with the computed one. The overall flow pattern changes little beyond this time, as in the CF case discussed above. A bubble of about 1 cm dia. was present in the observation and it moved very slowly along the heater during the test. As in the above CF test, the bubble stayed in the region where the fluid velocity was very small, so its effect on the whole flow was very small. The isotherms in Fig. B3 suggest that over most of the flow field the temperature is basically equal to the initial temperature except in the thermal boundary layer along the heater surface. The liquid initial temperature was about 0.5 °C below the side wall temperature.

The streamlines and isotherms at t = 10 min. are given in Figs. B5 and B6. The bulk fluid temperature is higher than that at t = 2 min. The isotherms show how the fluid is heated by convection: first heat spreads along the free surface and then into the bulk fluid along the cold wall. The isotherm pattern at t = 60 min. (Fig. B7) is nearly that of final steady state (Kamotani et al.[11]).

The velocity vectors determined from the particle motions at t = 10, 20, and 60 min. are presented in Figs. B8 - B10. The computed vectors are shown also in those figures for comparison. The velocity is relatively large in the region near the top half of the heater. Although there is a very strong flow along the free surface close to the heater, as seen in the computed results, the present flow visualization did not detect it because the tracer particles did not go into that small corner region. Except in that small region, the measured and computed vectors agree well. Kamotani et al.[13] analyzed the velocity data in more details.

The outputs from the thermistors TCR#1 - #3 are shown in Fig. B11, together with the numerical result. Good agreement is shown. The fluid temperature was nearly approaching to a steady state near the end of the test. As in the above CF test, the TCR#3 probe output seemed to be too high because, although it was placed below the TCR#2 probe, its reading was always above that of TCR#2, which does not seem to be correct. In any case the difference between the TCR#3 probe reading and the numerical prediction is at most 0.4 °C, which is only 3% of ΔT.

The IR imager data at t = 10 and 60 min. are given in Fig. B12. The numerical data and experimental data are compared in the same manner as they were for the CF one hour test, namely they are compared in terms of relative temperature variation. The comparison between the two are in good agreement. As seen in Fig. B12, the surface temperature drops sharply near the heater and, as a result, the surface velocity increases very sharply and attains its peak near the heater as the numerical results in Figs. B8 - B10 show. By comparing the profiles at t = 10 and 60 min. one sees that the overall profile does not change much with time, only it shifts as the fluid warms up, which explains why the velocity field does not change much with time, the driving force being dependent on the slope of the profile.

5.4 CF Flat Shorter Tests

After the one-hour test, shorter duration tests were conducted under various conditions to see whether the flow would become oscillatory. The short CF flat tests were run at times of 10 or 20 minutes. The results from those tests are given in Appendix C where the data are arranged in the following way. The laser and thermistor data are shown first (first three pages for each test) to show the laser power (first page) and thermal conditions (second page) of each test and also to show how the fluid temperature changed with time (third page). Then the velocity field data measured near the end of each test are given on the next three pages, together with the numerical result. Although each test was shorter than one hour, the velocity field was close to that of a steady state, as shown above. Therefore, the numerical result shown is that of the steady state which is computed based on the average thermal conditions over the duration of each test.

As seen in some tests (Run#1-Tests CF2, CF3, CF5; Run#3 Test CF2), the laser power fluctuated appreciably during the test. In all those cases the laser power setpoint was 3 W but the actual power did not go that high and ,because of it, the power control loop did not function. The power went up to only about 2 W and the power fluctuation level was ± 5 %. In two tests (Run#2-Tests CF2 and CF4) the laser power did go up to 3 W and remained constant. Even after an extensive investigation after the flight the cause of the problem has not been found, because it was not possible to reproduce the problem.

The cold wall, air, and floor temperature remained nearly constant for each individual test. The fluid temperature increased generally with time, but when the laser power of the previous test was much larger, the fluid temperature decreased. The laser power for Run#1 Test CF4 was around 0.3 W (Fig. C13) while the laser power for Run#1 Test CF3 was around 2.1 W (Fig. C7), so the fluid temperature continued to decrease during the ten-minute CF4 test (Fig. C15). The same trend can be seen in Run#2 Test CF3 (Fig. C39).

The overall flow structures were all simple unicellular as in the one-hour test. No secondary cells nor subregions were found. The computed streamlines agree well with the observed ones generally. The cell center location stays near halfway between the heater and the cold wall in all cases, nearly independent of the laser output and the laser beam diameter in the parametric ranges of the present study (actually, a close of examination of the velocity fields shows a small but systematic change of the cell center by those factors but it is not analyzed herein). For a given laser power the velocity increases with decreasing beam diameter (compare, for example, the velocity vectors for Run#1 Test CF3 with 30 mm beam dia. (Fig. C12) and those for Run#1 Test CF5 with 5 mm beam dia. (Fig. C24)) but the velocity decays more quickly away from the center with decreasing beam diameter. For a fixed beam diameter, the velocity increases with increasing laser power (compare, for example, the vectors for Run#1 Test CF4 (Fig. C18) and those for Run#1 Test CF5 (Fig. C24) noting the difference in the velocity scale between them).

No oscillations were found in any of the tests . The largest Ma was 2.9×10^5 (based on the average temperature of the heater and the cold wall) which was obtained in Run#2 Test CF2 with 5 mm beam diameter (note that the laser power remained constant in that test). Pr was 66 in that test. In our ground-based tests with smaller containers (less than 10 mm dia.) in the same laser heating mode the oscillations were found above about $Ma = 5 \times 10^4$ in the range $Pr = 20 - 55$ (Lee et al.[22]). Clearly, Ma is not a proper parameter to specify the onset of oscillations.

5.5 CT Flat Surface Tests

There were six shorter CT flat surface tests with 10 or 30 minutes in duration. The results from those tests are given in Appendix D. The thermistor data are given on the first two pages of each test, followed on the next three pages by the velocity field data measured near the end of each test together with the steady-state numerical calculation.

In most tests the chamber wall temperature and the air temperature increased with time, especially when the input to the heater was above 10 W. The heater power was boosted in the first 90 seconds in all the tests to warm-up the heater quickly. After the warm-up period, the heater temperature remained nearly constant, but in two tests (Run#2 CT1 and Run#3 CT2) the heater power fluctuated slightly and the thermistor in the fluid (TCR#1) detected the resultant fluid temperature fluctuation, as seen in Figs. D12 and D27. Even though the fluid temperature near the free surface varied almost periodically in Run#2 Test CT1 (Fig. D12), it was not caused by the flow oscillation phenomenon because the flow visualization did not show any appreciable change in the flow with time. There are also some disturbances in the thermistor data: the air and TCR#1 data for Run#1 CT3 (Figs. D6 and D7), the air data for Run#2 CT2 (Fig. D16), and the air data for Run#3 CT2 (Fig. D26). The cause of those disturbances are not known.

The overall flow structures were all unicellular and agree well with the computed patterns. Kamotani et al.[14] analyzed those velocity data in details and found that the cell moved toward the cold wall with increasing ΔT (or Ma). As discussed by Kamotani et al.[14], in the Ma range of the present experiment the extent of the important thermocapillary driving force region increases with increasing Ma, resulting in the above shift in the cell center. The velocity vector plots show that the maximum velocity always occurred near the heater at the surface where thermocapillary driving force is largest. As in the CF tests, the PIV technique did not detect very large velocities along the free surface very close to the heater because of lack of tracer particles in that region.

No oscillations were detected. The maximum value of Ma was 4.9×10^5 with $Pr = 50$ which was for Run#1 Test CT3. As noted above, there were some disturbances in the fluid temperature in that test but the fluid motion did not show any oscillatory behaviors.

In comparison, our ground-based experiments show that thermocapillary flow in the CT configuration but with smaller containers is known to become oscillatory even when Ma is as small as 6×10^4 in the range Pr = 11 - 23 (Kamotani et al.[23]). On the other hand, the value of the surface deformation parameter for Run#1 Test CT3 was S = 0.004, which was the largest in the STDCE, but in our ground-based tests with smaller containers in the CT configuration we found that the parameter must exceed about 0.007 to obtain oscillations. Therefore, the largest S-parameter of the STDCE tests was near the critical value, but did not exceed the surface deformation parameter requirement for the onset of oscillations, from which one can infer that free surface deformation plays an important role in the oscillation phenomenon.

5.6 CF Curved Surface Tests

There were nine CF curved surface tests and all were only 10 or 20 minutes in duration. The data from the tests are given in Appendix E. The laser power, the thermistor data, the velocity field data, and the steady numerical calculation are shown for each test. Although they were not in the original test matrix, two tests with a convex free surface were conducted (Run#3 Tests CF5 and CF6). The free surface remained very stationary during those tests. However, since the flow visualization system was not designed for a large convex shape, it was not possible to visualize an entire cross-section in those tests, as will be shown later. There was a technical problem in the thermistor data for Run#3 Test CF6, so they are not given here.

The laser power setpoint was 3 W in seven of the nine tests but the power went up to only about 2 W in all those seven tests. In some of the tests, the power fluctuated

(Run#1 CF67(Fig. E7), Run#2 CF6 (Fig. E19), and Run#3 CF3 (Fig. E31)). The thermistor data show mostly constant wall, air, and floor temperature. In one test, Run#3 CF3, since the fluid depth was shallow near the center, it caused a rise in the floor temperature (Fig. E32). The test chamber rakes and submerged heater rakes also exhibit the normal pattern of increasing temperature with time. In the case of concave free surface some thermistors were outside of the fluid. In all of the concave surface tests the center thermistor SHR#1 was outside the liquid and consequently its temperature reading was very high in those tests because it was heated directly by the laser beam. The top chamber thermistor TCR#1 was also outside when the free surface was concave so that it measured the air temperature near the free surface.

The overall flow structure was unicellular except in one test with a highly concave surface (Run#3 CF3) in which two cells appeared (Figs. E34). Since the cell near the heated region is very small, it is difficult to see in the streamline picture (Fig. E35) but it can be seen in the original videotape. When the free surface is highly concave, the fluid is very shallow near the center so that the return flow cannot easily go into the heated region and, as a result, some of the surface flow near the heated region turns around for recirculation to compensate for the lack of return flow from the cold region, which results in a small recirculation cell in the heated region. Kamotani et al.[13] analyzed the velocity data in details and showed that: (i) For given beam diameter and laser power, the center of the cell moves toward the container centerline as the free surface becomes more concave, and (ii) The computed results agree well with the measured velocity distributions (except in certain areas where not enough tracer particles are found, as described earlier for other tests).

In Appendix E the numerically computed vectors are plotted in two ways; the plot at the top left corner shows the vectors at unevenly spaced points (as in the numerical calculation) to show more points where the flow is strong, while the top right plot is an evenly spaced plot to compare with the experimental plot. In Figs. E47 and E53 for the convex surface tests the top region was blocked out because the camera viewing area was not big enough, so the experimental vector plots in Figs. E48 and E54 are shown only in the viewing area

5.7 CT Curved Surface Tests

11 CT curved surface tests were conducted with various concave free surface shapes. No convex surface test was conducted in the CT configuration because the heater was not designed to go above the flat free surface position. The results from those tests are given in Appendix F. The thermistor data, the flow field data, and the steady state computation are shown.

As in the curved CF tests some thermistors are outside the fluid when the surface is concave, so their readings do not show the fluid temperature. Again as in other tests there are some disturbances in the thermistor data, notably the outputs of the thermistors TCR#1 and TCR#3 in Run#2 Test CT3 (Fig. F12). The fluid temperature in Run#1 Test CT4 decreased through the entire experiment (Fig. F2), which was caused by the power setting of the previous test being higher.

Since the flow field was observed through the bottom wall, various reflections from the free surface made it somewhat difficult to understand the whole camera view, especially when the surface was highly curved (e.g. Fig. F54). After identifying the free surface location the reflected portion was blocked out for the PTV analysis. As in the CF curved tests the computed vectors are plotted in two ways; the plot at the top left corner shows the vectors at unevenly spaced points as in the numerical analysis, while the top right plot is an evenly spaced plot to compare with the experimental plot.

The overall flow structure was unicellular in all CT curved tests. For a given shape the cell center moves toward the cold wall with increasing heater temperature (or Ma). Compare, for example, Run#1 CT4 (Figs. F3 and F4) with $Ma = 2.9 \times 10^4$ and Run#1 CT5 (Figs. F8 and F9) with $Ma = 3.1 \times 10^5$. For a given heater temperature the flow slows down when the surface is more concave, as the overall flow passage becomes narrower. Unlike in the CF configuration, it is possible in the CT configuration to vary the free surface shape near the heater where the flow is mainly driven. The experimental conditions for tests Run#2 CT4 and Run#5 CT2 are rather close: same total fluid volume, same total free surface area, and the difference in Ma is about 25%. However, in Run#5 Test CT2 the free surface is more curved near the heater (Fig. 4). As discussed by Kamotani et al.[15], the overall flow rate (the maximum stream function) is nearly the same in both tests, but by comparing Figs. F18 and F19 and Figs. F48 and F49 one notices that the center of the cell is located further away from the heater in Run#5 Test CT2, which suggests that the flow near the heater is slower in that test due to the curved free surface. At present we are still analyzing the data from the CT curved surface tests.

CHAPTER VI. SUMMARY

The Surface Tension Driven Convection Experiment (STDCE) was conducted aboard the USML-1 Spacelab in 1992 to investigate steady and transient thermocapillary flows in cylindrical containers under two different modes of heating. It was generally a successful experiment and more than ten hours of data were brought back. It was the first thermocapillary flow experiment in microgravity using state-of-the-art diagnostic techniques in an interactive mode. Thermocapillary flows with large curved free surfaces had not been studied experimentally before. The STDCE was a combined theoretical, numerical, and experimental work to increase our understanding of complex thermocapillary flow with substantially reduced buoyancy.

The data from the STDCE are presented in this report. Since the flow visualization and IR imager data are on videotapes, they need to be reduced to obtain quantitative information. We have so far analyzed only the main data, the results of which are given herein. Since the rest of the data also contains useful information about thermocapillary flows, we will continue to analyze those data. The videotapes are also archived so that interested scientists have access to those tapes. More detailed information about the data presented herein will be supplied upon request.

With the STDCE we accomplished our objective of investigating thermocapillary flows at large Marangoni numbers with various free surface shapes. There were a few technical problems but they did not affect our study significantly. Based on the data analyzed so far, we can conclude that the velocity and temperature distributions in steady and transient thermocapillary flows can be predicted with reasonable accuracy by numerical analysis as long as it employs sufficiently fine numerical mesh to resolve the thin velocity and temperature boundary layers in the heated region.

No oscillatory thermocapillary flows were observed although Ma went above 10^5, which was much beyond the 'critical' Ma found in our ground-based tests with smaller containers. Most of the flows in the STDCE were not exactly in steady state because it took at least an hour to heat up the bulk fluid. However, thermocapillary flow in the present configurations and in the present parametric ranges is mainly driven in a relatively small hot-corner region and thus once the temperature field in the hot-corner region is established, the subsequent long period to heat up the bulk fluid does not have significant influence on the flow as long as the fluid initial temperature is close to the side wall temperature, as evidenced by the fact that the velocity field became nearly steady within a few minutes in each test. Therefore, the flow unsteadiness is not significant enough to explain the above difference between the STDCE and the ground-based tests. Clearly, Ma alone cannot specify the onset conditions of oscillations. According to our concept of oscillations, the surface deformation parameter is also important and its value was not large enough in the STDCE to cause oscillations. Accordingly, we have redesigned the STDCE to obtain oscillatory thermocapillary flow and the experiment called STDCE-2 will be conducted aboard the USML-2 Spacelab in the fall of 1995. STDCE-2 will measure free surface deformation during oscillations and study the role of the deformation in the oscillation phenomenon.

REFERENCES

1. Ostrach, S., "Low Gravity Fluid Flows," Annual Review of Fluid Mechanics, Vol. 14, 1982, pp. 314-375.

2. Fu, B. and Ostrach, S., "Numerical Simulation of Floating-Zone Thermocapillary Flows," Proceedings of the 4th European Symposium on Materials Sciences under Microgravity, Madrid, Spain (ESA SP-191), 1983, pp. 239-245.

3. Zebib, A., Homsy, G.M. and Meiburg, E.," High Marangoni Number Convection in a Square Cavity," Physics of Fluids, Vol. 28,1985, pp. 3467-3476.

4. Carpenter, B.M. and Homsy, G.M., "High Marangoni Number Convection in a Square Cavity: Part II," Physics of Fluids A, Vol. 2, 1990, pp.137-149.

5. Kamotani, Y. and Platt, J., "Effects of Free Surface Shape on Combined Thermocapillary and Natural Convection," J. Thermophysics and Heat Transfer, Vol. 6, 1992, pp. 721-726.

6. Schwabe, D., Scharmann, A., Preisser, F., and Oeder, R., "Experiments on Surface Tension Driven Flow in Floating Zone Melting," J. Crystal Growth, Vol. 43, 1978, pp. 305-312.

7. Chun, C.-H. and Wuest, W., "Experiments on the Transition from Steady to the Oscillatory Marangoni Convection of a Floating Zone under Reduced Gravity Effect," Acta Astronautica, Vol. 6, 1979, pp. 1073-1082.

8. Kamotani, Y., Ostrach, S., and Vargas, M., "Oscillatory Thermocapillary Convection in a Simulated Floating-Zone Configuration," Journal of Crystal Growth, Vol. 66, 1984, pp. 83-90.

9. Kamotani, Y., Lee, J.H., and Ostrach, S., "An Experimental Study of Oscillatory Thermocapillary Convection in Cylindrical Containers," Physics of Fluids A, Vol. 4, 1992, pp. 955-962.

10. Ostrach, S., Kamotani, Y., and Lai, C.L., "Oscillatory Thermocapillary Flows," PCH Physico-Chemical Hydrodynamics, Vol. 6, 1985, pp. 585-599

11. Kamotani, Y., Ostrach, S. and Pline, A., "A Thermocapillary Convection Experiment in Microgravity," in Heat Transfer in Microgravity (Avedesian, C.T. and Arpaci, V.A., eds.), ASME HTD-Vol. 1, 1993, pp. 23-30 (also to appear in Journal of Heat Transfer).

12. Ostrach, S., Kamotani, Y., and Pline, A., "Surface Tension Driven Convection Experiment (STDCE)," Proceedings of Launch+One Year Science Review of USML-1 and USMP-1 with the Microgravity Measurement Group (NASA CP-3272), Vol. 1, 1993, pp. 271-300..

13. Kamotani, Y., Ostrach, S., and Pline, A., "Analysis of Velocity Data Taken in Surface Tension Driven Convection Experiment in Microgravity," Physics of Fluids, Vol. 6, 1994, pp. 3601-3609.

14. Kamotani, Y., Ostrach, S., and Pline, A., "Some Velocity Fields Results from the Thermocapillary Flow Experiment aboard USML-1 Spacelab," presented at the COSPAR Meeting, Hamburg, Germany, July, 1994 (to be published in Advances in Space Research).

15. Kamotani, Y., Ostrach, S., and Pline, A., "Summary of Results from the Surface Tension Driven Convection Experiments in Microgravity," Paper IAF-94-J.3.238, presented at the 45th Congress of the International Astronautical Federation, Jerusalem, Israel, October, 1994.

16. Kamotani, Y. and Ostrach, S., "Design of a Thermocapillary Flow Experiment in Reduced Gravity," J. Thermophysics and Heat Transfer, Vol. 1, 1987, pp. 83-89.

17. Pline, A., Jacobson, T.P., Wanhainen, J.S., and Petrarca, D.A., "Hardware Development for Surface Tension Driven Convection Experiment," Journal of Spacecraft and Rockets, Vol. 27, 1990, pp. 312-317.

18. Pline, A., Jacobson, T., Kamotani, Y., and Ostrach, S., "Surface Tension Driven Convection Experiment," AIAA Paper No. 93-4312, 1993.

19. Wernet, M. and Pline, A., "Particle Image Velocimetry for the Surface Tension Driven Convection Experiment Using a Particle Displacement Tracking Technique," NASA TM 104482, 1991.

20. Pline, A. and Butcher, R., "Spacelab Qualified Infrared Imager for Microgravity Science Experiments," SPIE Vol. 1313, Thermosense XII, 1990, pp. 250-258.

21. Patanker, S.V., <u>Numerical Heat Transfer and Fluid Flow</u>, Hemisphere Publication, 1980.

22. Lee, J. H., Ostrach, S., and Kamotani, Y., "A Study of Oscillatory Thermocapillary Convection in Circular Containers with CO_2 Laser Heating," Report EMAE/TR-94-213, Case Western Reserve University, 1994.

23. Kamotani, Y., Masud, J., Lee, J. H., and Pline, A., "Oscillatory Convection due to Combined Buoyancy and Thermocapillarity," AIAA Paper 95-0817, 1995.

Property	Value/Units
ρ	0.935 g/cm^3
μ	0.094 dynes sec/cm^2
α	9.51 x 10^{-4} cm^2/sec
σ	20.1 dynes/cm
σ_T	-0.06 dynes/cm °C
c_p	0.36 cal/g °C
Pr	105

Table 1. Properties of 10 cs silicone oil at 25 °C

Test Name	Power* (W)	Heating Zone Dia. (mm)	Free Surface Shape Flat/Curved (See Figs. 2-4)	Test Start Time Mission Elapsed Time Day/Time	Duration (min)
Run#1 CF1	0.48	10.0	F	4/09:53:03	60
CF2	2.07	10.0	F	4/10:53:12	10
CF3	2.10	30.0	F	4/11:03:12	10
CF4	0.31	5.0	F	4/11:14:03	10
CF5	2.05	5.0	F	4/11:24:13	10
CF6	2.00	5.0	CF shape 3	4/12:05:12	10
CF7	2.00	30.0	CF shape 3	4/12:15:39	10
Run#1 CT1	1.2		F	4/13:51:06	60
CT2	4.0		F	4/14:51:16	10
CT3	12.9		F	4/15:01:26	10
CT4	1.2		CT shape 2	4/15:35:19	10
CT5	12.9		CT shape 2	4/15:45:36	10
Run#2 CF1	1.50	5	F	6/08:53:07	20
CF2	3.00	5	F	6/09:13:13	20
CF3	1.50	30	F	6/09:33:44	10
CF4	3.00	30	F	6/09:43:54	10
CF5	1.50	5.2	CF shape 2	6/10:35:26	20
CF6	1.85	5.2	CF shape 2	6/10:55:36	20
CF7	1.90	10.0	CF shape 2	6/11:16:10	20
Run#2 CT1	3.0		F	6/13:09:13	30
CT2	10.1		F	6/13:39:23	30
CT3	1.2		CT shape 10	6/15:02:55	20
CT4	12.9		CT shape 10	6/15:23:05	20
Run#3 CT1	5.0		F	8/07:57:15	30
CT2	12.9		F	8/08:27:25	30
CT3	3.0		CT shape 7	8/09:10:50	20
CT4	10.1		CT shape 7	8/09:31:01	20
Run#3 CF1	1.80	10	F	8/11:14:14	20
CF2	1.80	5	F	8/11:34:47	20
CF3	1.95	4.9	CF shape 4	8/12:22:26	20
CF4	1.95	31.6	CF shape 4	8/12:42:53	20
CF5	1.90	5.7	CF shape 5	8/13:31:58	10
CF6	1.94	27.6	CF shape 5	8/13:42:26	10
Run#4 CT1	5.0		CT shape 5	8/14:49:33	30
CT2	12.9		CT shape 5	8/15:19:43	10
Run#5 CT1	10.1		CT shape 8	10/17:18:44	20
CT2	12.9		CT shape 9	10/17:48:45	20
CT3	10.0		CT shape 6	10/18:18:34	20

* Excludes boost power in CT tests. Average laser power over duration of test in CF tests.

Table 2. STDCE test conditions

	Ma based on two different temperatures*		Pr based on two different temepratures*		Hr
Test Name	T_c	$(T_h+T_c)/2$	T_c	$(T_h+T_c)/2$	
Run#1 CF1	3.2×10^4	3.5×10^4	100	92	0.10
CF2	8.9×10^4	1.1×10^5	98	78	0.10
CF3	4.0×10^4	4.4×10^4	97	88	0.30
CF4	4.4×10^4	4.9×10^4	97	87	0.05
CF5	1.5×10^5	2.2×10^5	97	66	0.05
CF6	1.6×10^5	2.1×10^5	95	63	0.05
CF7	4.6×10^4	5.1×10^4	95	84	0.30
Run#1 CT1	4.6×10^4	5.2×10^4	96	86	0.11
CT2	1.4×10^5	1.9×10^5	95	67	0.11
CT3	2.6×10^5	4.9×10^5	94	50	0.11
CT4	2.7×10^4	2.9×10^4	94	88	0.11
CT5	2.0×10^5	3.1×10^5	93	55	0.11
Run#2 CF1	1.1×10^5	1.5×10^5	110	80	0.05
CF2	1.8×10^5	2.9×10^5	109	66	0.05
CF3	2.9×10^4	3.1×10^4	108	100	0.30
CF4	4.8×10^4	5.4×10^4	107	95	0.30
CF5	1.1×10^5	1.5×10^5	106	77	0.052
CF6	1.3×10^5	1.8×10^5	105	73	0.052
CF7	8.3×10^4	1.0×10^5	104	83	0.10
Run#2 CT1	9.7×10^4	1.3×10^5	105	81	0.11
CT2	2.3×10^5	4.3×10^5	104	56	0.11
CT3	1.7×10^4	1.7×10^4	104	99	0.11
CT4	1.7×10^5	2.5×10^5	103	64	0.11
Run#3 CT1	1.6×10^5	2.4×10^5	103	68	0.11
CT2	2.5×10^5	4.9×10^5	101	52	0.11
CT3	1.1×10^5	1.5×10^5	100	73	0.11
CT4	2.4×10^5	4.1×10^5	99	52	0.11
Run#3 CF1	8.1×10^4	9.8×10^4	98	80	0.10
CF2	1.4×10^5	1.9×10^5	98	69	0.05
CF3	1.6×10^5	2.2×10^5	97	64	0.049
CF4	5.0×10^4	5.6×10^4	96	85	0.316
CF5	1.3×10^5	1.7×10^5	97	68	0.057
CF6	4.1×10^4	4.5×10^4	96	86	0.276
Run#4 CT1	1.0×10^5	1.3×10^5	97	74	0.11
CT2	2.0×10^5	3.2×10^5	97	56	0.11
Run#5 CT1	1.8×10^5	2.8×10^5	107	64	0.11
CT2	1.9×10^5	3.1×10^5	105	61	0.11
CT3	1.4×10^5	2.0×10^5	104	69	0.11

* Both T_h and T_c are average temperatures over duration of each test.

Table 3. Parametric Ranges of STDCE tests

Test Name	Appendix	Figures
Run#1 CF1	A	A1 - A14
CF2	C	C1 - C6
CF3	C	C7 - C12
CF4	C	C13 - C18
CF5	C	C19 - C24
CF6	E	E1 - E6
CF7	E	E7 - E12
Run#1 CT1	B	B1 - B12
CT2	D	D1 - D5
CT3	D	D6 - D10
CT4	F	F1 - F5
CT5	F	F6 - F10
Run#2 CF1	C	C25 - C30
CF2	C	C31 - C36
CF3	C	C37 - C42
CF4	C	C43 - C48
CF5	E	E13 - E18
CF6	E	E19 - E24
CF7	E	E25 - E30
Run#2 CT1	D	D11 - D15
CT2	D	D16 - D20
CT3	F	F11 - F15
CT4	F	F16 - F20
Run#3 CT1	D	D21 - D25
CT2	D	D26 - D30
CT3	F	F21 - F25
CT4	F	F26 - F30
Run#3 CF1	C	C49 - C54
CF2	C	C55 - C60
CF3	E	E31 - E36
CF4	E	E37 - E42
CF5	E	E43 - E48
CF6	E	E49 - E51
Run#4 CT1	F	F31 - F35
CT2	F	F36 - F40
Run#5 CT1	F	F41 - F45
CT2	F	F46 - F50
CT3	F	F51 - F55

Table 4. Figure location in Appendices

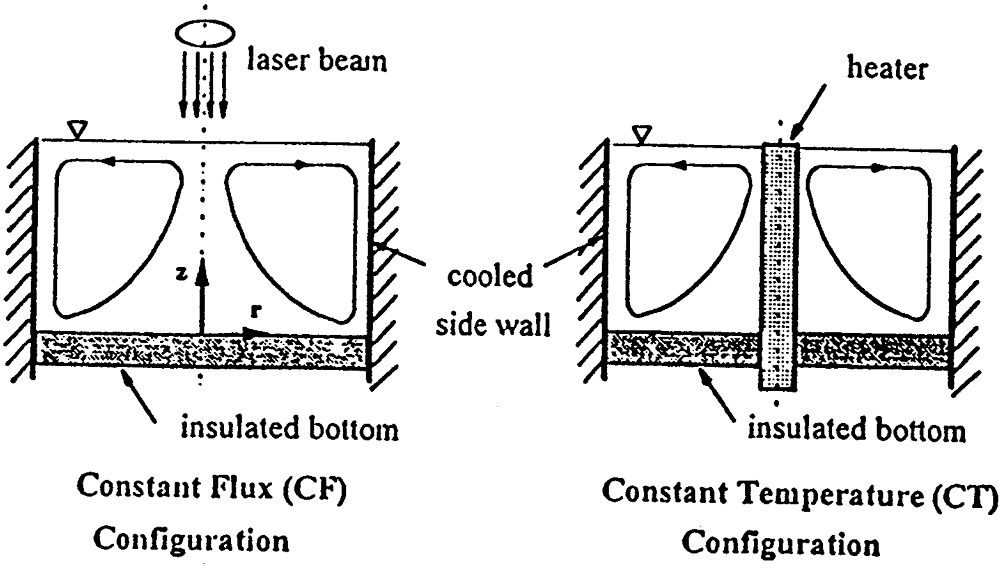

Figure 1 Two heating modes of STDCE

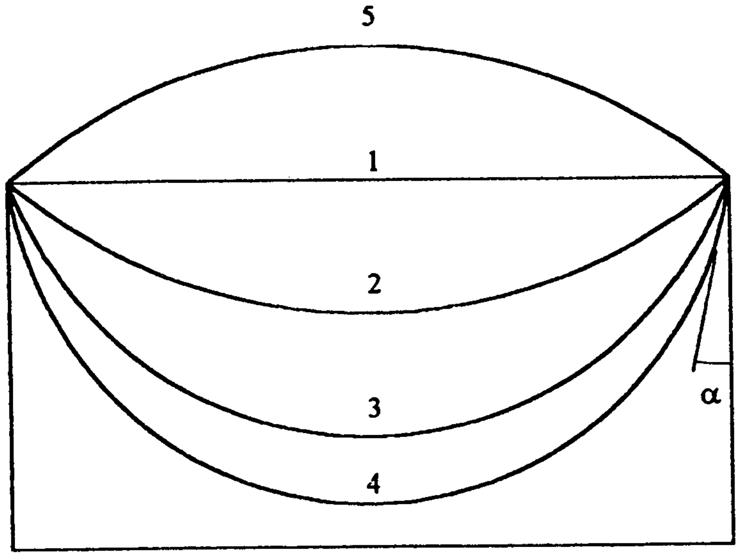

shape	1	2	3	4	5
volume	1	0.81	0.76	0.44	1.19
α	90	50	20	7	130

Figure 2 Free surface shapes in CF tests

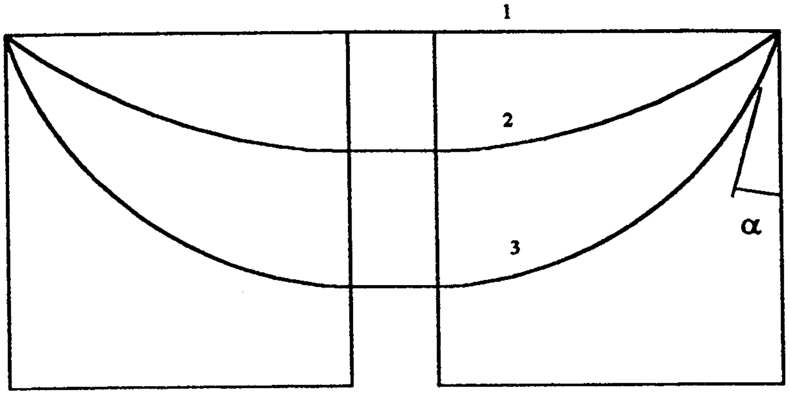

shape	1	2	3
volume	1	0.82	0.56
α	90	51	16

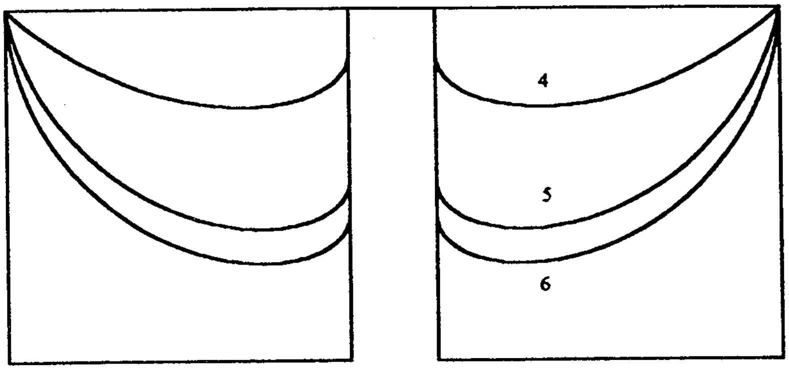

shape	4	5	6
volume	0.82	0.56	0.47
α	45	10	2

Figure 3 Free surface shapes in CT tests

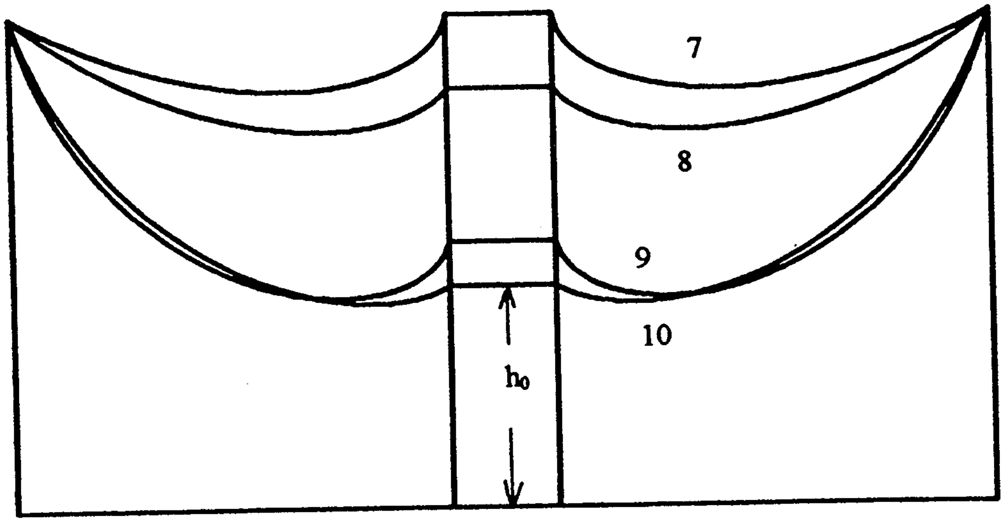

shape	7	8	9	10
volume	0.94	0.85	0.61	0.62
α	70	52	15	19
h_0	1	0.85	0.54	0.45

Figure 4 Additional free surface shapes in CT tests

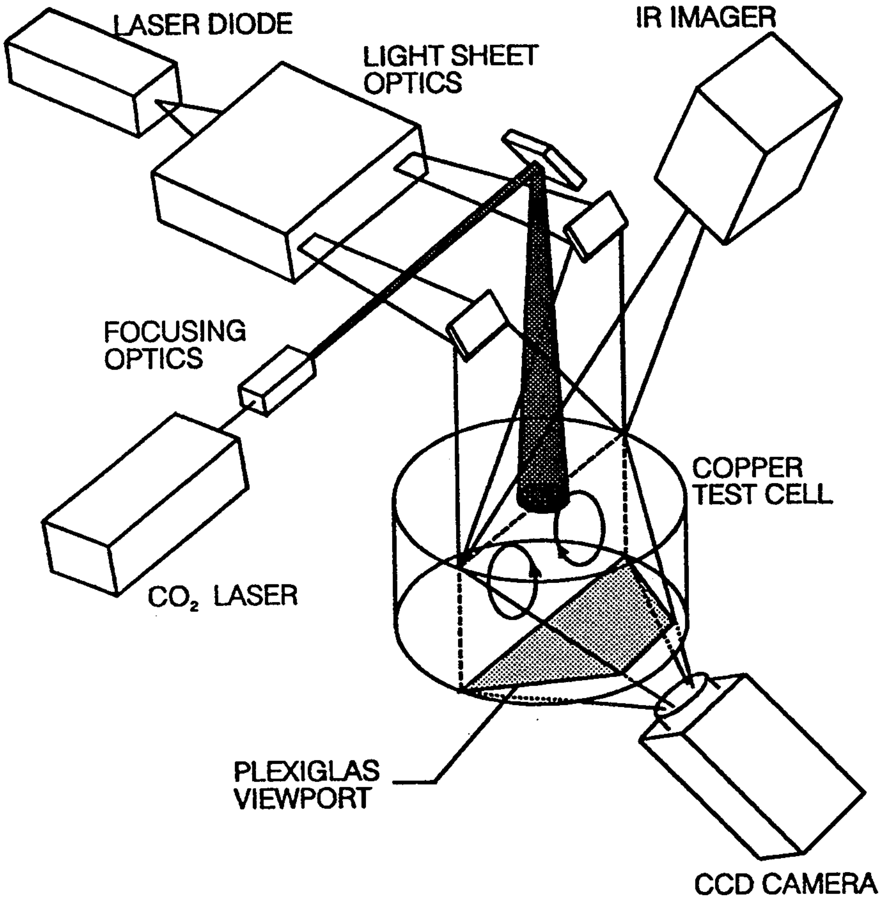

Figure 5 Experimental arrangement of STDCE

CONSTANT TEMPERATURE EXPERIMENT

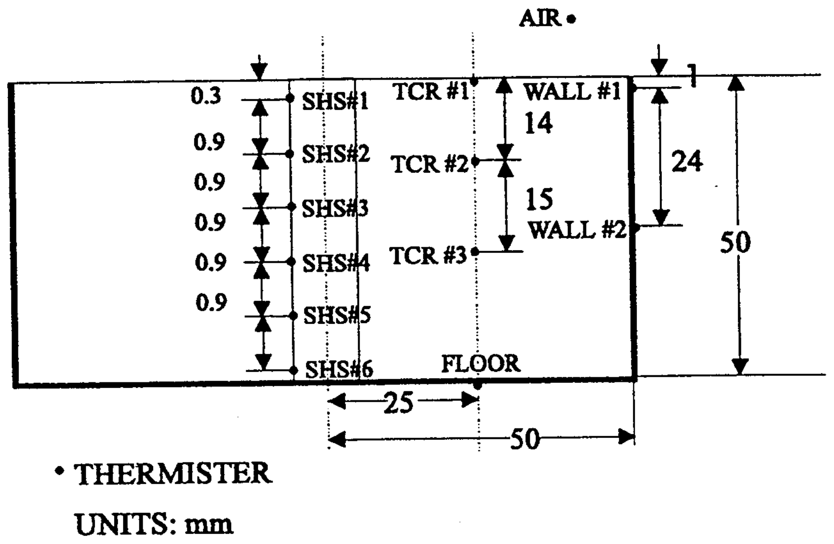

CONSTANT FLUX EXPERIMENT

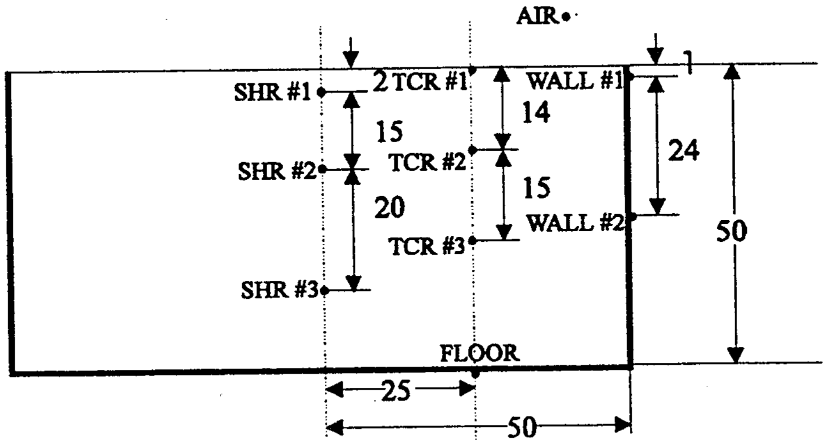

Figure 6 Thermistor locations

APPENDIX A

CF ONE HOUR TEST

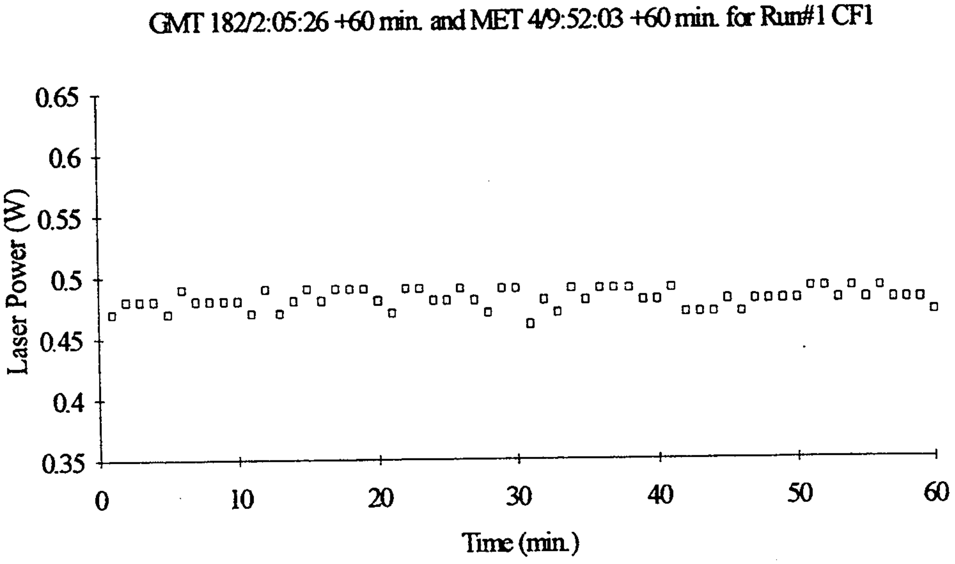

Figure A1 Laser power

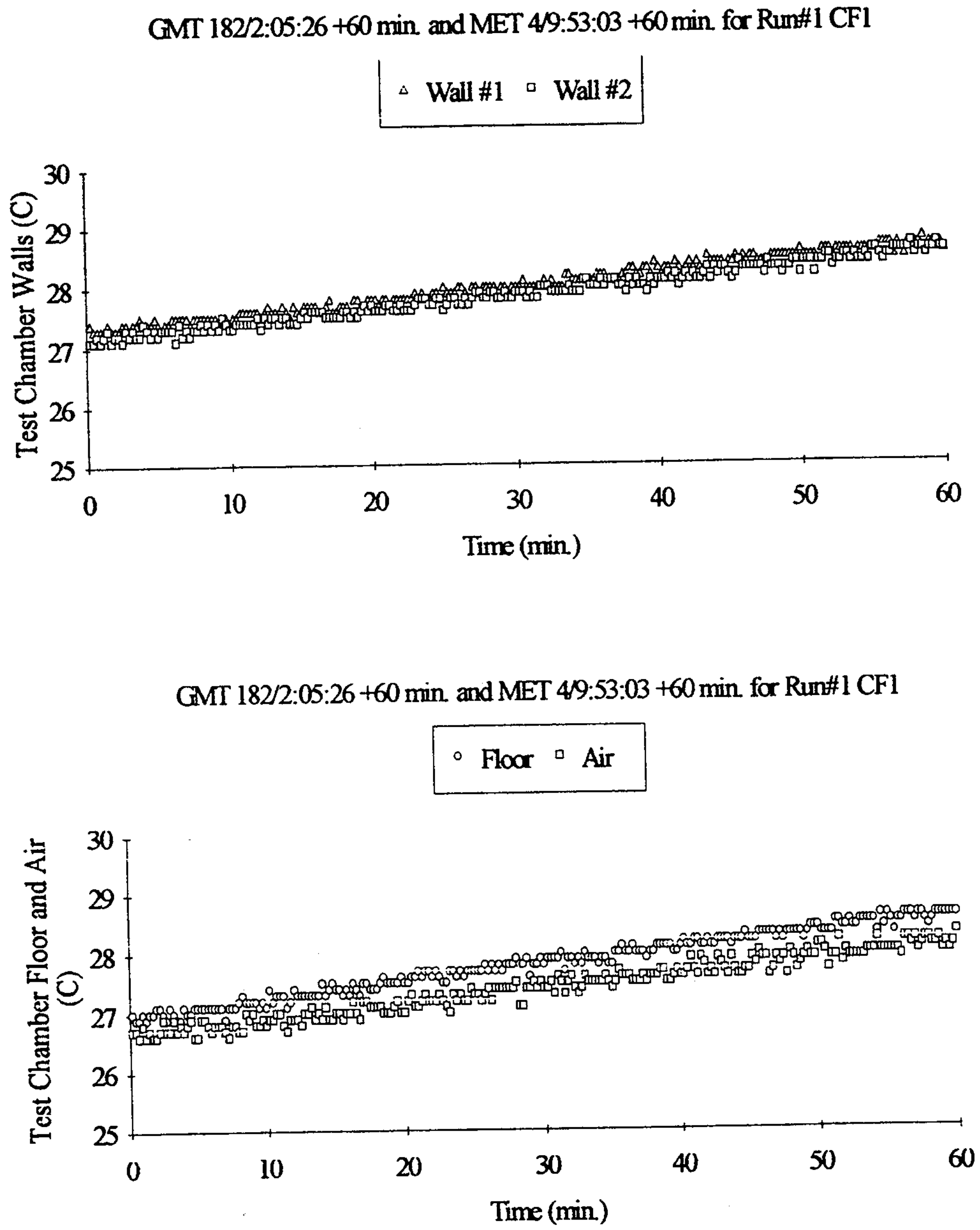

Figure A2 Thermistor data

Streamlines for Run#1 Test CF1 at 2 min.

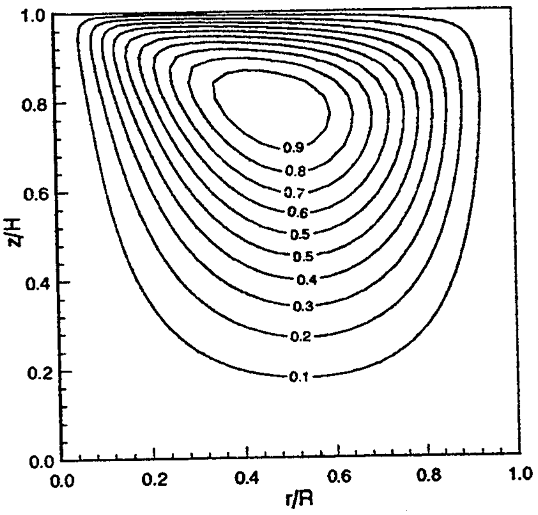

Isotherms for Run#1 Test CF1 at 2 min.

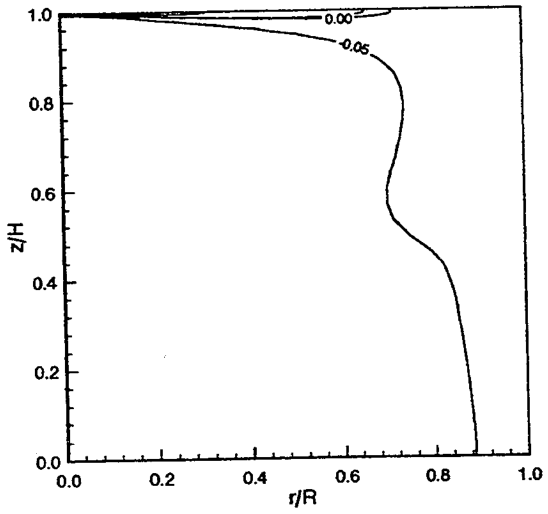

Figure A3 Numerical data at t = 2 min.

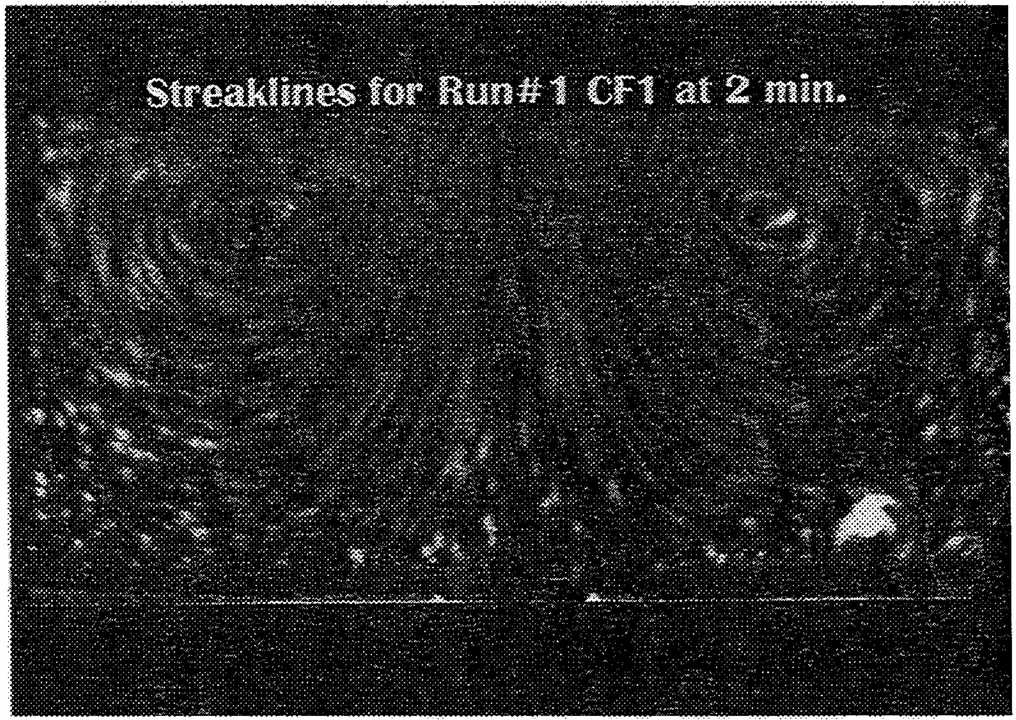

Figure A4 Experimental pathlines at t = 2 min.

Streamlines for Run#1 Test CF1 at 10 min.

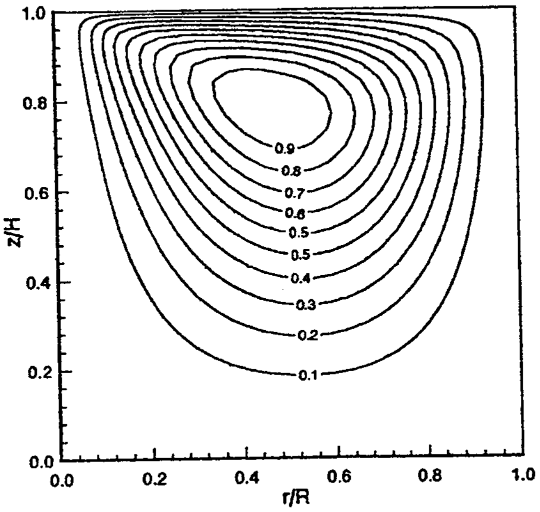

Isotherms for Run#1 CF1 at 10 min.

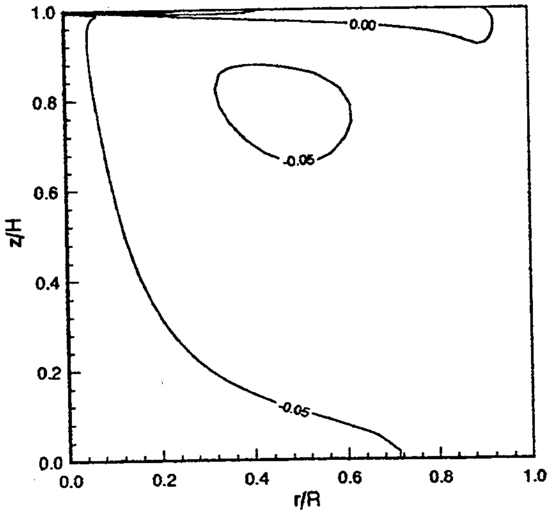

Figure A5 Numerical data at t = 10 min.

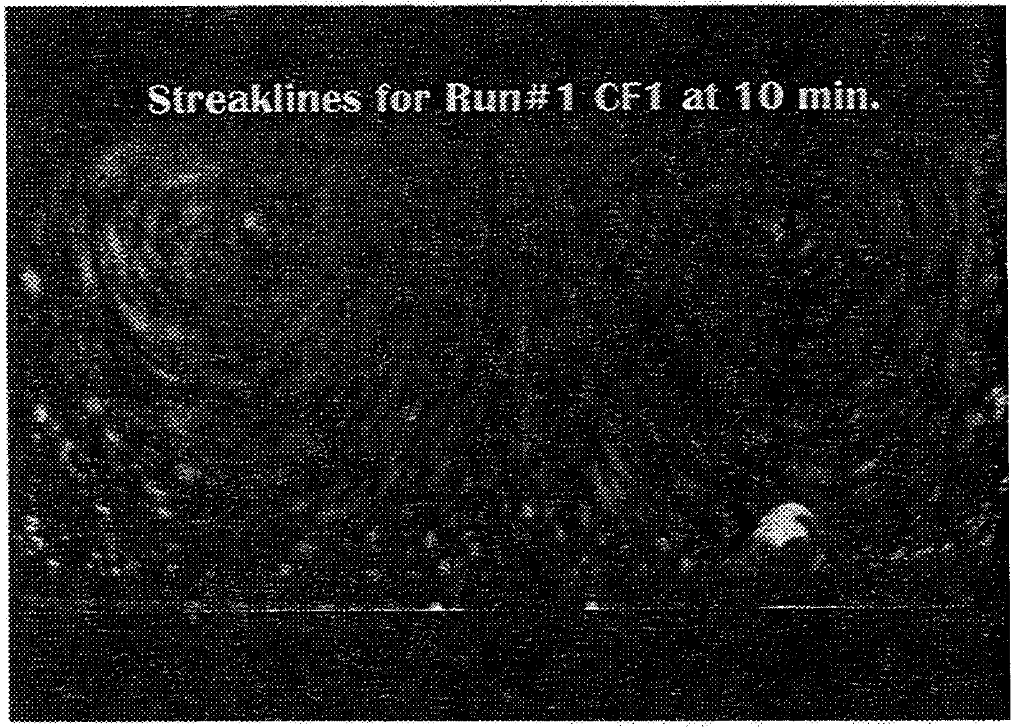

Figure A6 Experimental pathlines at t = 10 min.

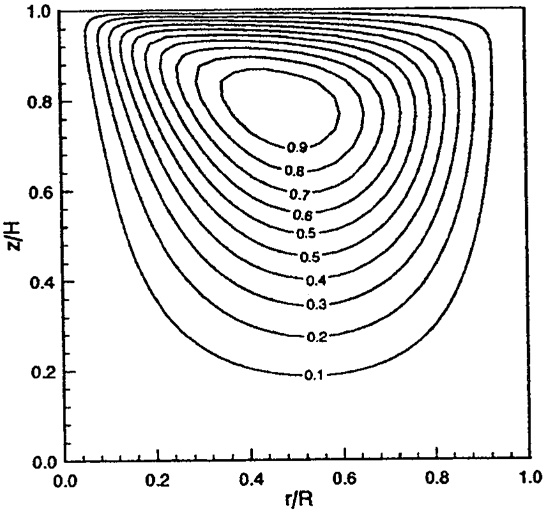
Streamlines for Run#1 Test CF1 at 30 min.

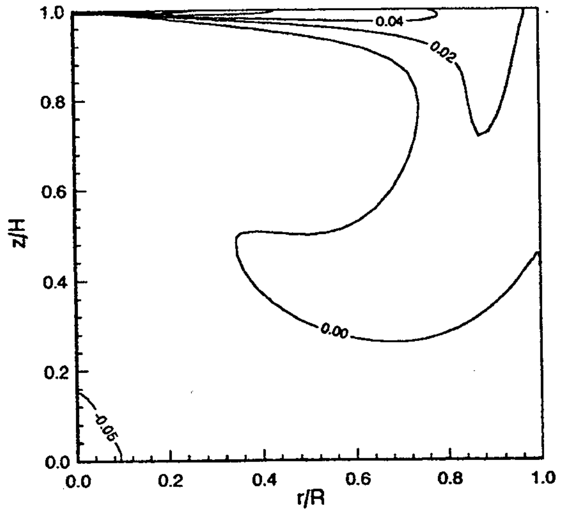
Isotherms for Run#1 Test CF1 at 30 min.

Figure A7 Numerical data at t = 30 min.

Streamlines for Run#1 Test CF1 at 60 min.

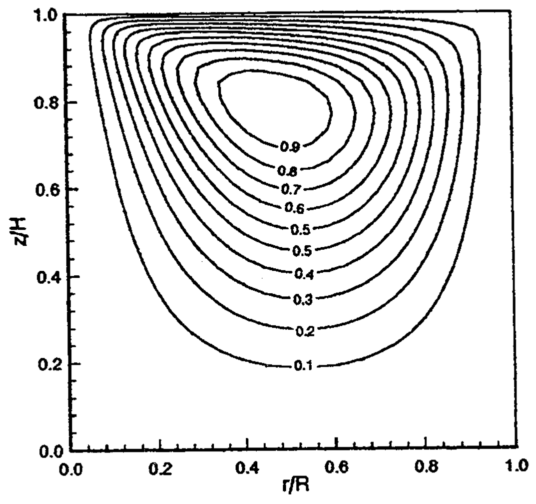

Isotherms for Run#1 Test CF1 at 60 min.

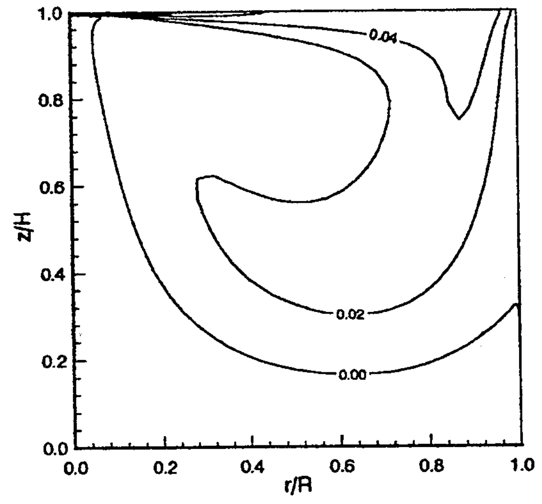

Figure A8 Numerical data at t = 60 min.

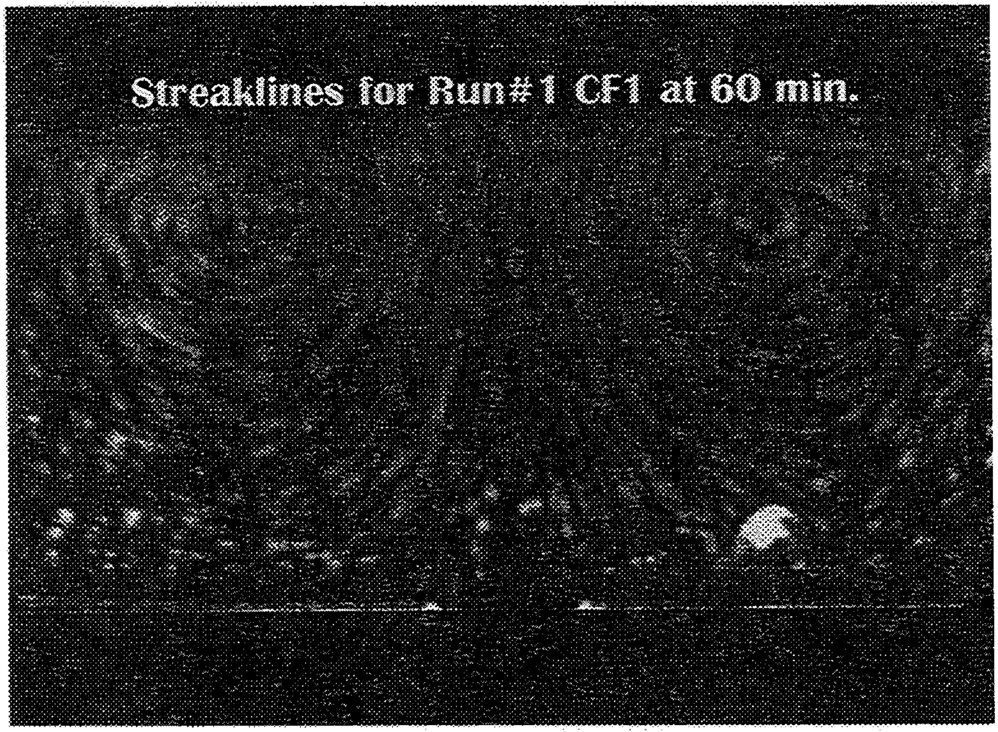

Figure A9 Experimental pathlines at t = 60 min.

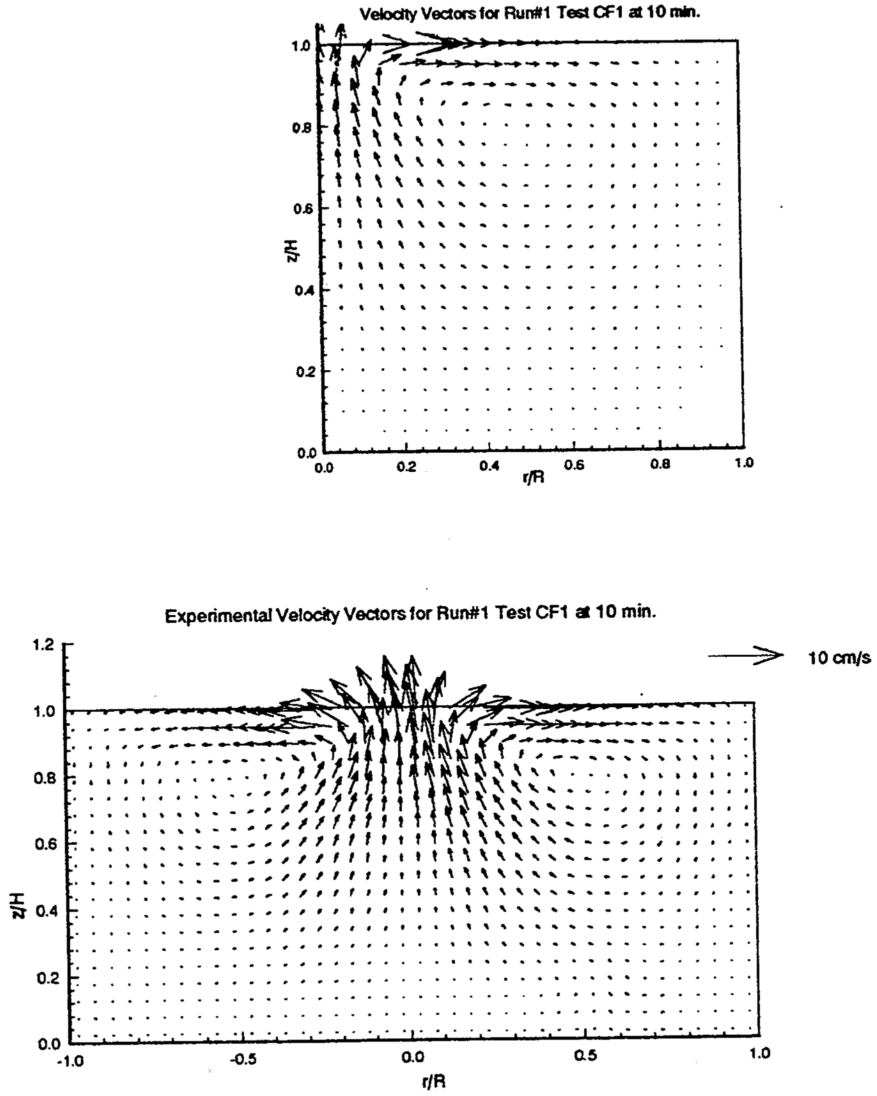

Figure A10 Computed and measured velocity vectors at t = 10 min.

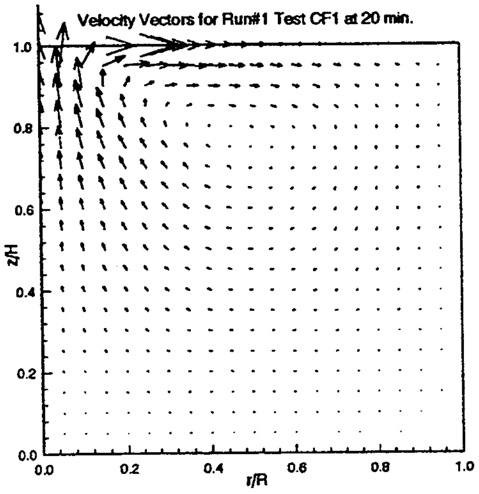
Velocity Vectors for Run#1 Test CF1 at 20 min.

Experimental Velocity Vectors for Run#1 Test CF1 at 20 min.

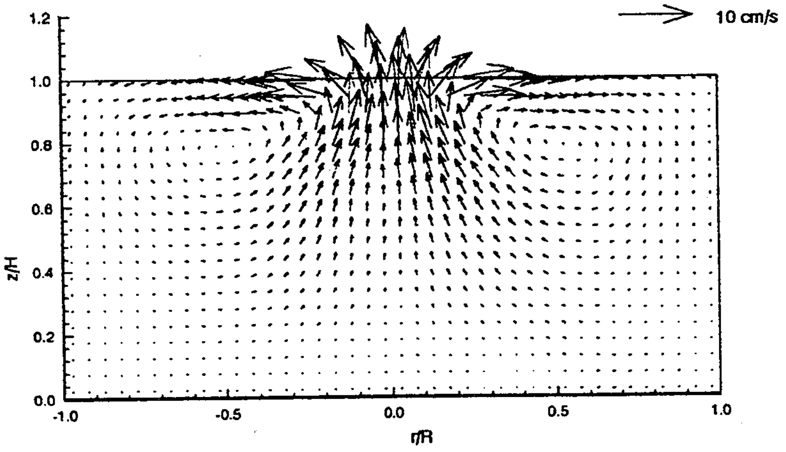

Figure A11 Computed and measured velocity vectors at t = 20 min.

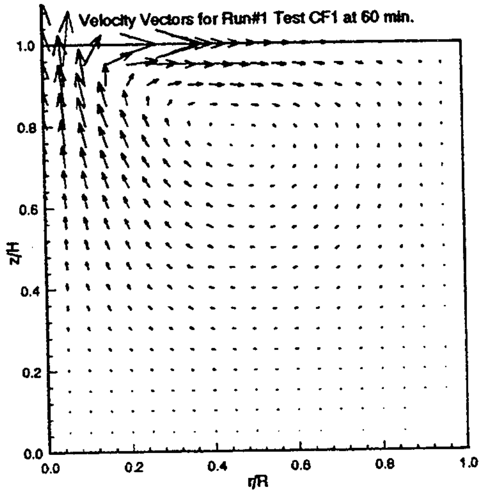

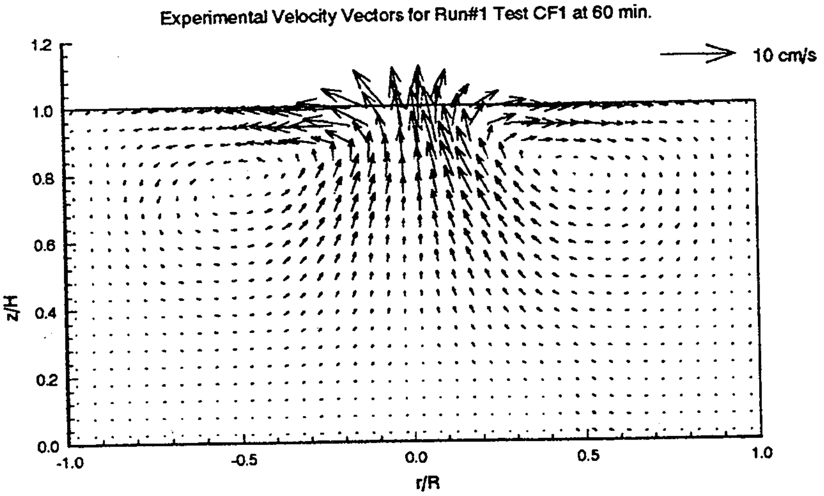

Figure A12 Computed and measured velocity vectors at t = 60 min.

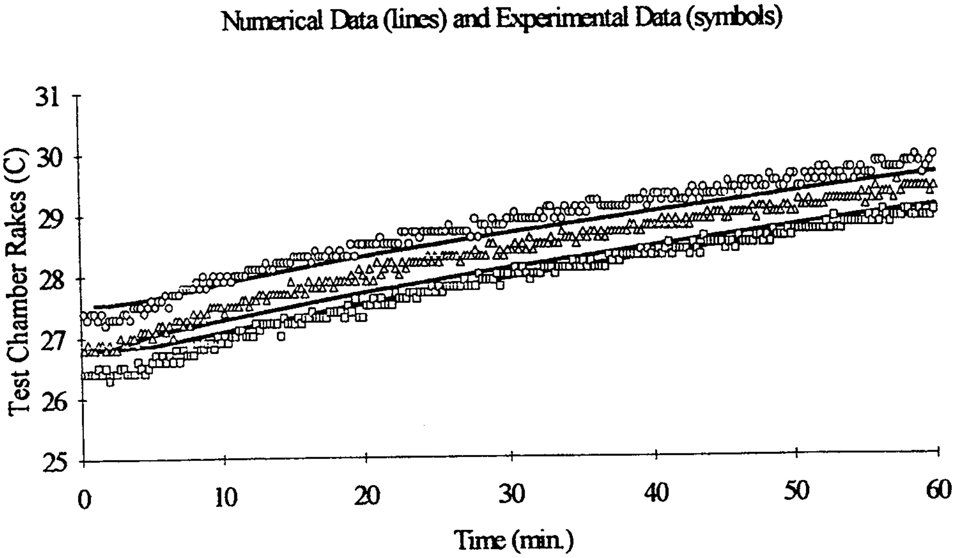

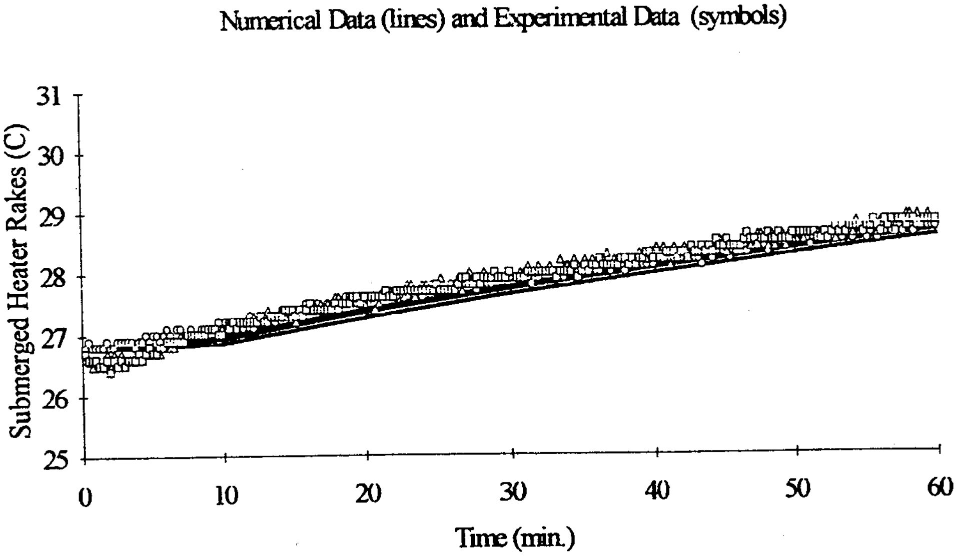

Figure A13 Thermistor data and numerical results

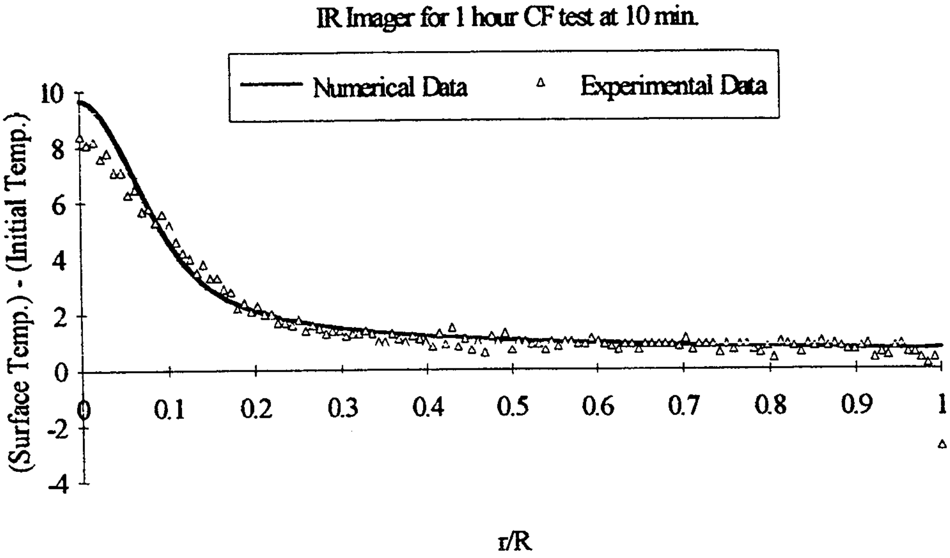

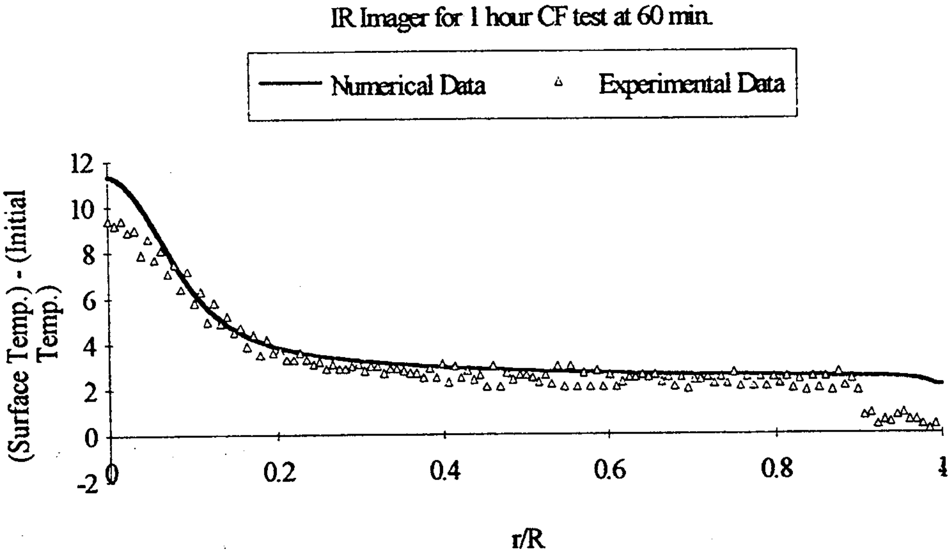

Figure A14 IR Imager data and numerical results

APPENDIX B

CT ONE HOUR TEST

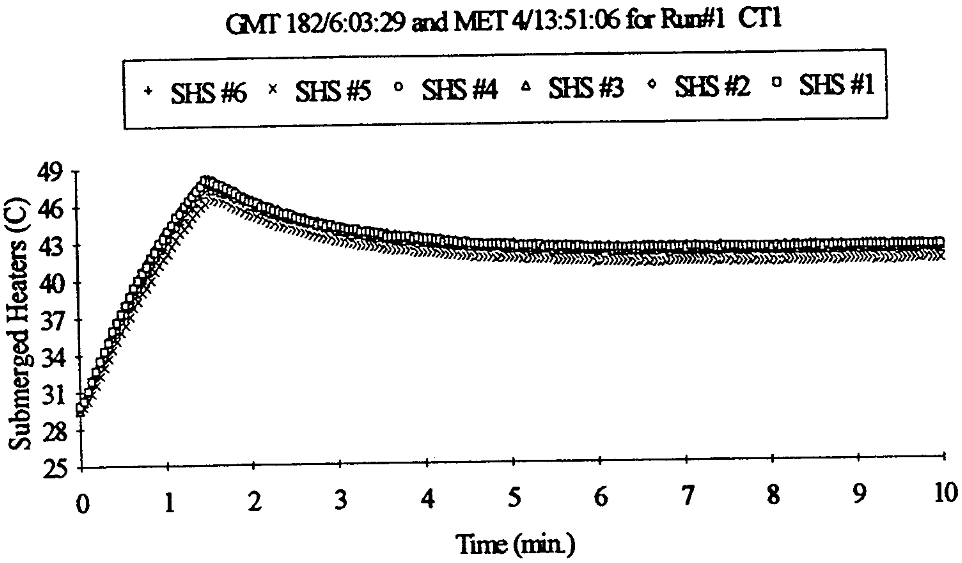

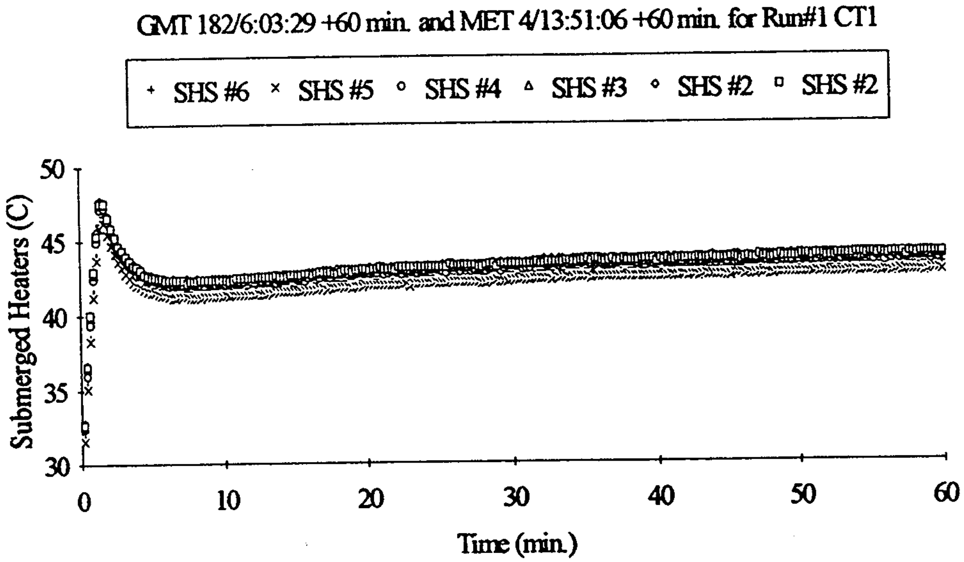

Figure B1 Thermistor data

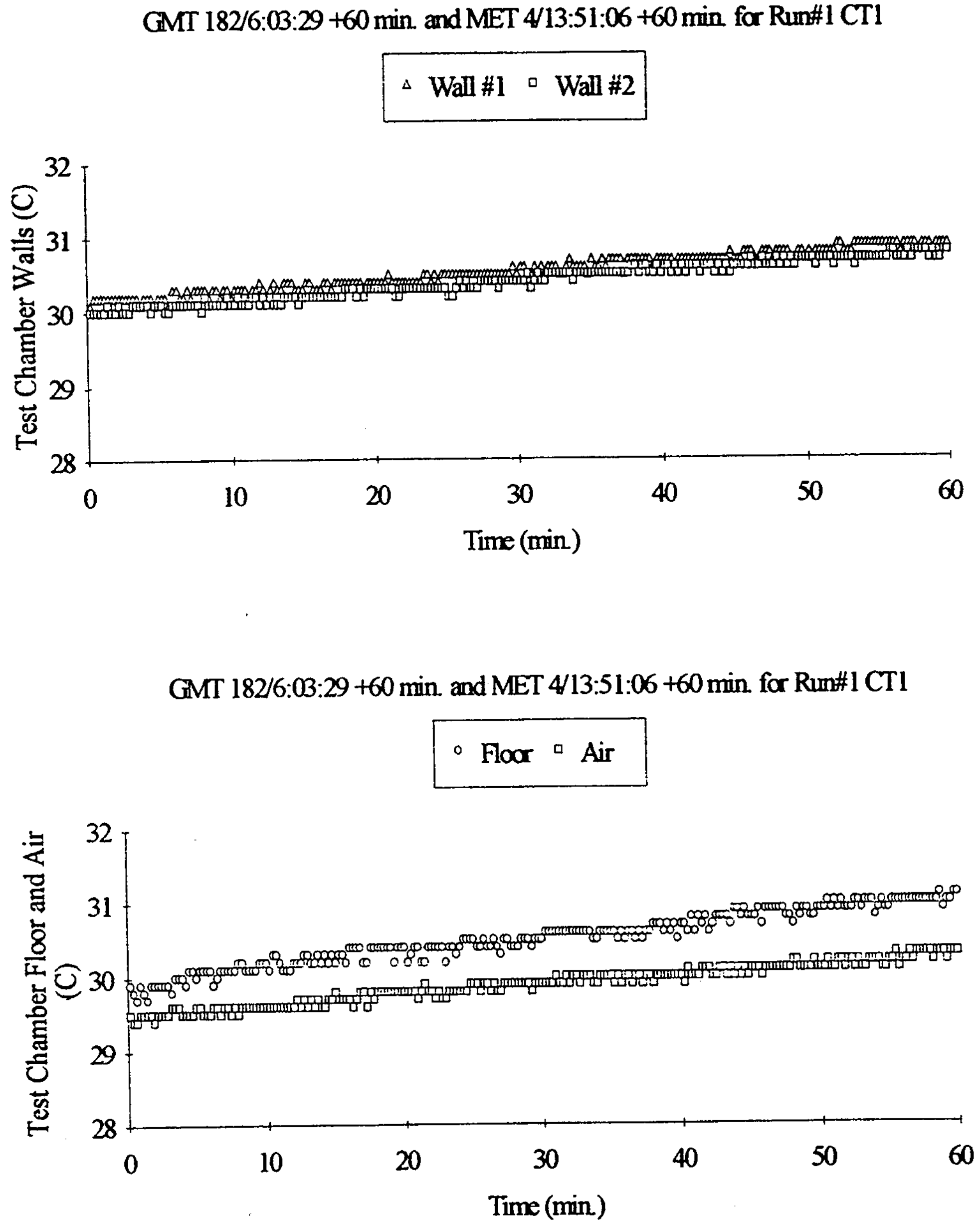

Figure B2 Thermistor data

Isotherms for Run#1 CT1 at 2 min.

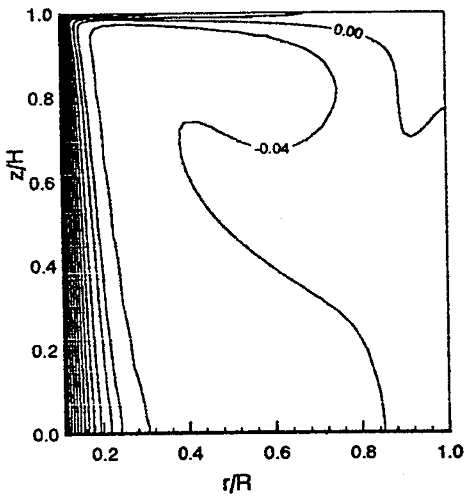

Streamlines for Run#1 CT1 at 2 min.

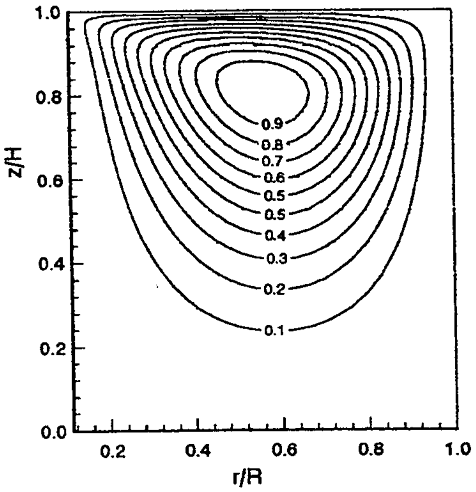

Figure B3 Computed isotherms and streamlines at t = 2 min.

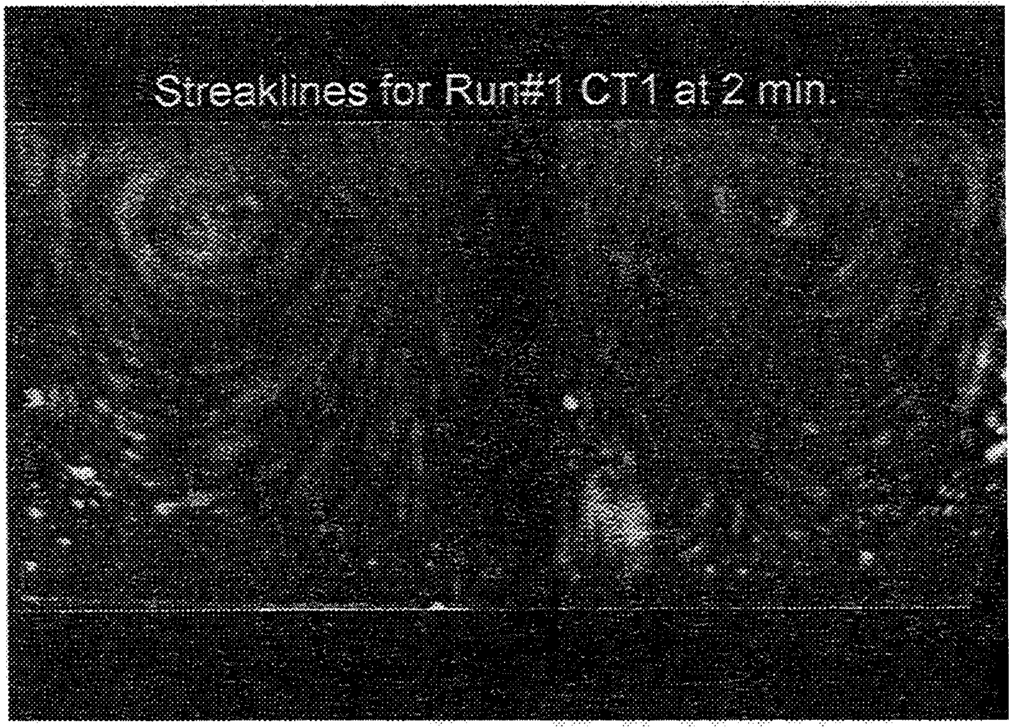

Figure B4 Experimental pathlines

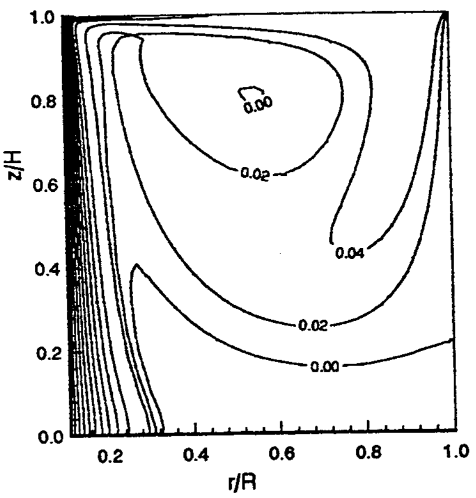

Isotherms for Run#1 CT1 at 10 min.

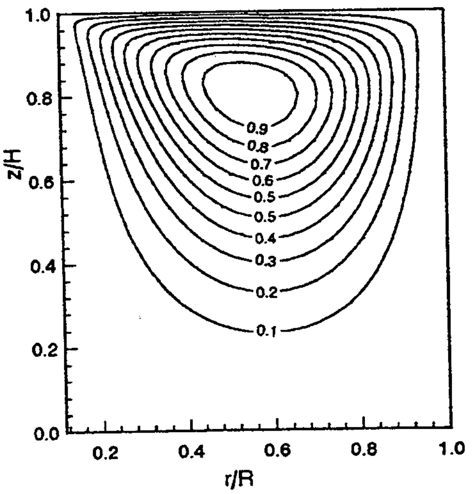

Streamlines for Run#1 CT1 at 10 min,

Figure B5 Computed isotherms and streamlines at t = 10 min.

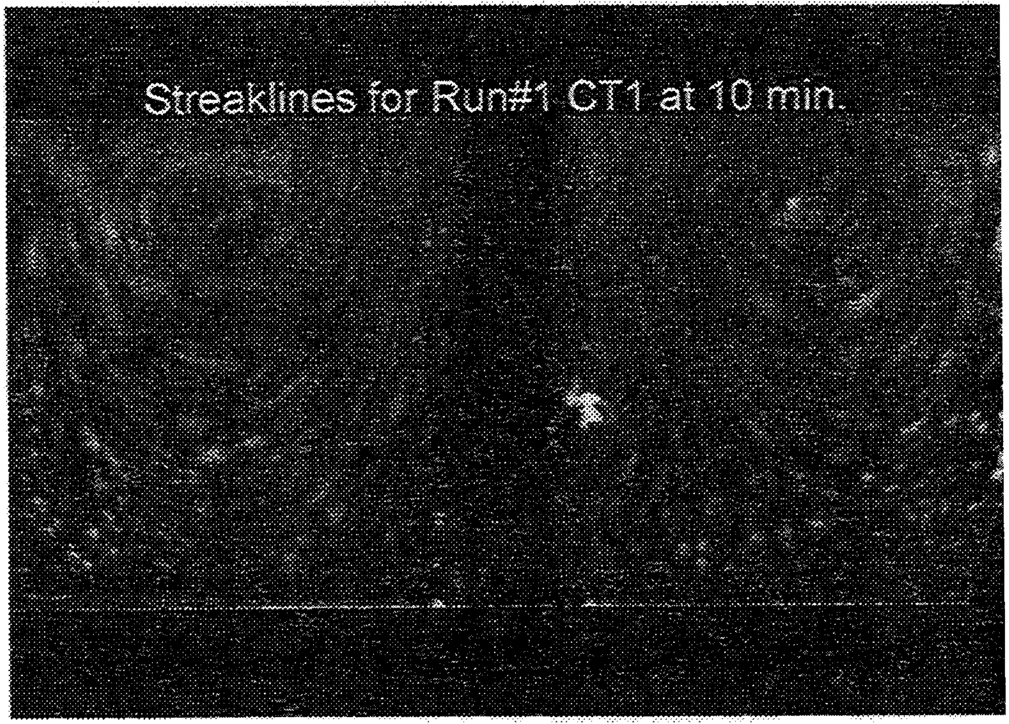

Figure B6 Experimental pathlines

Streamlines for Run#1 CT1 at 60 min.

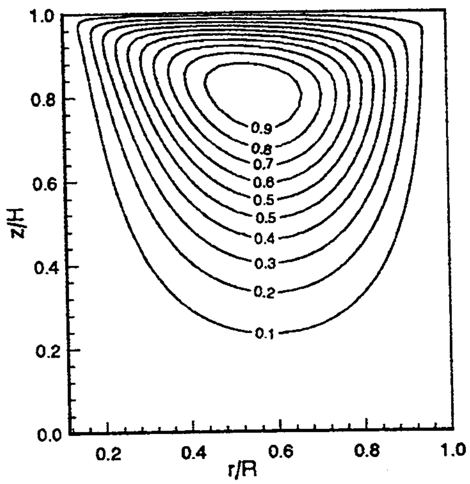

Isotherms for Run#1 CT1 at 60 min.

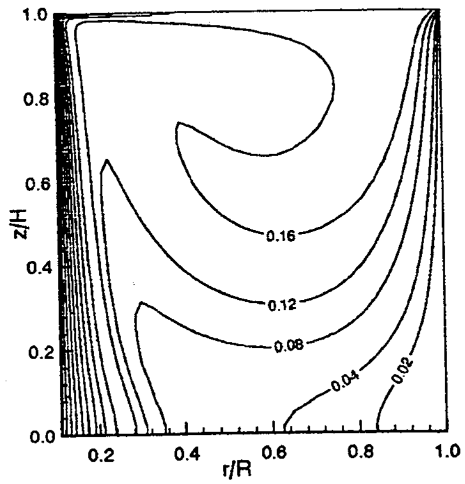

Figure B7 Computed streamlines and isotherms at t = 60 min.

Velocity Vectors for Run#1 CT1 at 10 min.

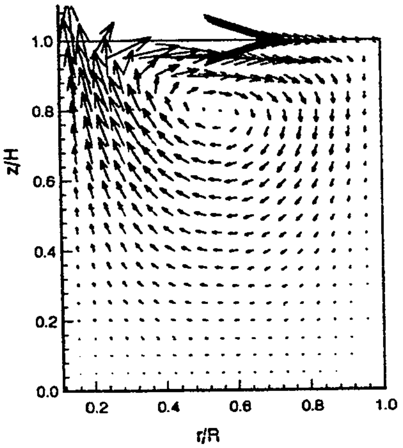

Experimental Velocity Vectors for Run#1 Test CT1 at 10 min.

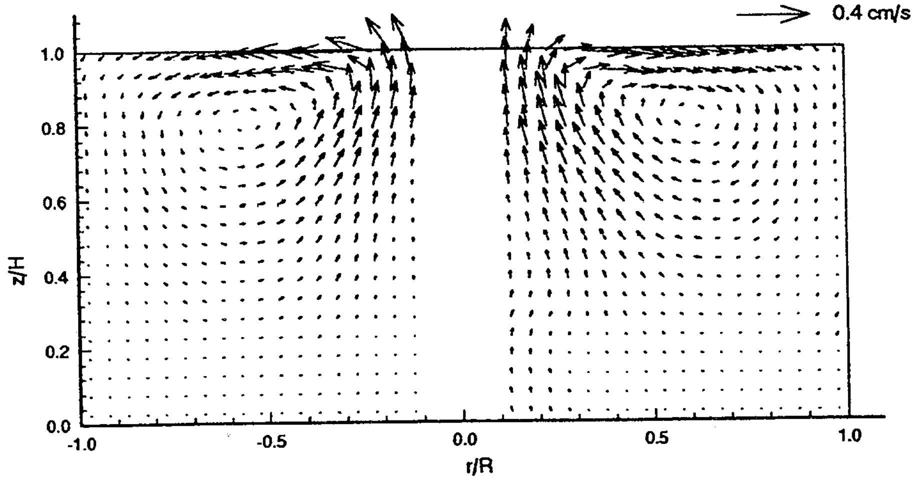

Figure B8 Computed and measured velocity vectors at t = 10 min.

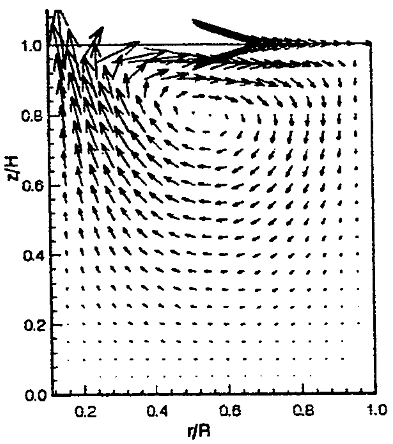

Velocity Vectors for Run#1 CT1 at 20 min.

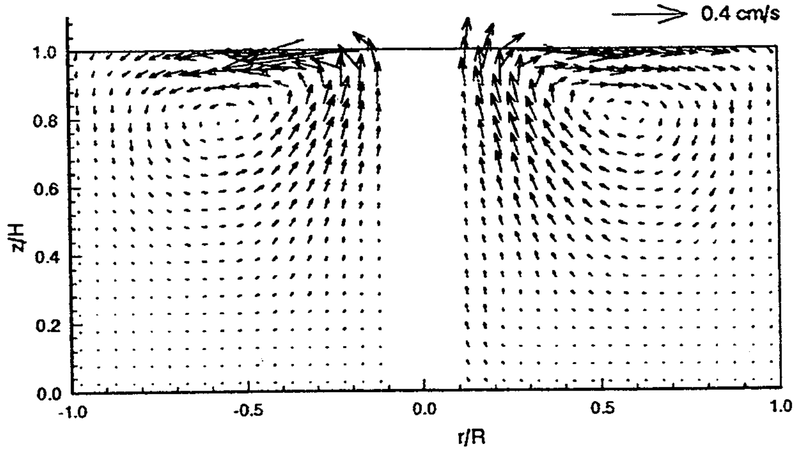

Experimental Velocity Vectors for Run#1 Test CT1 at 20 min.

Figure B9 Computed and measured velocity vectors at t = 20 min.

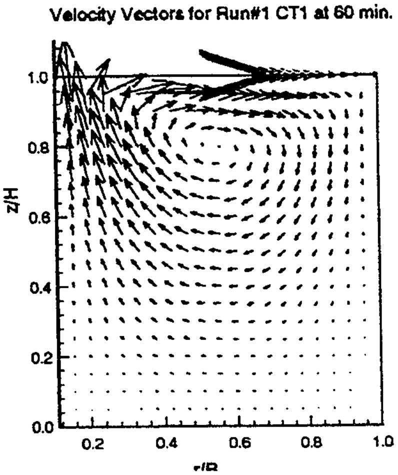

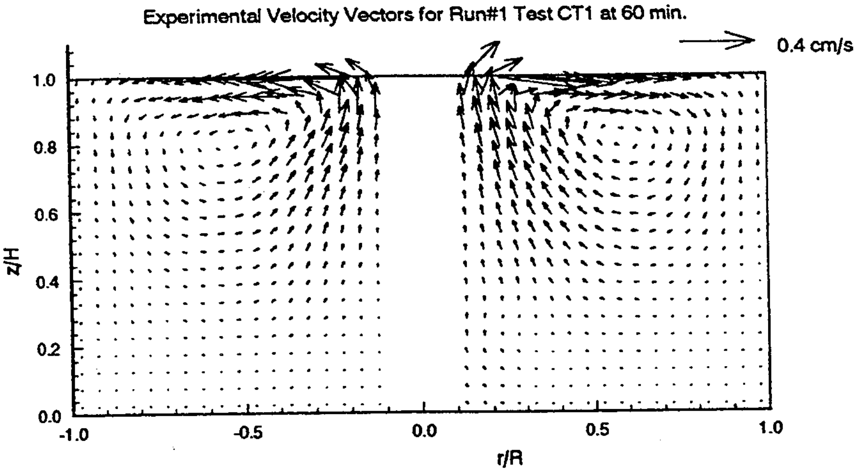

Figure B10 Computed and measured velocity vectors at t = 60 min.

GMT 182/6:03:29 and MET 4/13:51:06 for Run#1 CT1

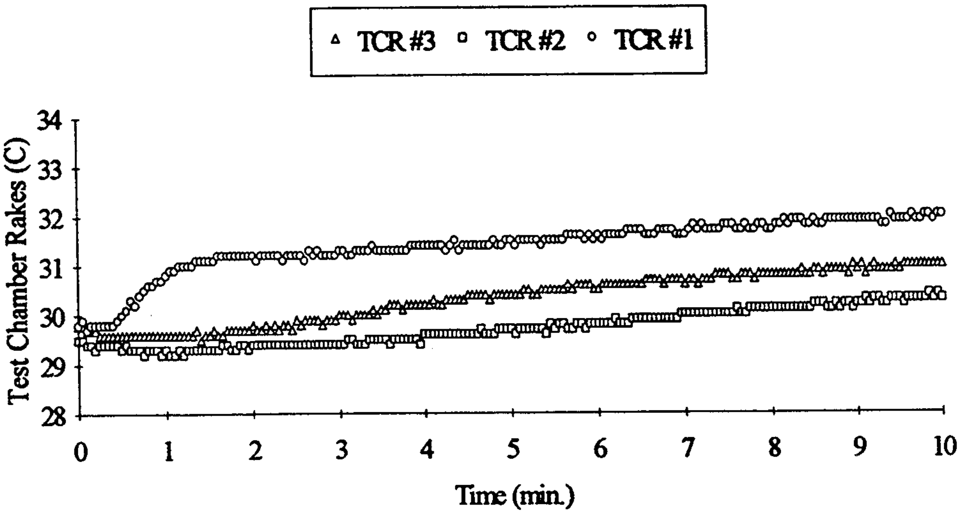

Numerical Data (lines) and Experimental Data (symbols)

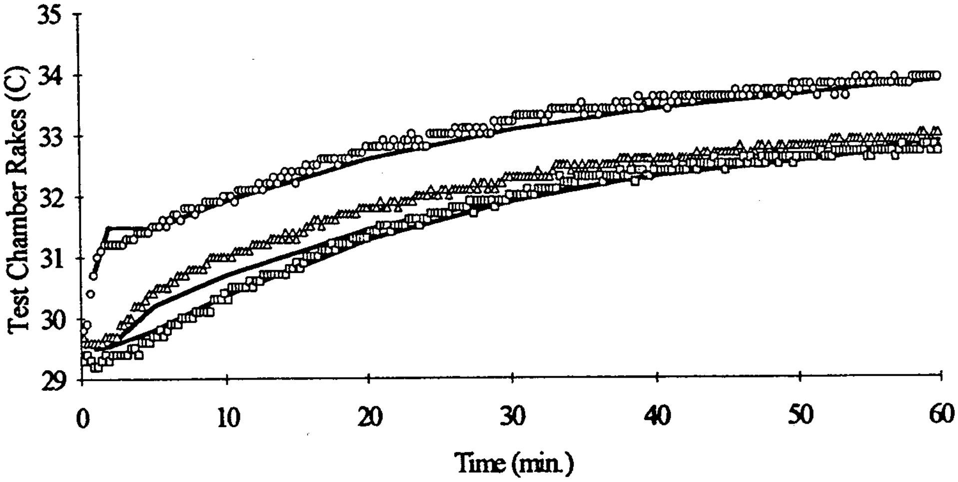

Figure B11 Measured and computed fluid temperature variations

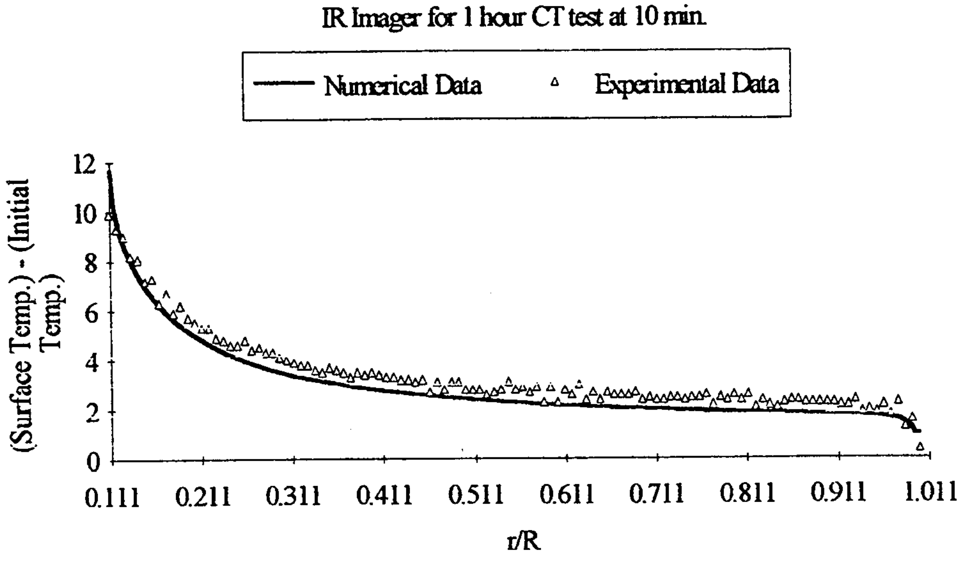

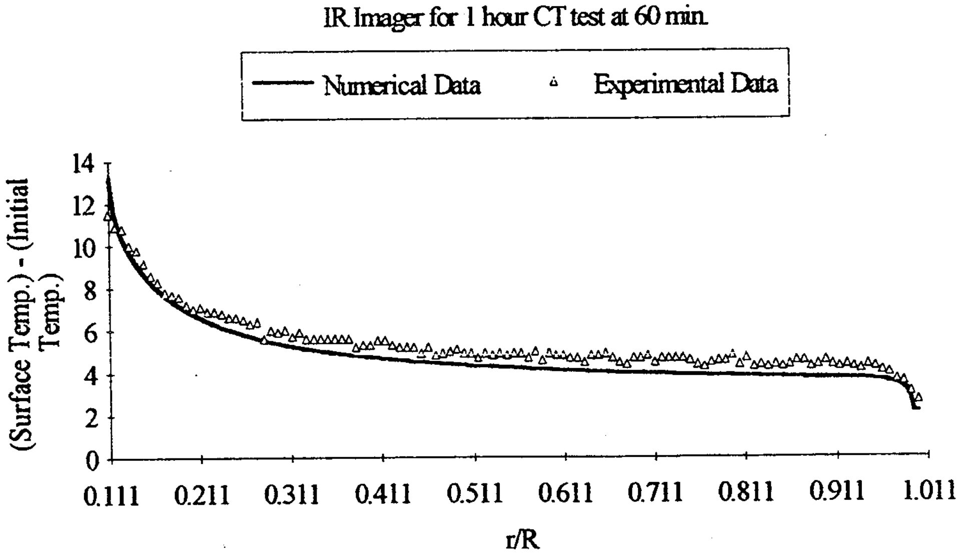

Figure B12 IR Imager data and computed results

APPENDIX C

CF FLAT SHORTER TESTS

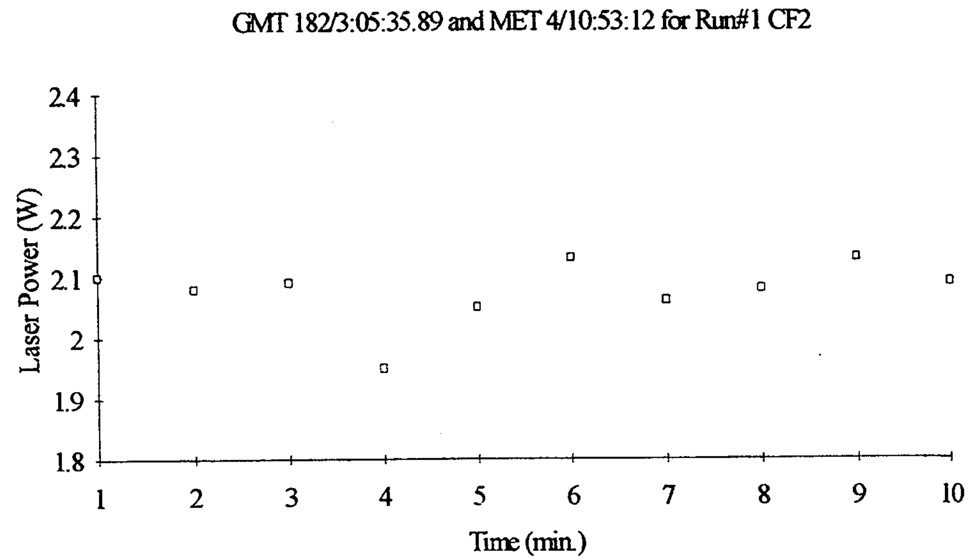

Figure C1 Laser power

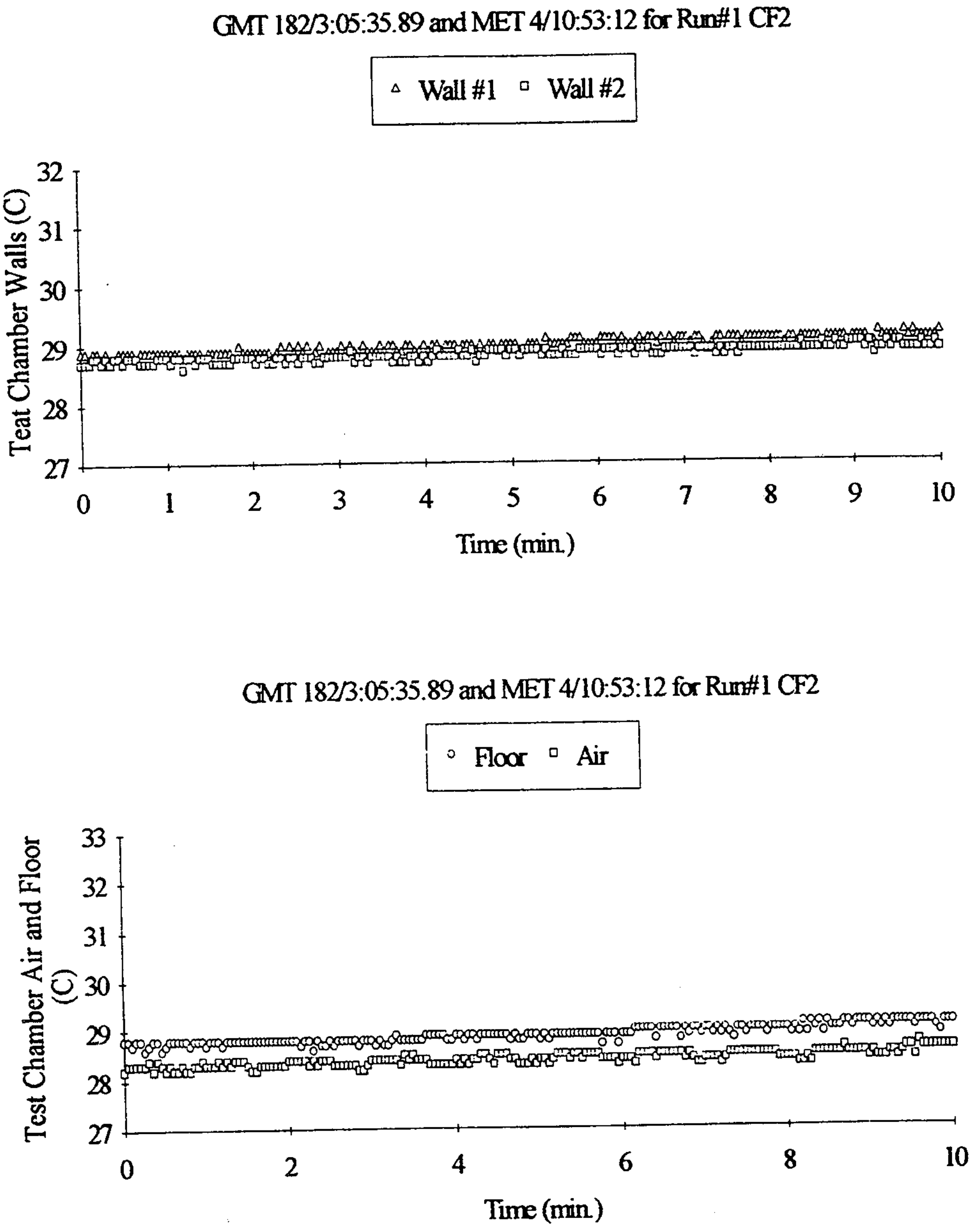

Figure C2 Thermistor data

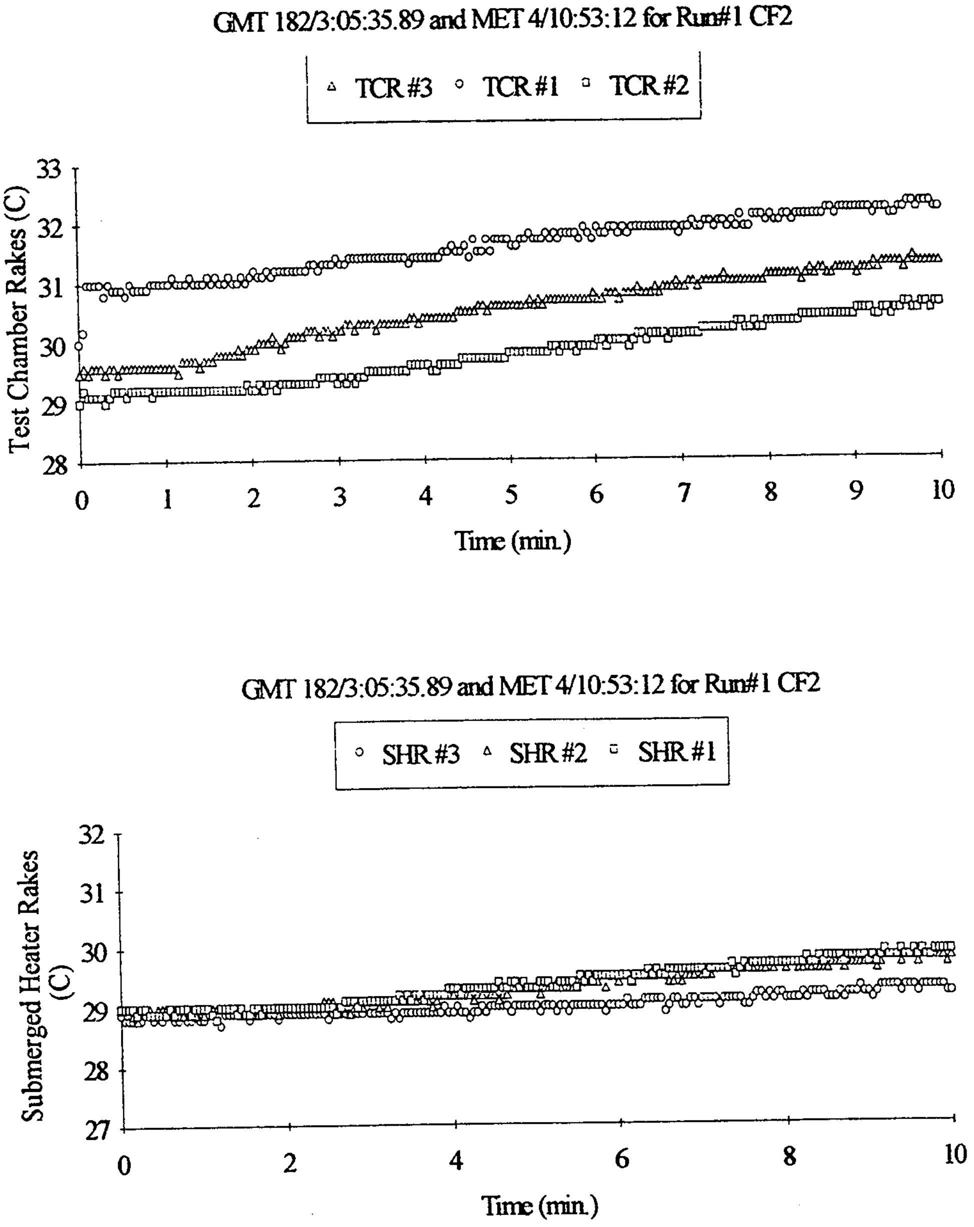

Figure C3 Thermistor data

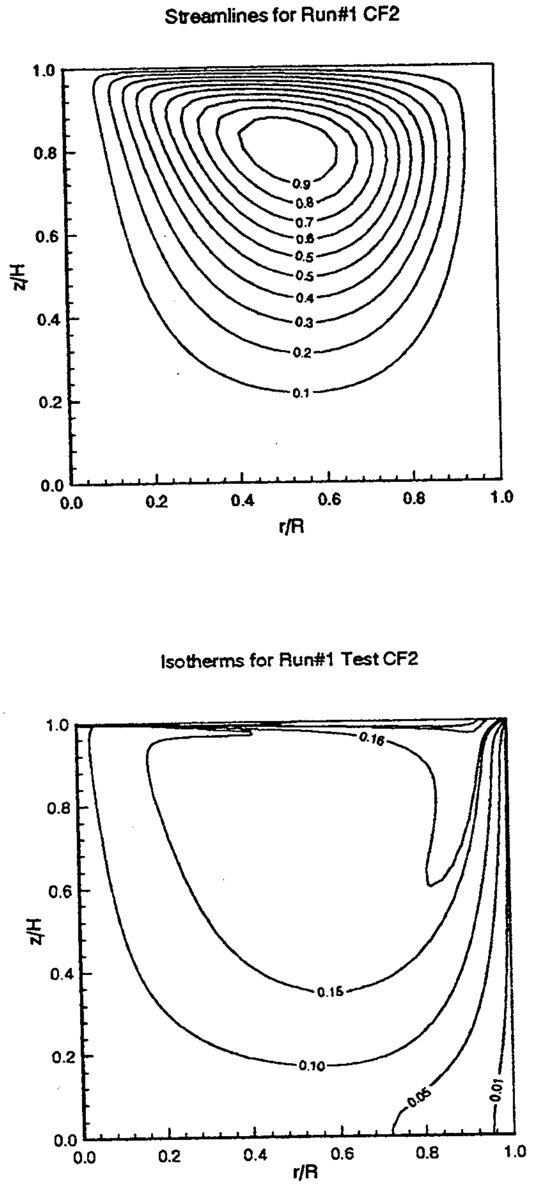

Figure C4 Computed streamlines and isotherms

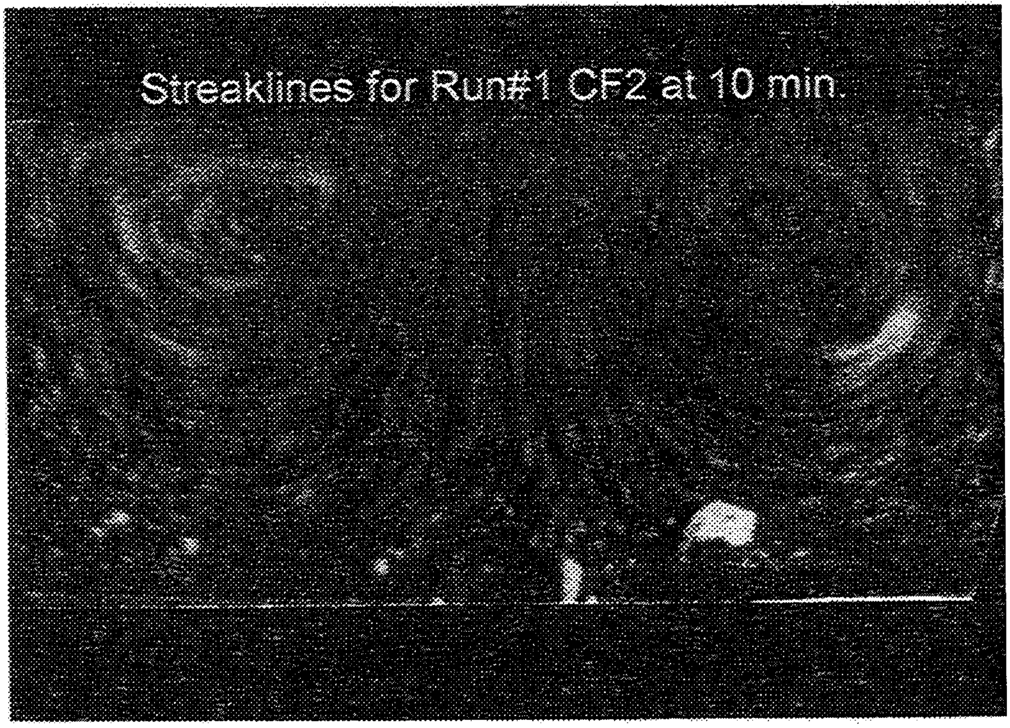

Figure C5 Experimental pathlines

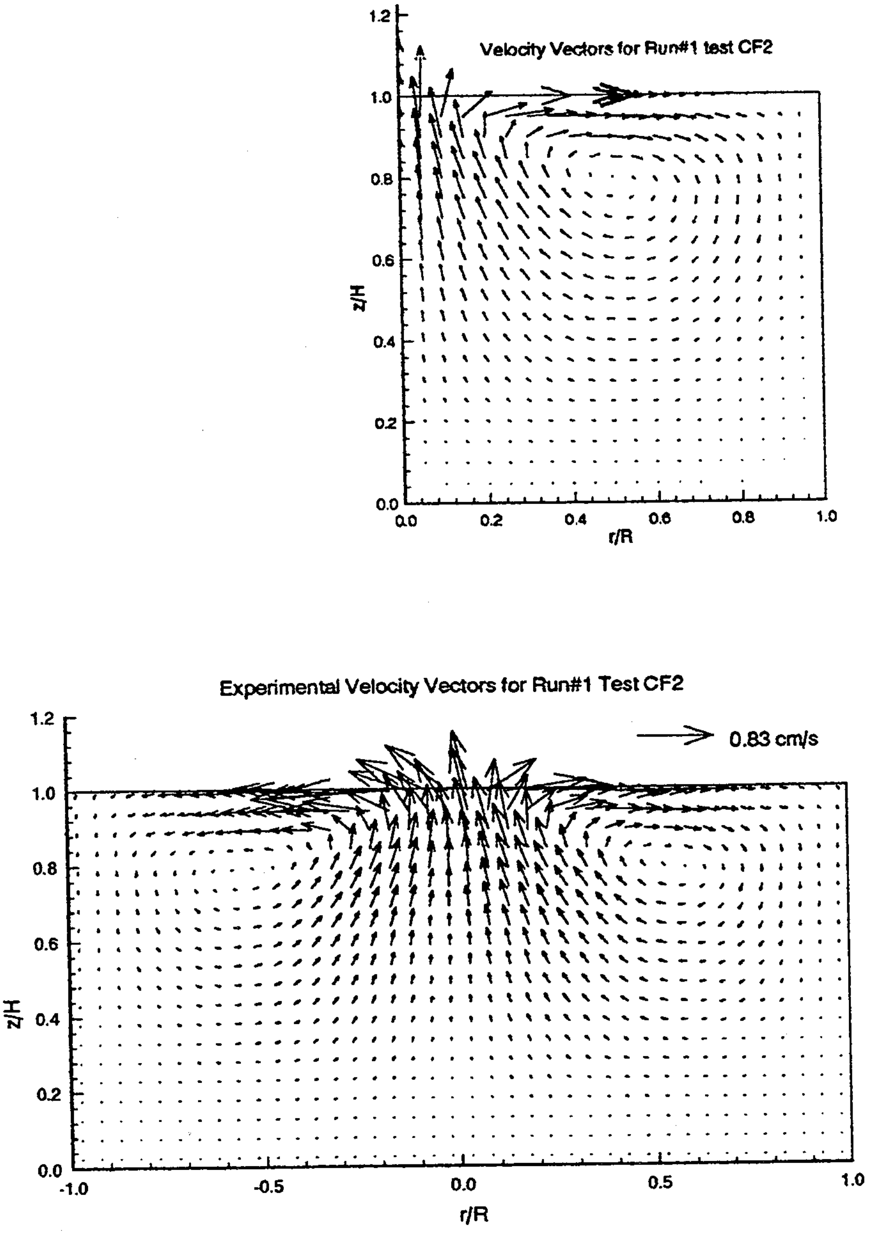

Figure C6 Computed and measured velocity vectors

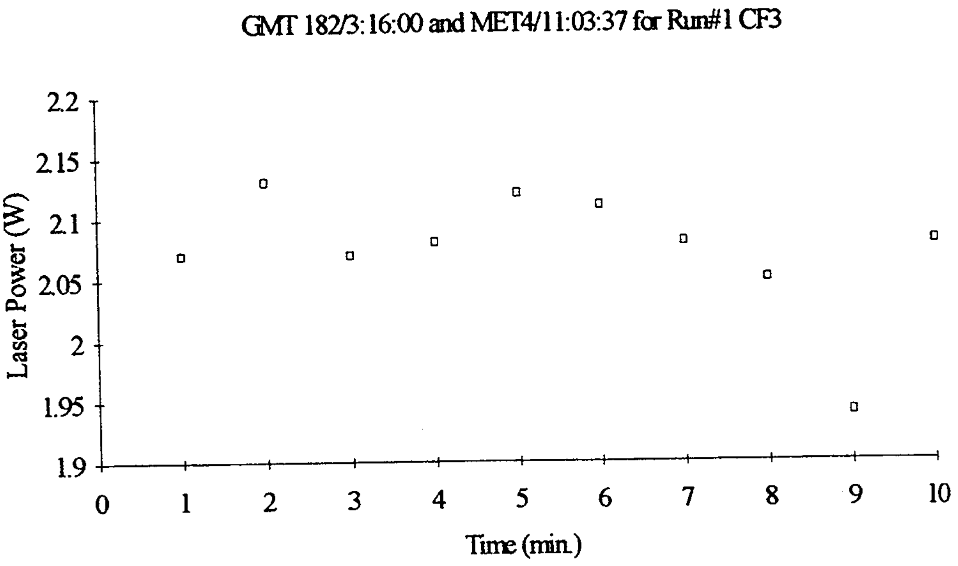

Figure C7 Laser power

GMT 182/3:16:00.16 and MET 4/11:03:37 for Run#1 CF3

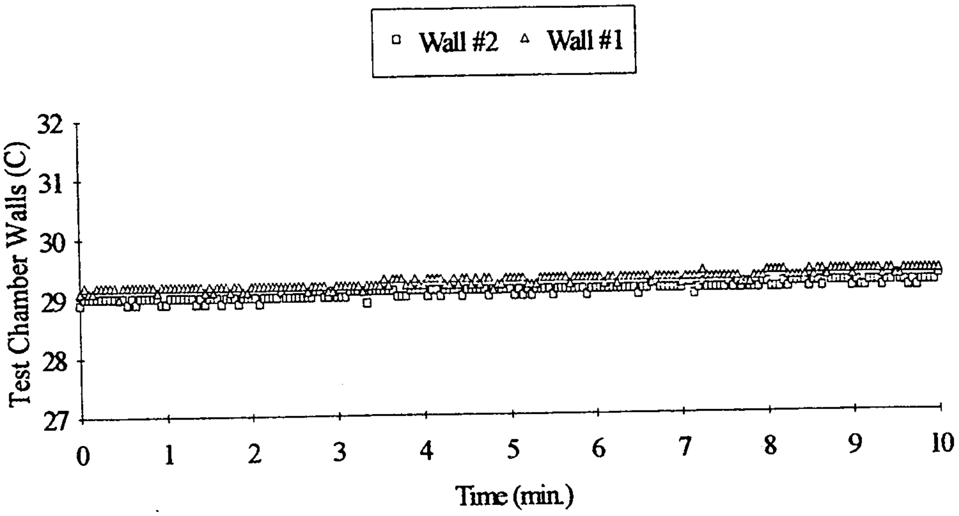

GMT 182/3:16:00.16 and MET 4/11:03:37for Run#1 CF3

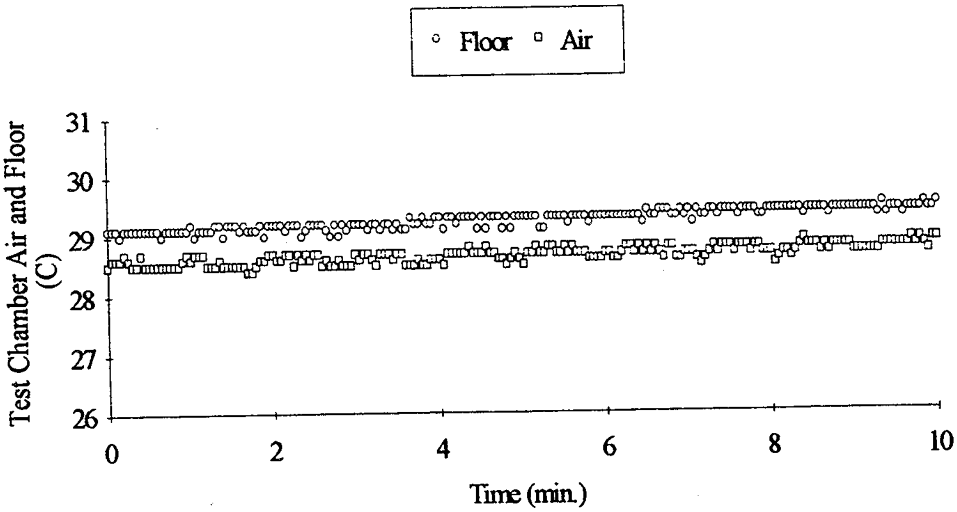

Figure C8 Thermistor data

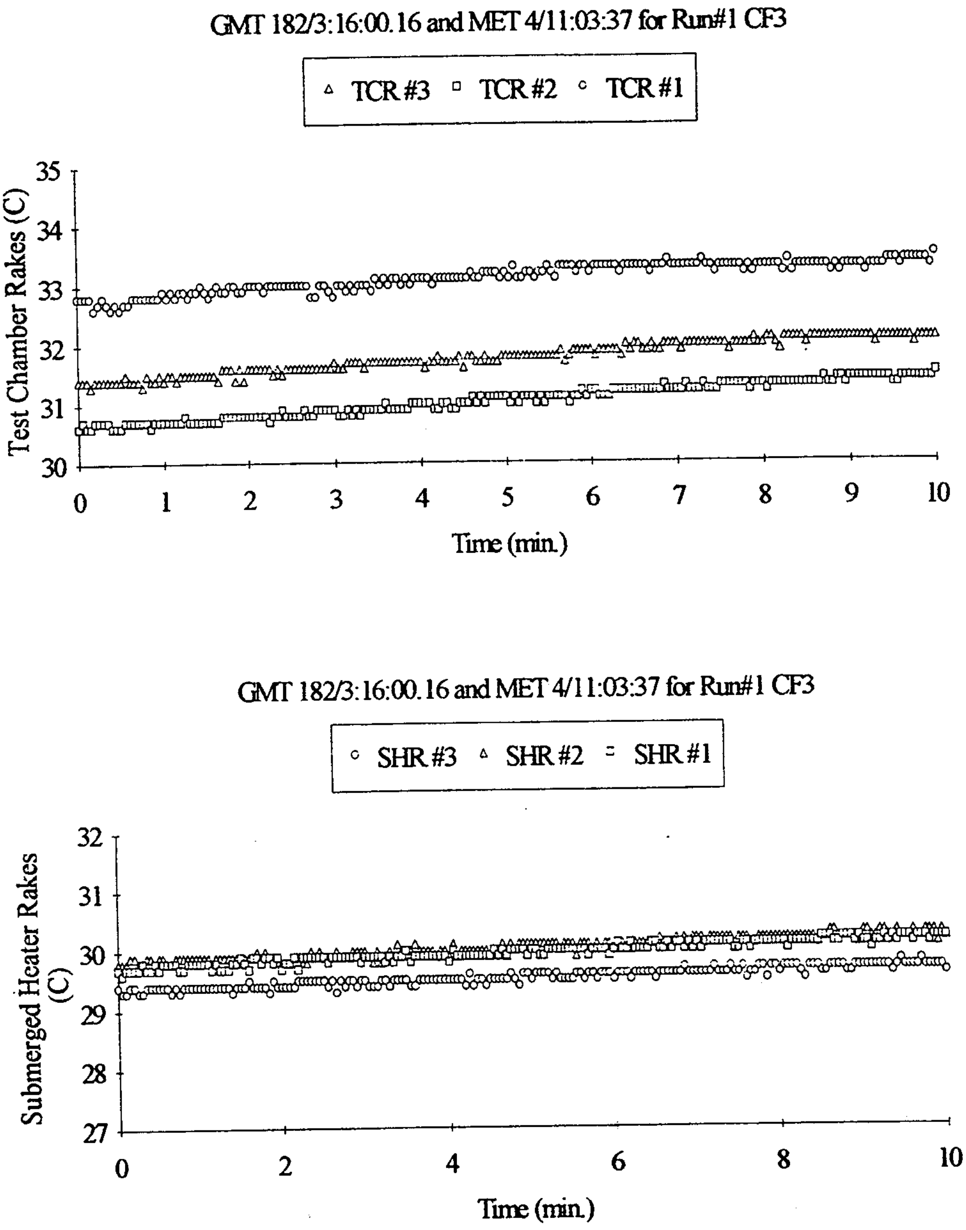

Figure C9 Thermistor data

Streamlines for Run#1 Test CF3

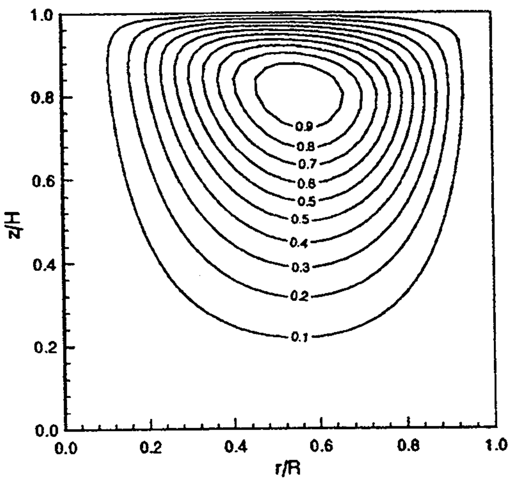

Isotherms for Run#1 Test CF3

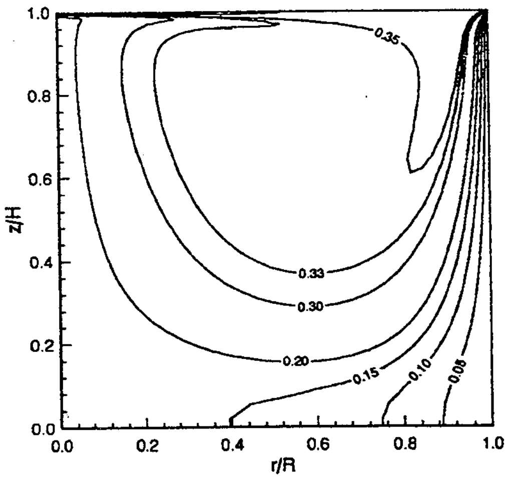

Figure C10 Computed streamlines and isotherms

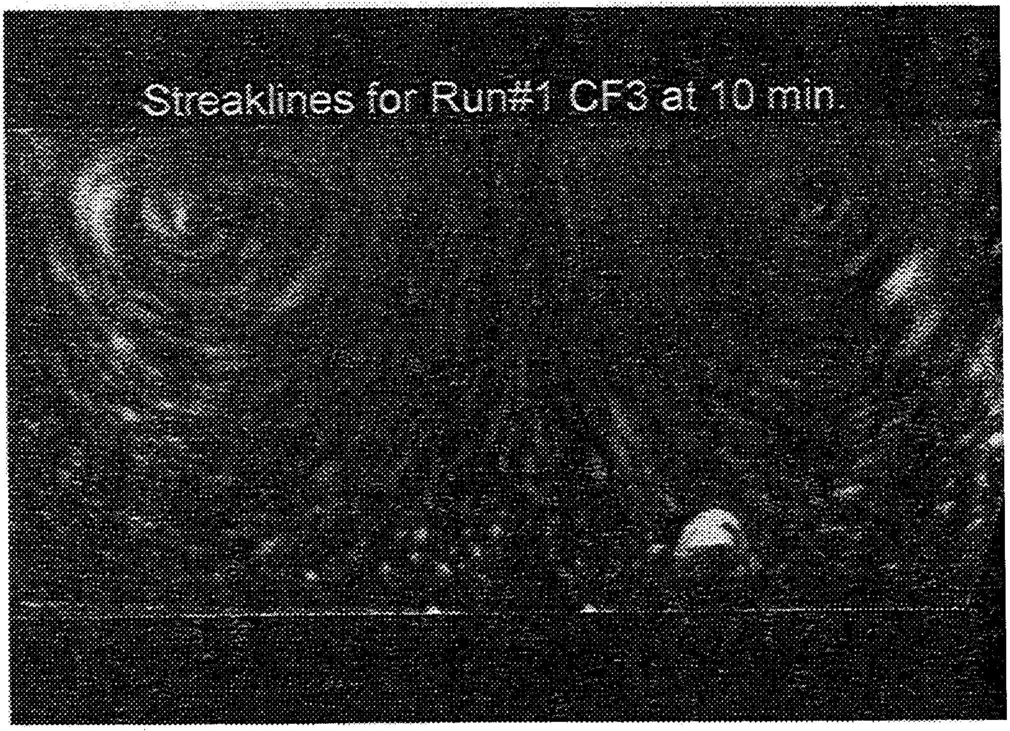

Figure C11 Experimental pathlines

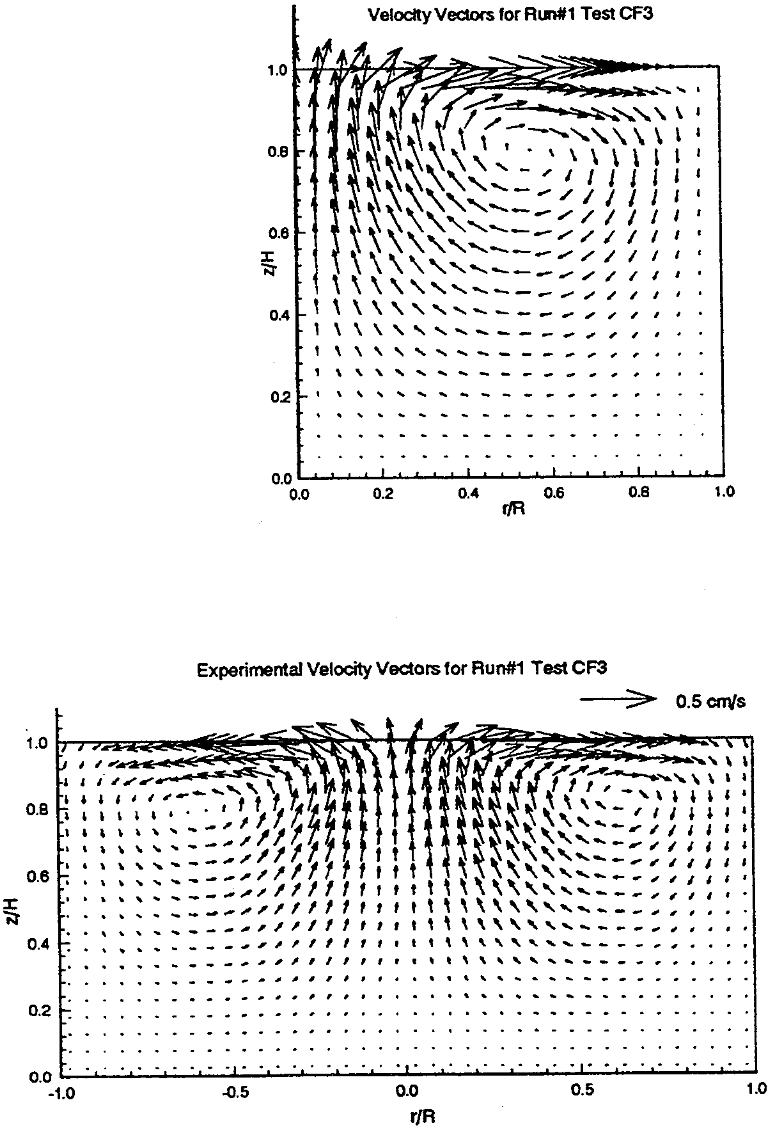

Figure C12 Computed and measured velocity vectors

GMT 182/3:26:26 and MET 4/11:14:03 for Run#1 CF4

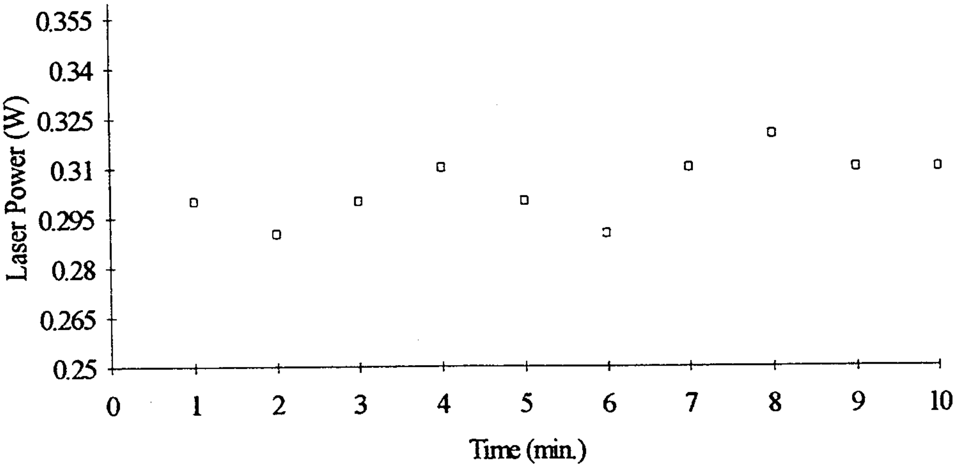

Figure C13 Laser power

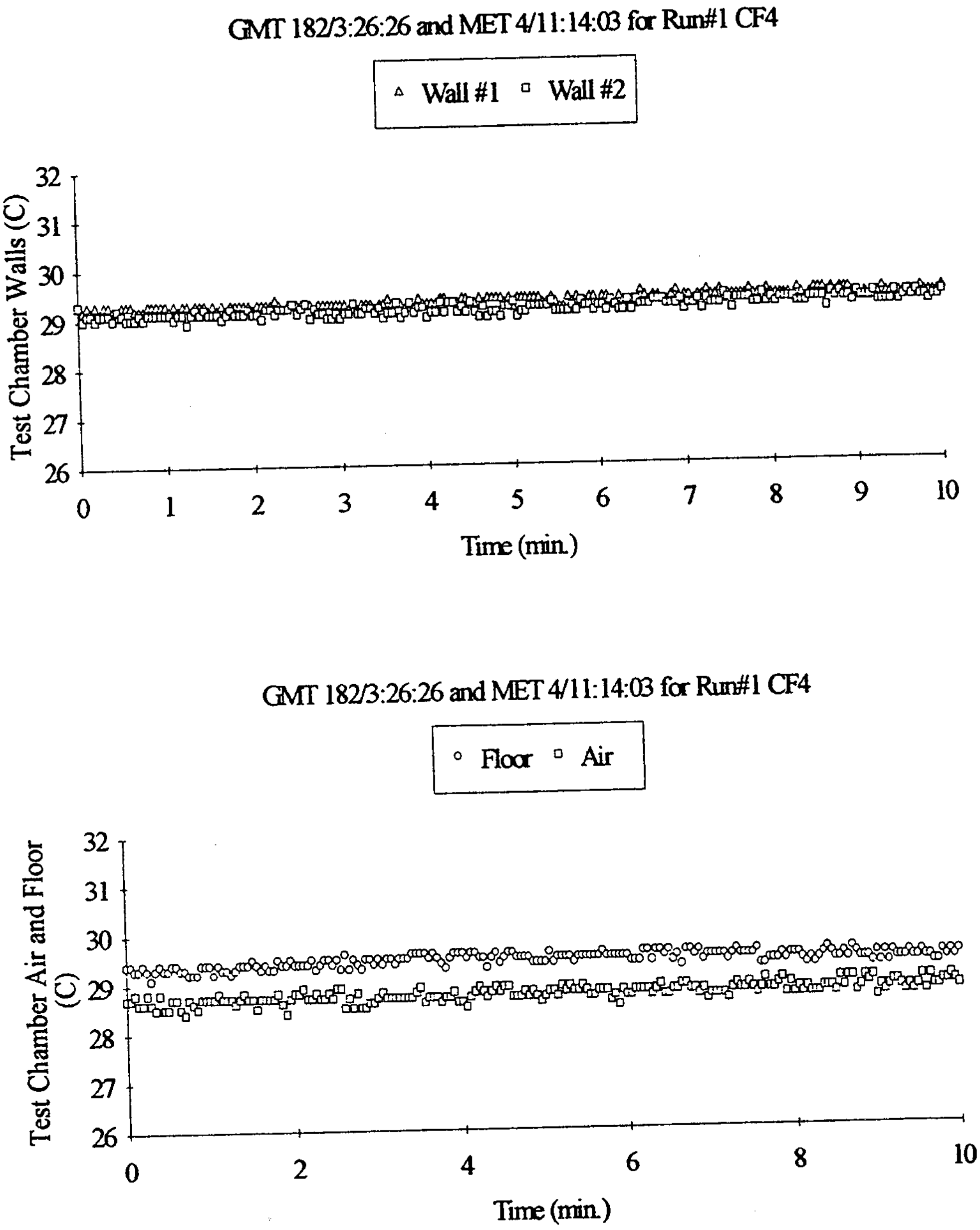

Figure C14 Thermistor data

Streamlines for Run#1 Test CF4

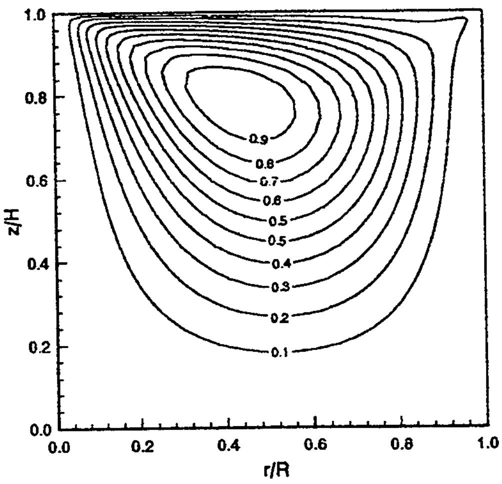

Isotherms for Run#1 Test CF4

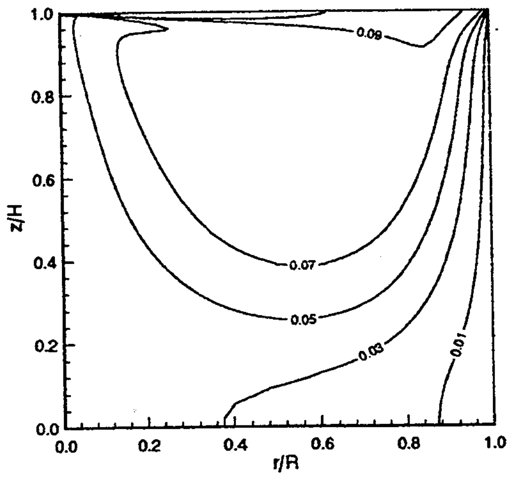

Figure C16 Computed streamlines and isotherms

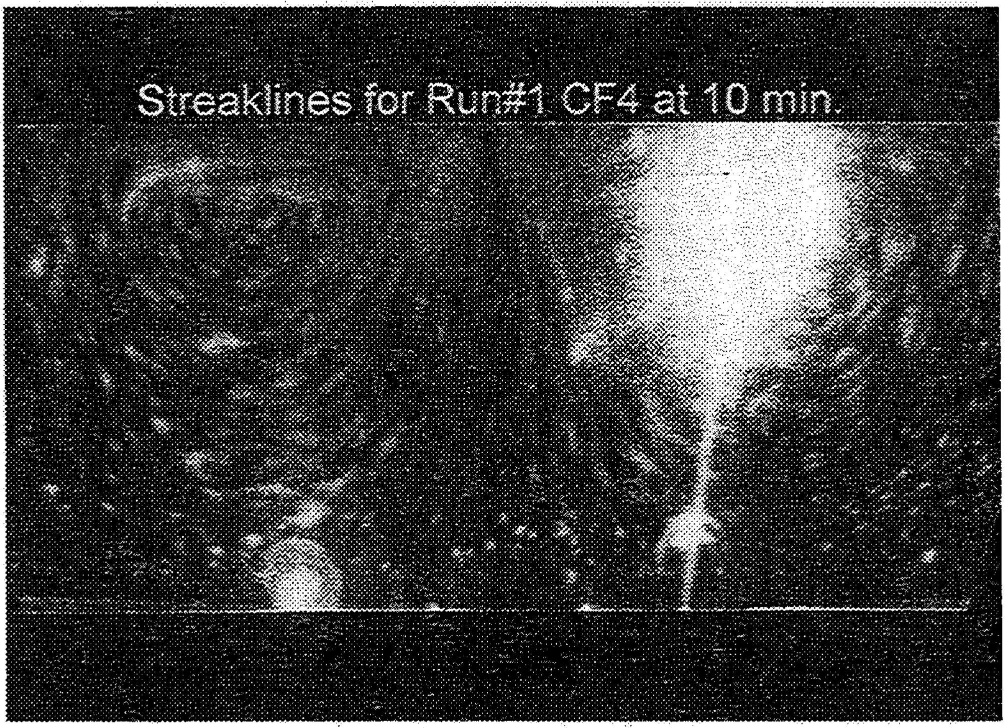

Figure C17 Experimental pathlines

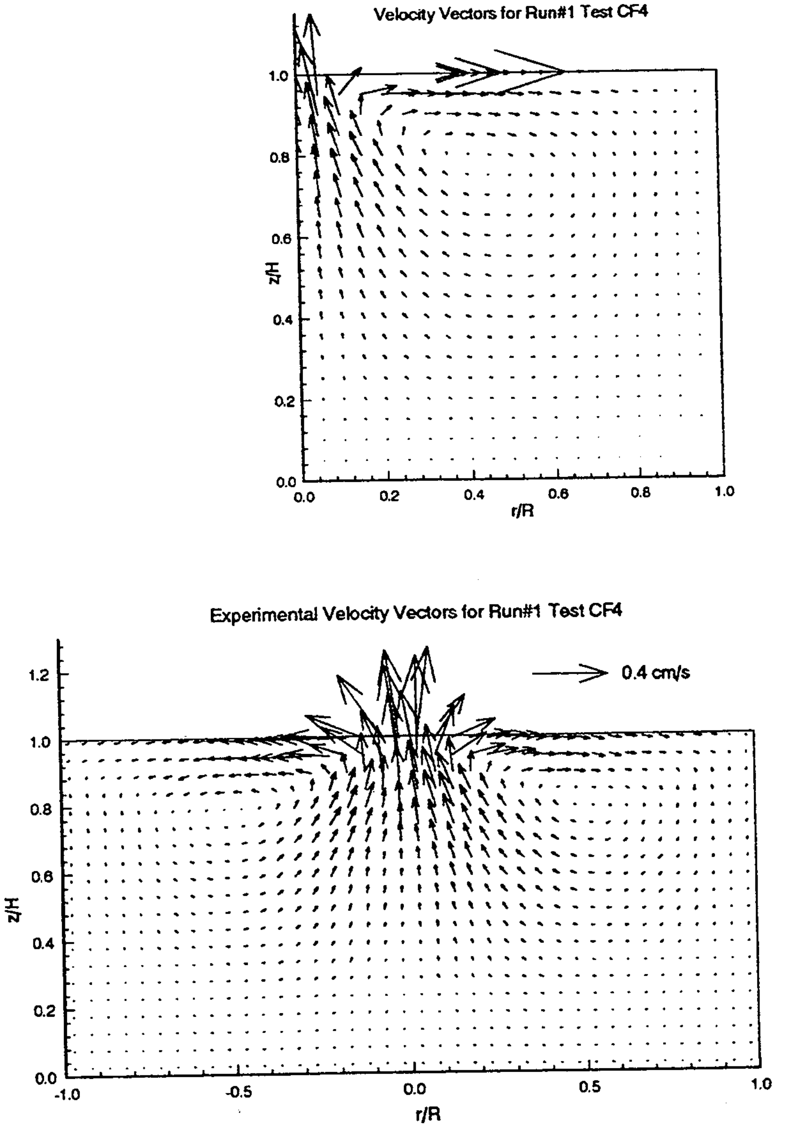

Figure C18 Computed and measured velocity vectors

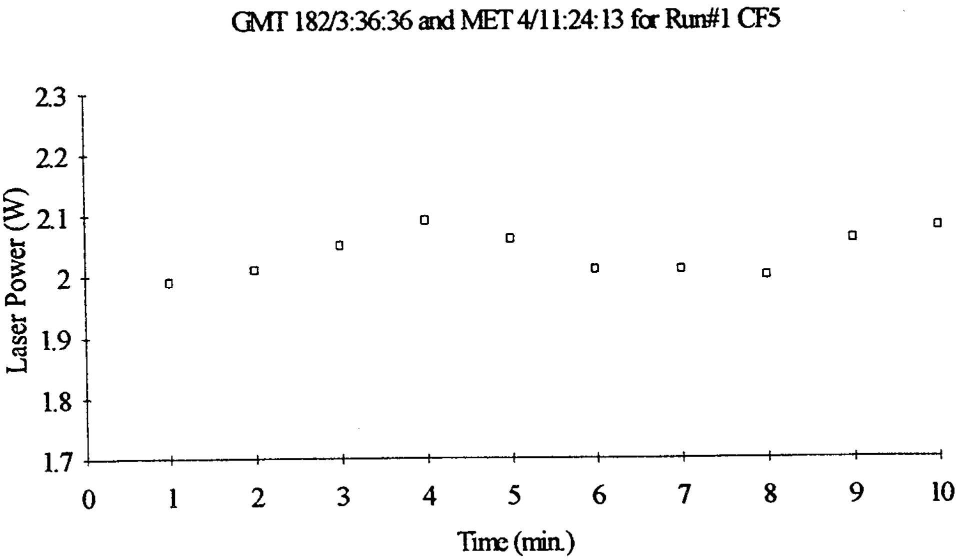

Figure C19 Laser power

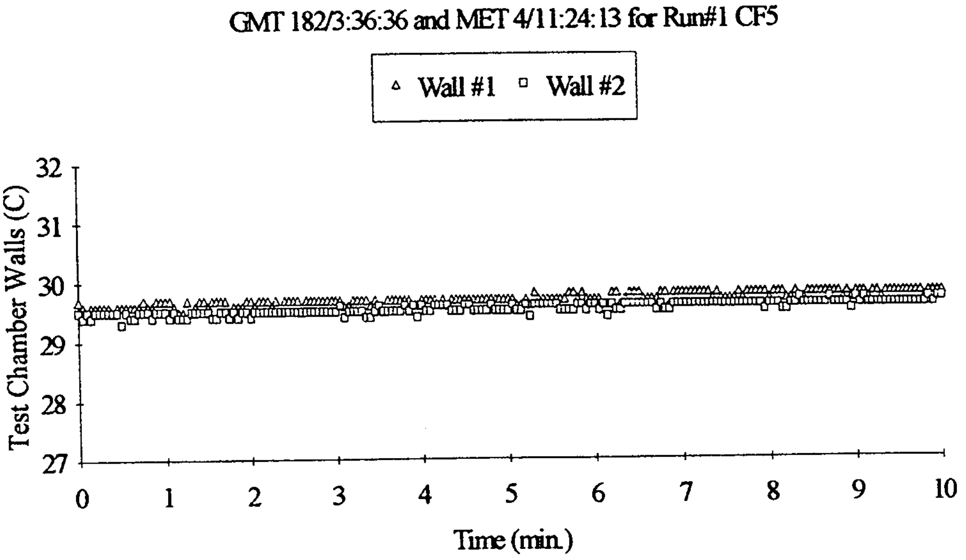

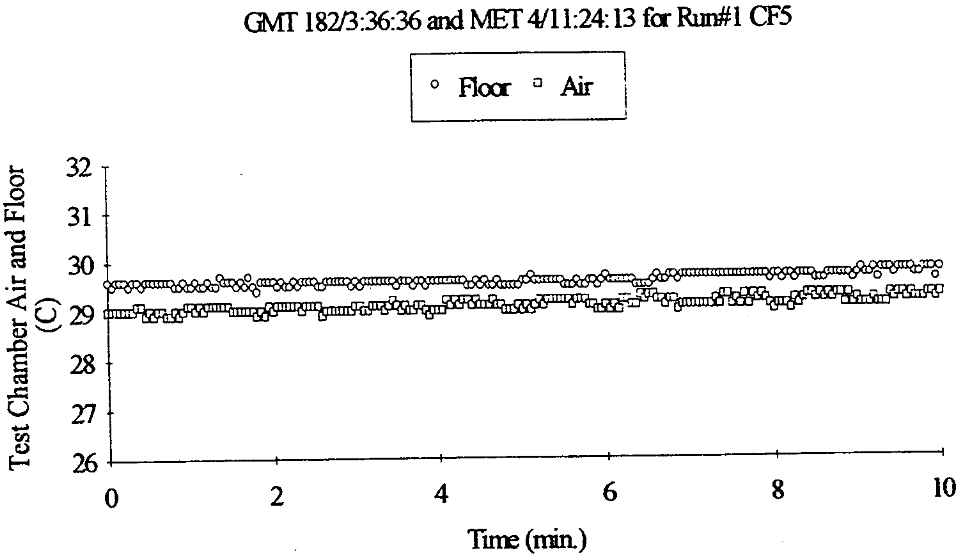

Figure C20 Thermistor data

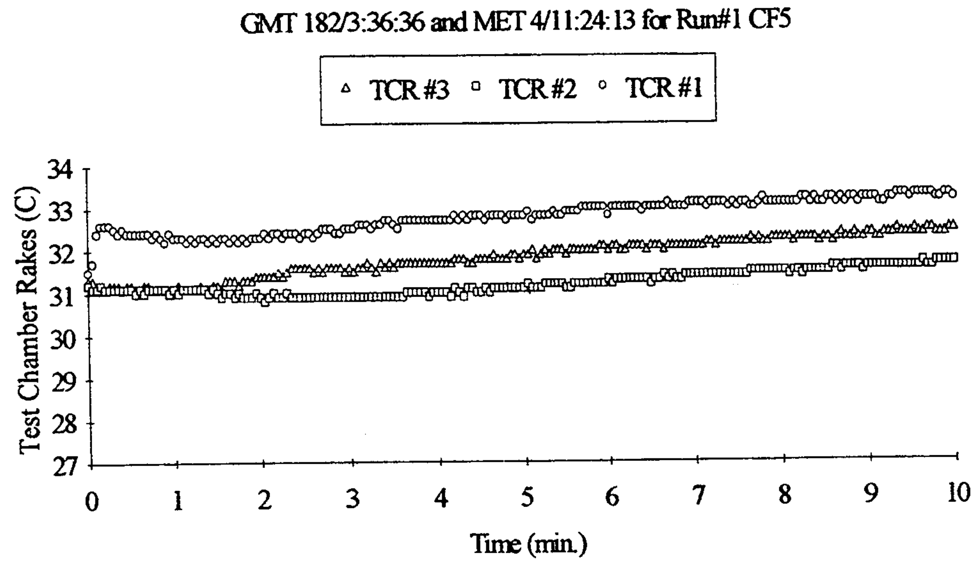

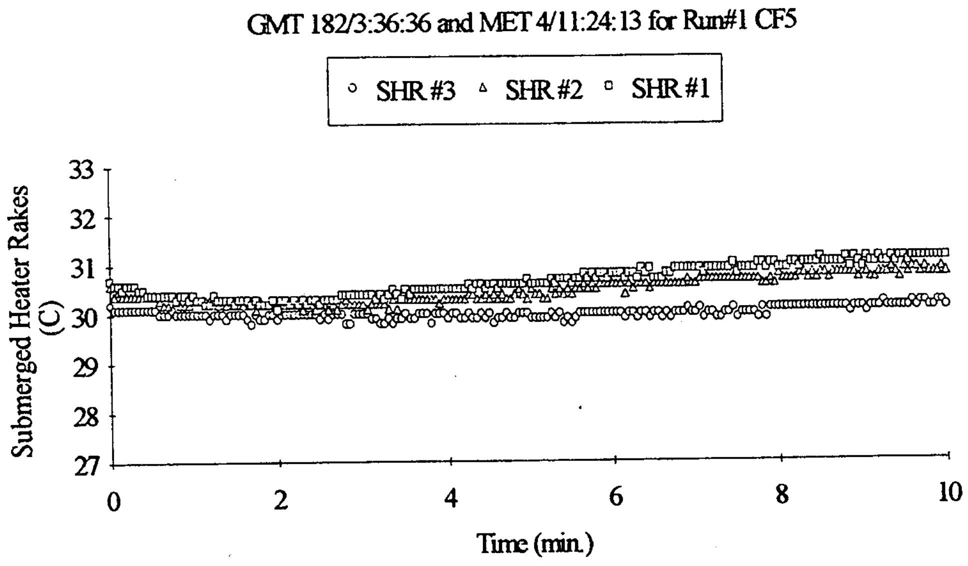

Figure C21 Thermistor data

Streamlines for Run#1 Test CF5

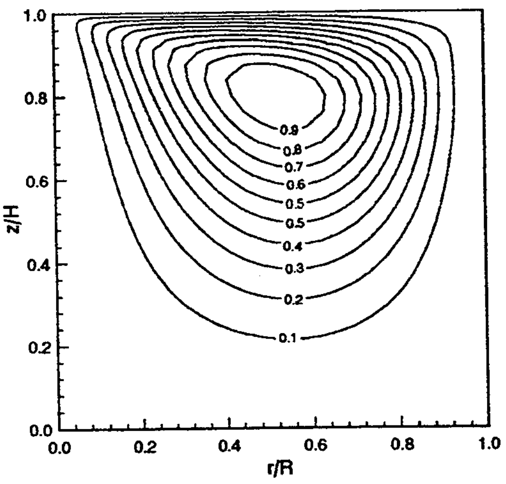

Isotherms for Run#1 Test CF5

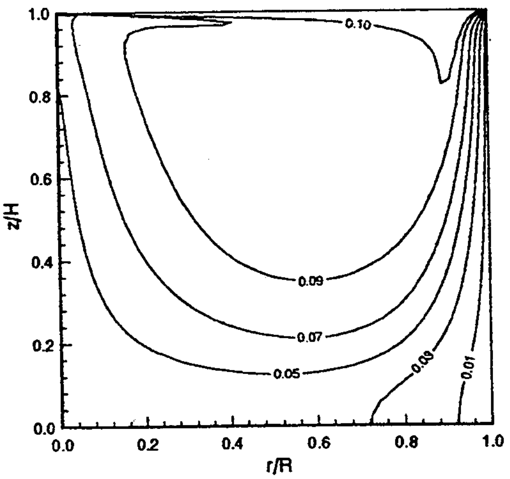

Figure C22 Computed streamlines and isotherms

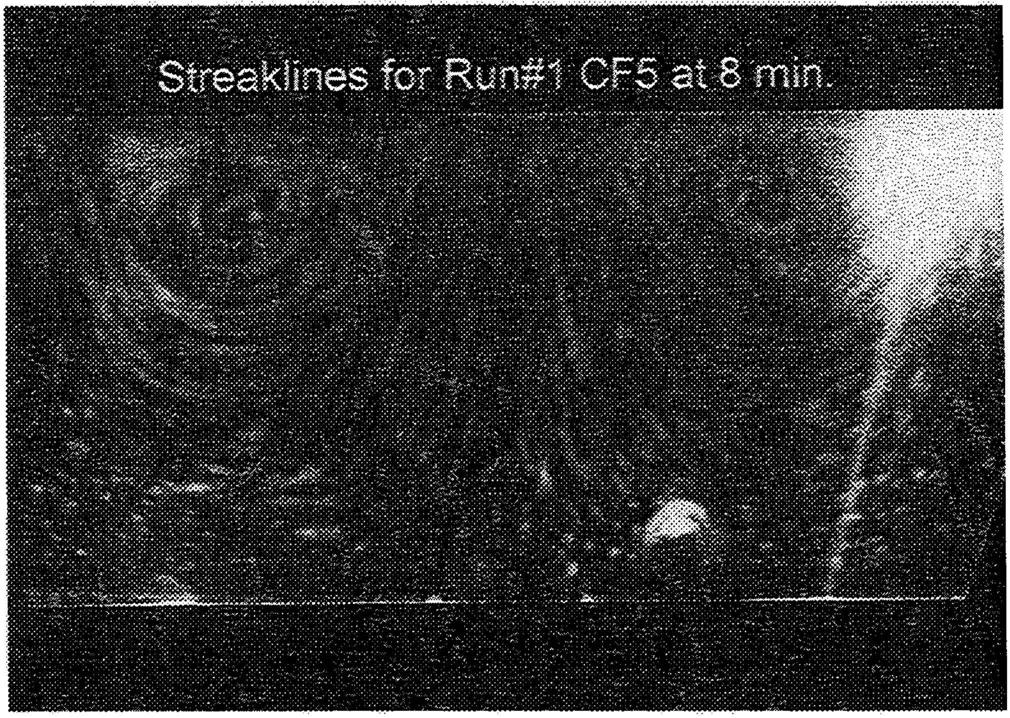

Figure C23 Experimental pathlines

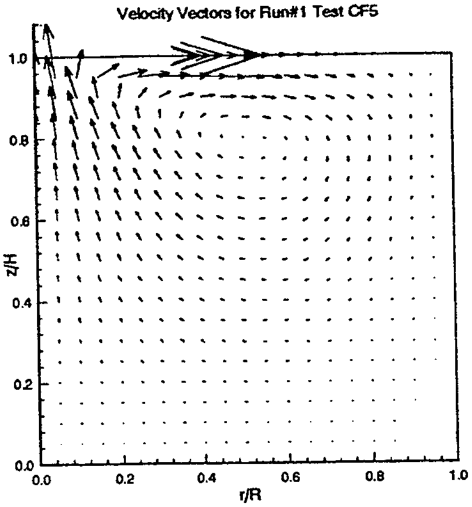

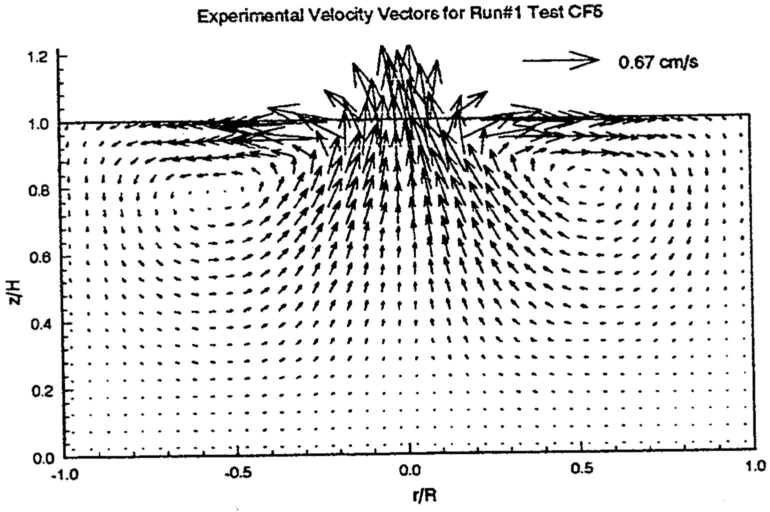

Figure C24 Computed and measured velocity vectors

GMT 184/1:05:30 +20 min. and MET 6/8:53:07 +20 min. for Run#2 CF1

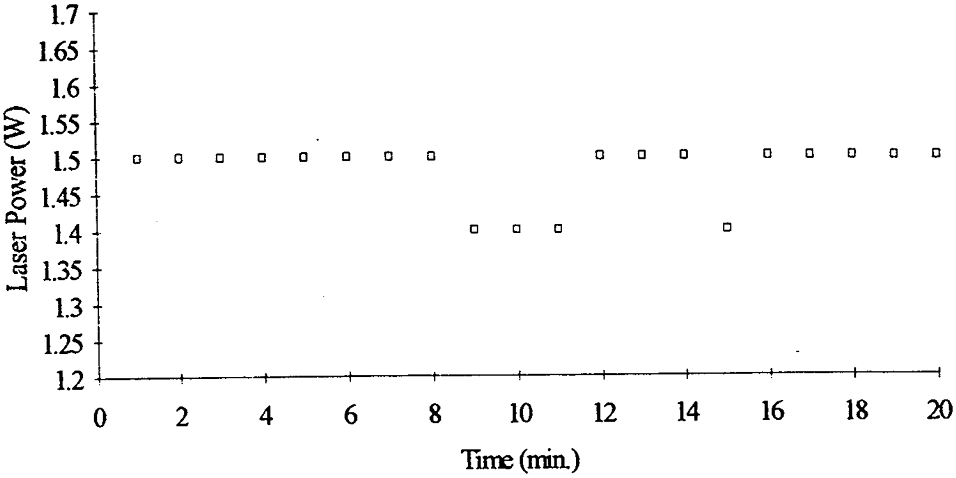

Figure C25 Laser power

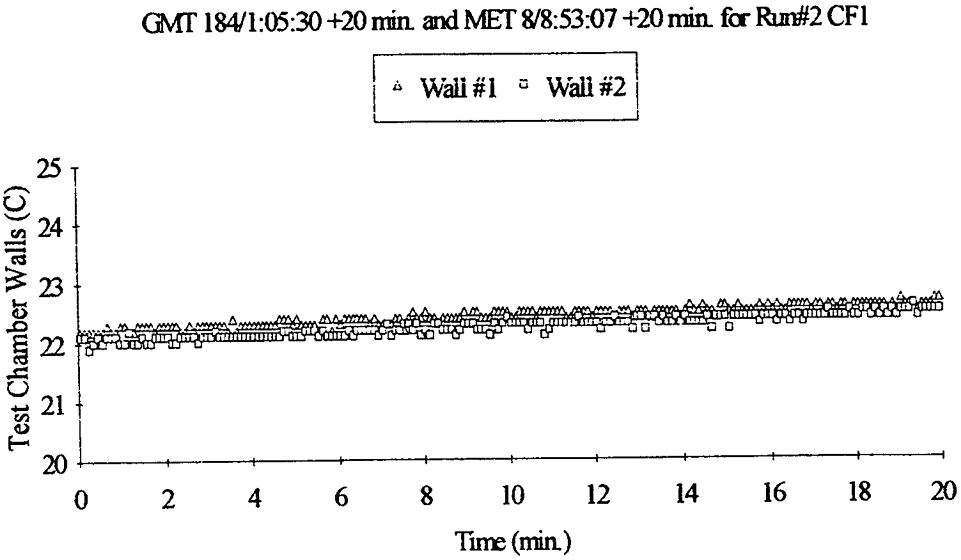

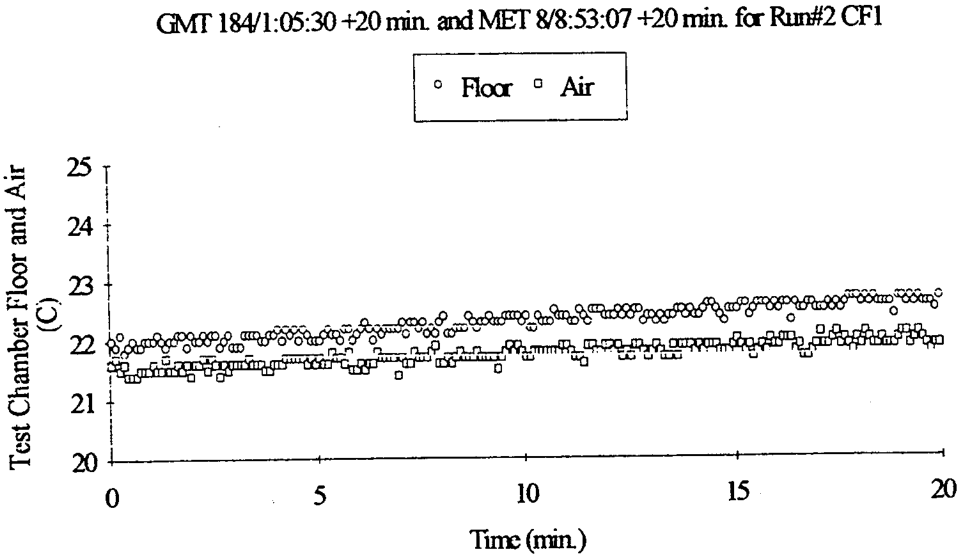

Figure C26 Thermistor data

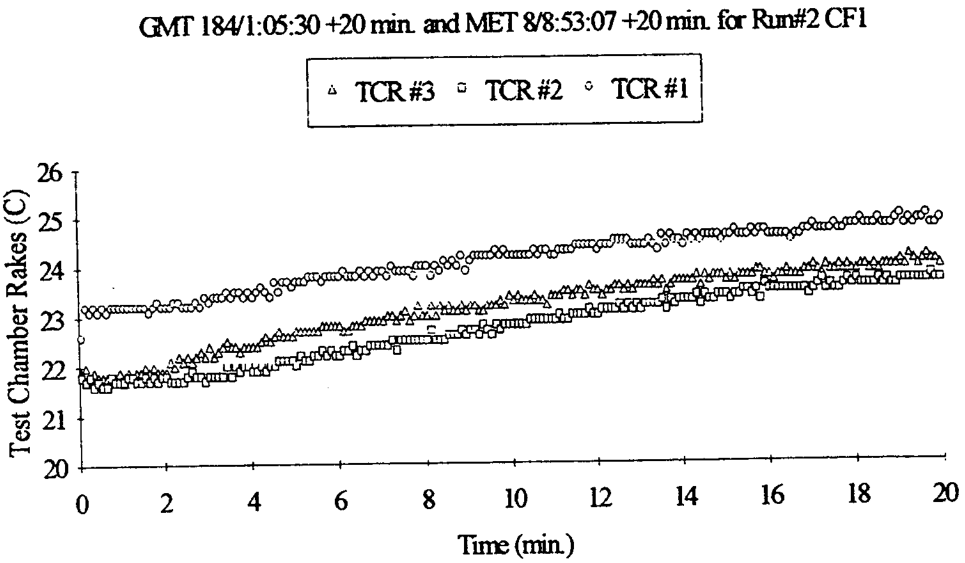
GMT 184/1:05:30 +20 min. and MET 8/8:53:07 +20 min. for Run#2 CF1

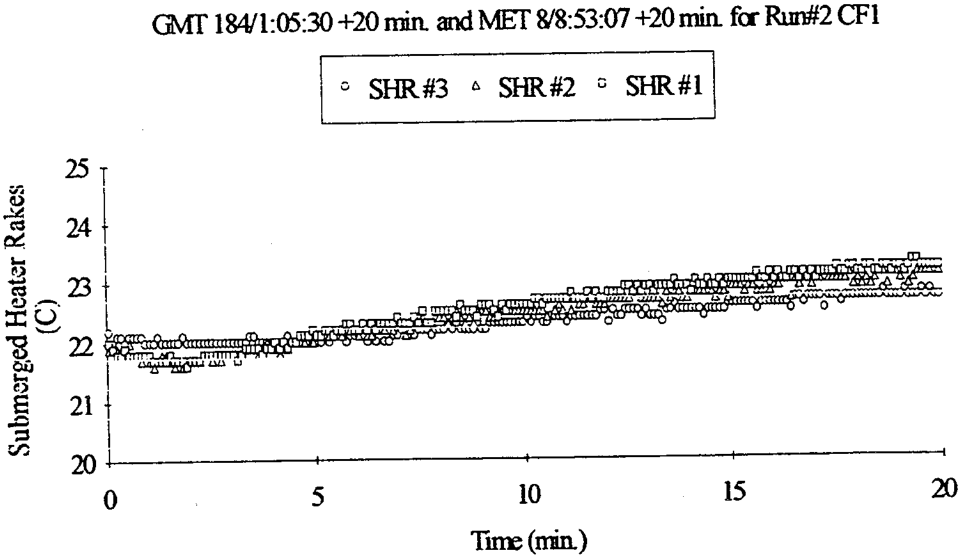
GMT 184/1:05:30 +20 min. and MET 8/8:53:07 +20 min. for Run#2 CF1

Figure C27 Thermistor data

Streamlines for Run#2 Test CF1

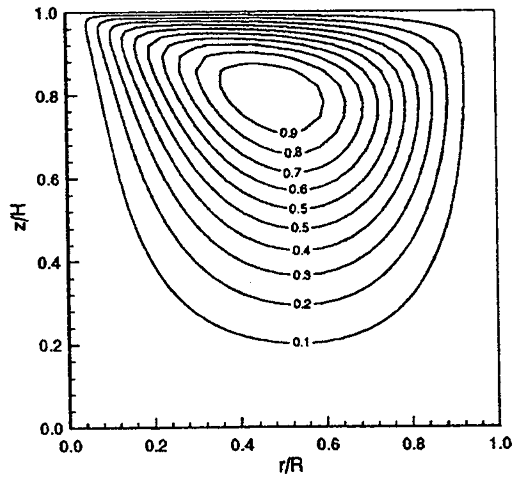

Isotherms for Run#2 Test CF1

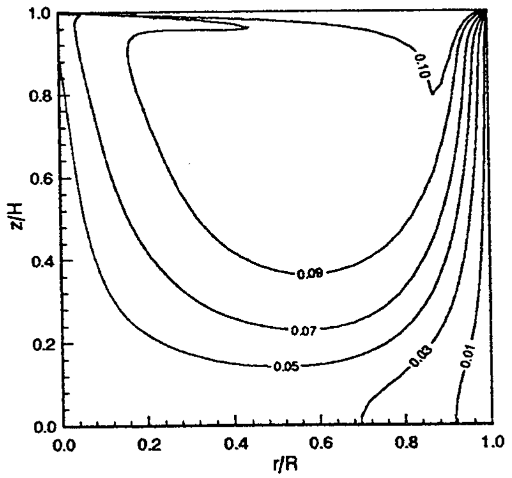

Figure C28 Computed streamlines and isotherms

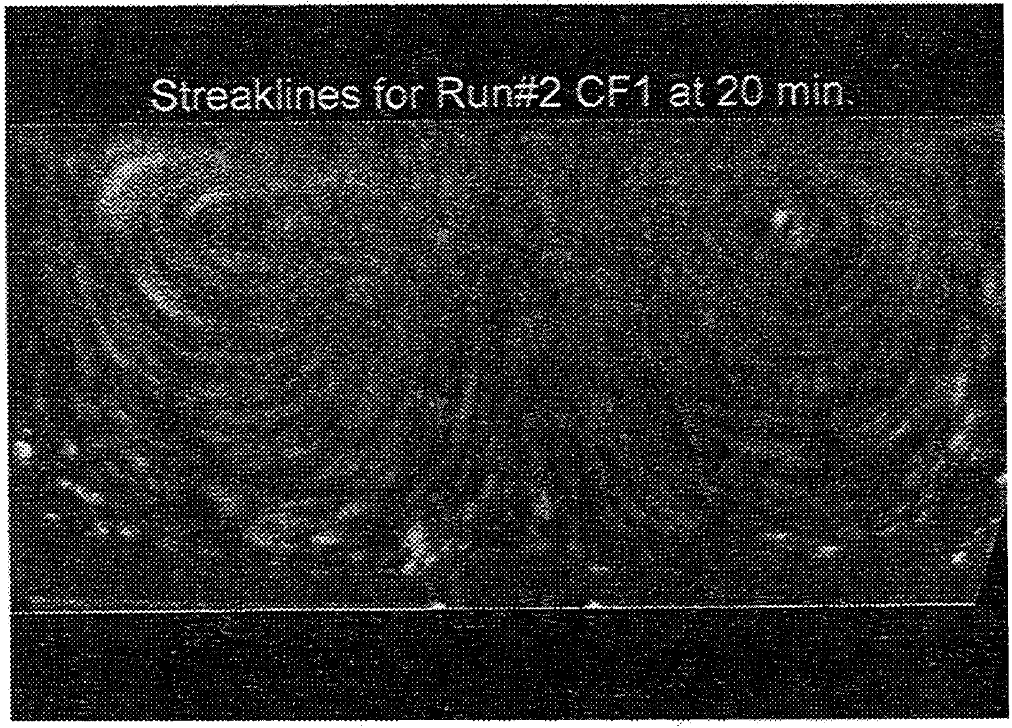

Figure C29 Experimental data pathlines

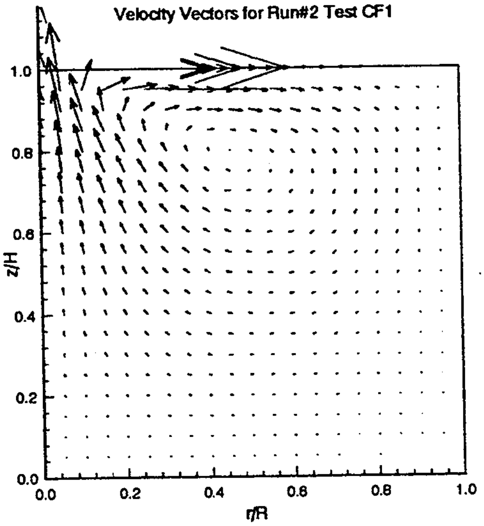

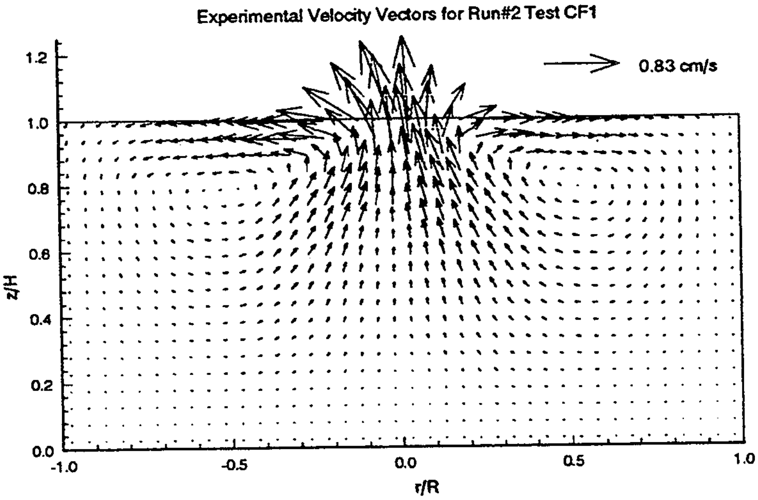

Figure C30 Computed and measured velocity vectors

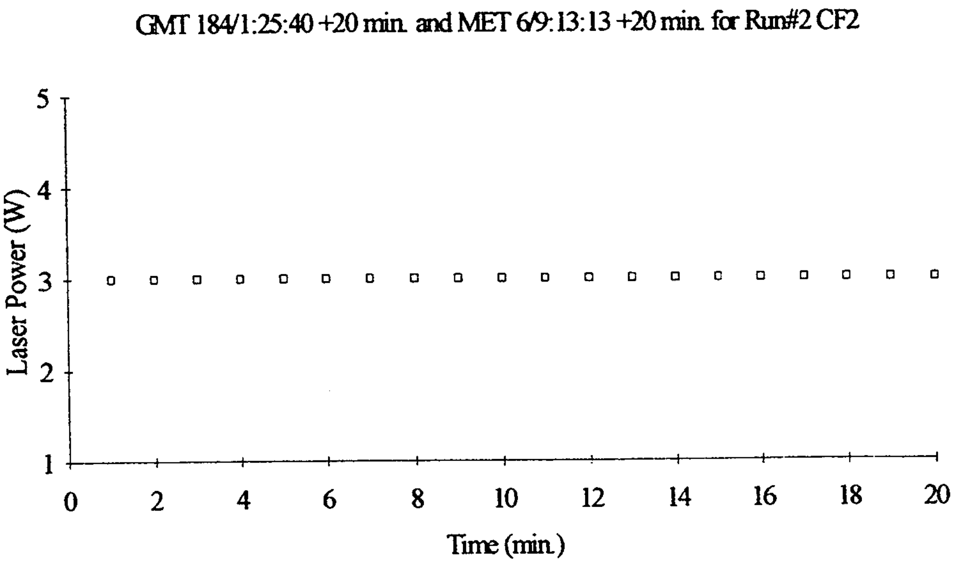

Figure C31 Laser power

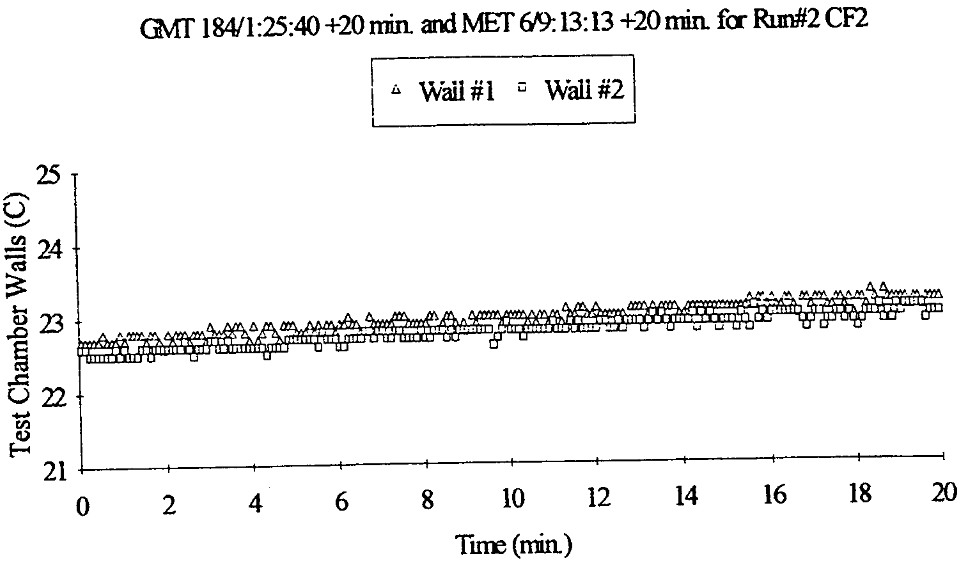

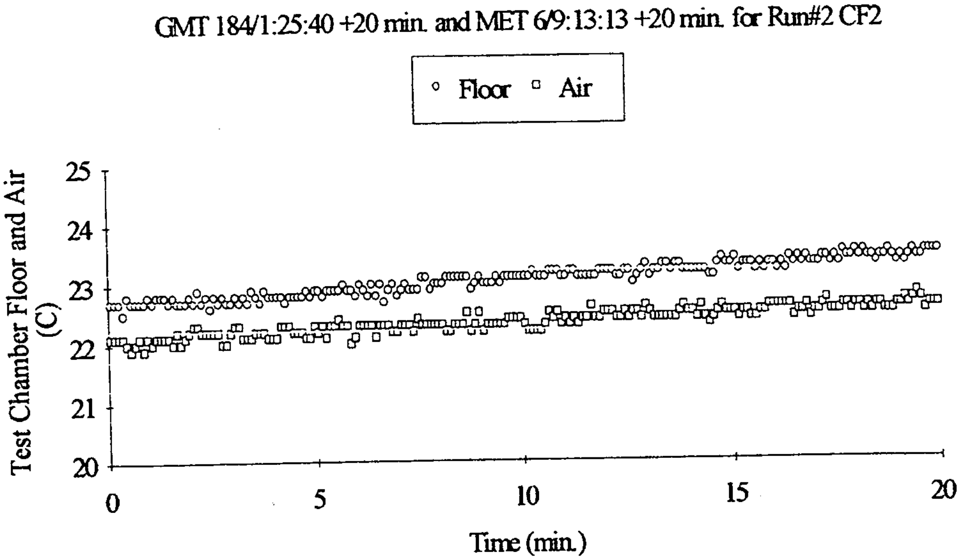

Figure C32 Thermistor data

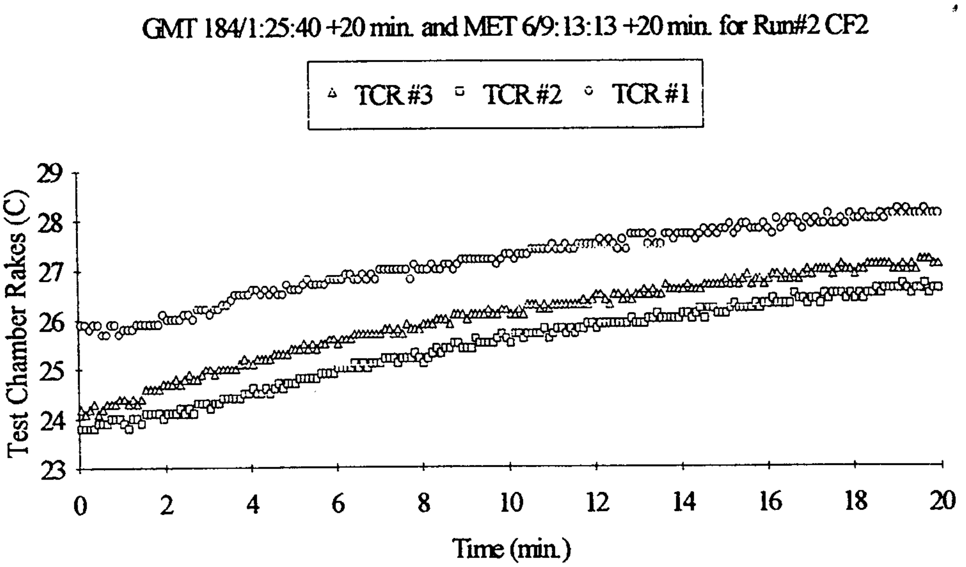

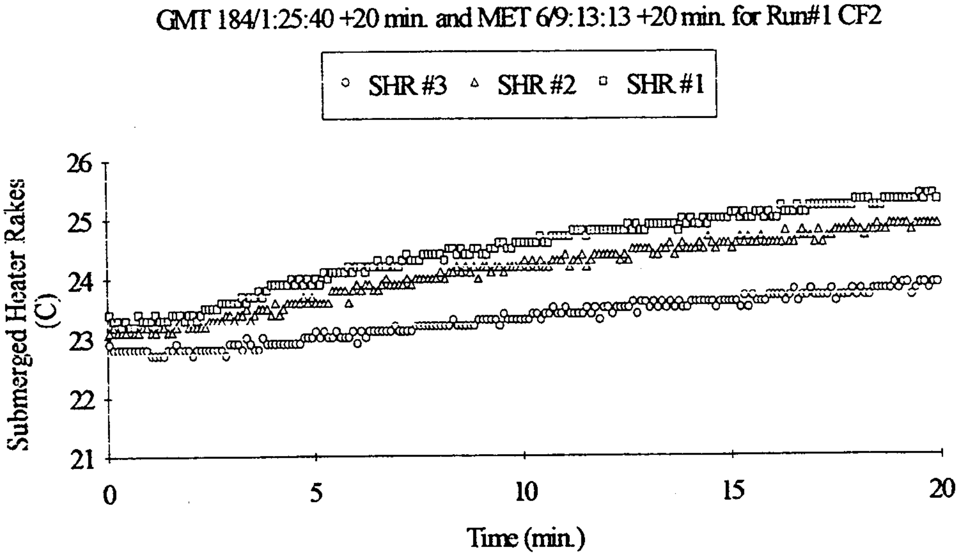

Figure C33 Thermistor data

Streamlines for Run#2 Test CF2

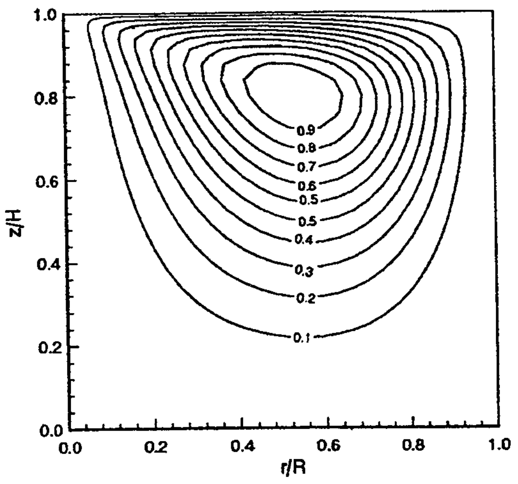

Isotherms for Run#2 Test CF2

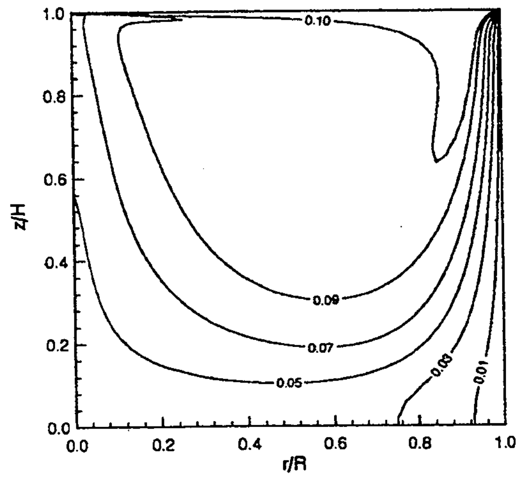

Figure C34 Computed streamlines and isotherms

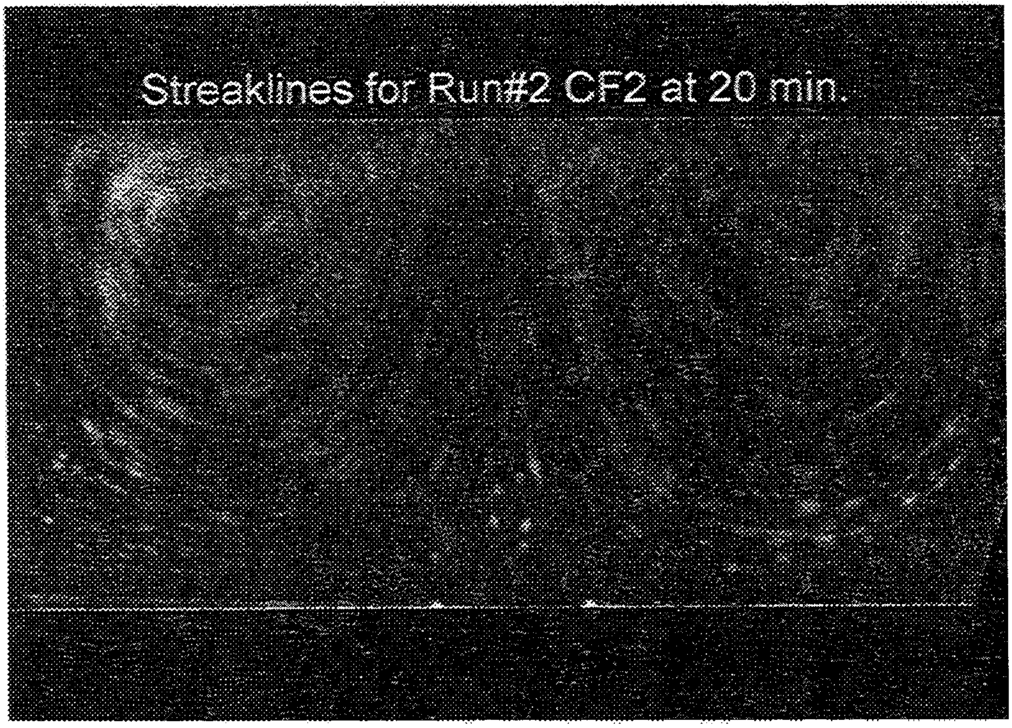

Figure C35 Experimental pathlines

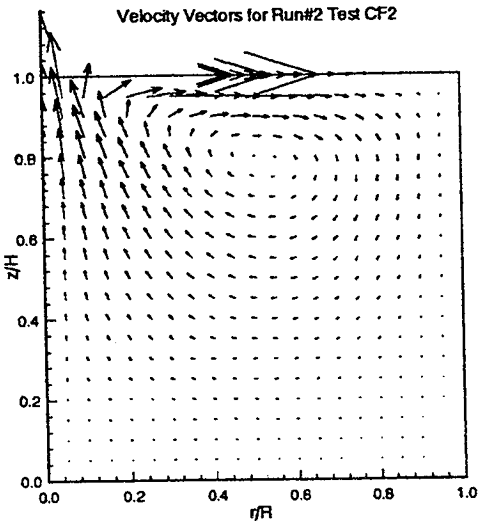

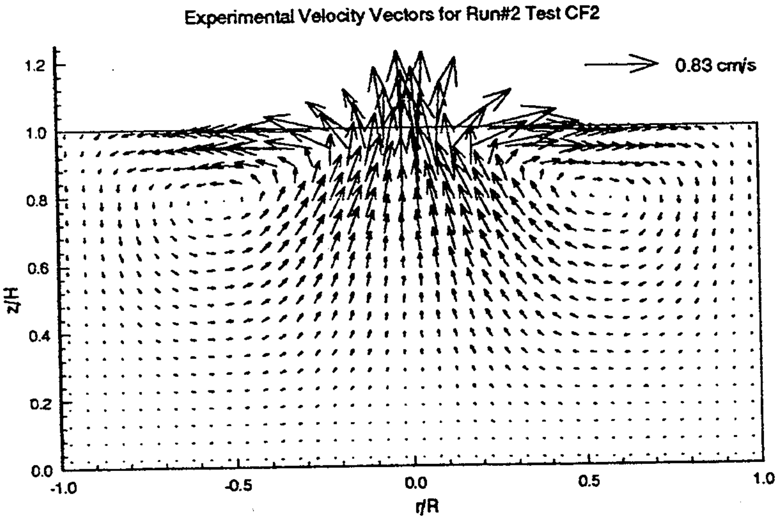

Figure C36 Computed and measured velocity vectors

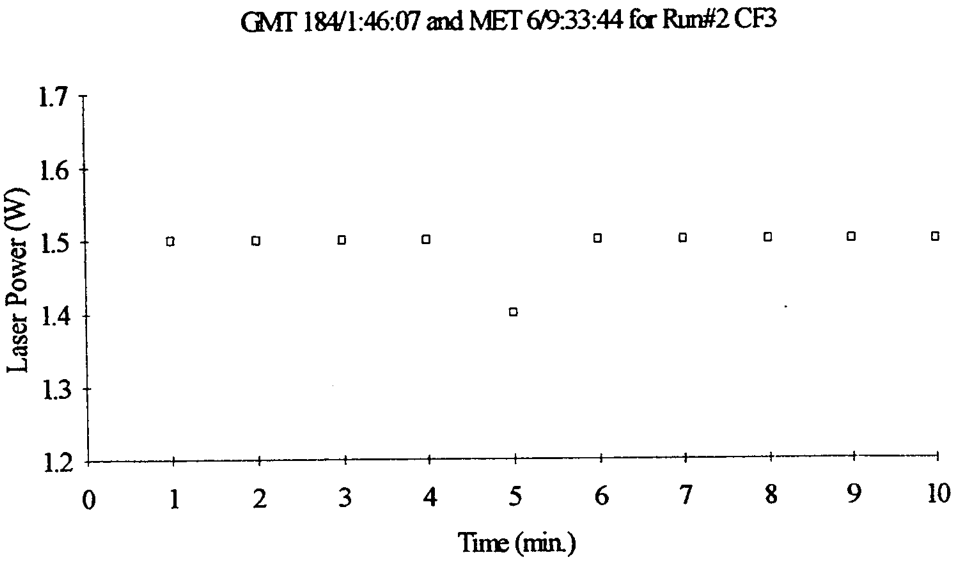

Figure C37 Laser power

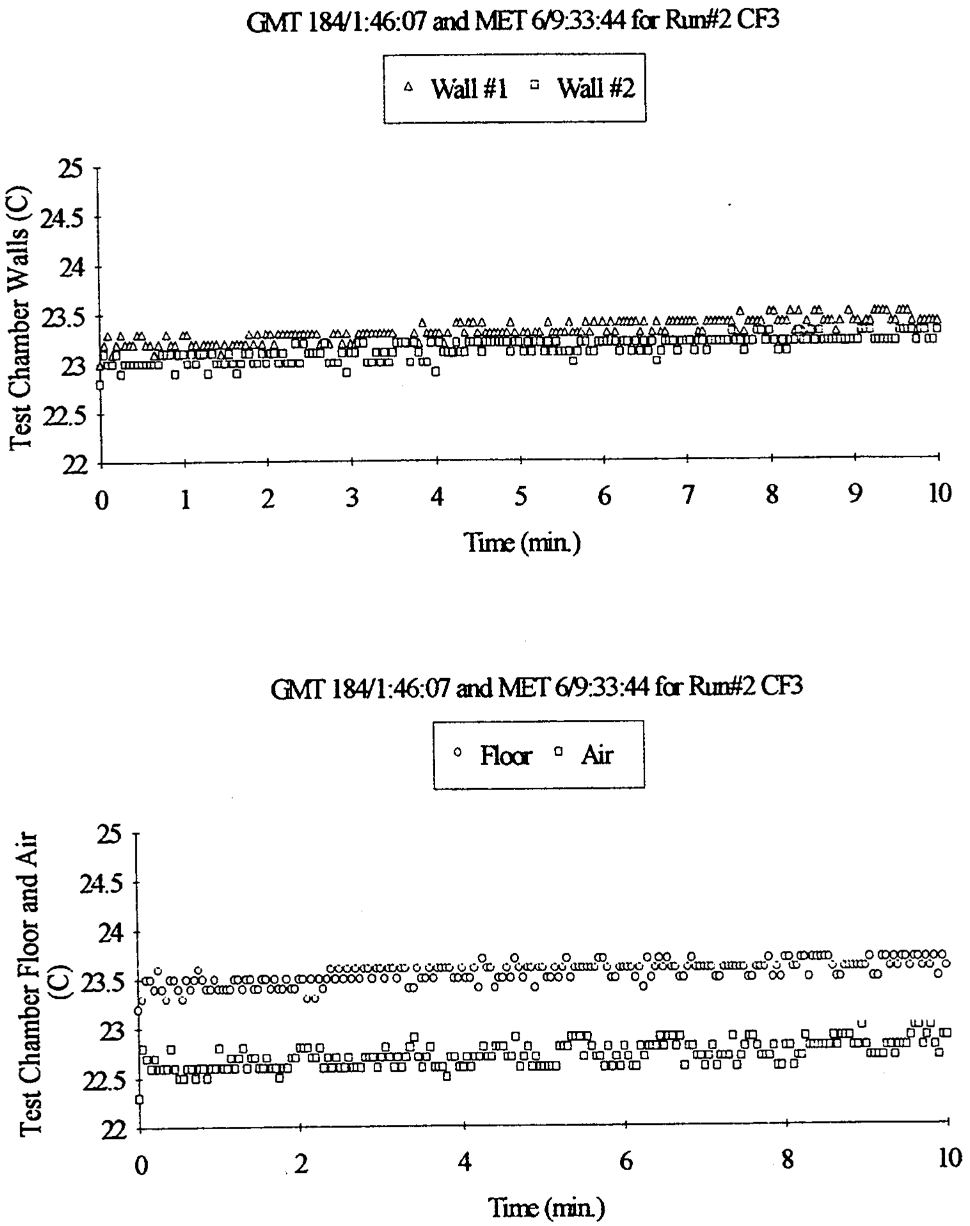

Figure C38 Thermistor data

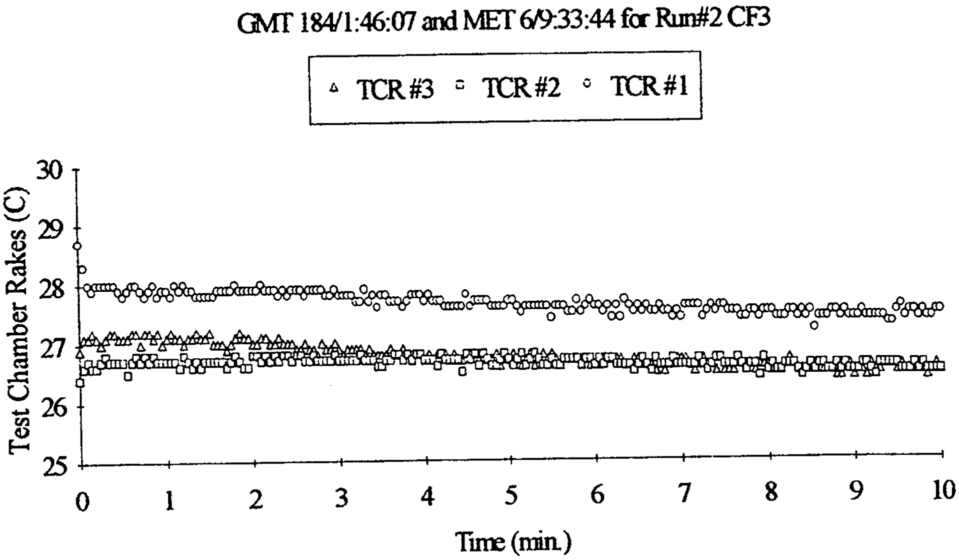

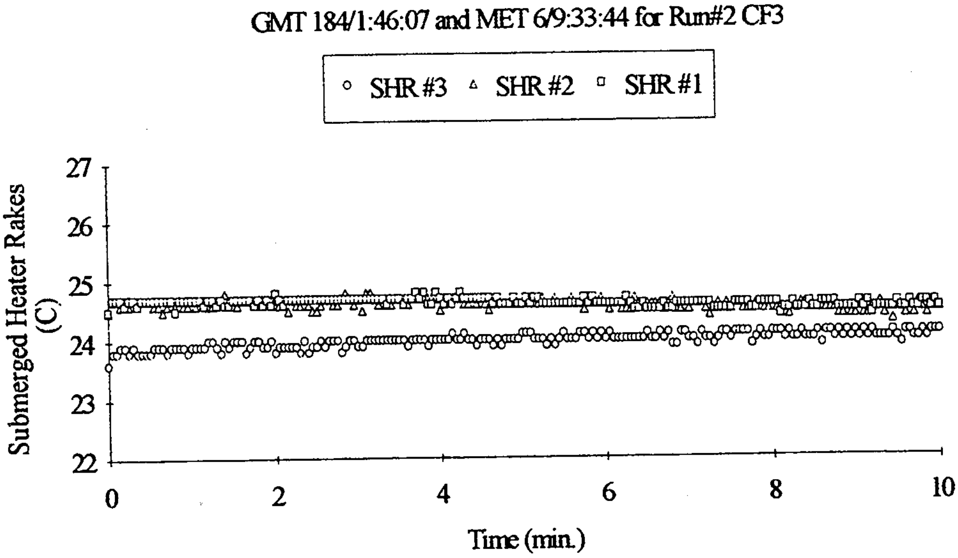

Figure C39 Thermistor data

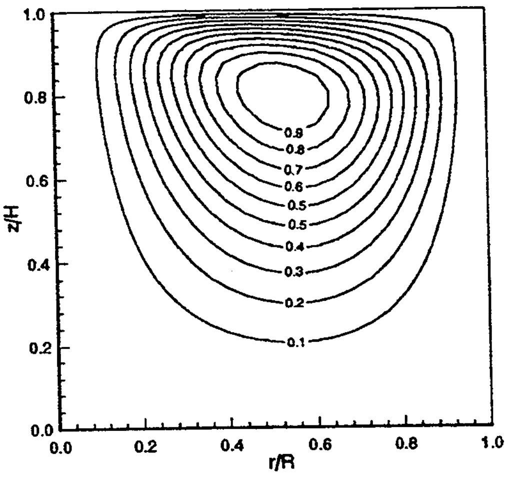
Streamlines for Run#2 Test CF3

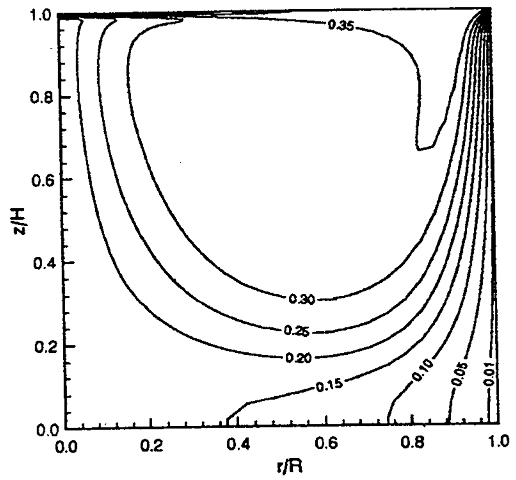
Isotherms for Run#2 Test CF3

Figure C40 Computed streamlines and isotherms

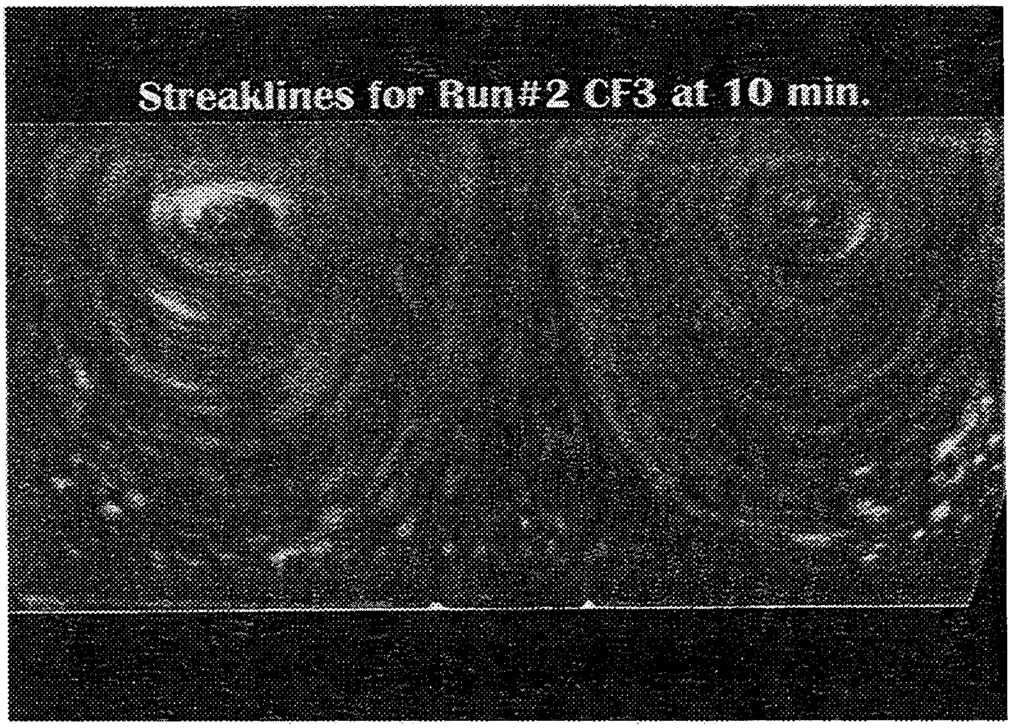

Figure C41 Experimental pathlines

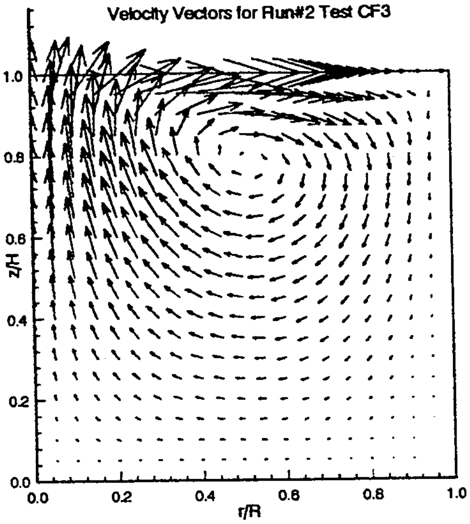
Velocity Vectors for Run#2 Test CF3

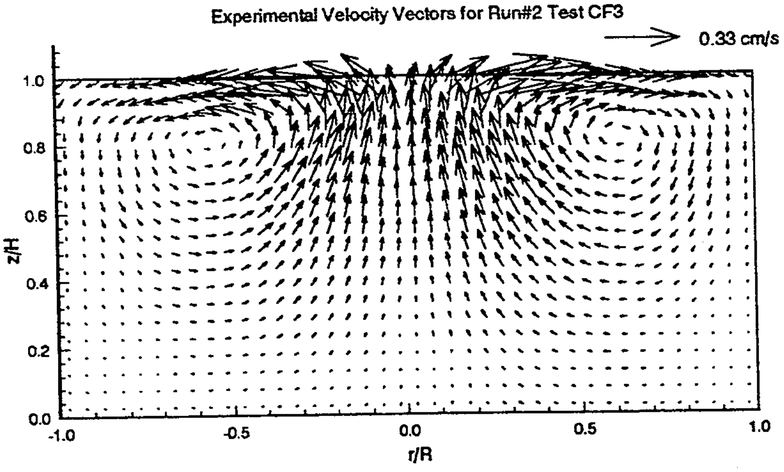
Experimental Velocity Vectors for Run#2 Test CF3

Figure C42 Computed and measured velocity vectors

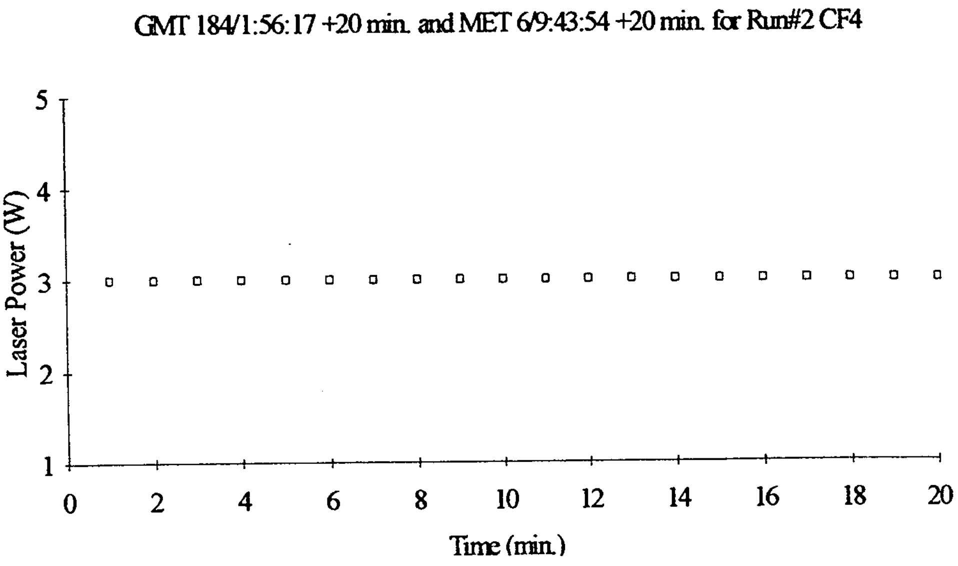

Figure C43 Laser power

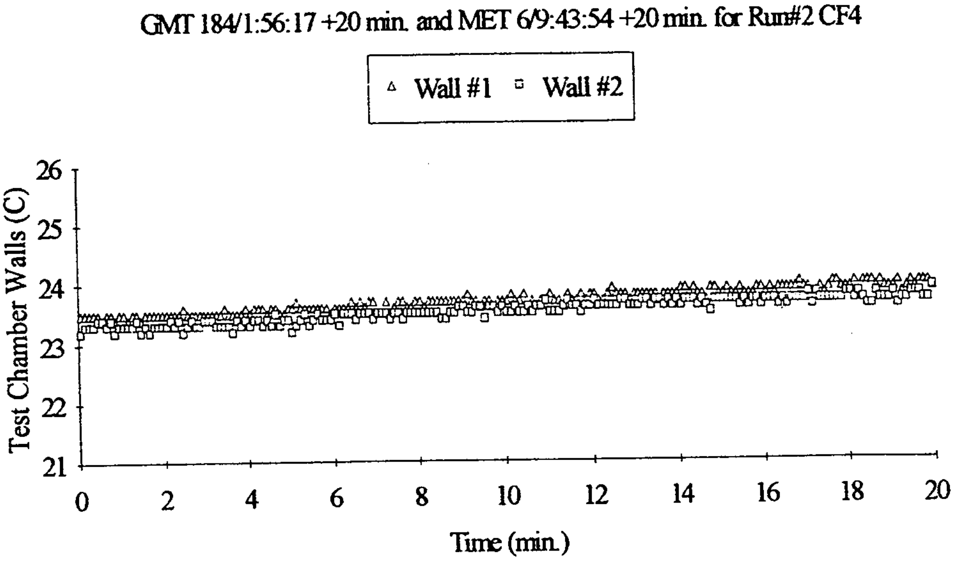

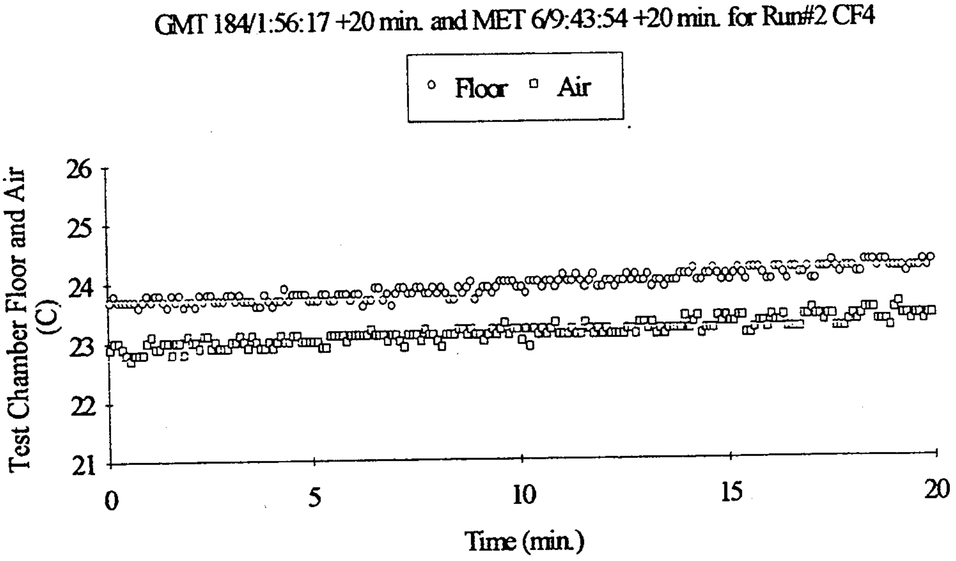

Figure C44 Thermistor data

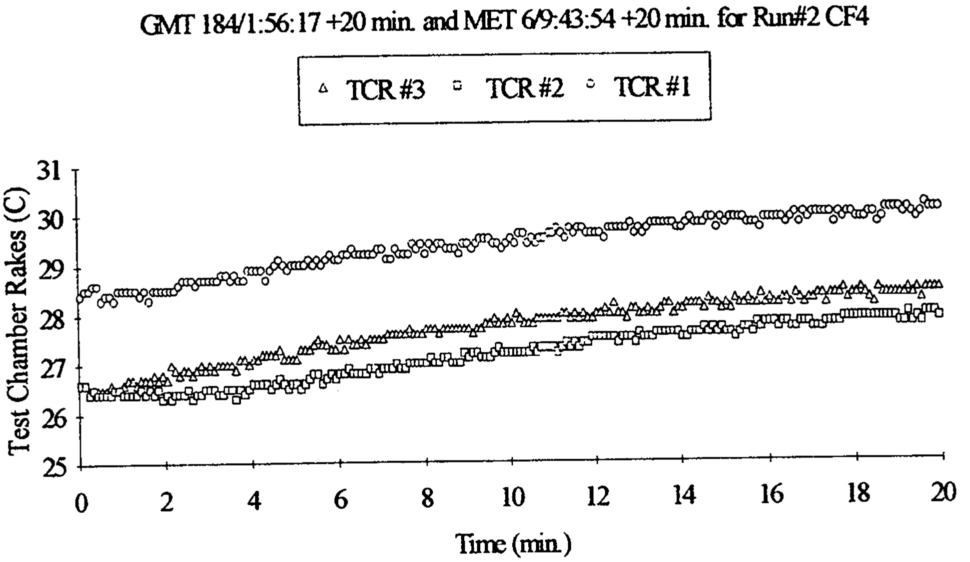

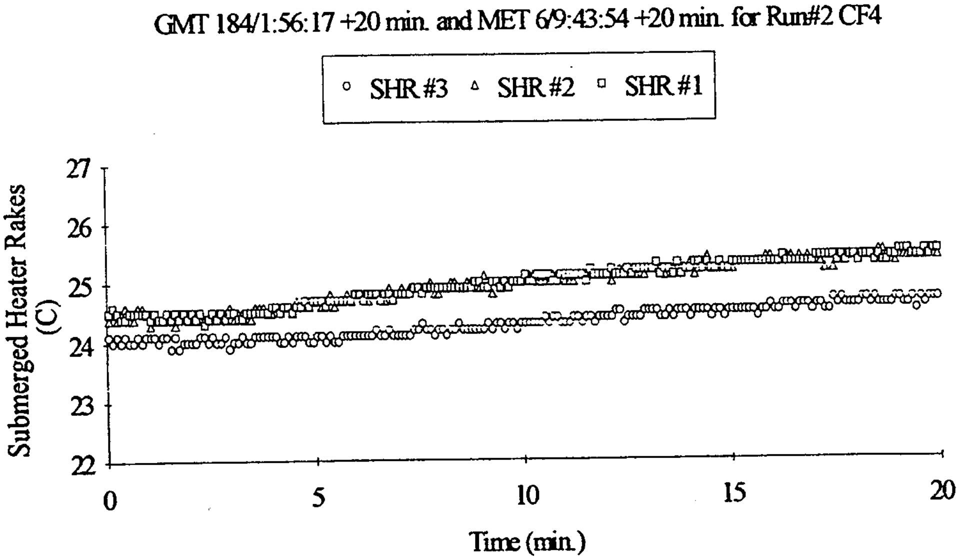

Figure C45 Thermistor data

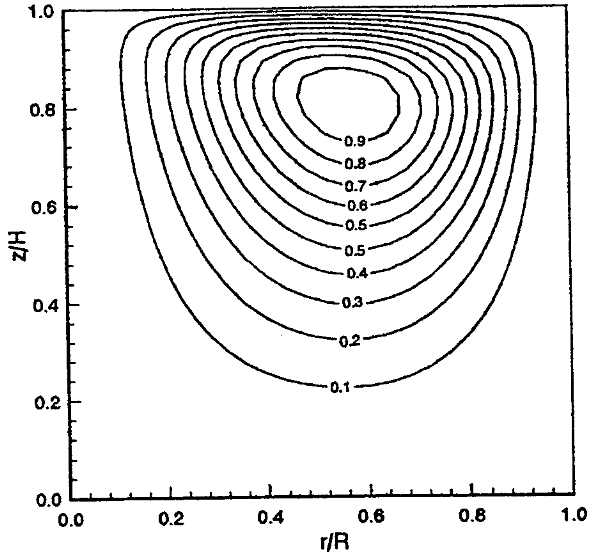
Streamlines for Run#2 Test CF-4

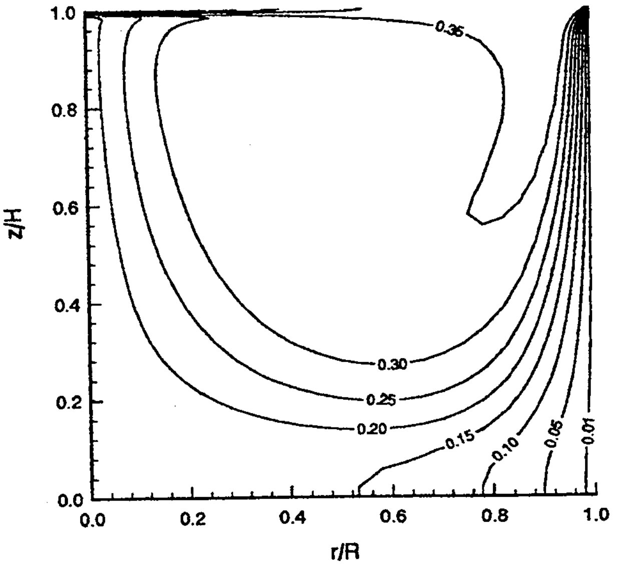
Isotherms for Run#2 Test CF4

Figure C46 Computed streamlines and isotherms

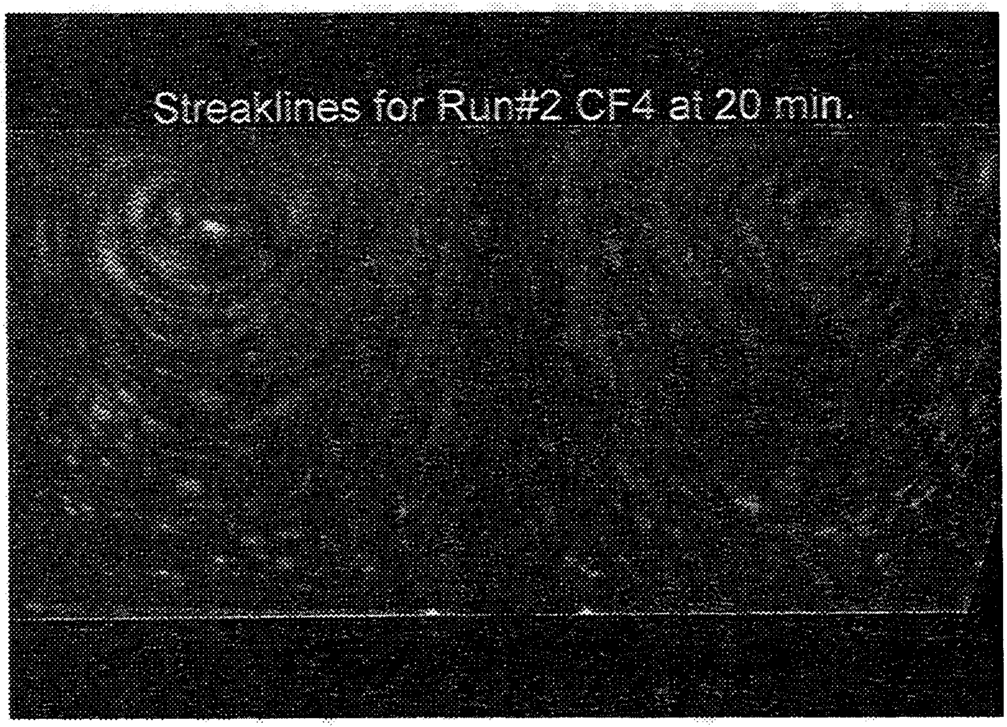

Figure C 47 Experimental pathlines

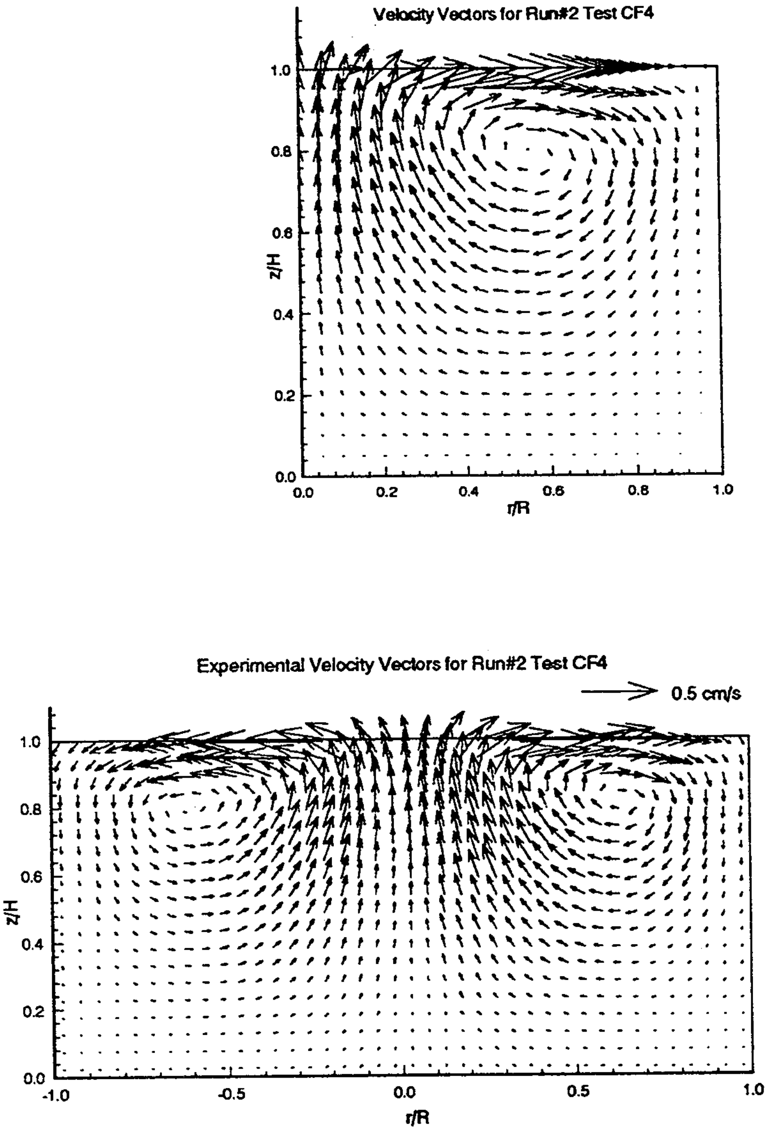

Figure C48 Computed and measured velocity vectors

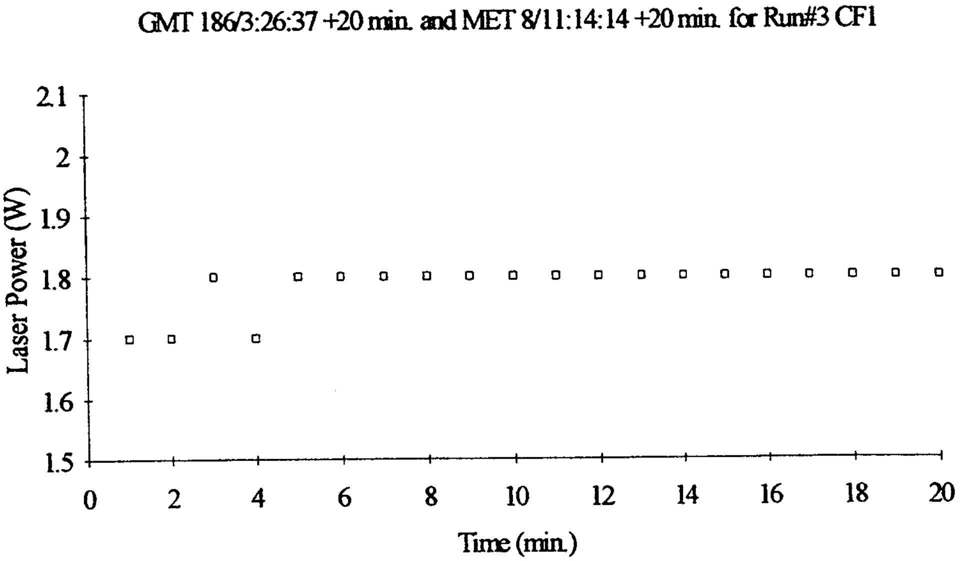

Figure C49 Laser power

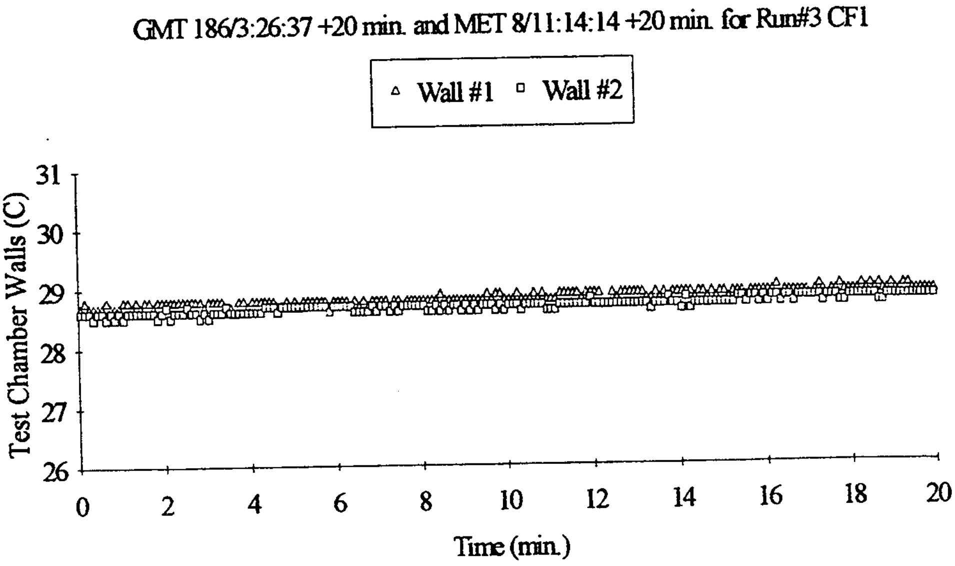

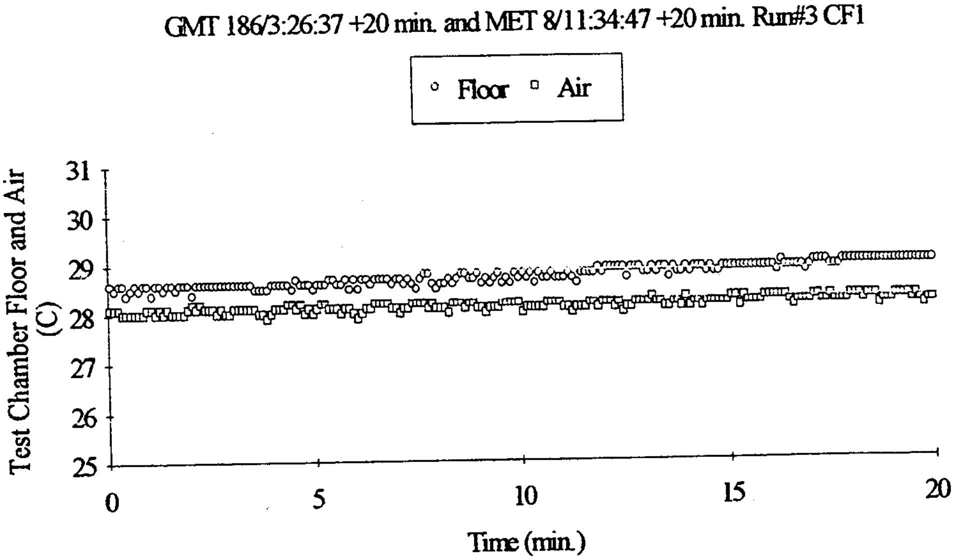

Figure C50 Thermistor data

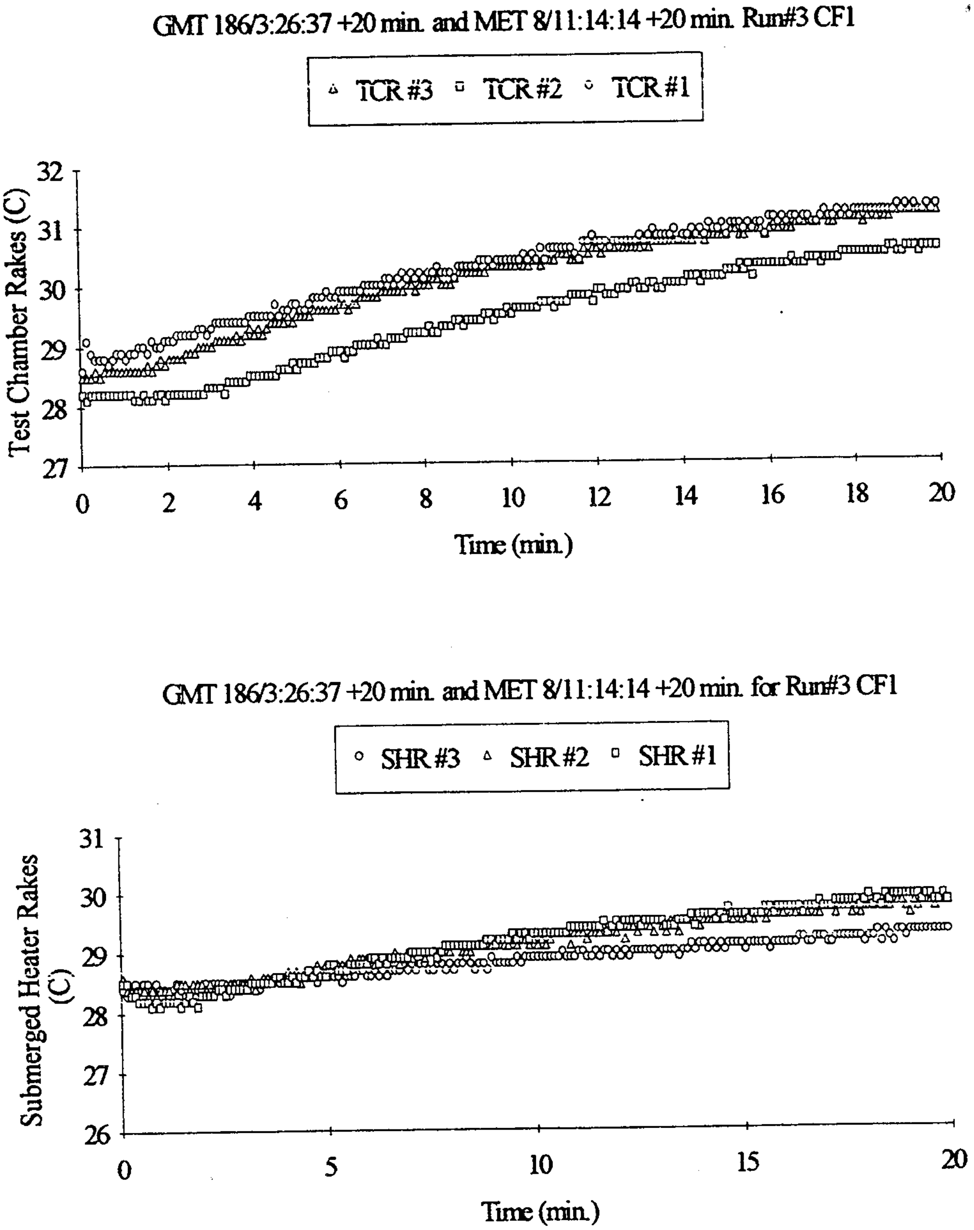

Figure C51 Thermistor data

Streamlines for Run#3 Test CF1

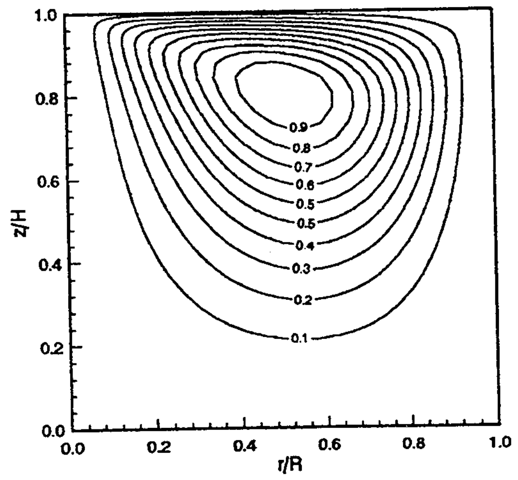

Isotherms for Run#3 Test CF1

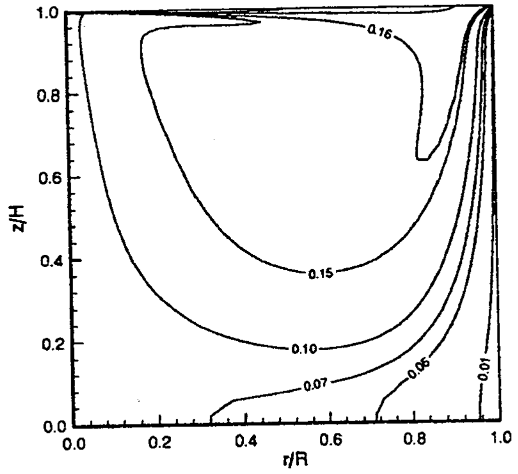

Figure C52 Computed streamlines and pathlines

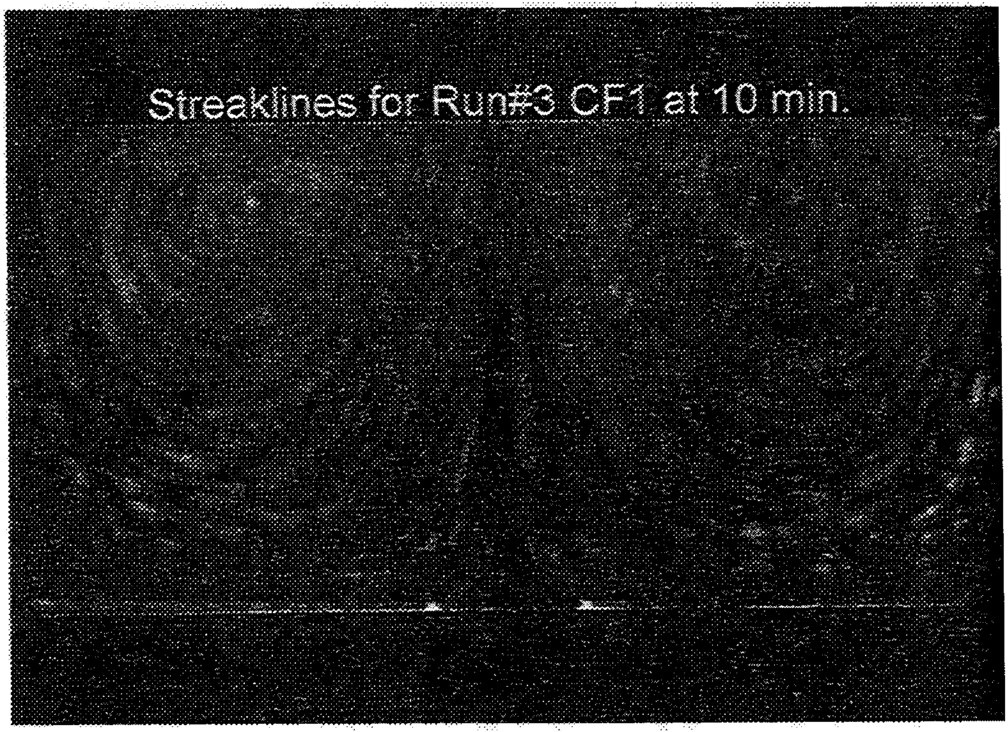

Figure C53 Experimental pathlines

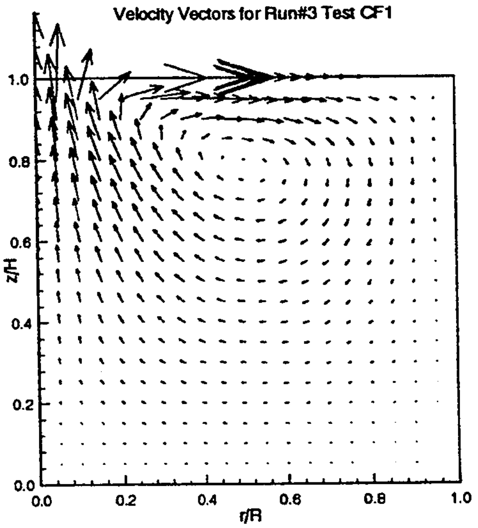

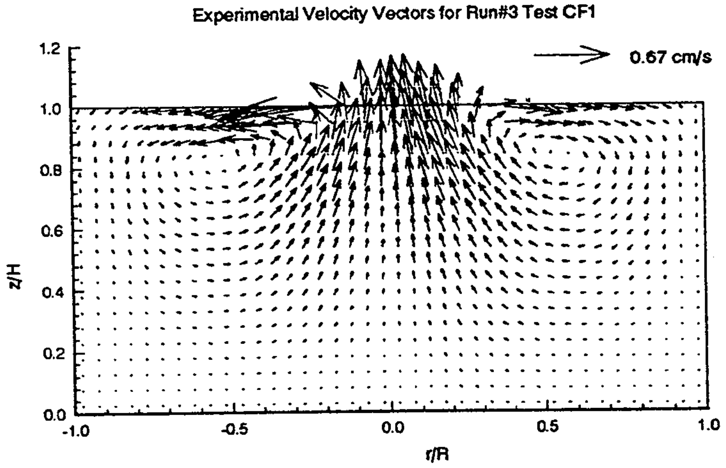

Figure C54 Computed and measured velocity vectors

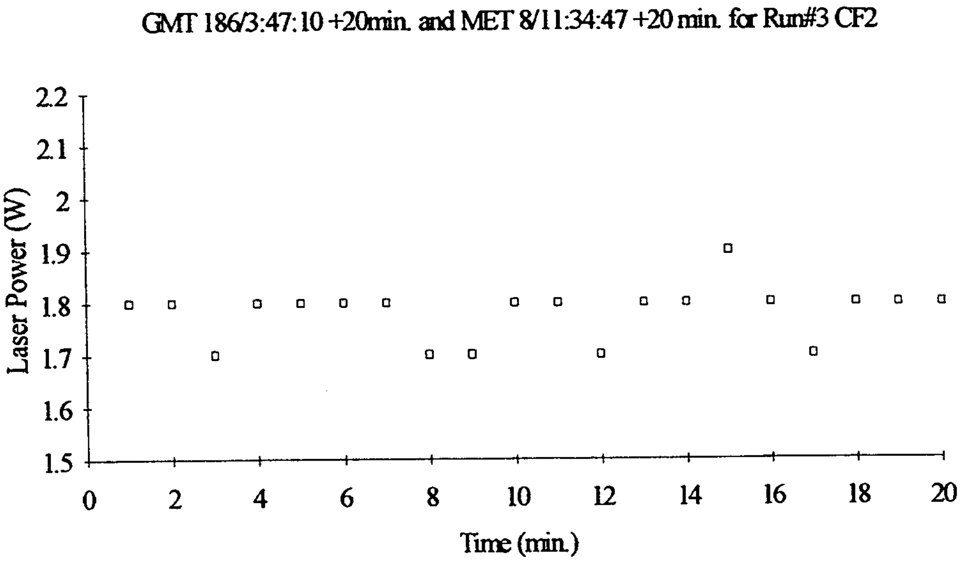

Figure C55 Laser power

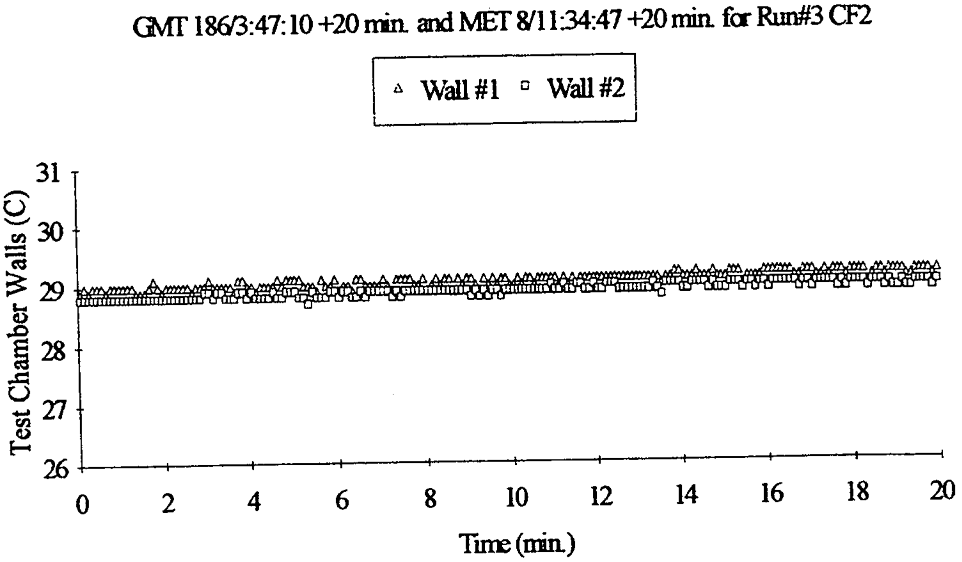

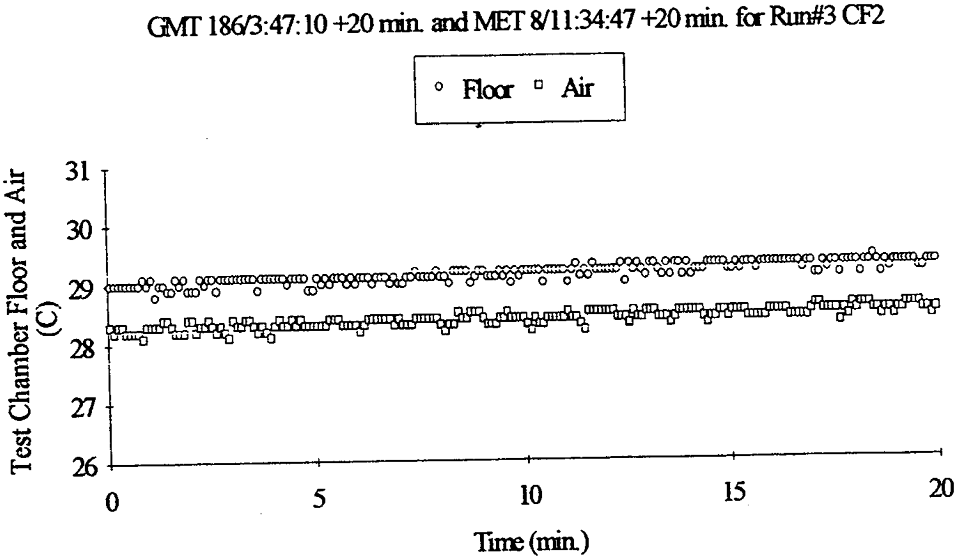

Figure C56 Thermistor data

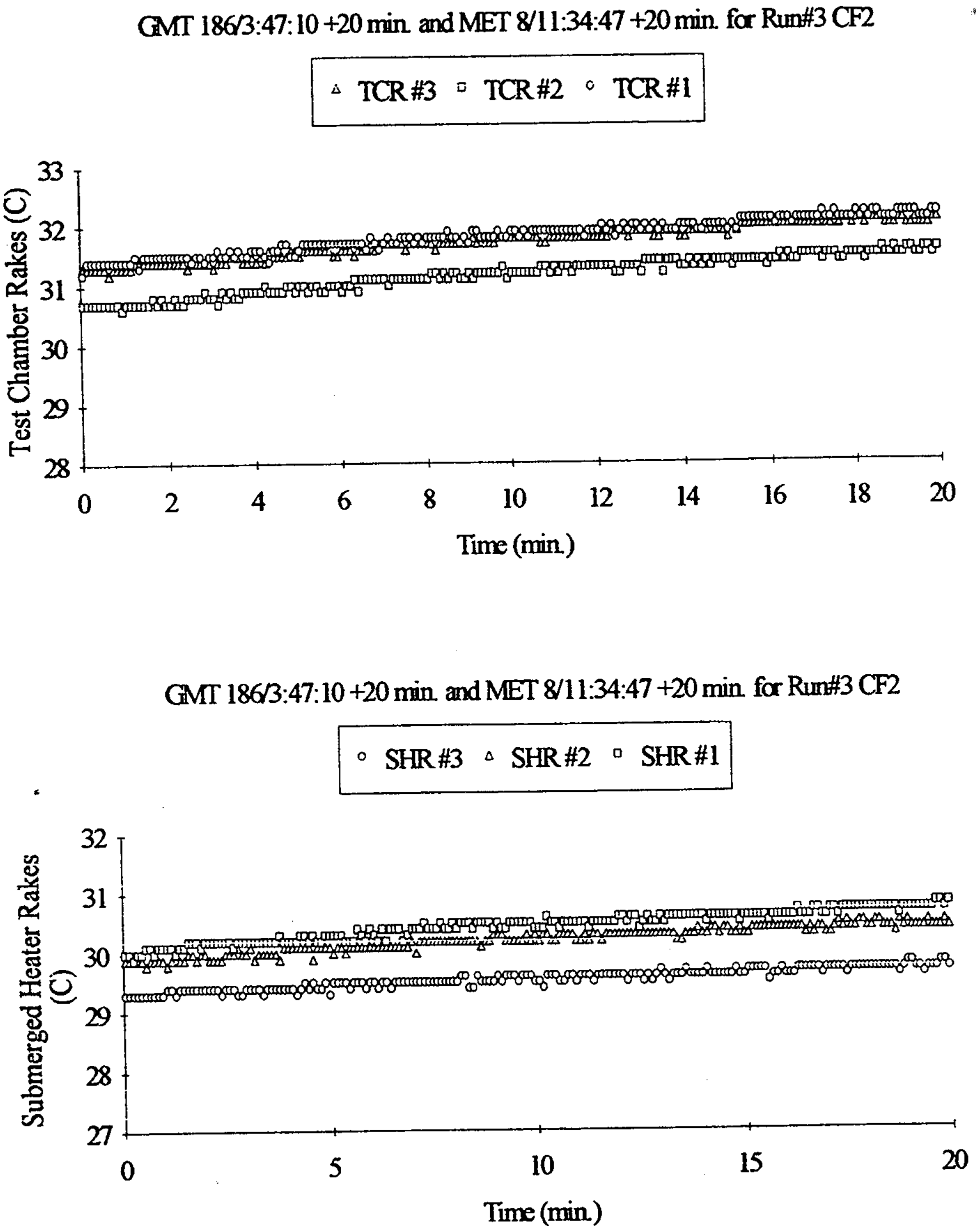

Figure C57 Thermistor data

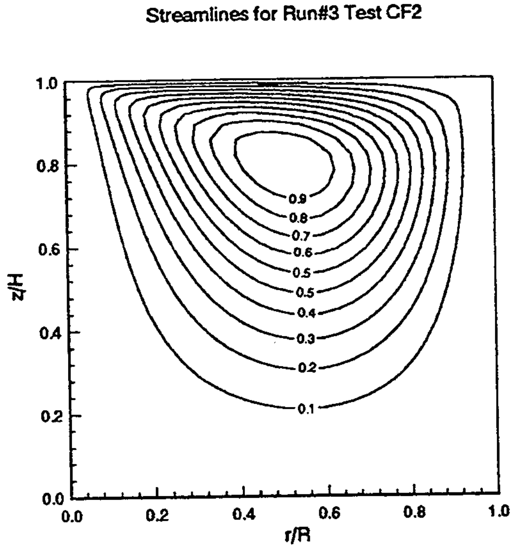

Streamlines for Run#3 Test CF2

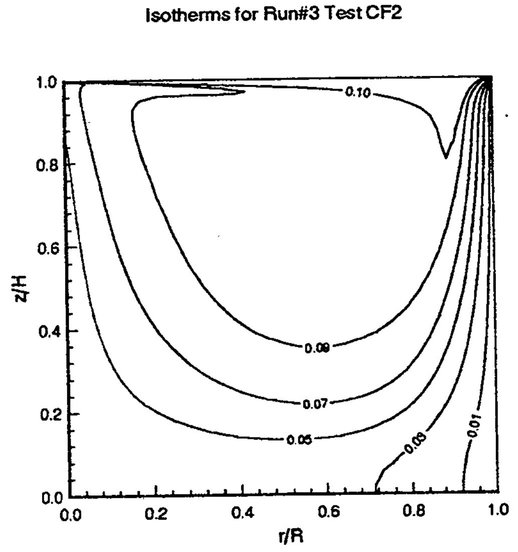

Isotherms for Run#3 Test CF2

Figure C58 Computed streamlines and isotherms

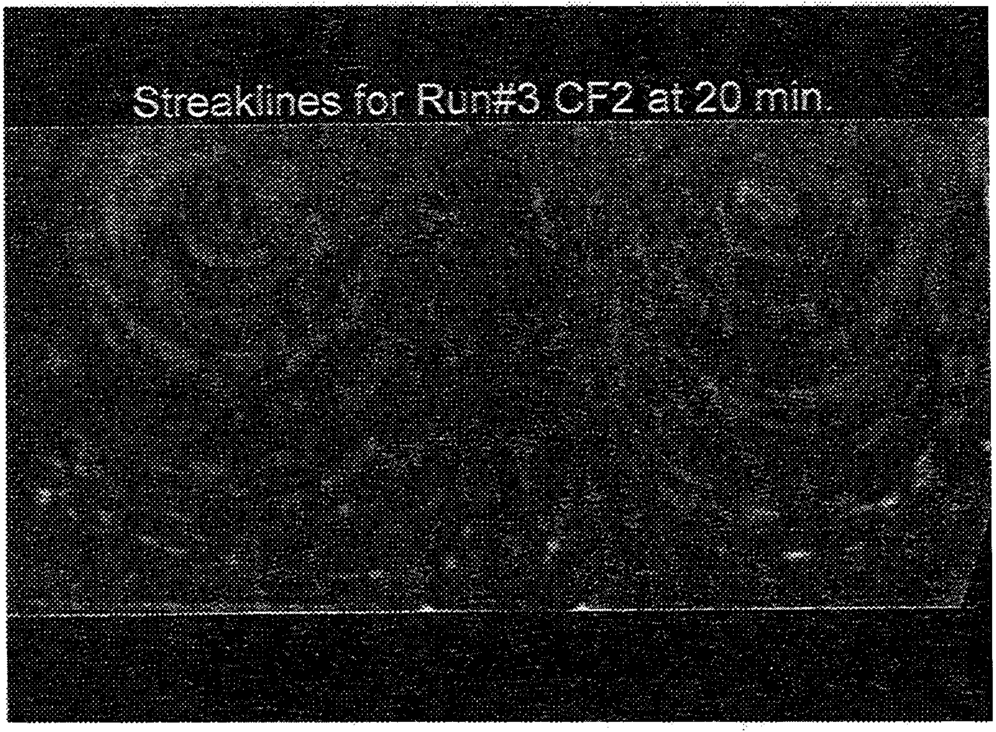

Figure C59 Experimental pathlines

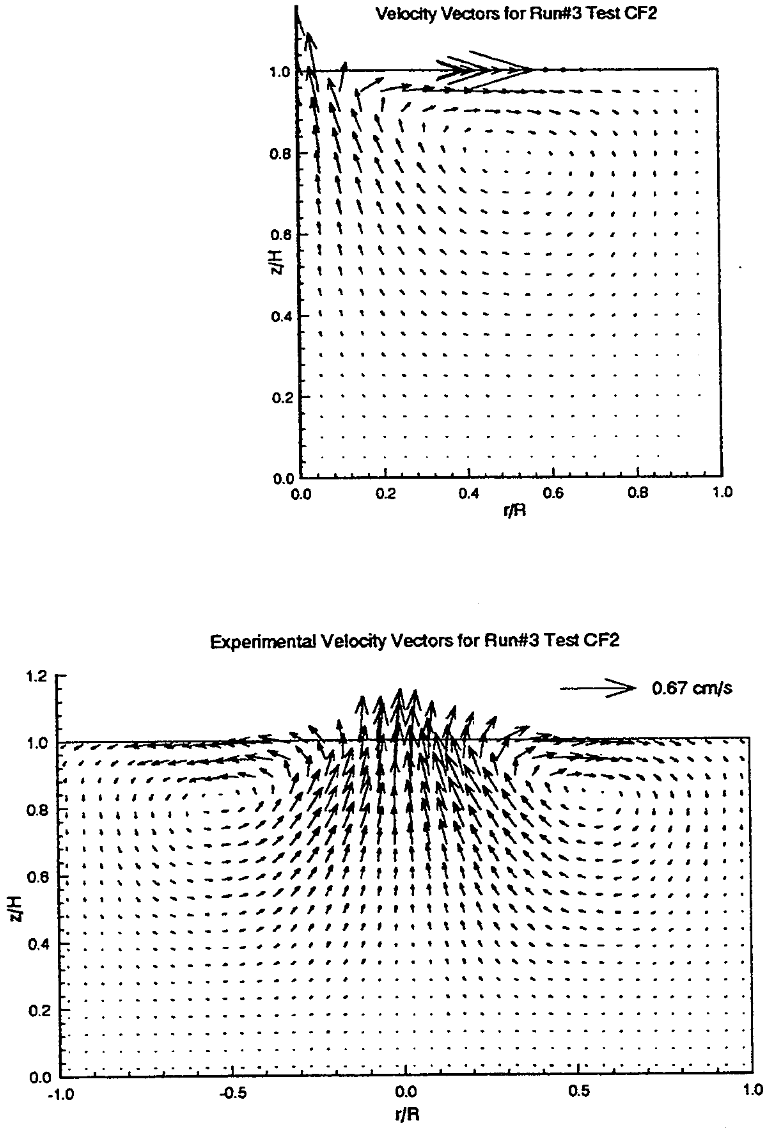

Figure C60 Computed and measured velocity vectors

APPENDIX D

CT FLAT SHORTER TESTS

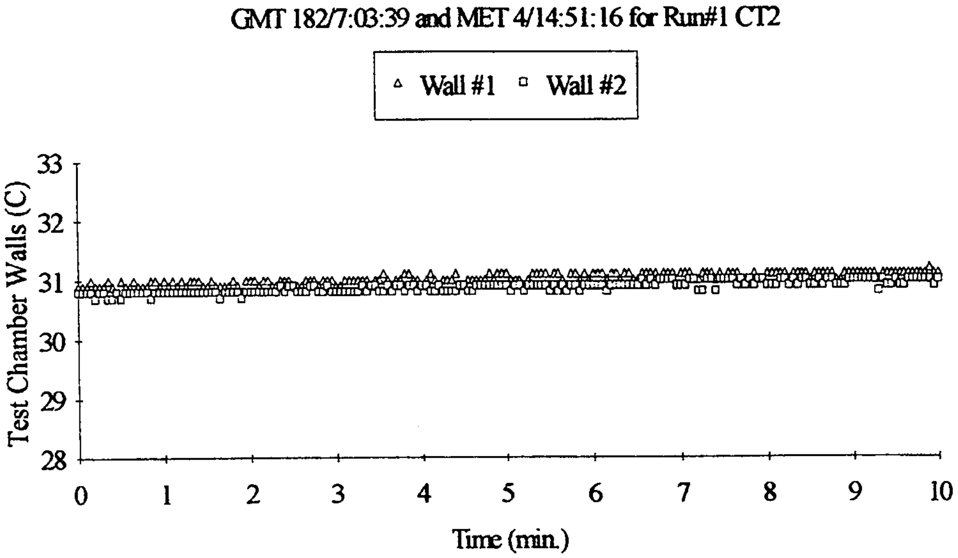

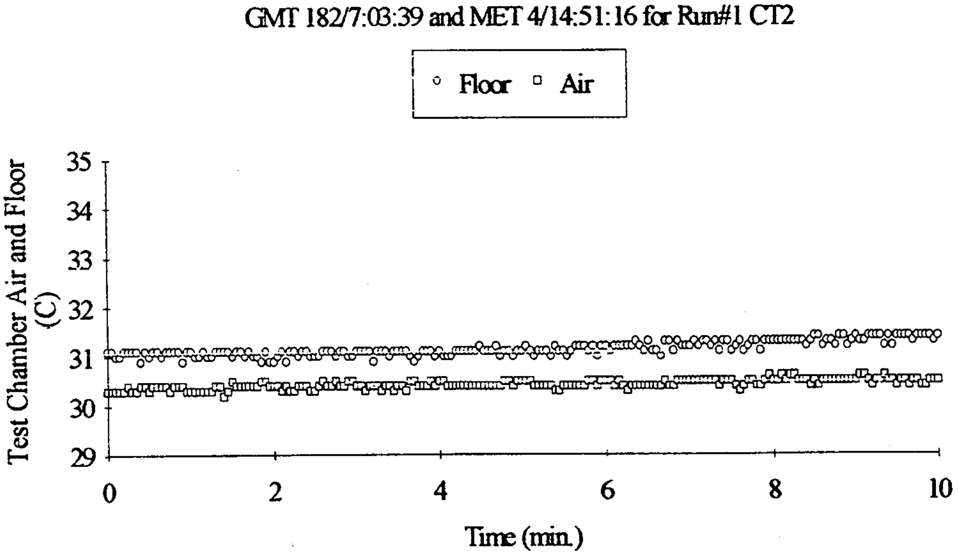

Figure D1 Thermistor data

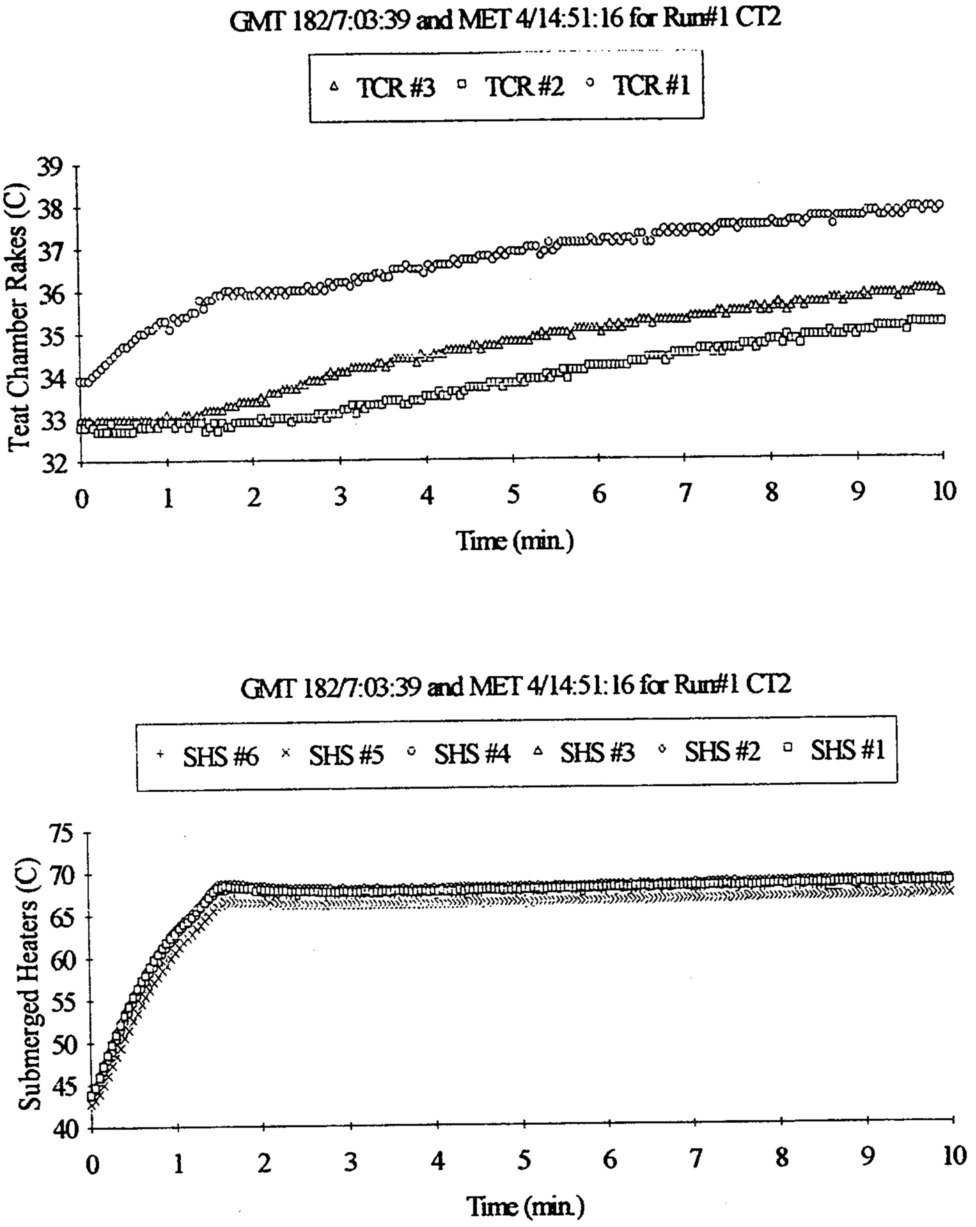

Figure D2 Thermistor data

Streamlines for Run#1 Test CT2

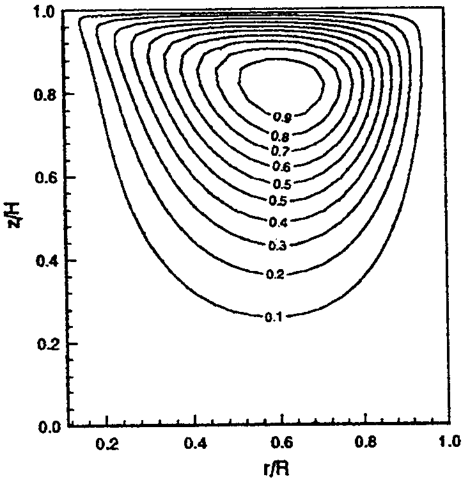

Isotherms for Run#1 Test CT2

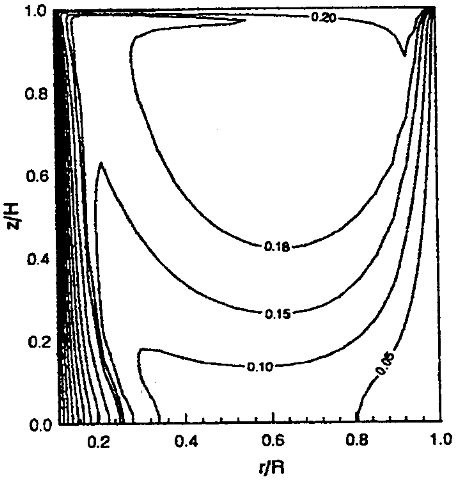

Figure D3 Computed streamlines and isotherms

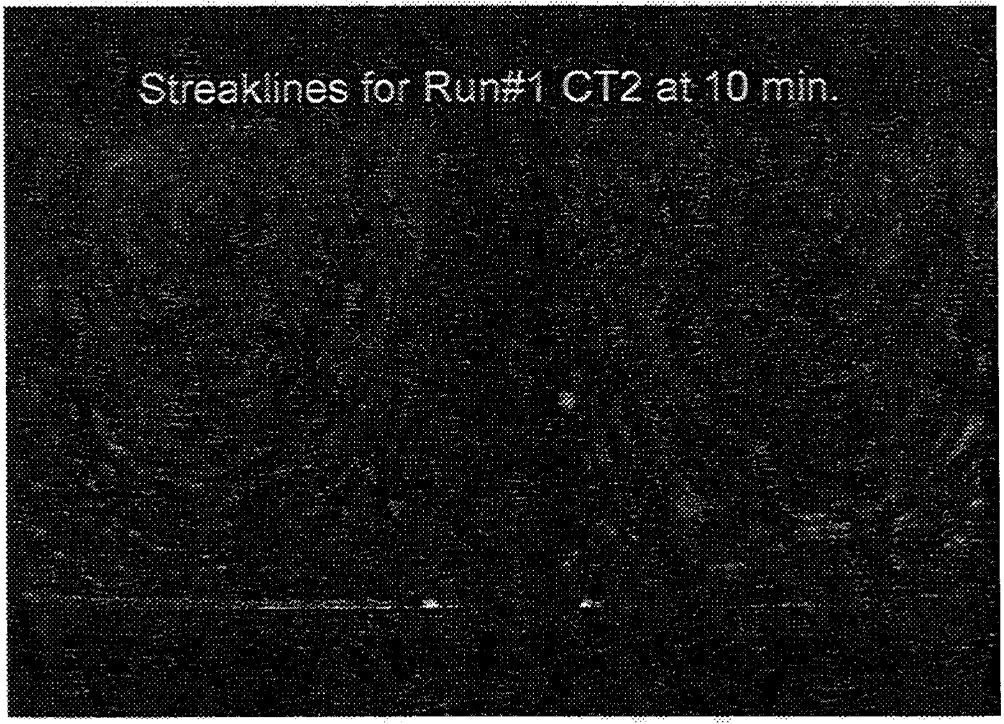

Figure D4 Experimental pathlines

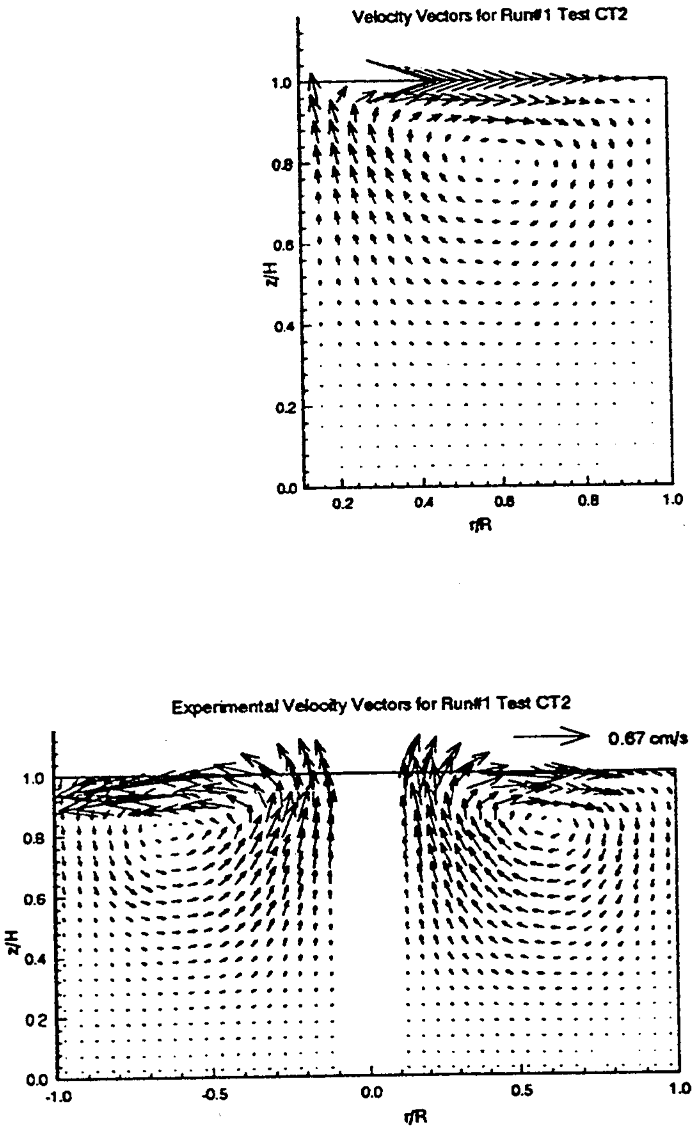

Velocity Vectors for Run#1 Test CT2

Experimental Velocity Vectors for Run#1 Test CT2

Figure D5 Computed and experimental velocity vectors

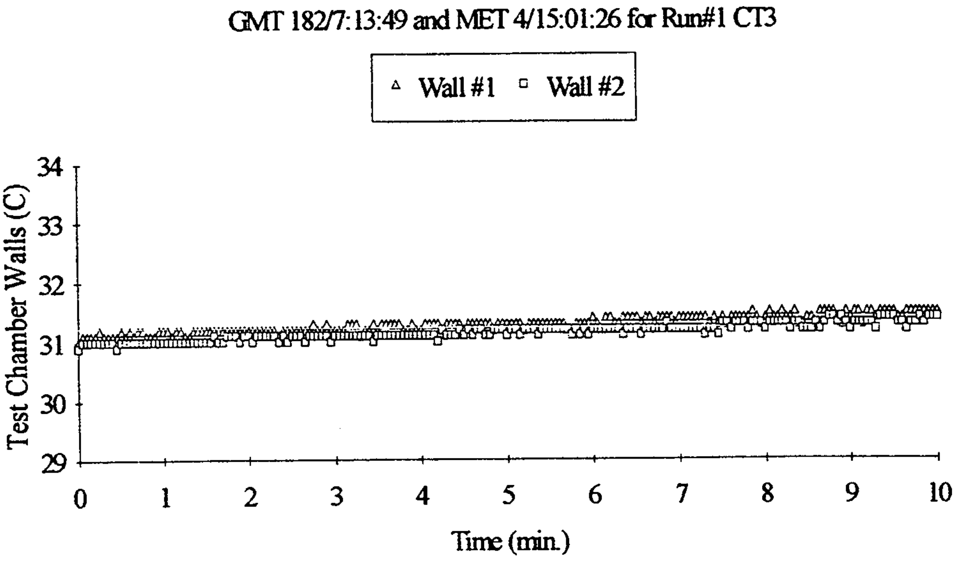
GMT 182/7:13:49 and MET 4/15:01:26 for Run#1 CT3

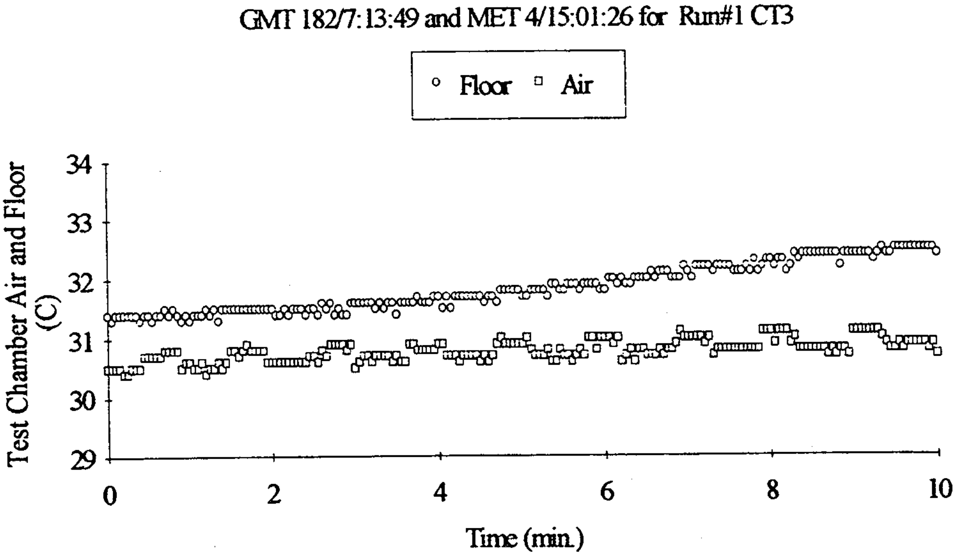
GMT 182/7:13:49 and MET 4/15:01:26 for Run#1 CT3

Figure D6 Thermistor data

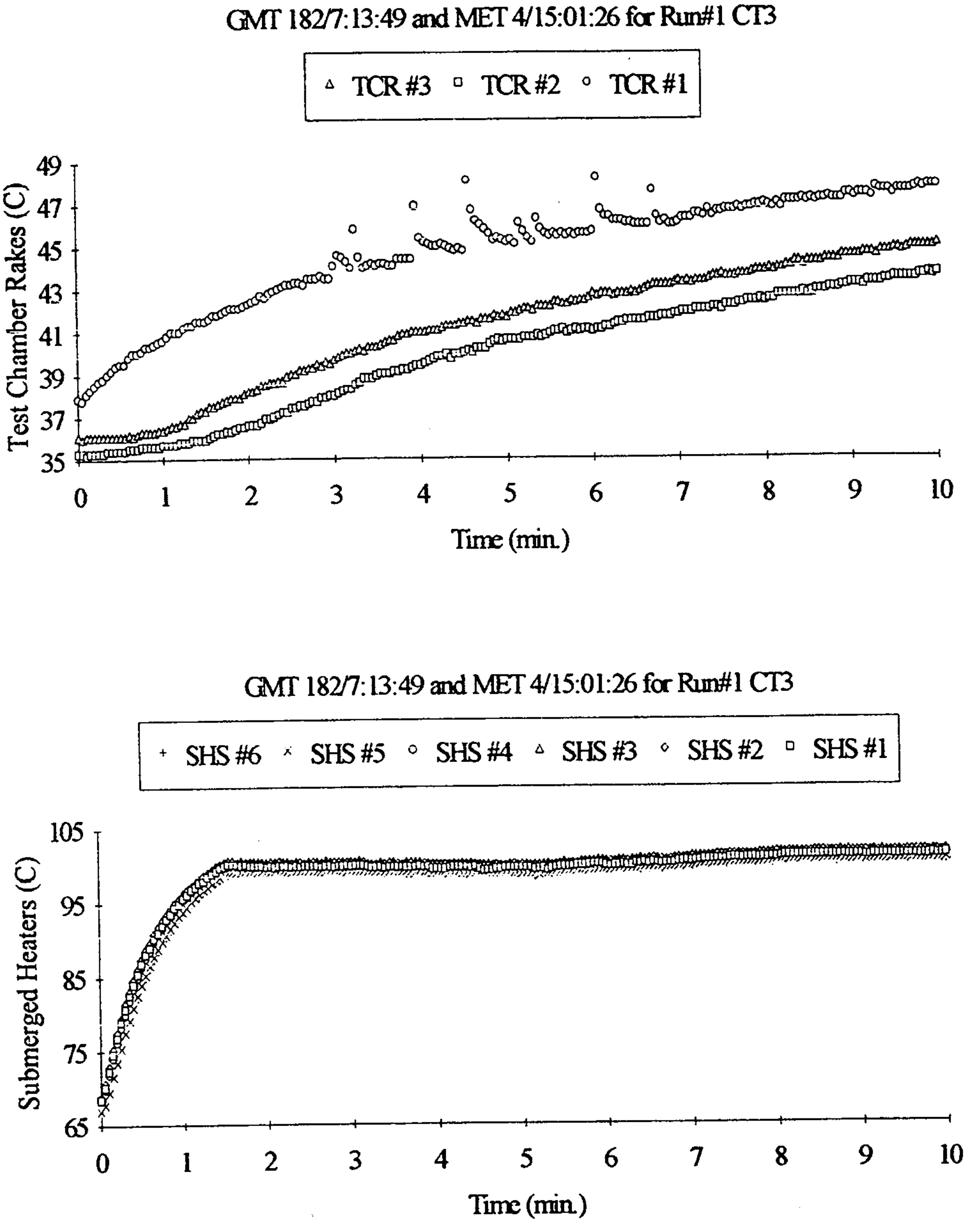

Figure D7 Thermistor data

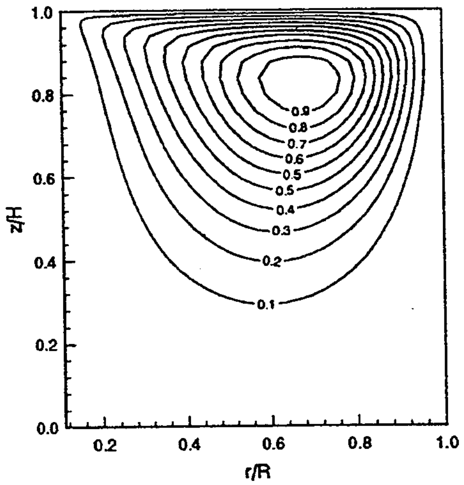
Streamlines for Run#1 Test CT3

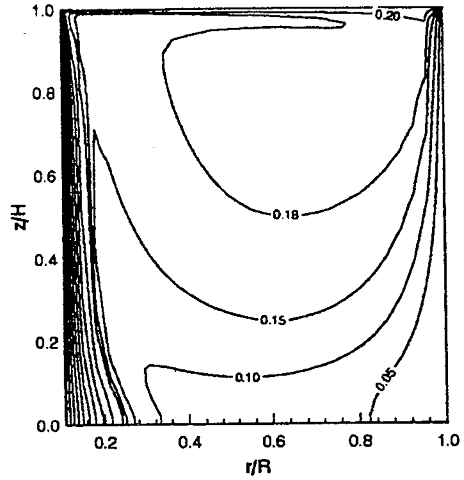
Isotherms for Run#1 Test CT3

Figure D8 Computed streamlines and isotherms

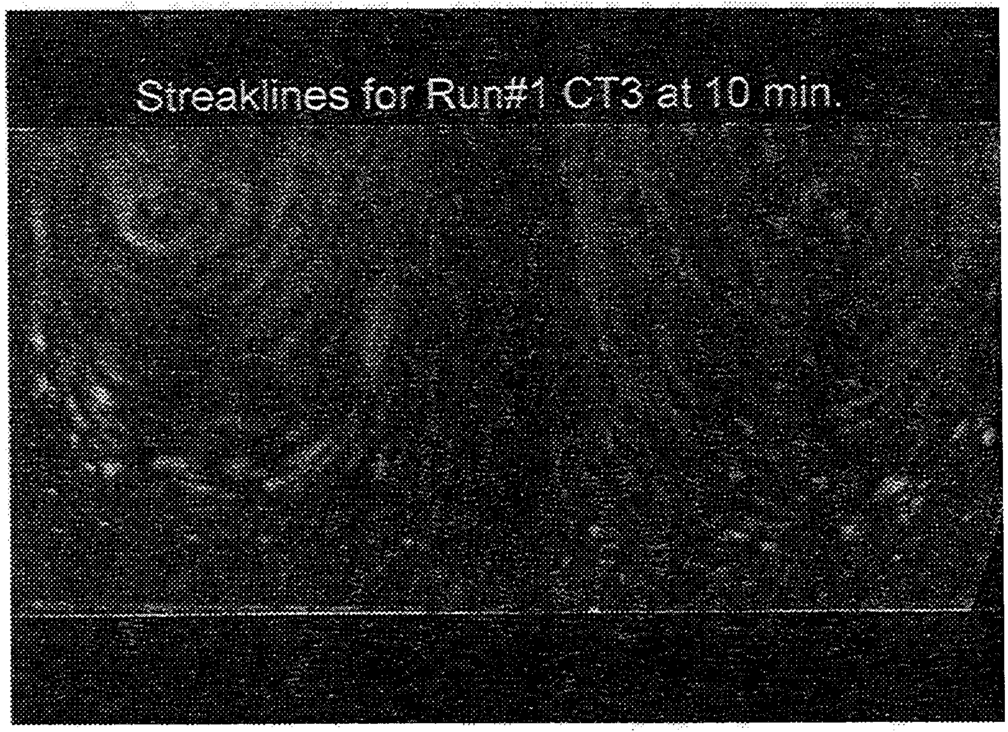

Figure D9 Experimental pathlines

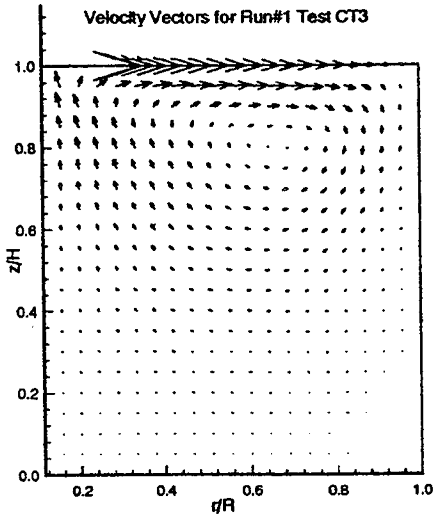

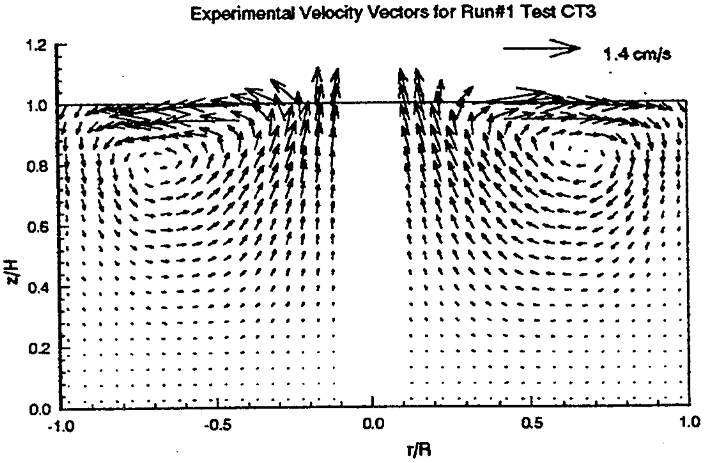

Figure D10 Computed and measured velocity vectors

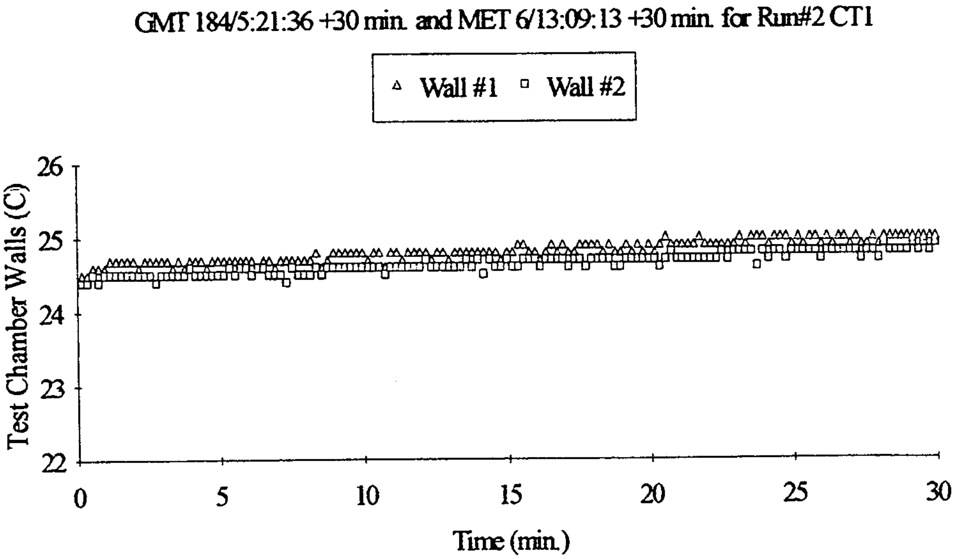

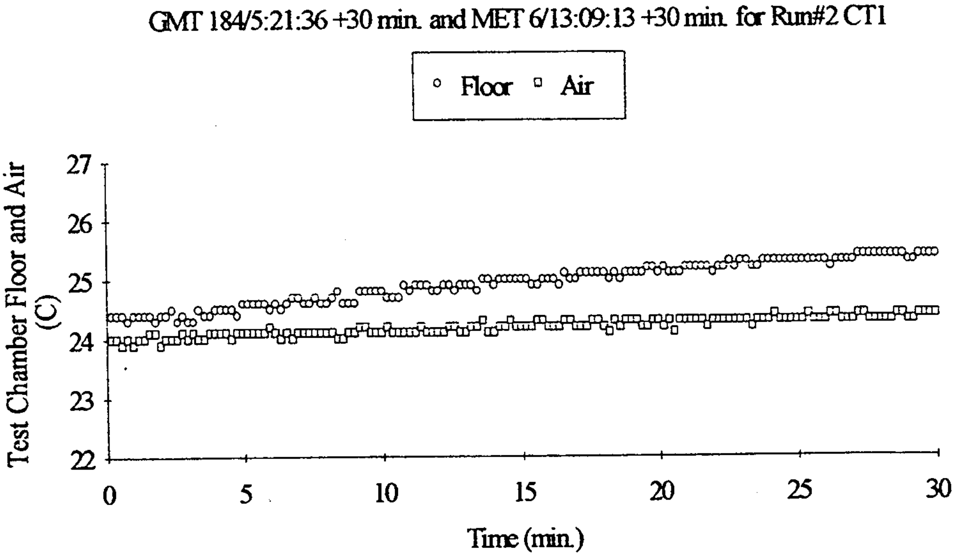

Figure D11 Thermistor data

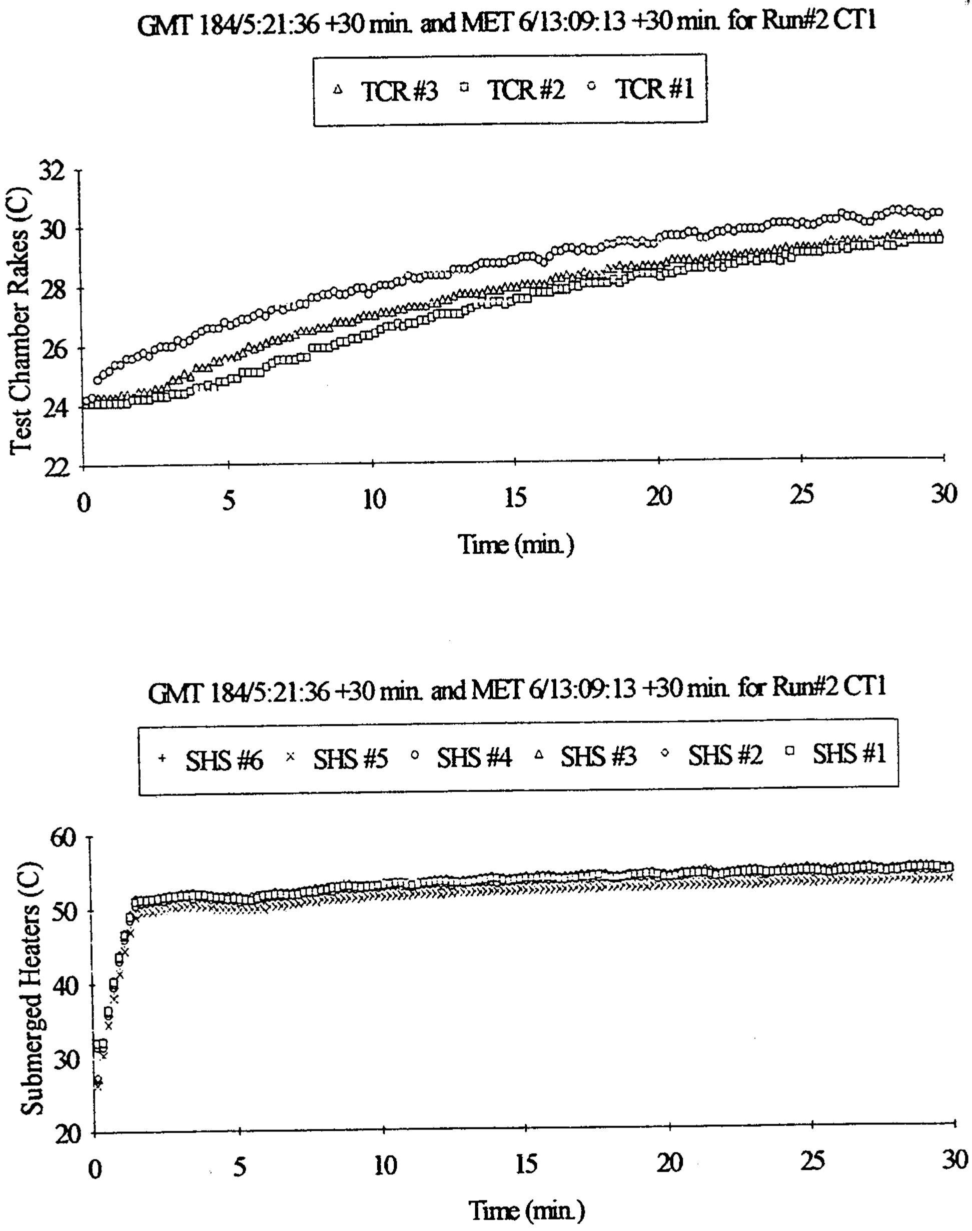

Figure D12 Thermistor data

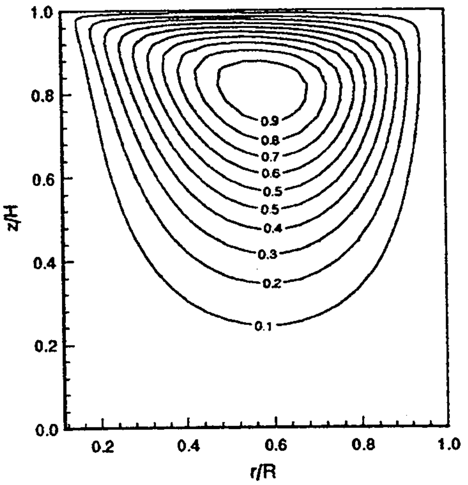
Streamlines for Run#2 Test CT1

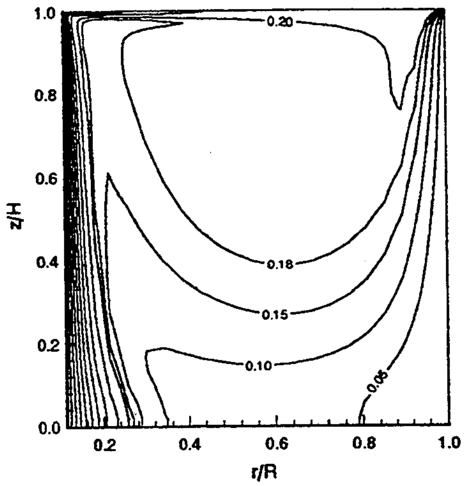
Isotherms for Run#2 Test CT1

Figure D13 Computed streamlines and isotherms

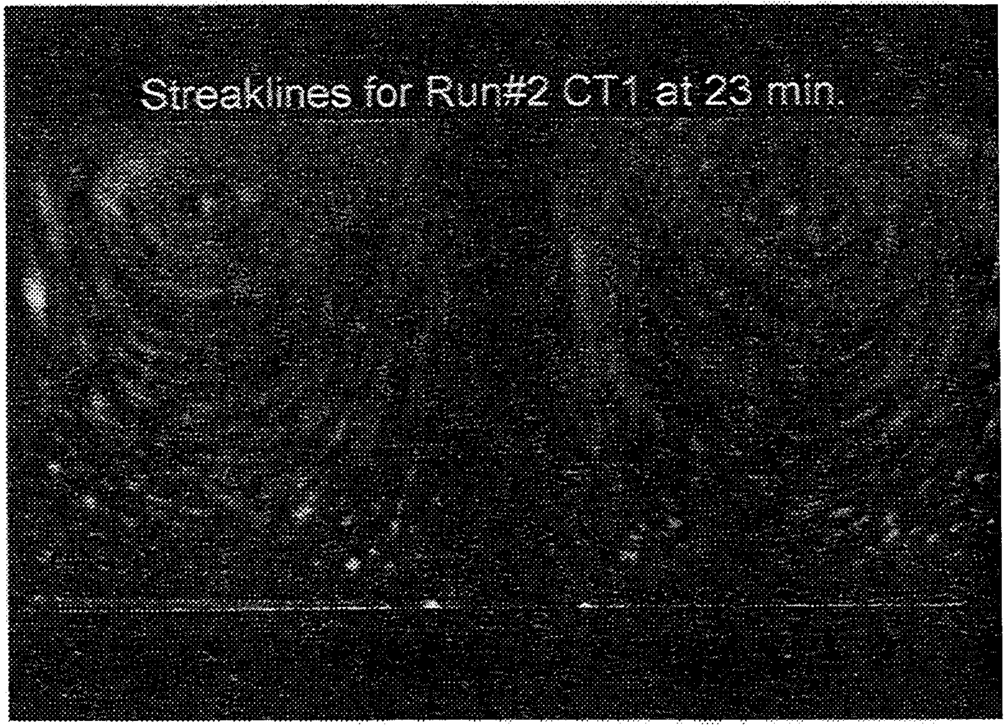

Figure D14 Experimental pathlines

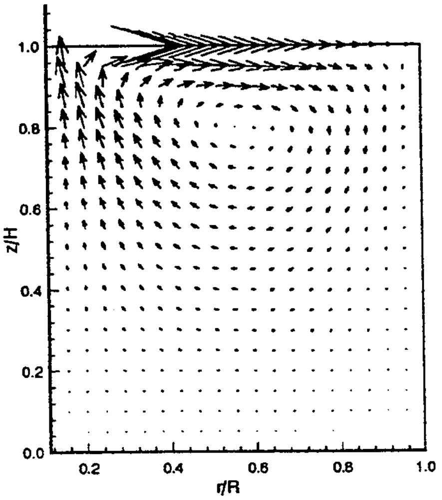

Velocity Vector for Run#2 Test CT1

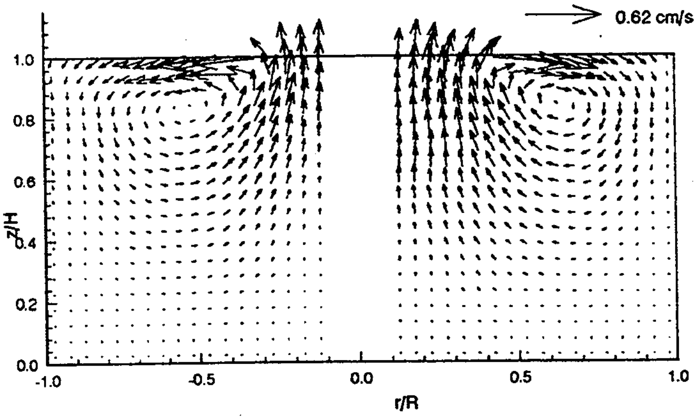

Experimental velocity Vectors for Run#2 Test CT1

Figure D15 Computed and measured velocity vectors

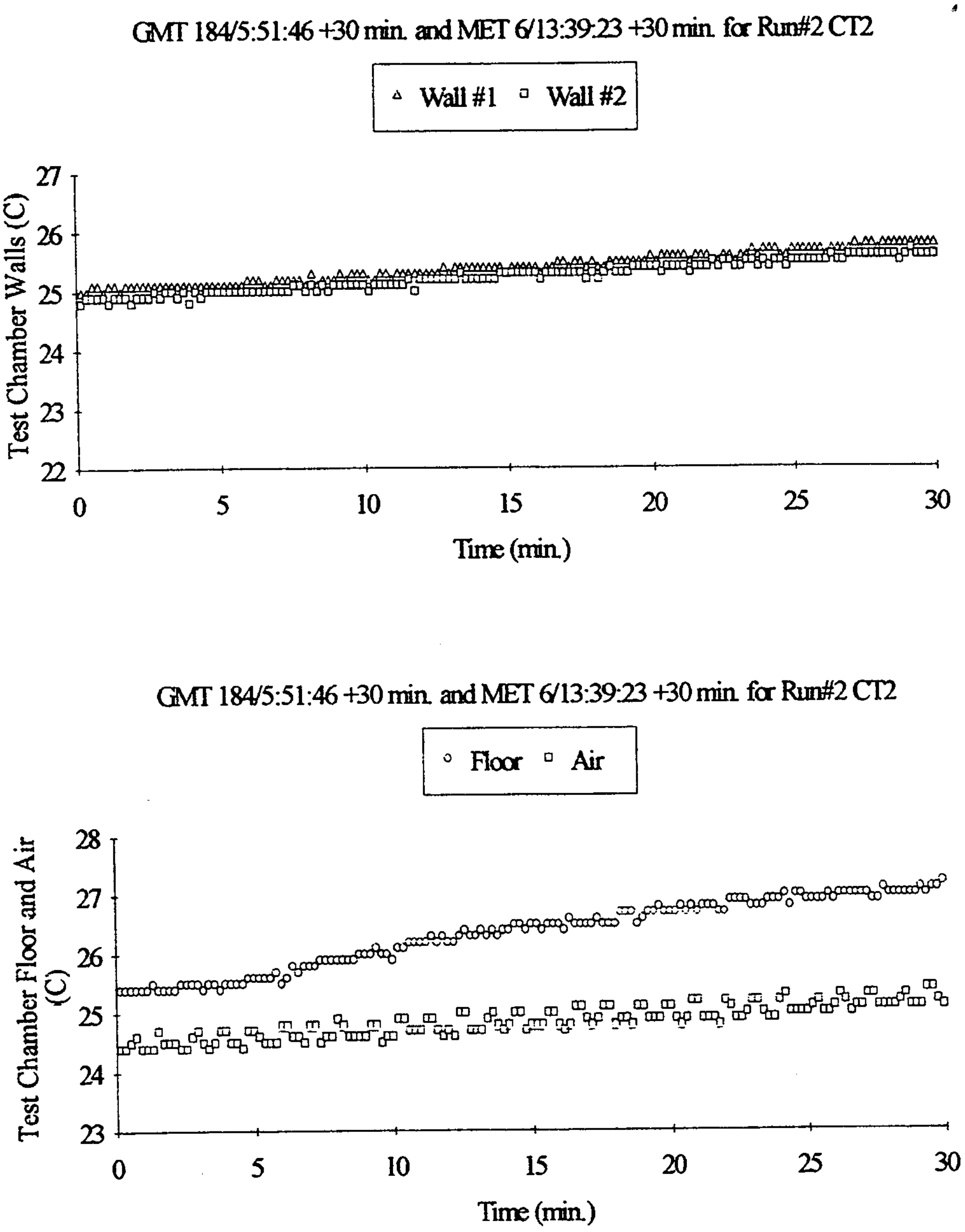

Figure D16 Thermistor data

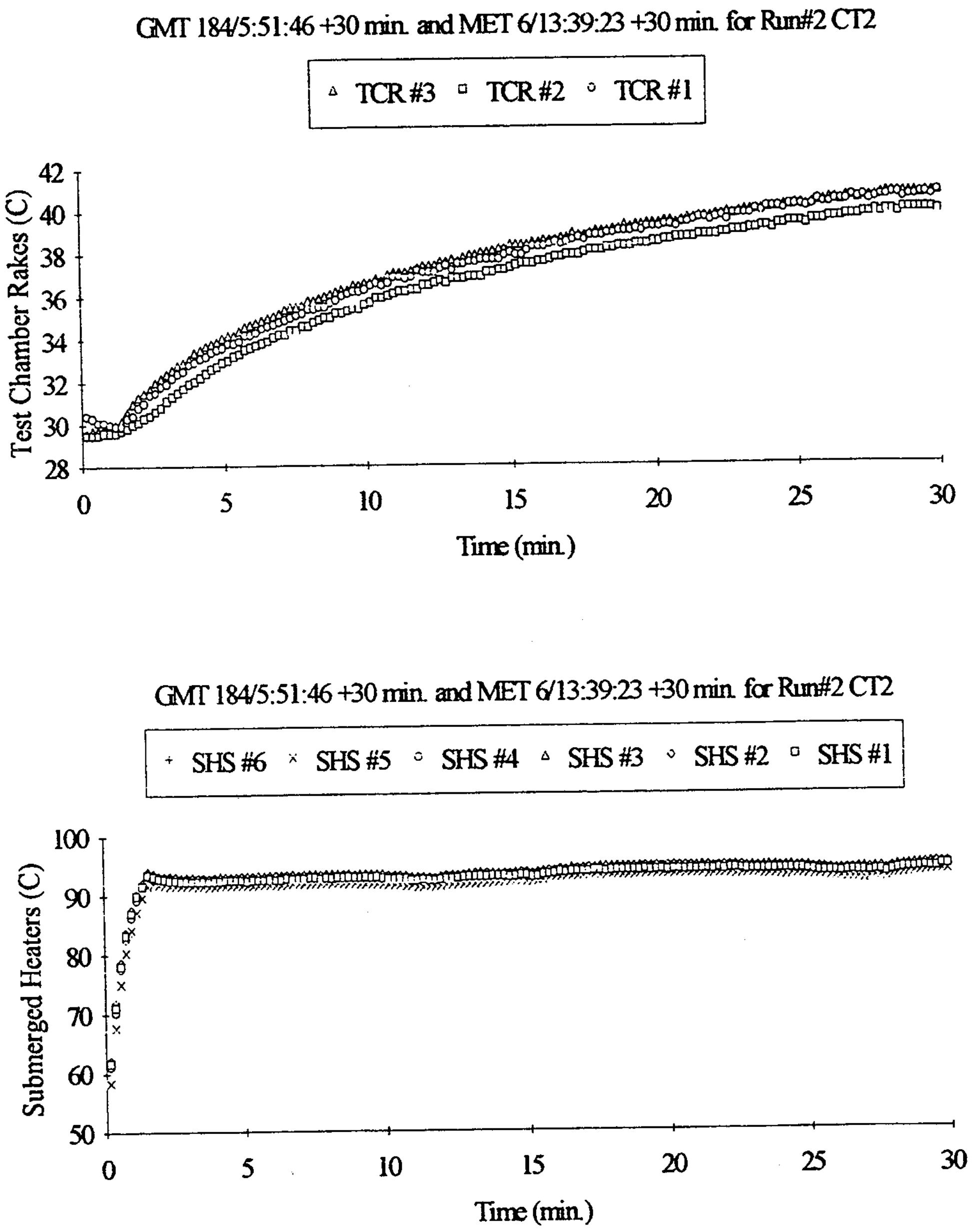

Figure D17 Thermistor data

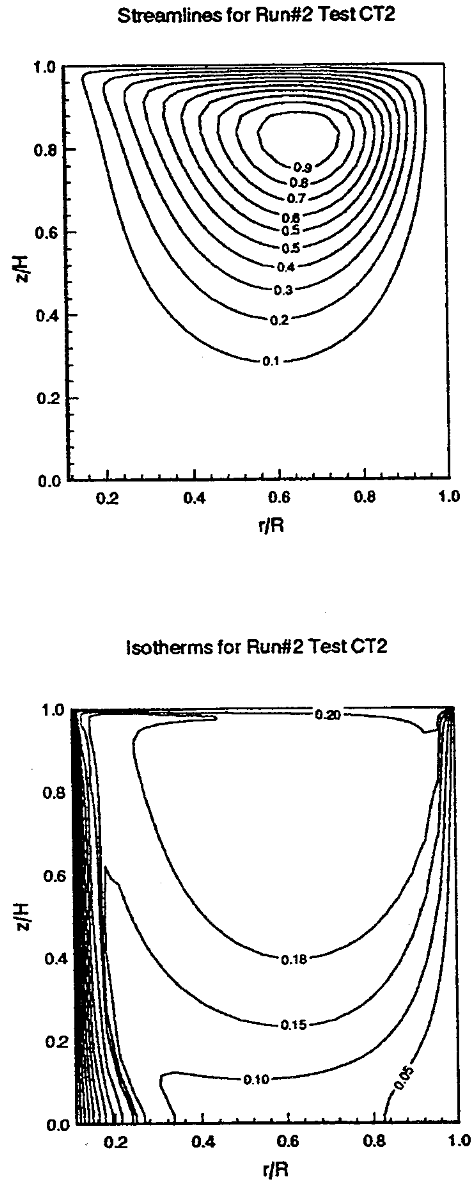

Figure D18 Computed streamlines and isotherms

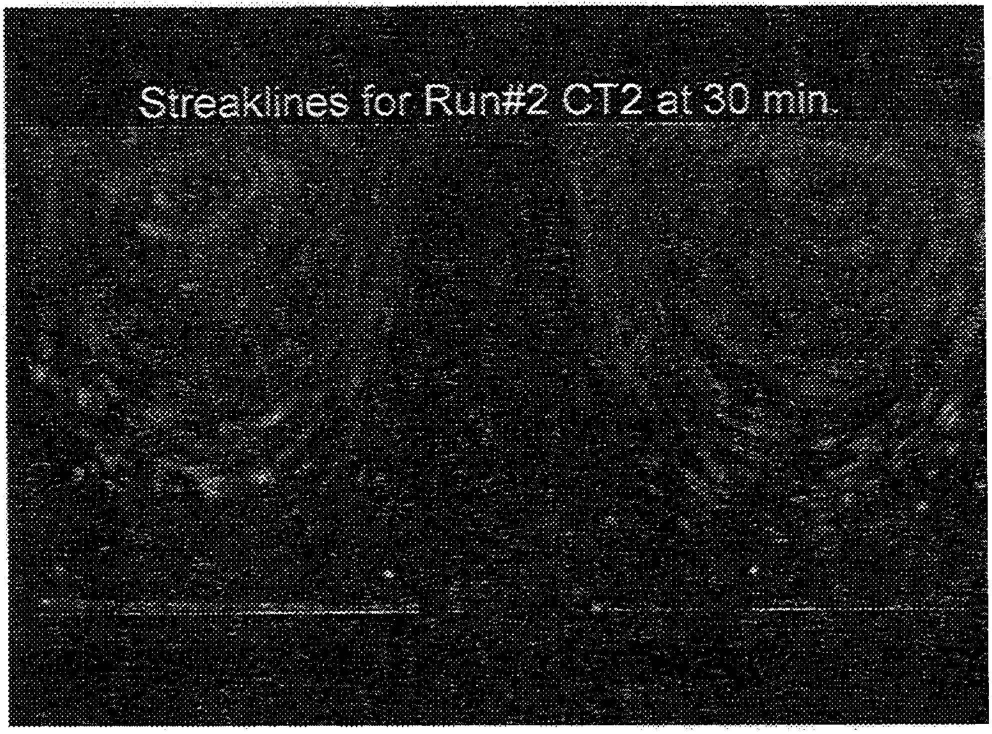

Figure D19 Experimental pathlines

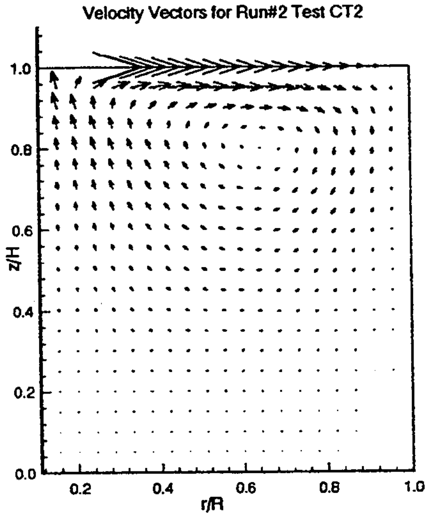

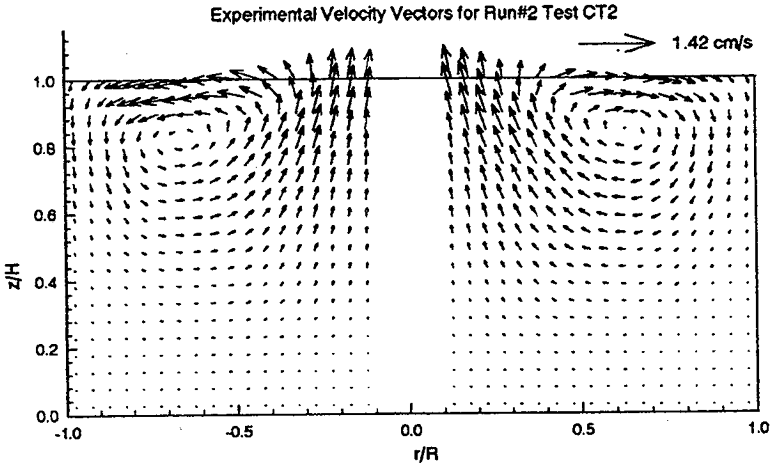

Figure D20 Computed and measured velocity vectors

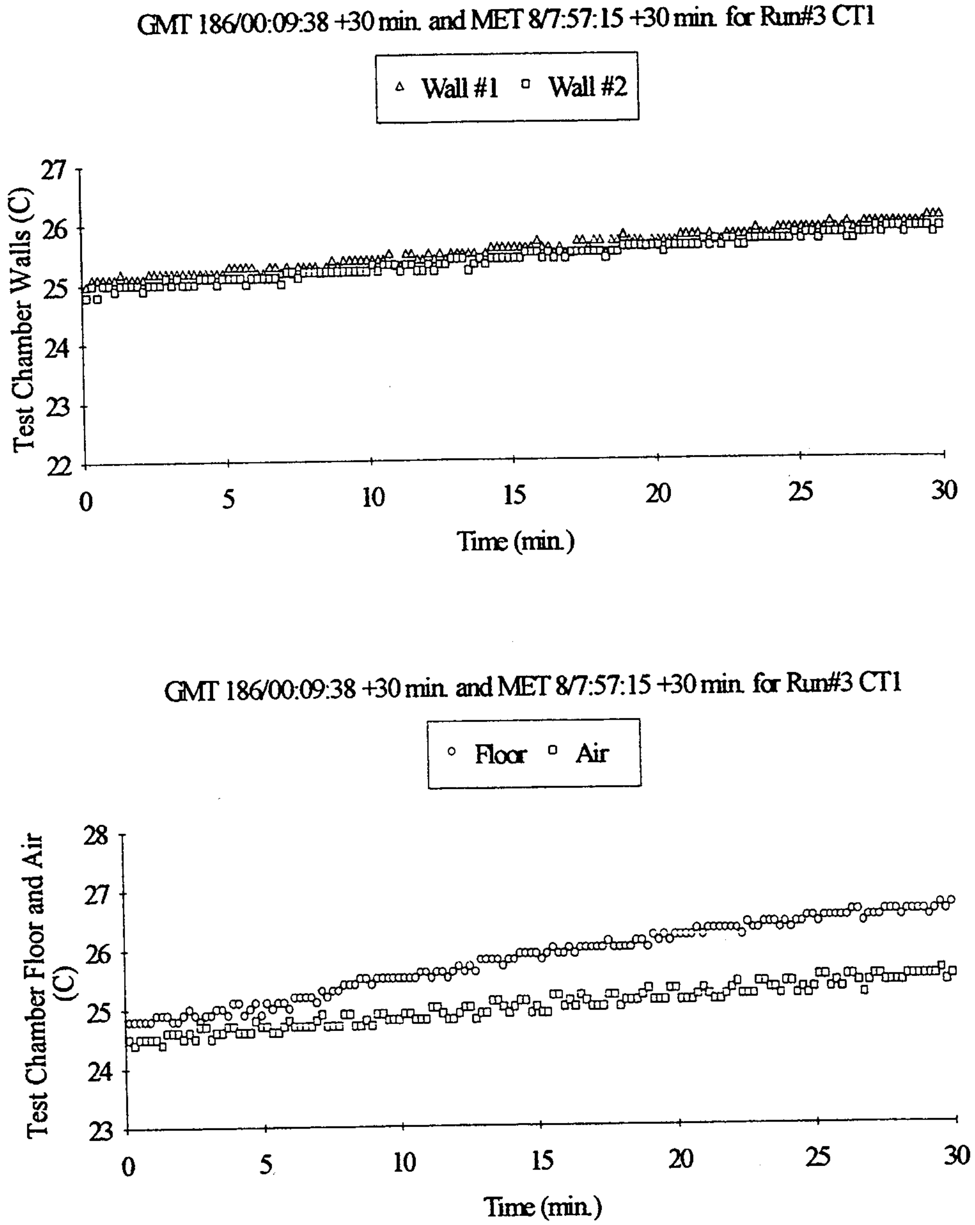

GMT 186/00:09:38 +30 min. and MET 8/7:57:15 +30 min. for Run#3 CT1

GMT 186/00:09:38 +30 min. and MET 8/7:57:15 +30 min. for Run#3 CT1

Figure D21 Thermistor data

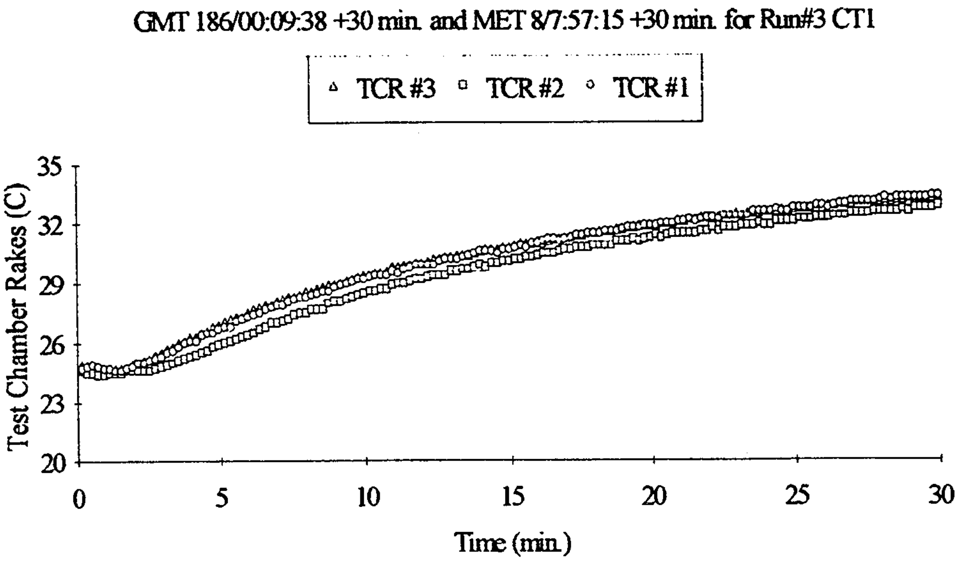

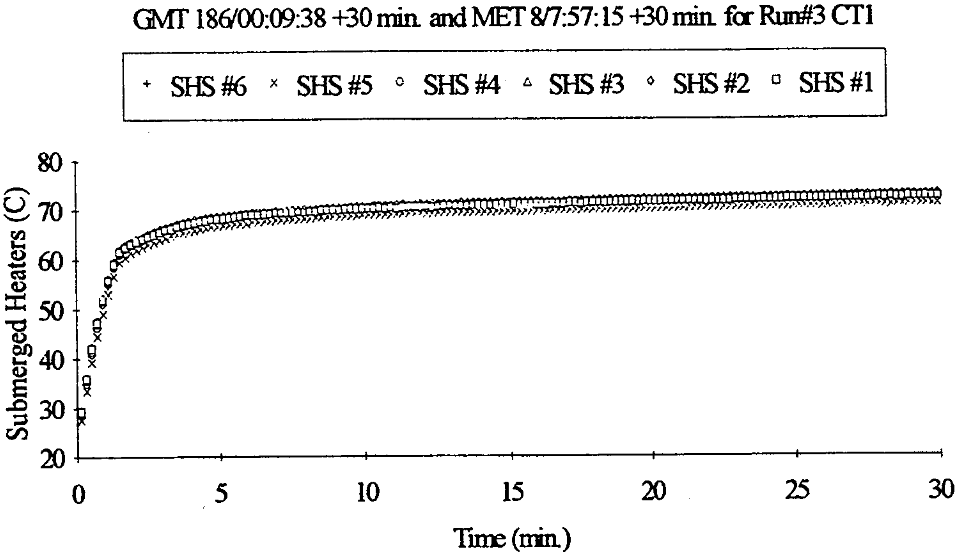

Figure D22 Thermistor data

Streamlines for Run#3 Test CT1

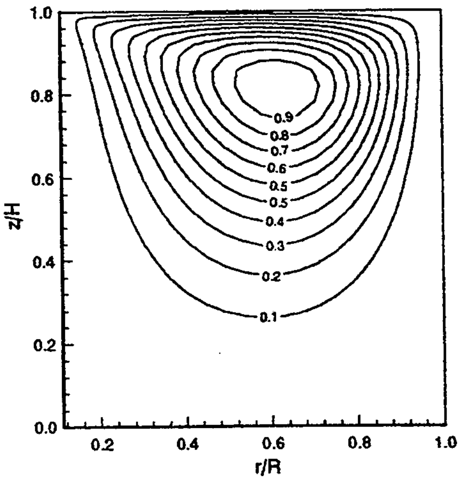

Isothems for Run#3 Test CT1

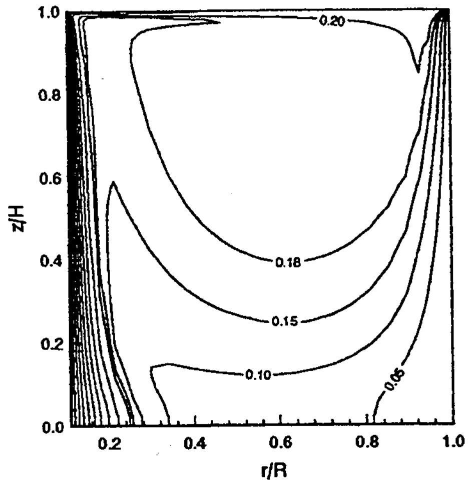

Figure D23 Computed streamlines and isotherms

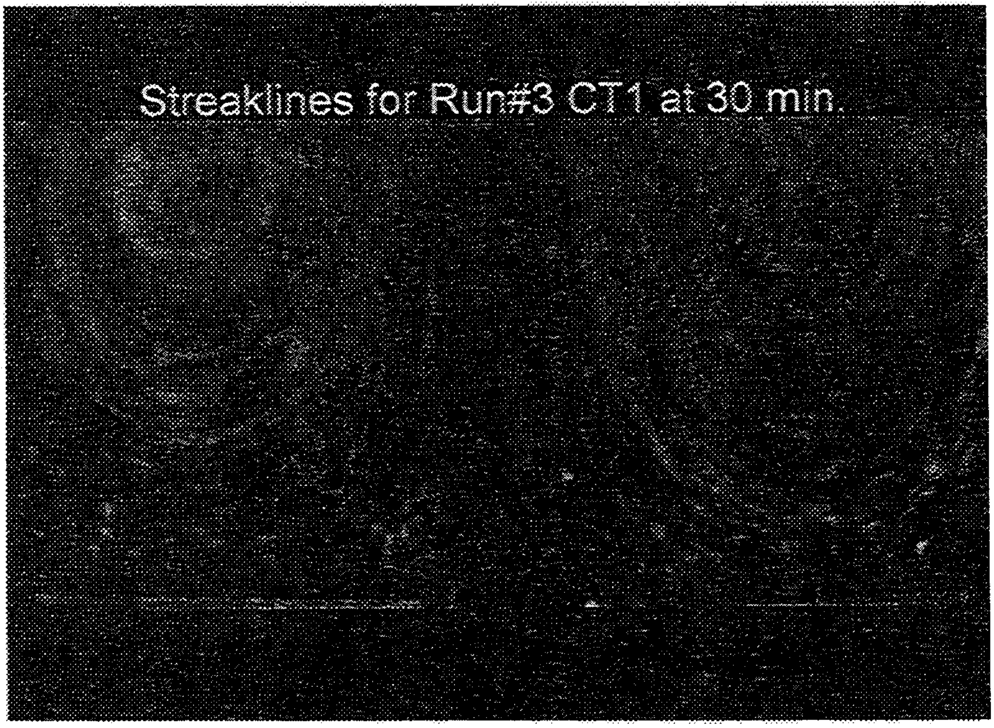

Figure D24 Experimental pathlines

Velocity Vectors for Run#3 Test CT1

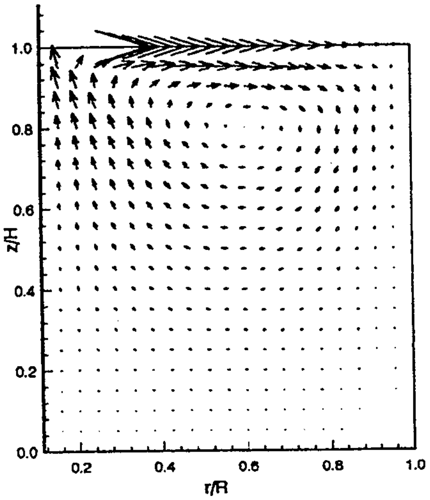

Experimental Velocity Vectors for Run#3 Test CT1

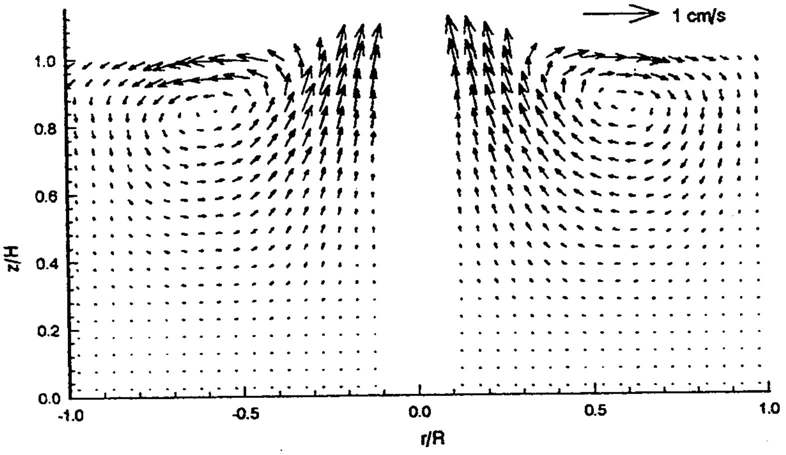

Figure D25 Computed and measured velocity vectors

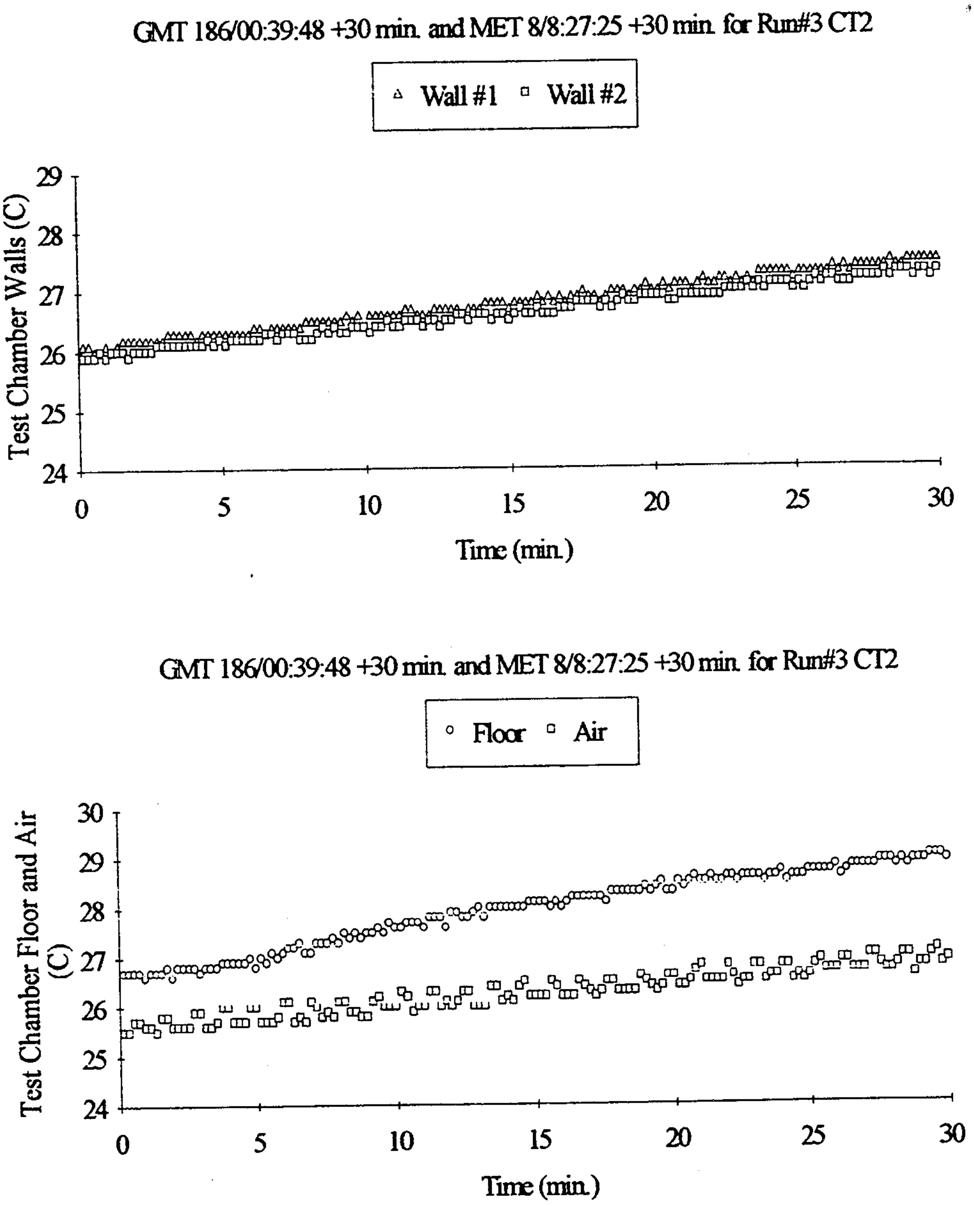

Figure D26 Thermistor data

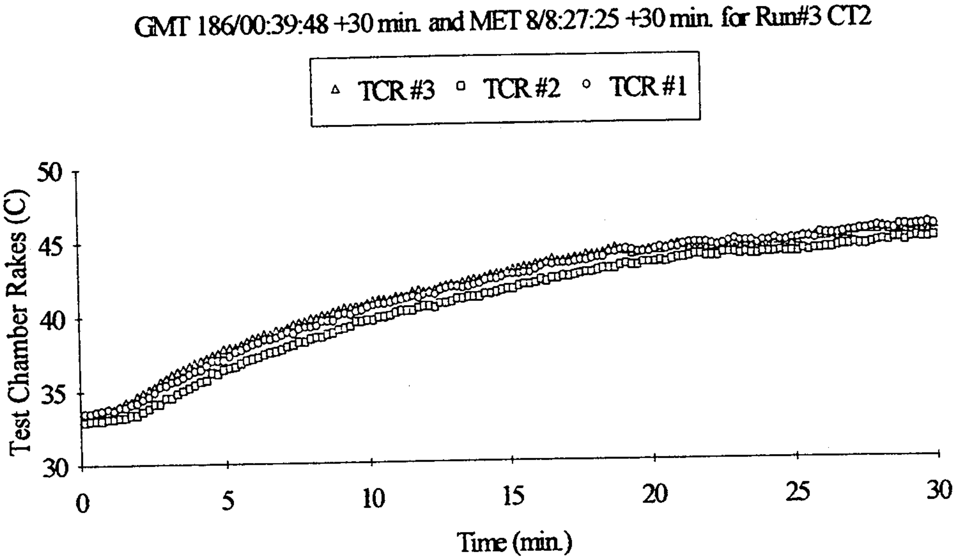

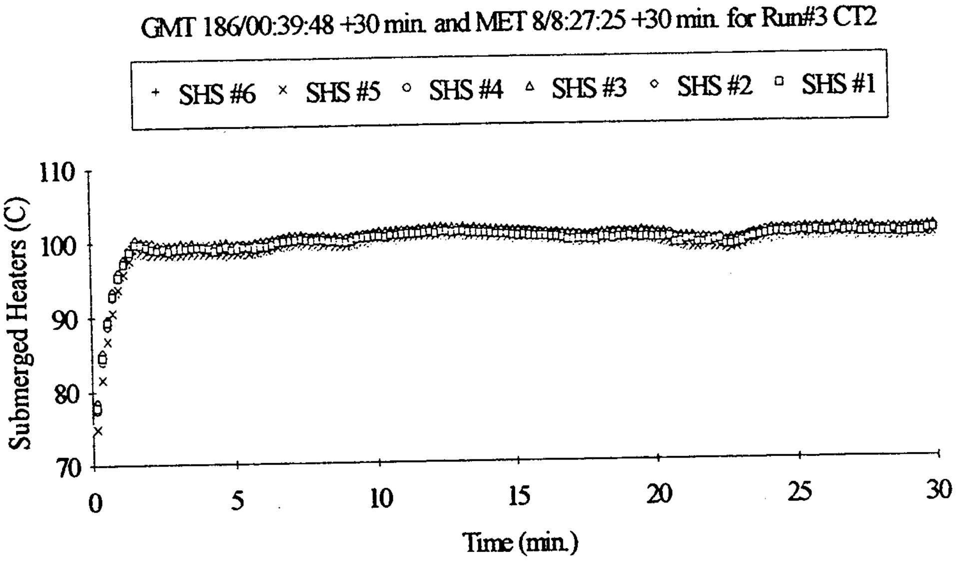

Figure D27 Thermistor data

Streamlines for Run#3 Test CT2

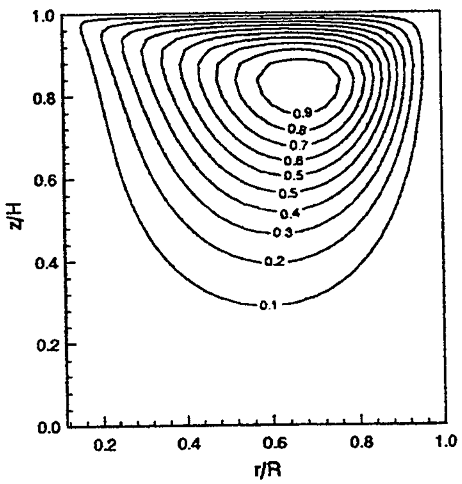

Isotherms for Run#3 Test CT2

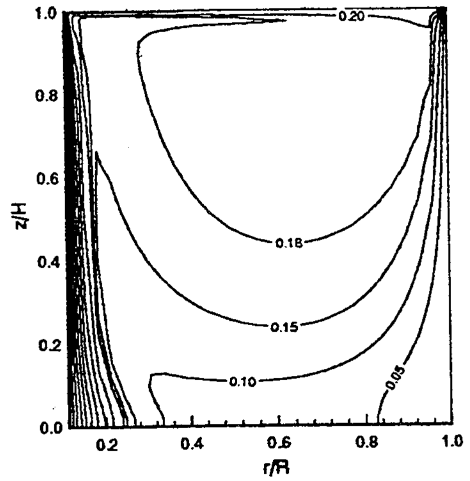

Figure D28 Computed streamlines and isotherms

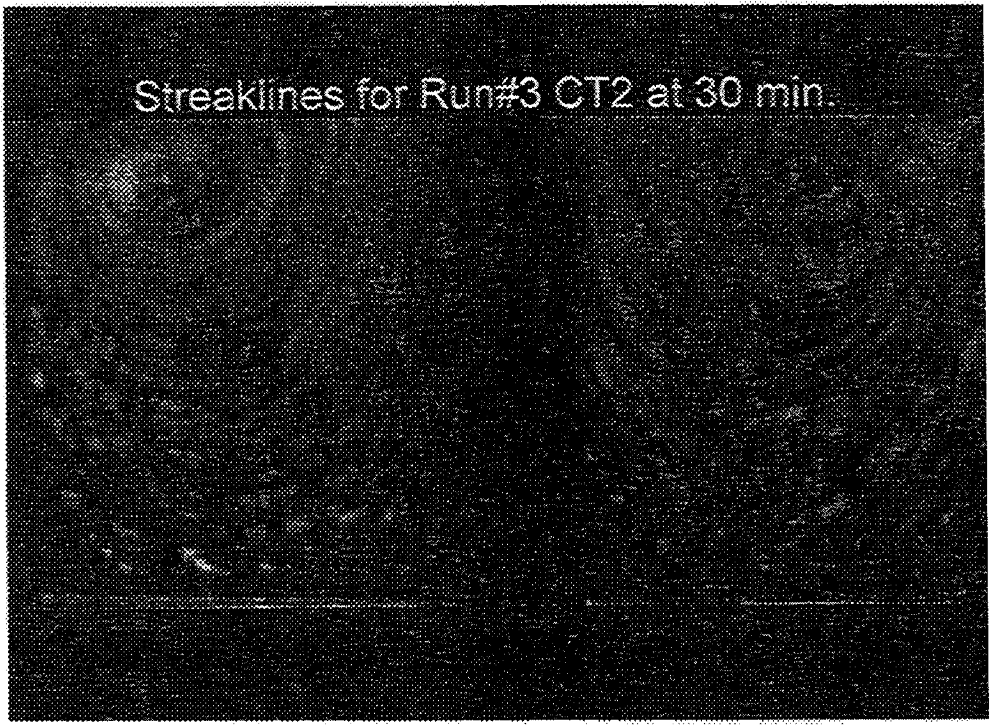

Figure D29 Experimental pathlines

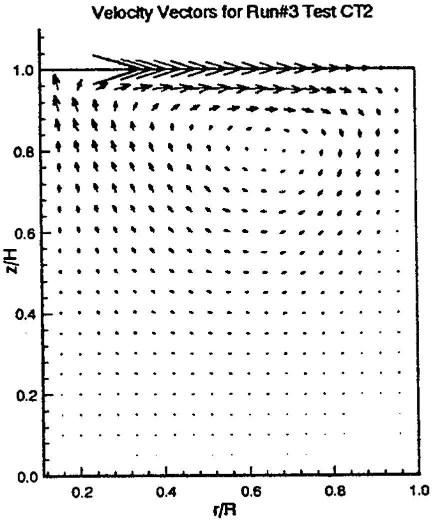

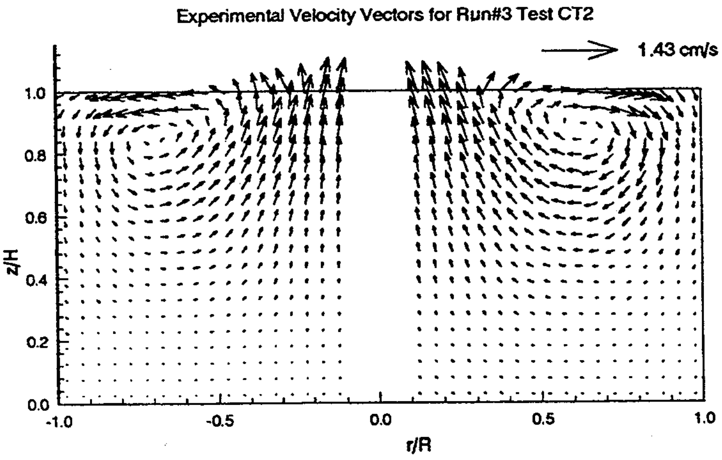

Figure D30 Computed and measured velocity vectors

APPENDIX E

CF CURVED SHORTER TESTS

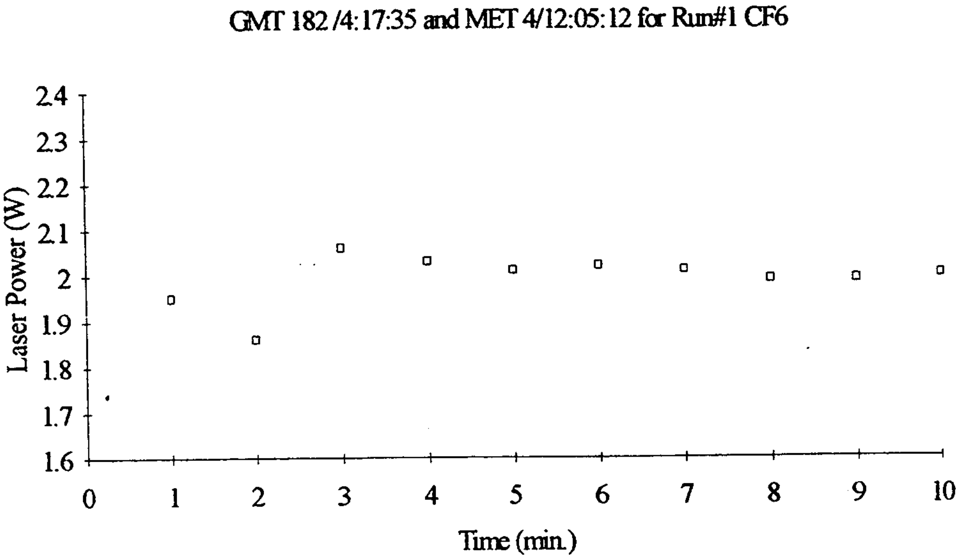

Figure E1 Laser power

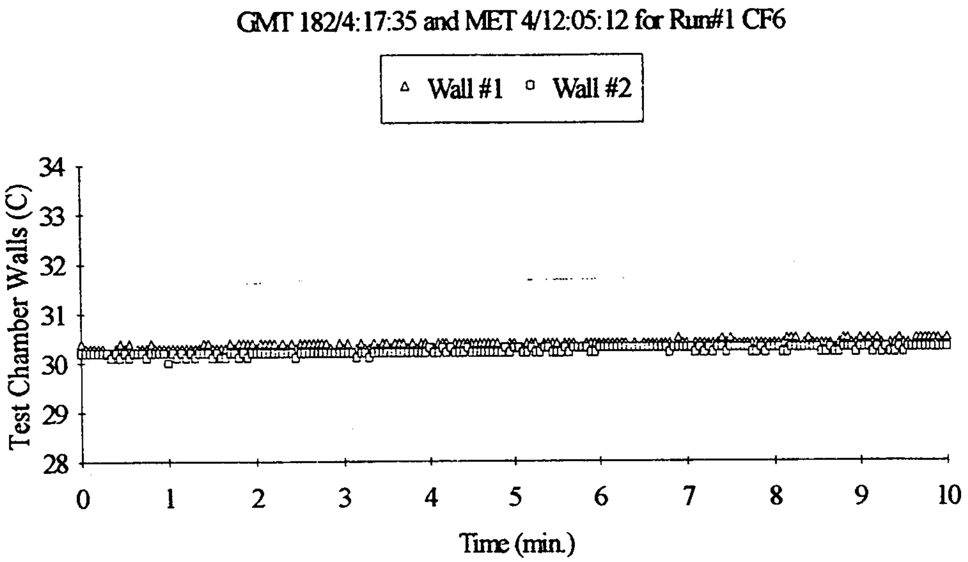

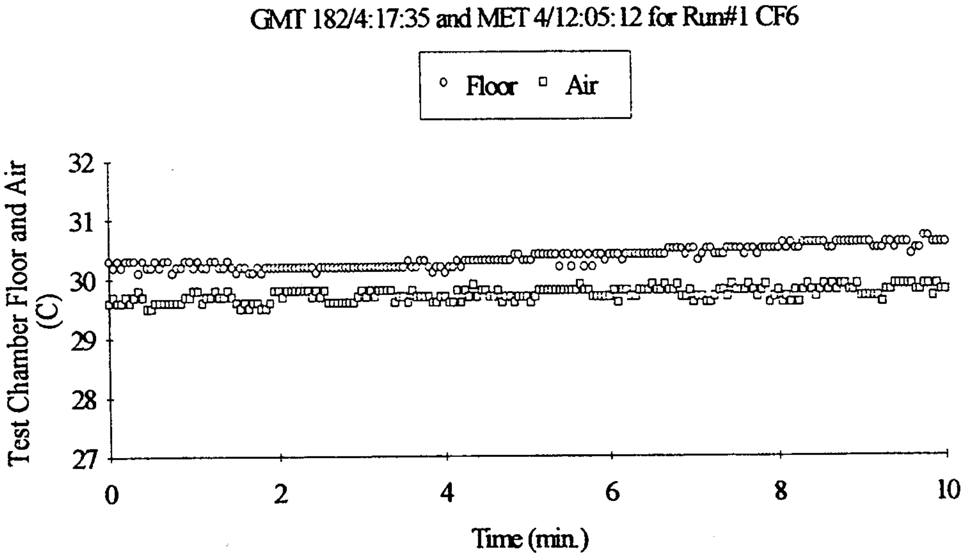

Figure E2 Thermistor data

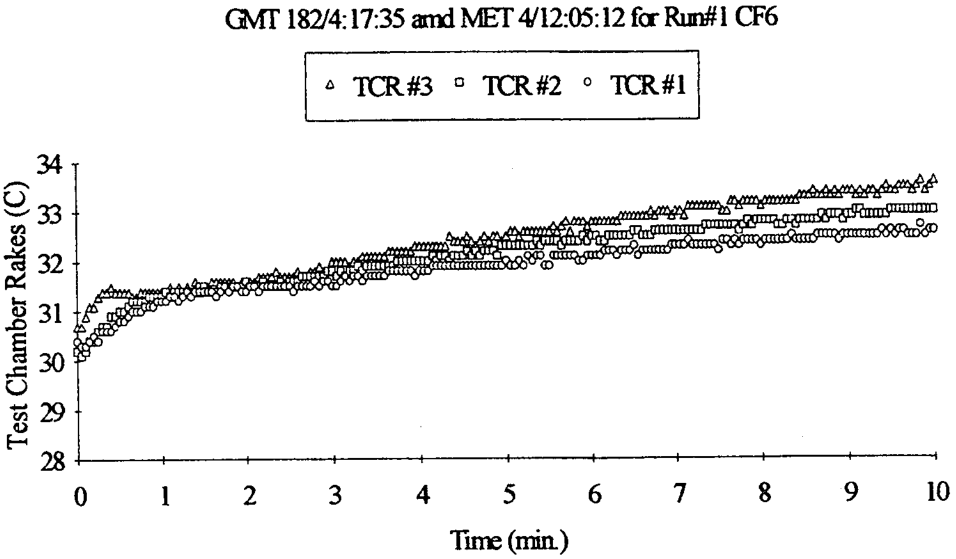

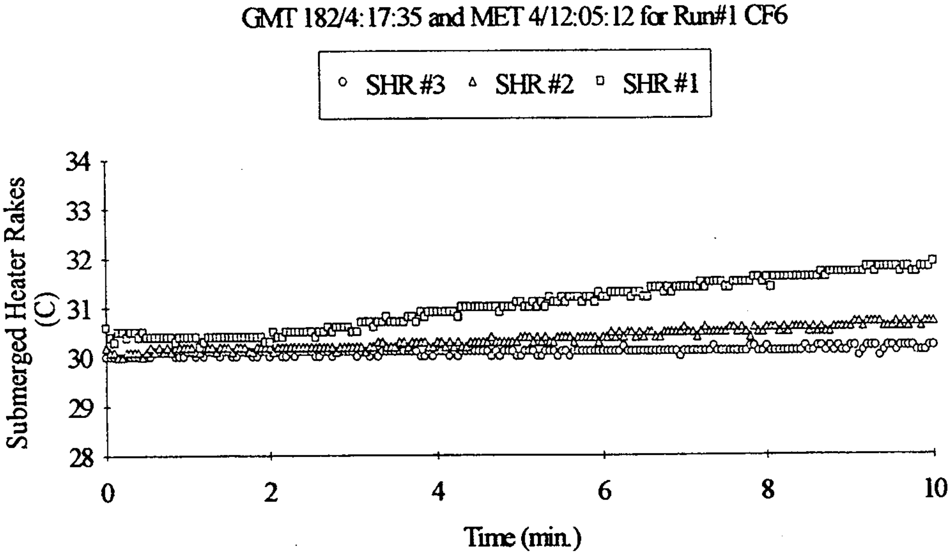

Figure E3 Thermistor data

Streamlines for Run#1 Test CF6

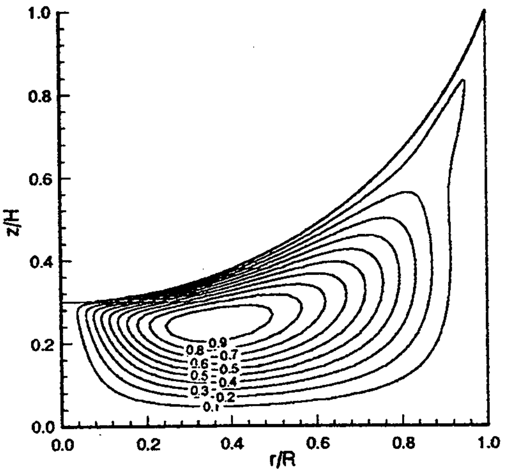

Isotherms for Run#1 Test CF6

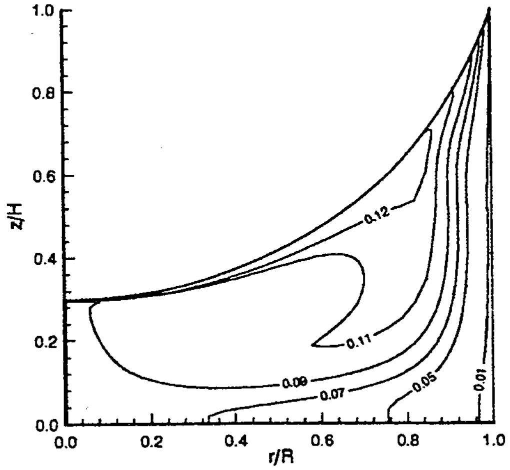

Figure E4 Computed streamlines and isotherms

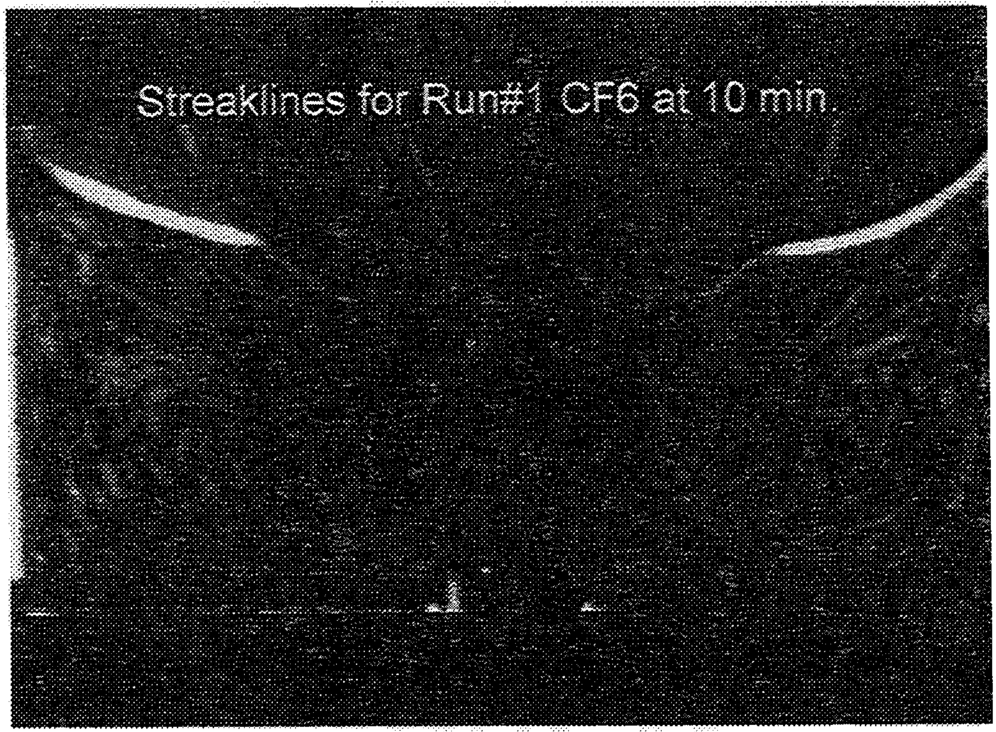

Figure E5 Experimental pathlines

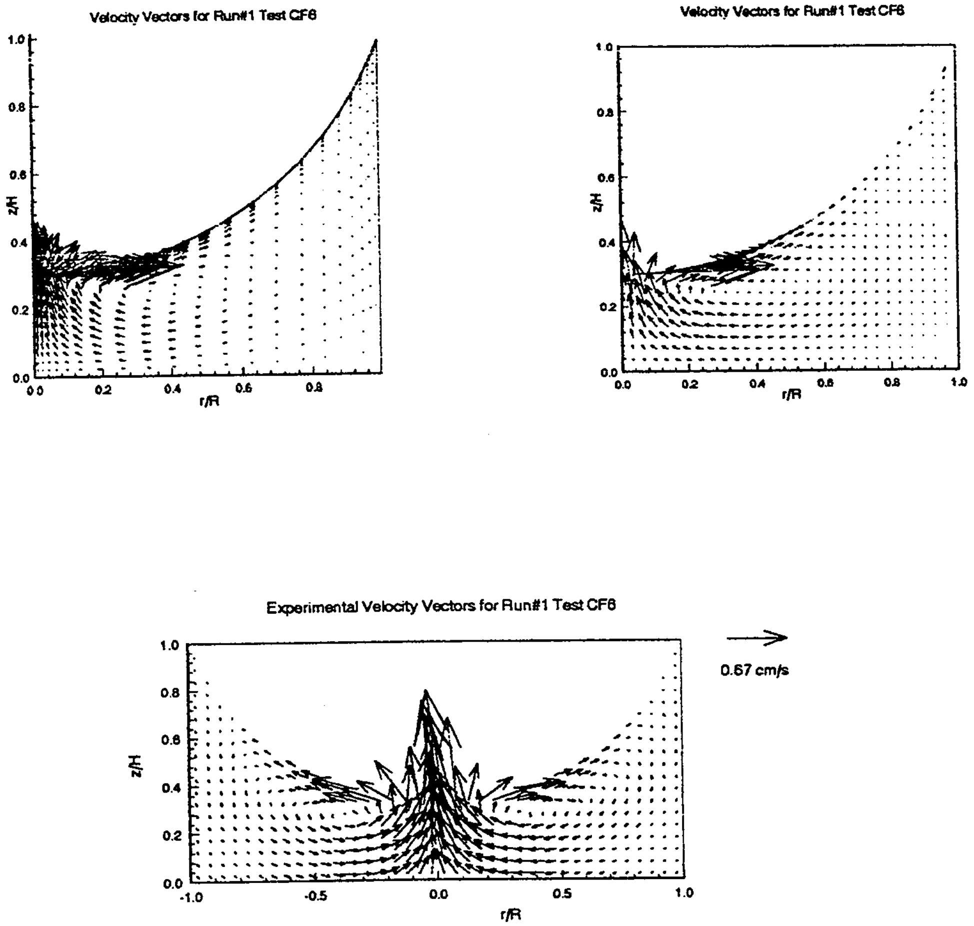

Figure E6 Computed and measured velocity vectors

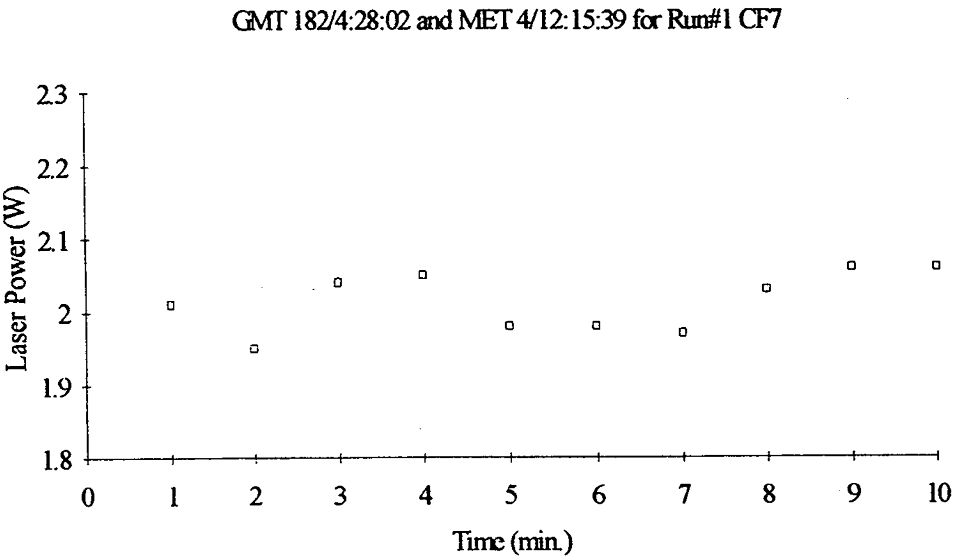

Figure E7 Laser power

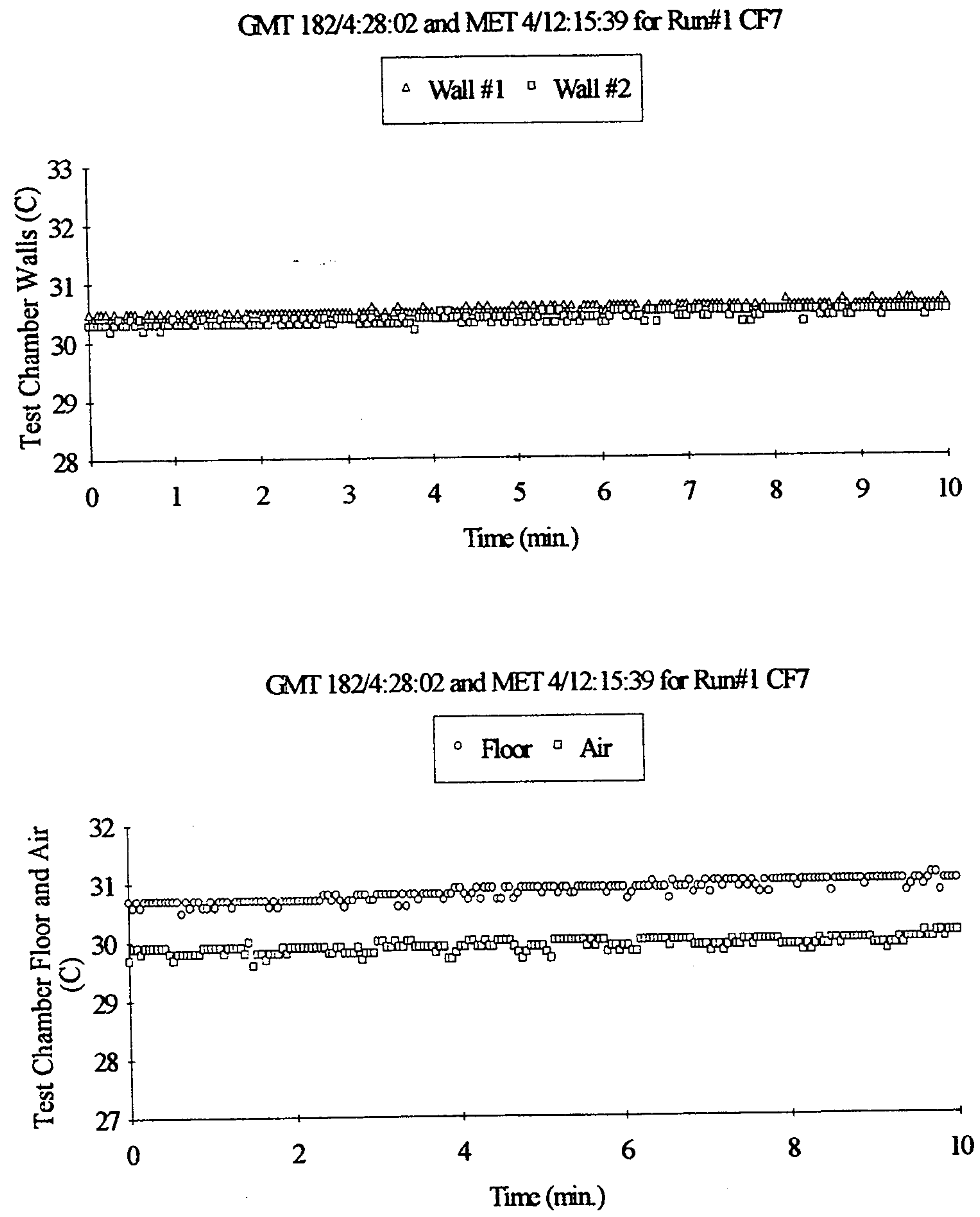

Figure E8 Thermistor data

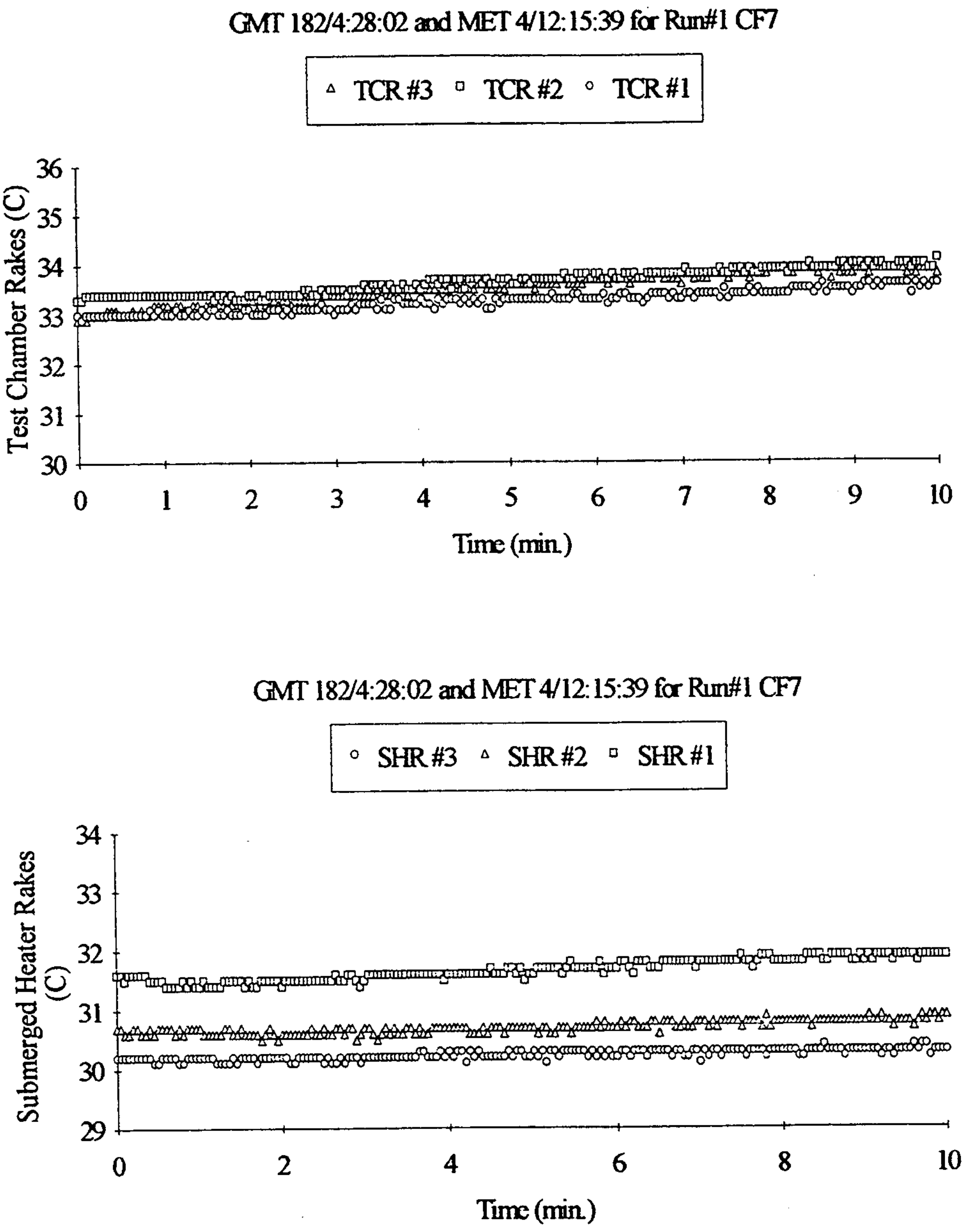

Figure E9 Thermistor data

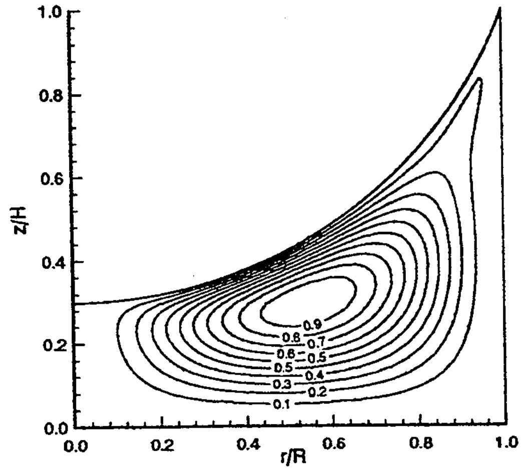

Streamlines for Run#1 Test CF7

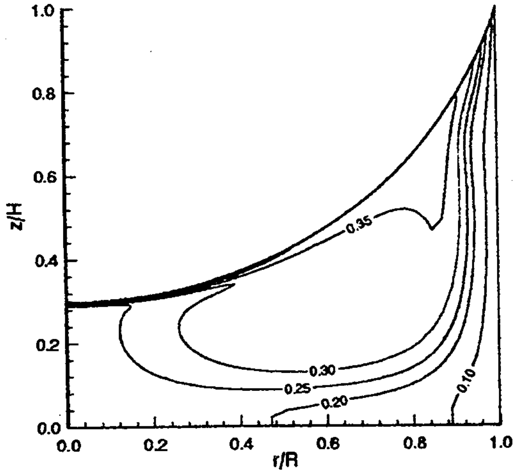

Isotherms for Run#1 Test CF7

Figure E10 Computed streamlines and isotherms

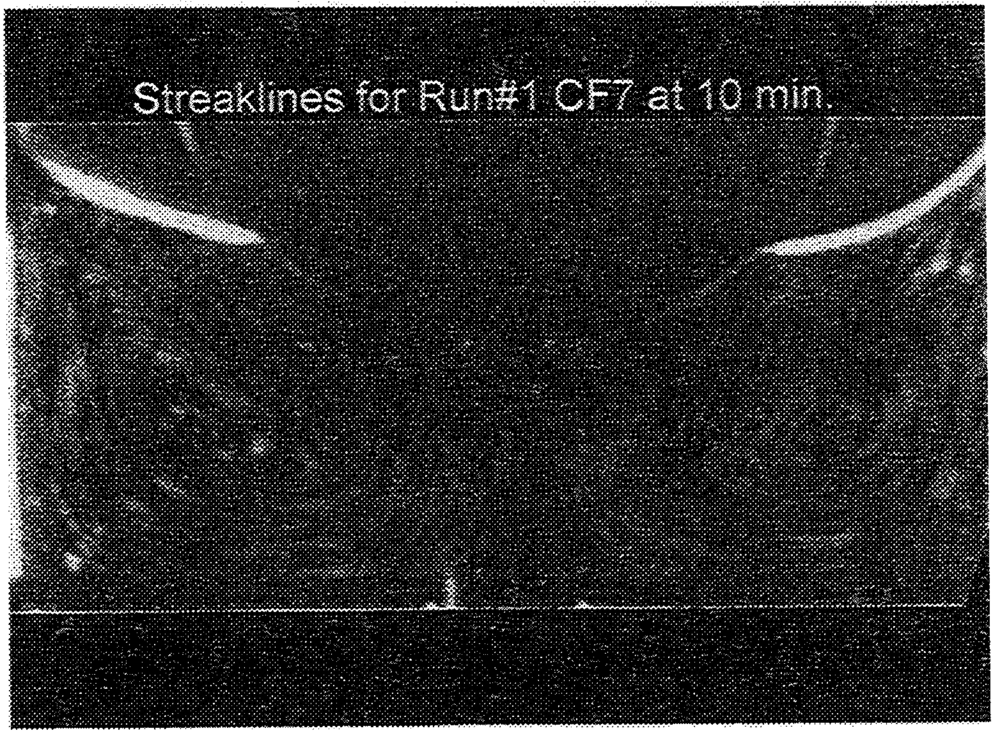

Figure E11 Experimental pathlines

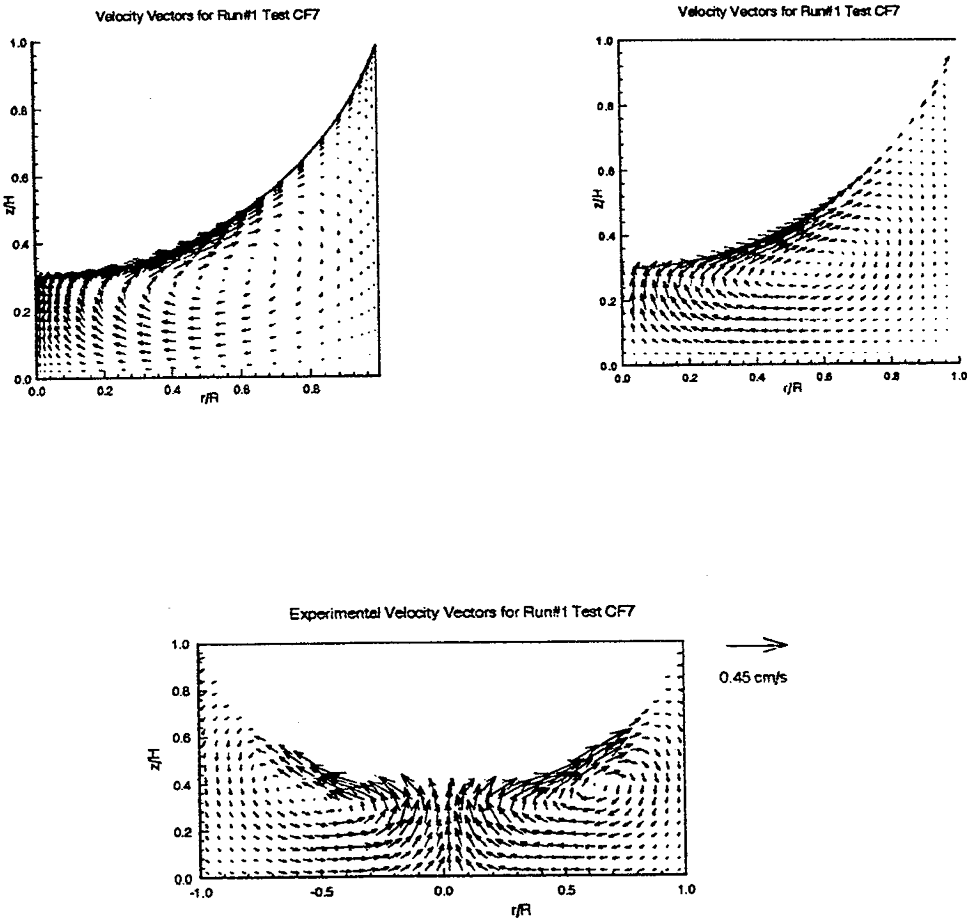

Figure E12 Computed and measured velocity vectors

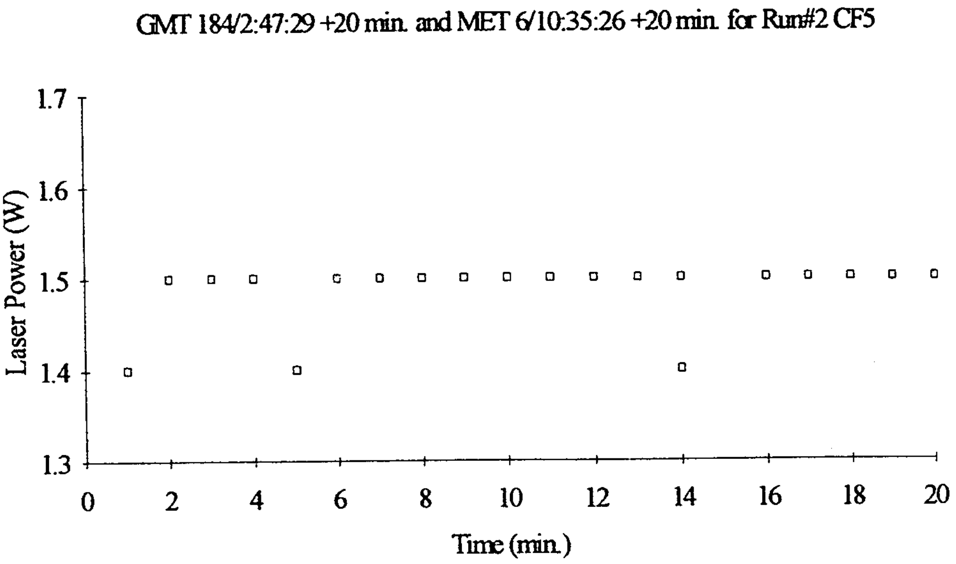

Figure E13 Laser power

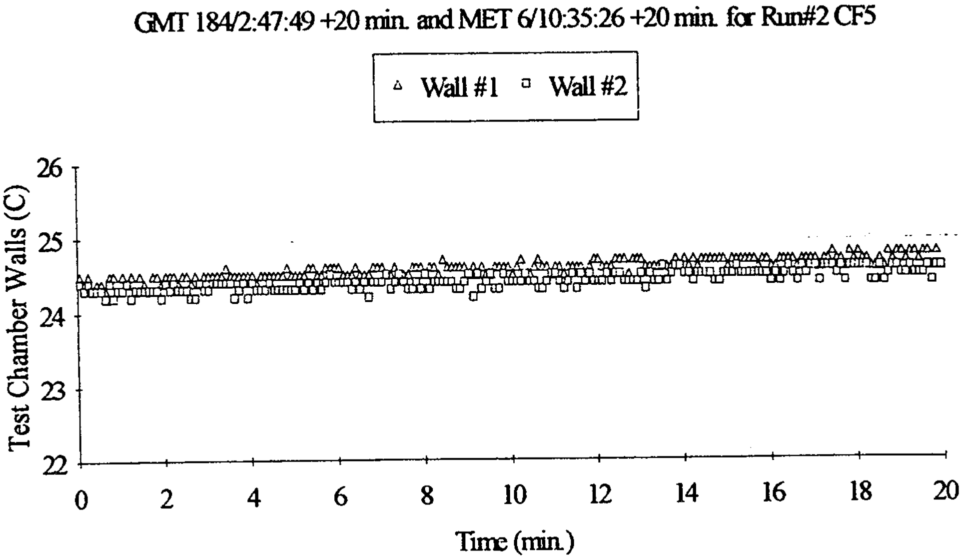

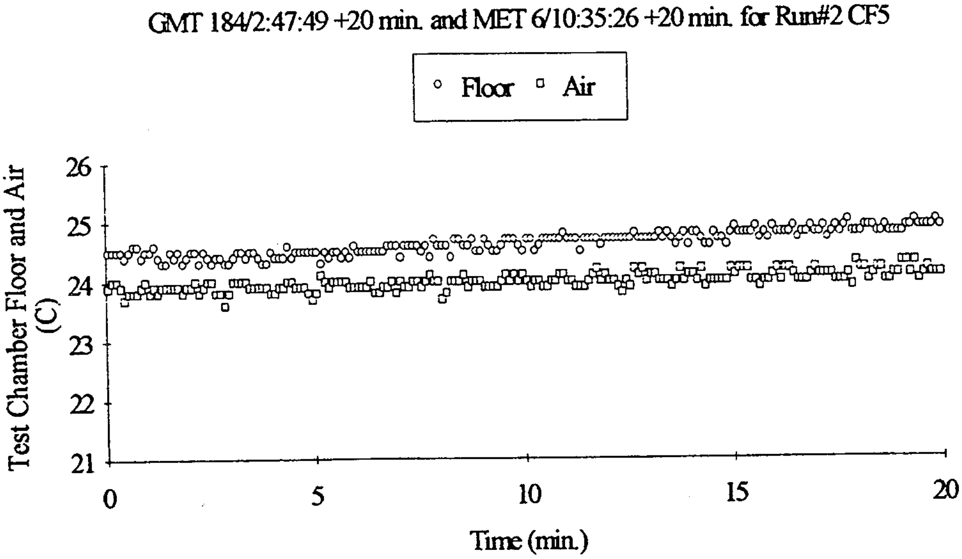

Figure E14 Thermistor data

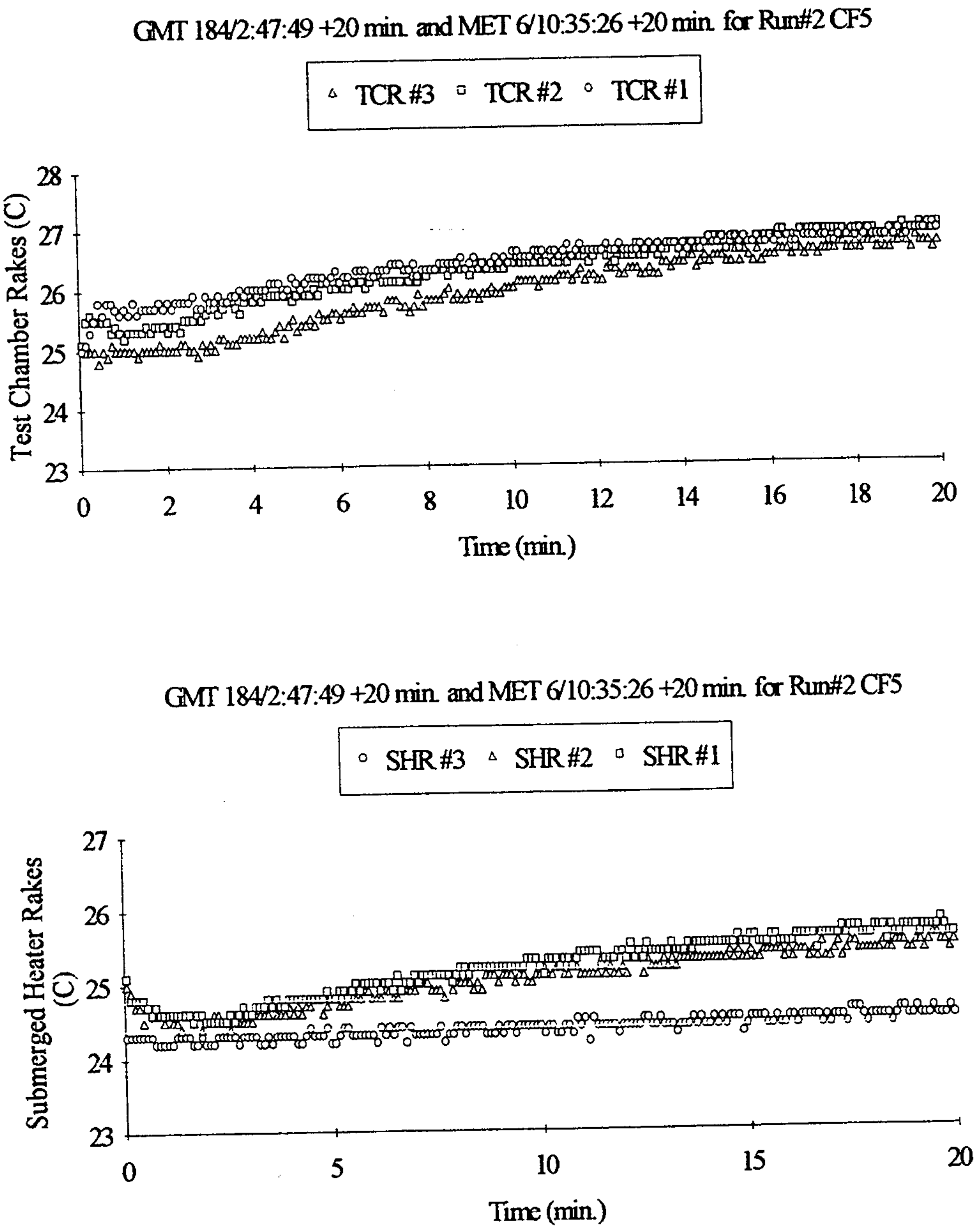

Figure E15 Thermistor data

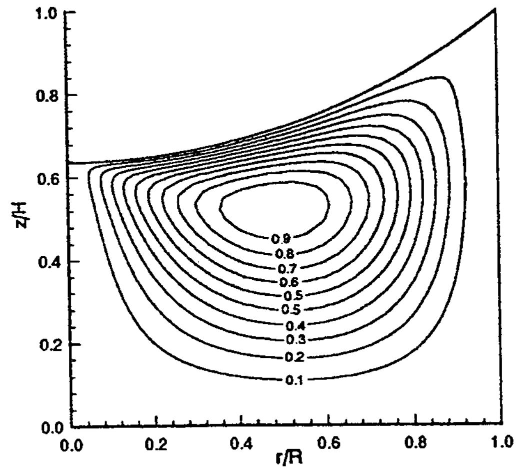
Streamlines for Run#2 Test CF5

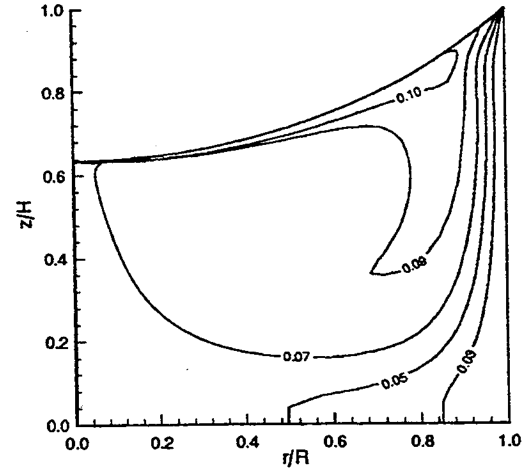
Isotherms for Run#2 Test CF5

Figure E16 Computed streamlines and isotherms

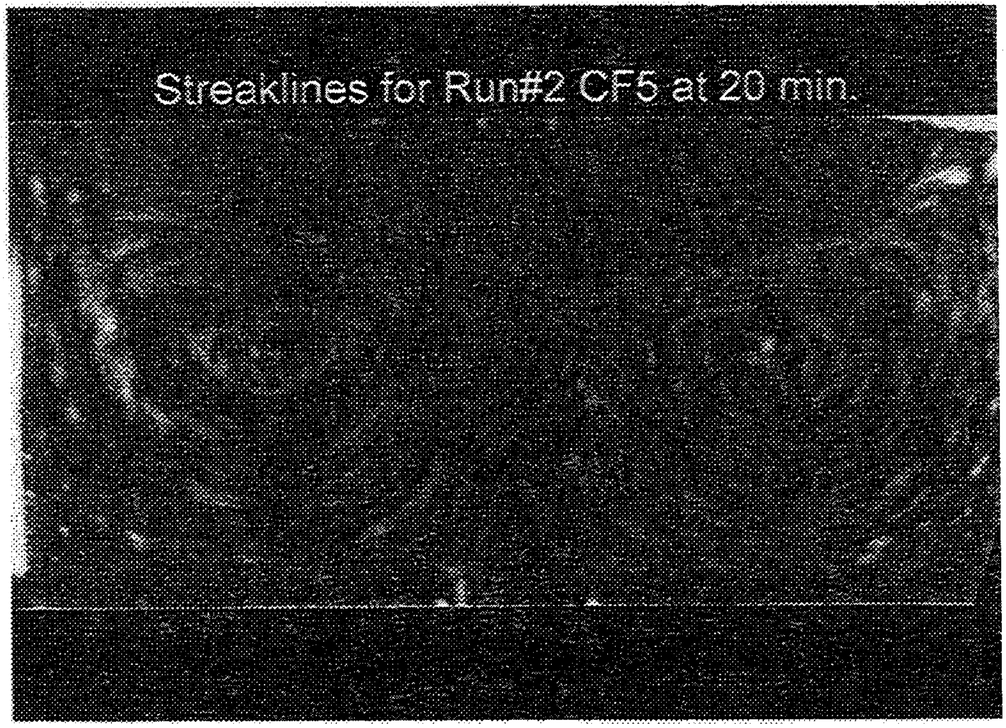

Figure E17 Experimental pathlines

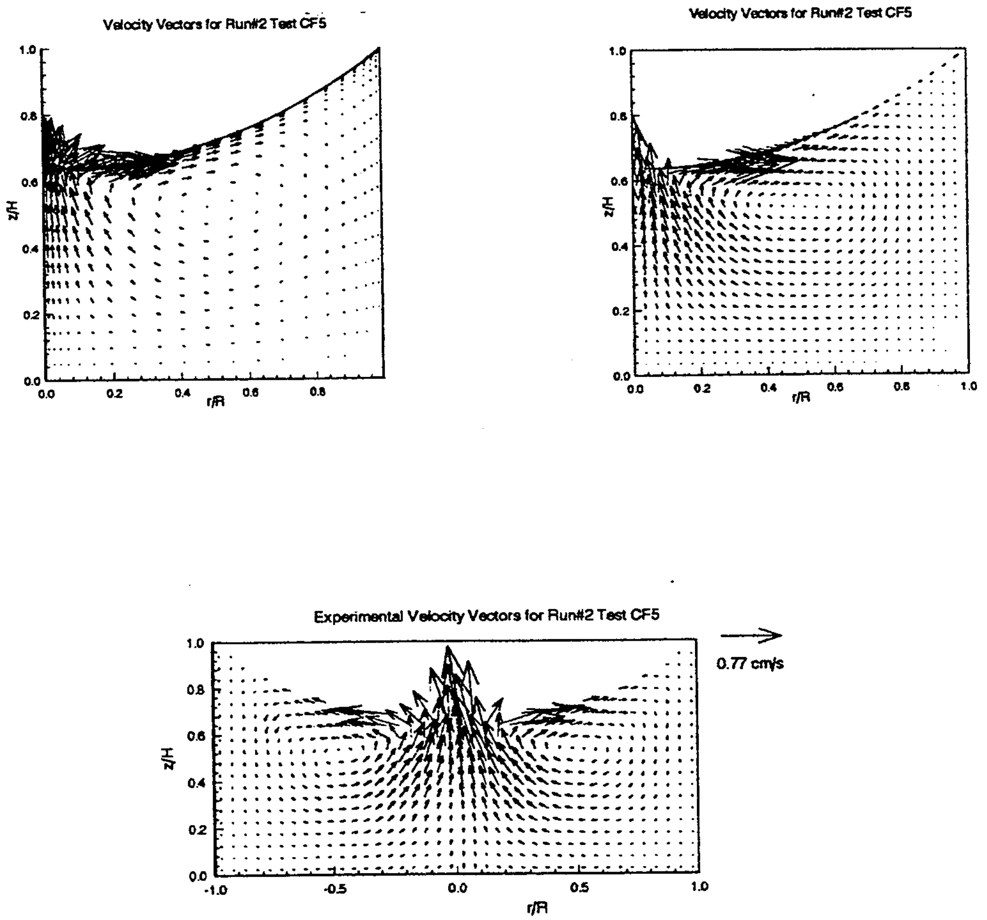

Figure E18 Computed and measured velocity vectors

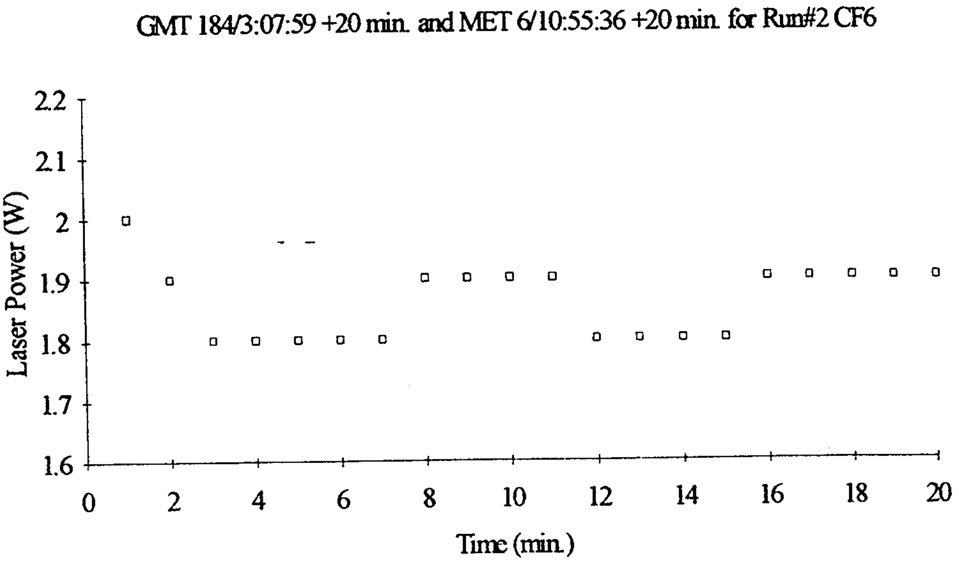

Figure E19 Laser power

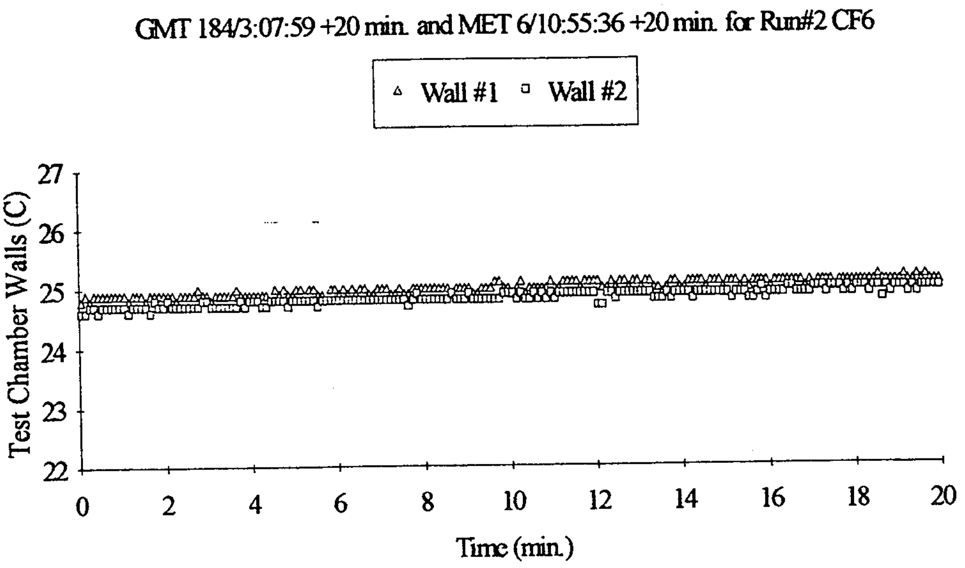

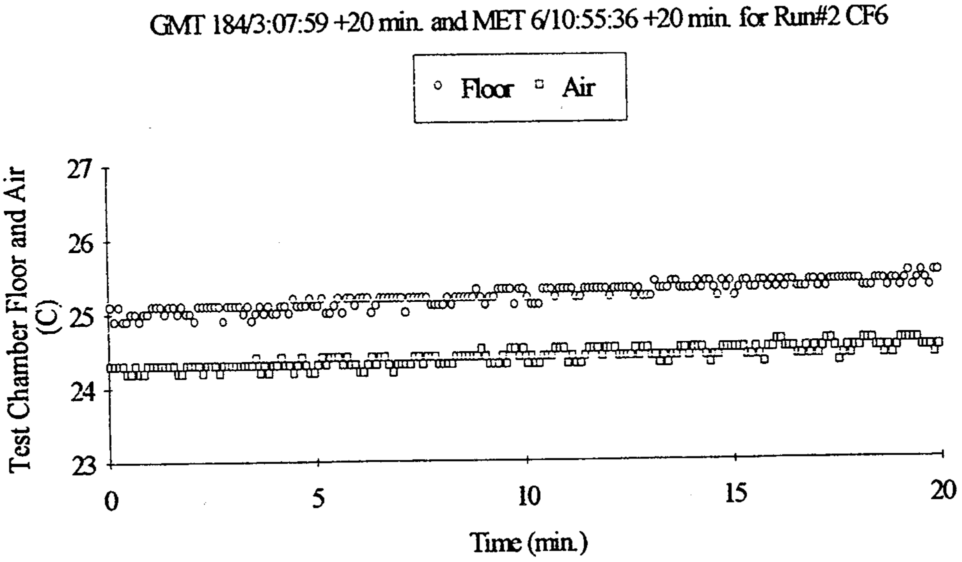

Figure E20 Thermistor data

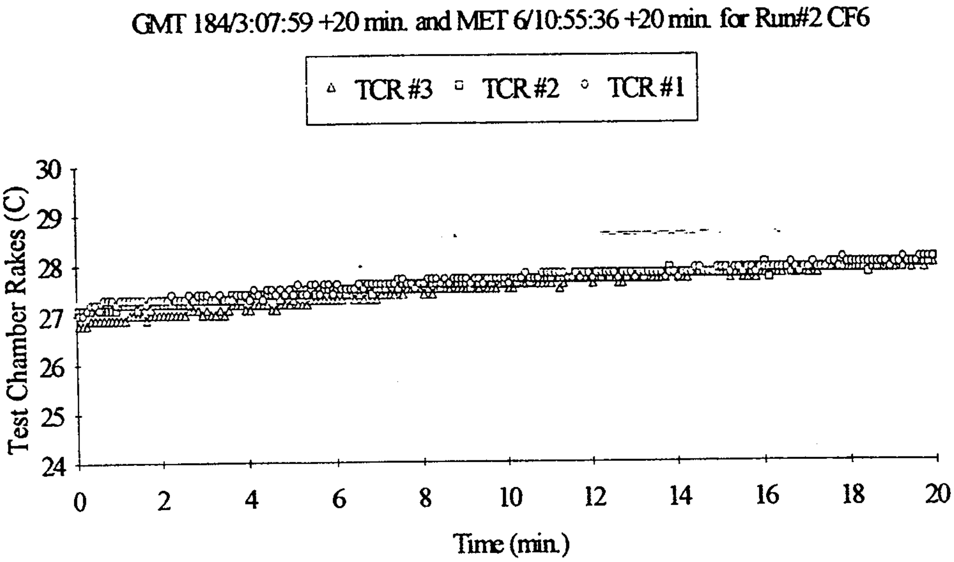

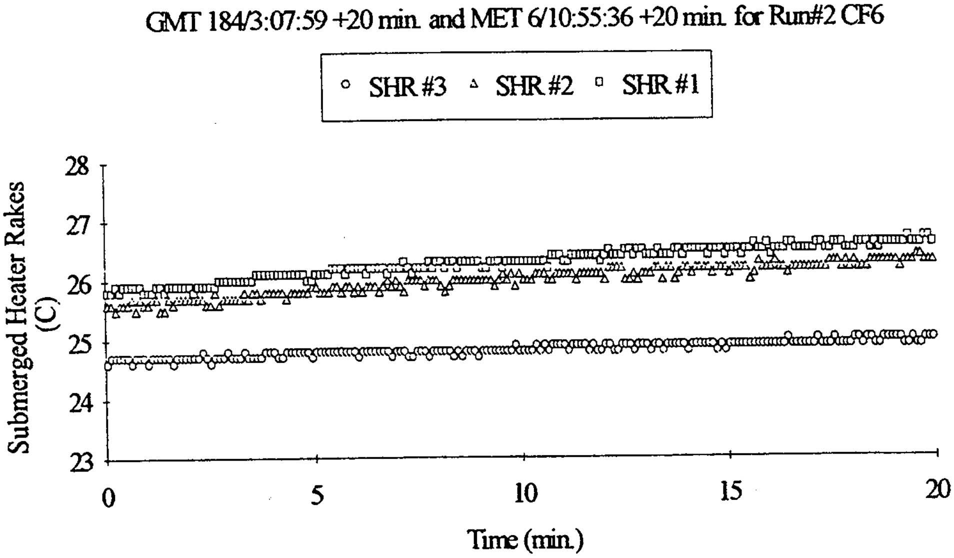

Figure E21 Thermistor data

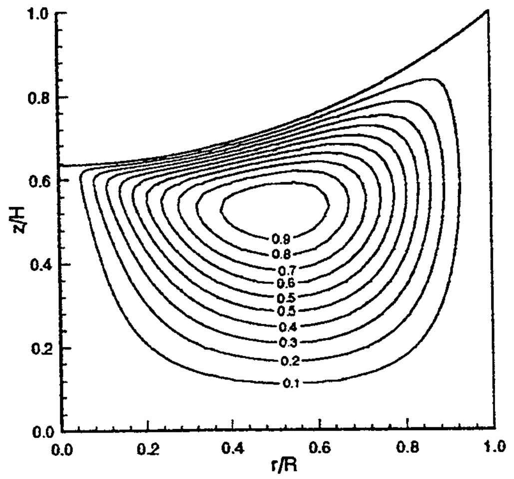

Streamlines for Run#2 Test CF6

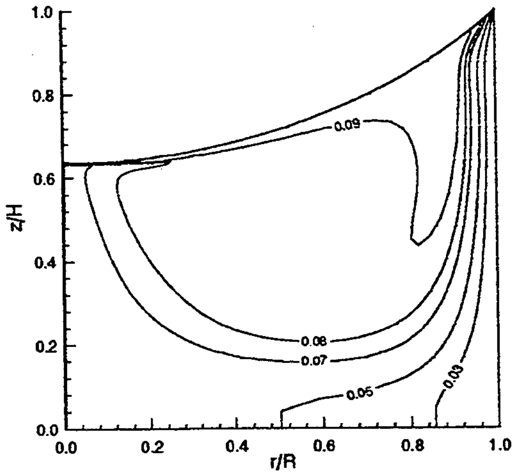

Isotherms for Run#2 Test CF6

Figure E22 Computed streamlines and isotherms

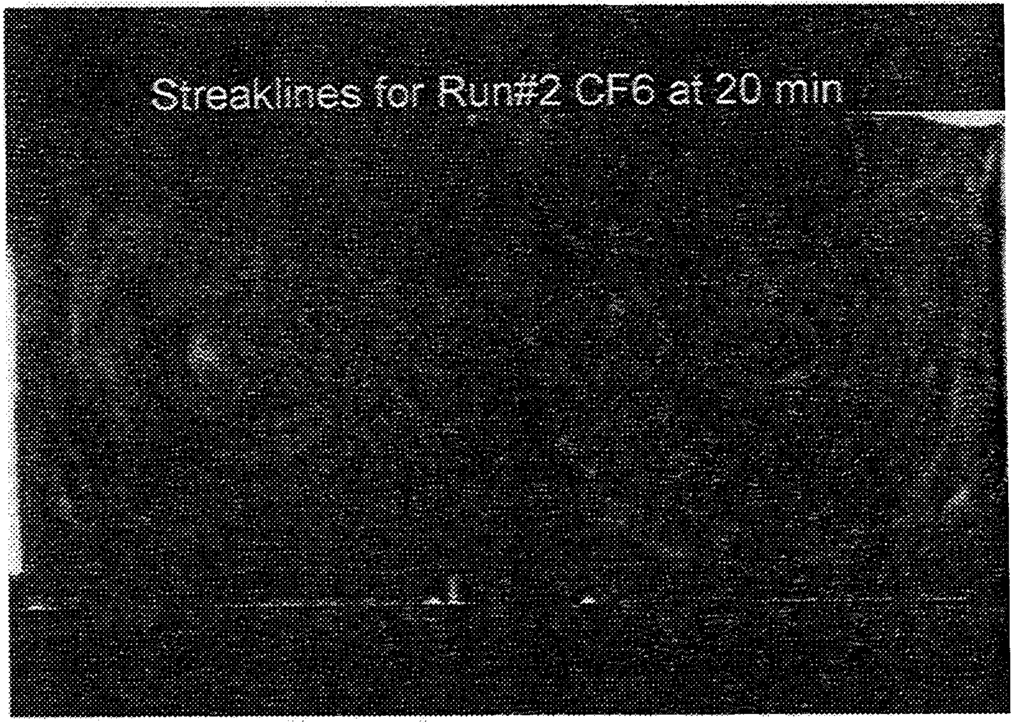

Figure E23 Experimental pathlines

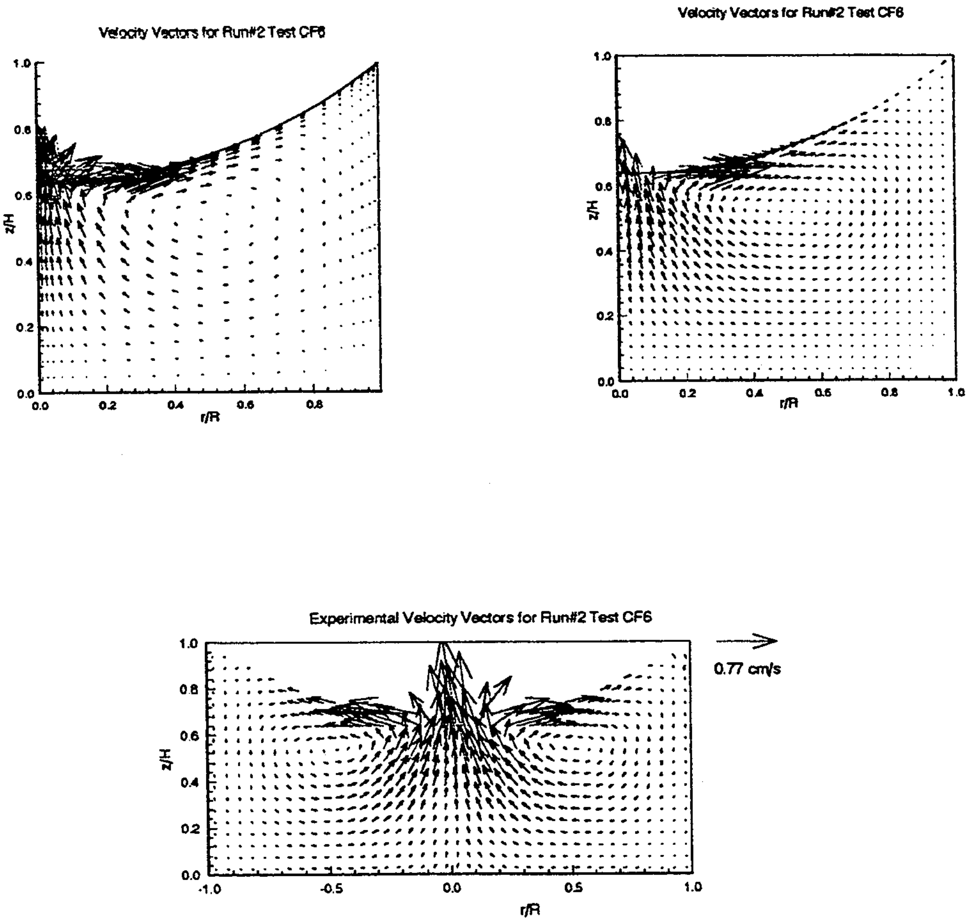

Figure E24 Computed and measured velocity vectors

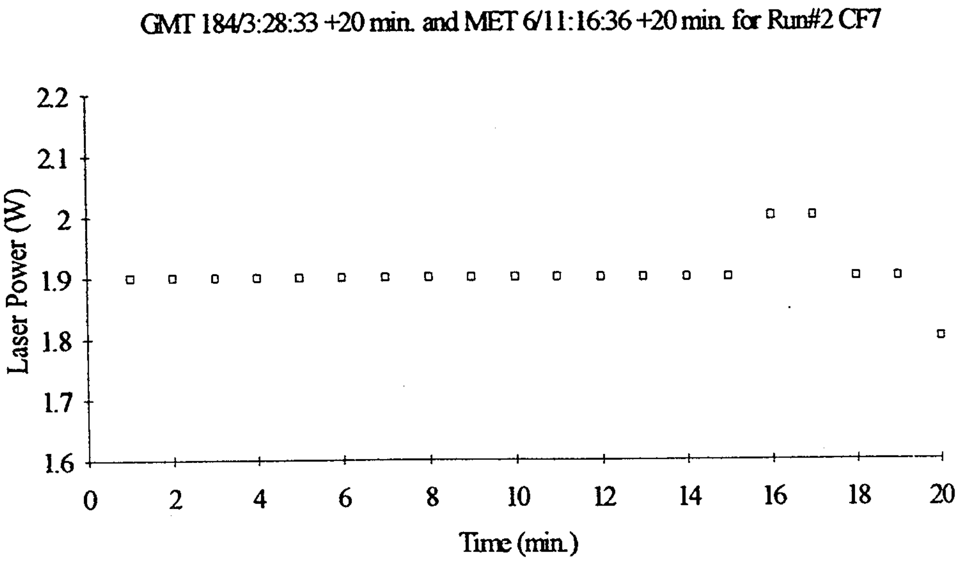

Figure E25 Laser power

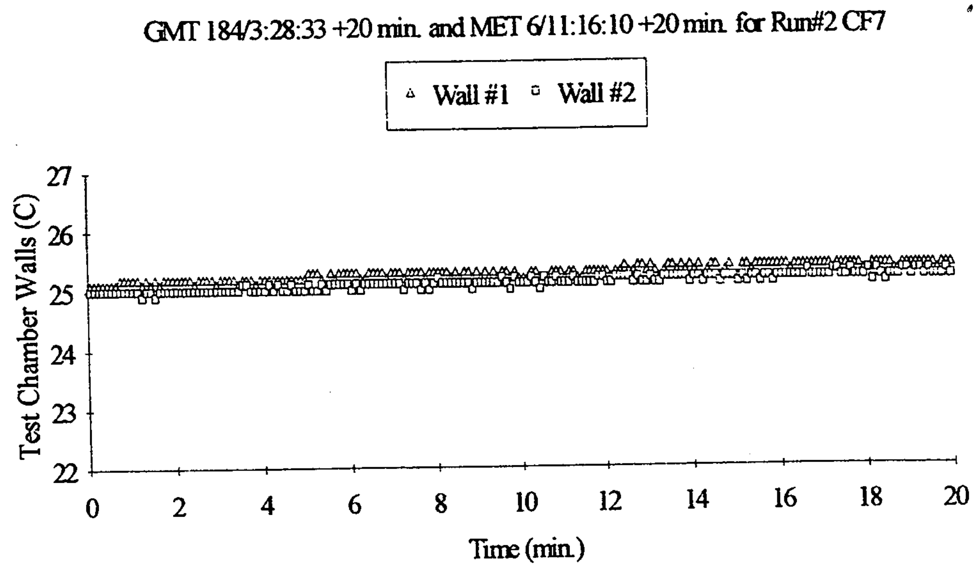

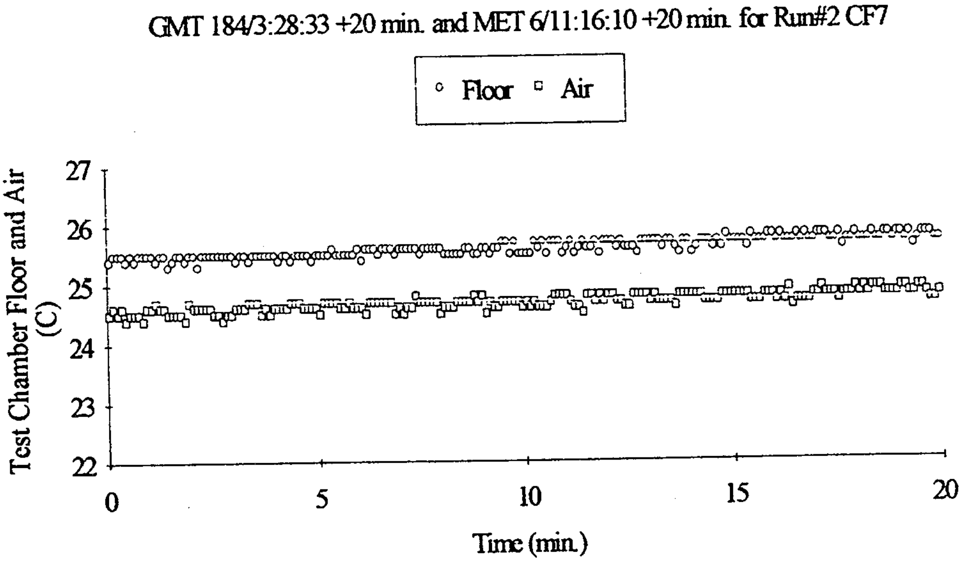

Figure E26 Thermistor data

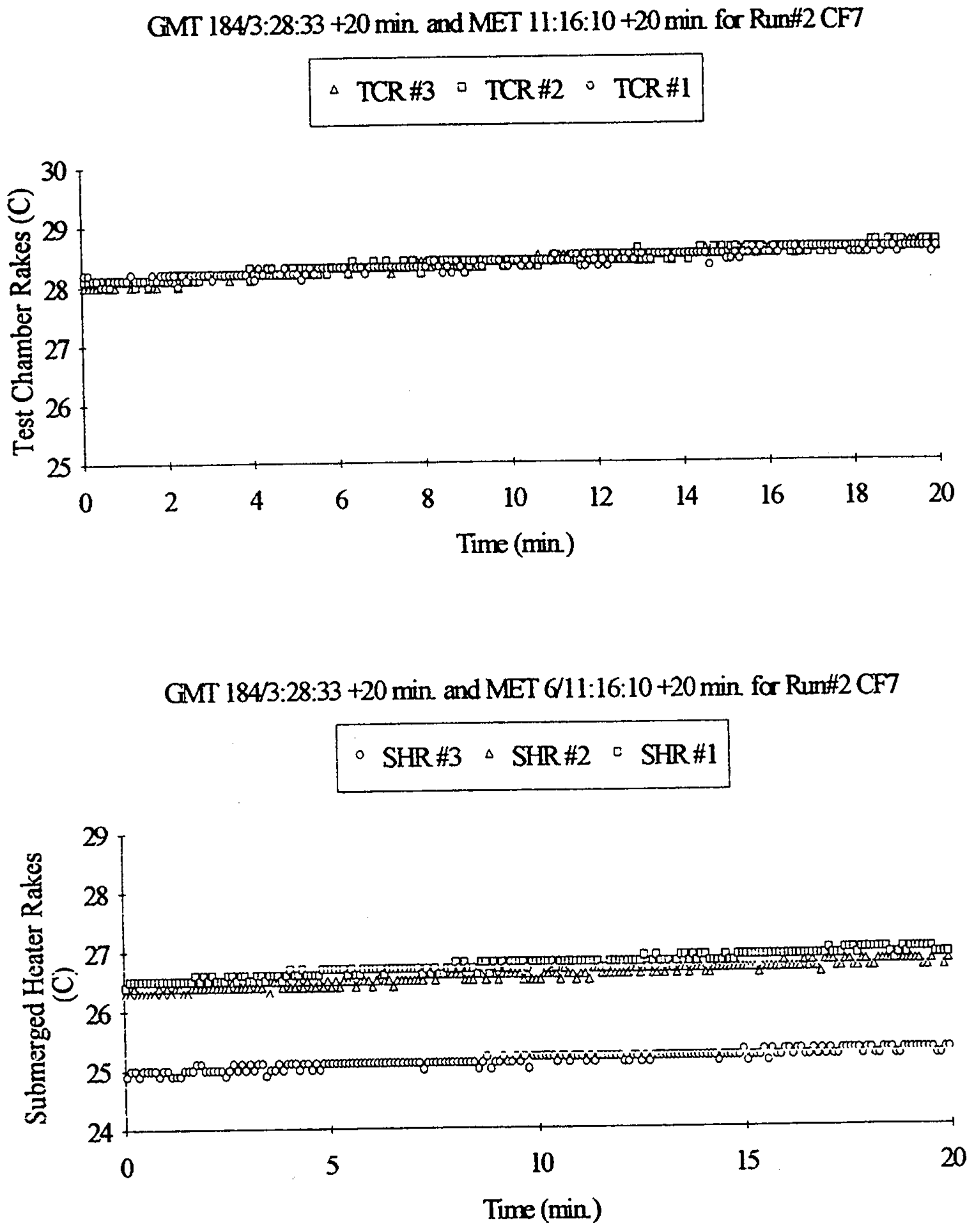

Figure E27 Thermistor data

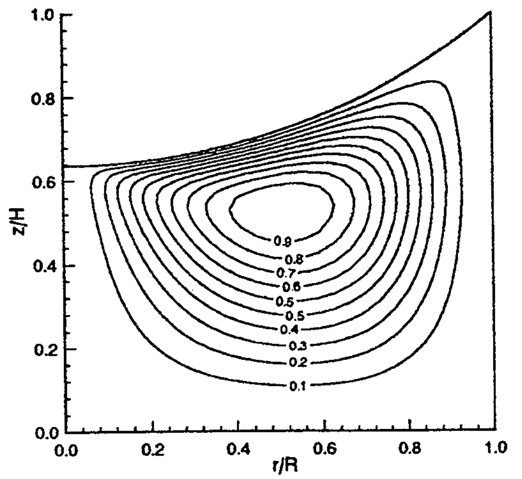

Streamlines for Run#2 Test CF7

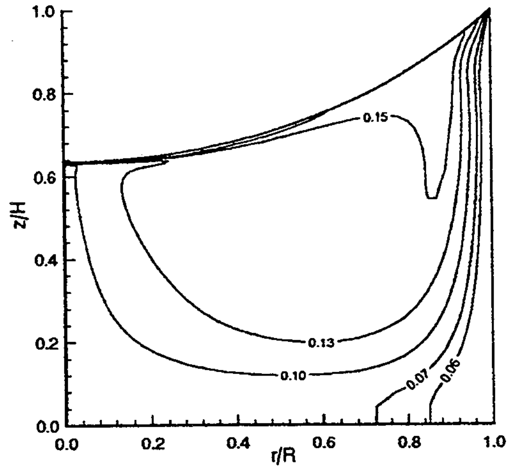

Isotherms for Run#2 Test CF7

Figure E28 Computed streamlines and isotherms

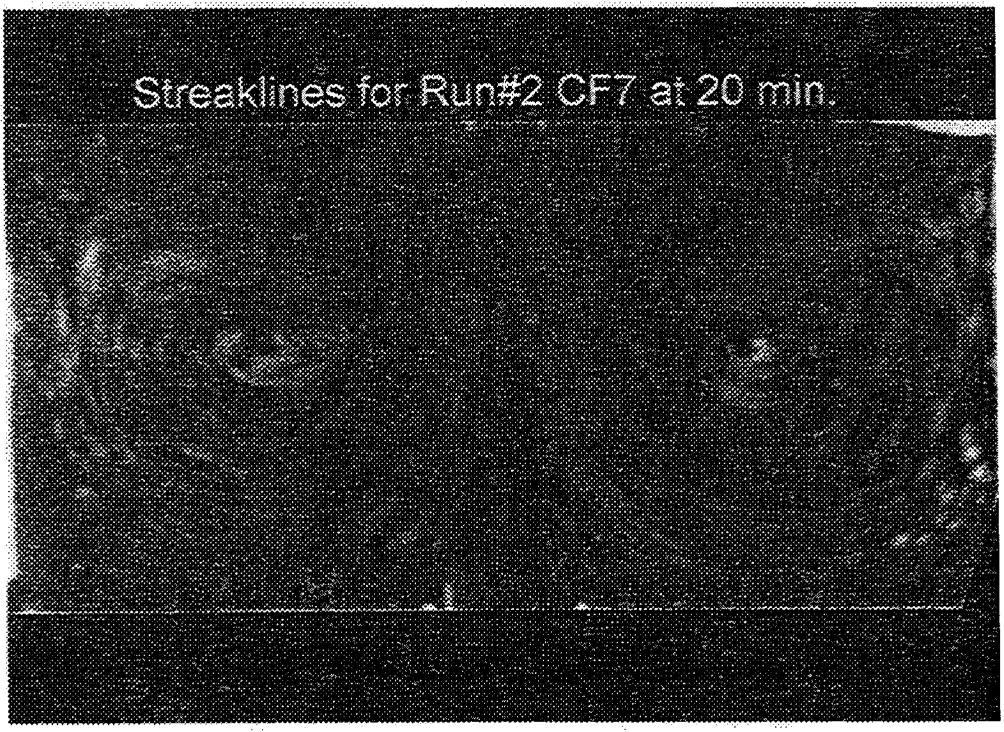

Figure E29 Experimental pathlines

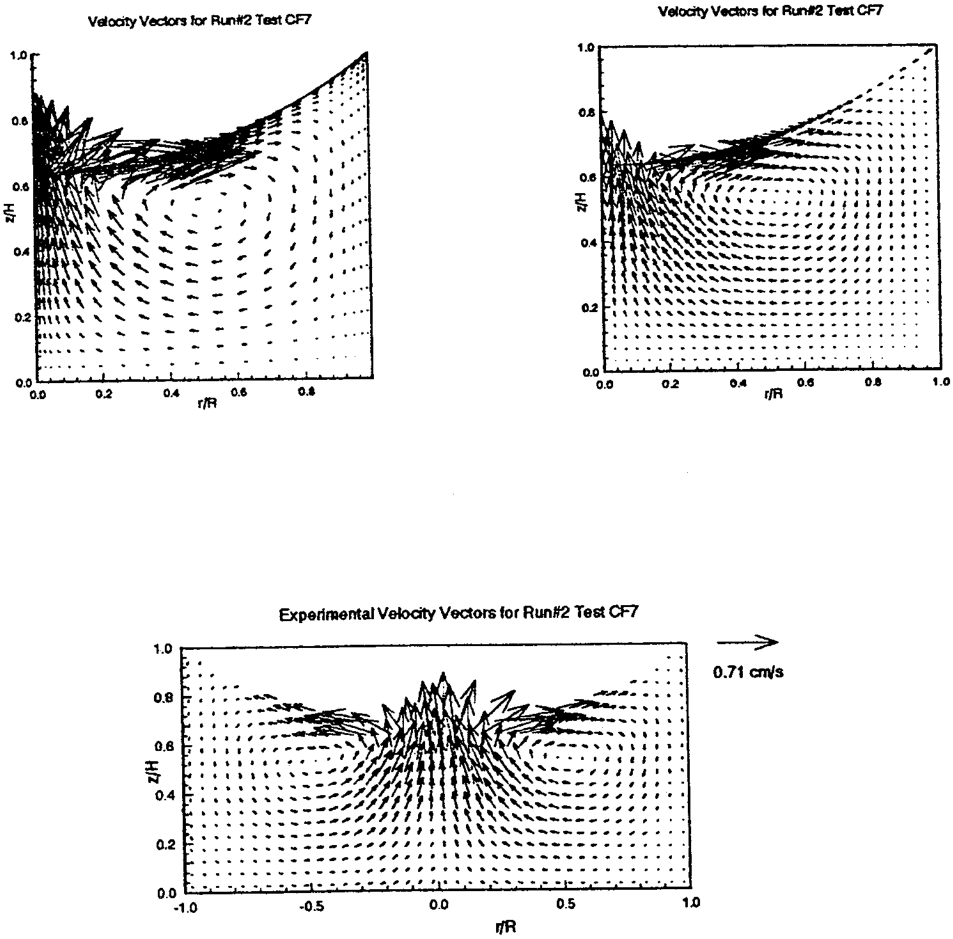

Figure E30 Computed and measured velocity vectors

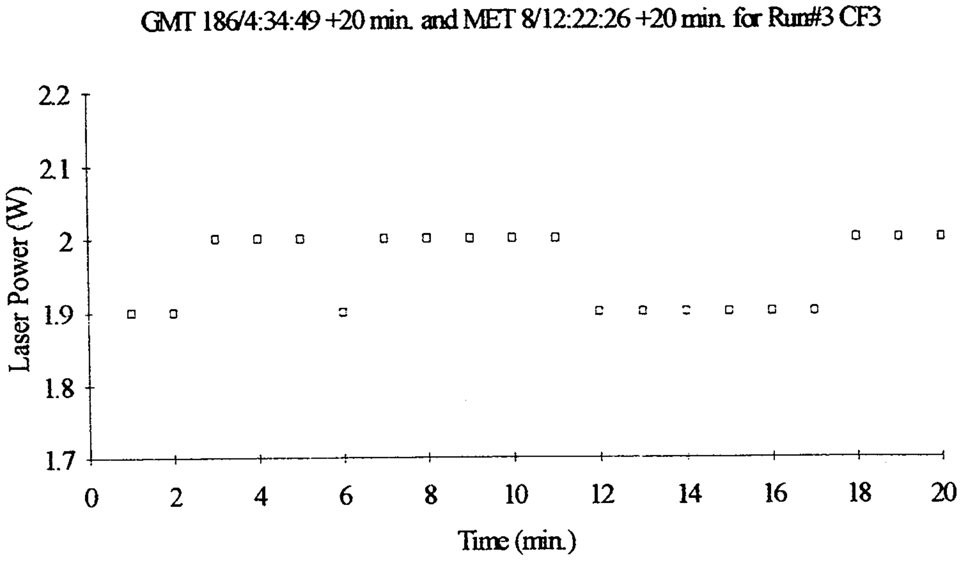

Figure E31 Laser power

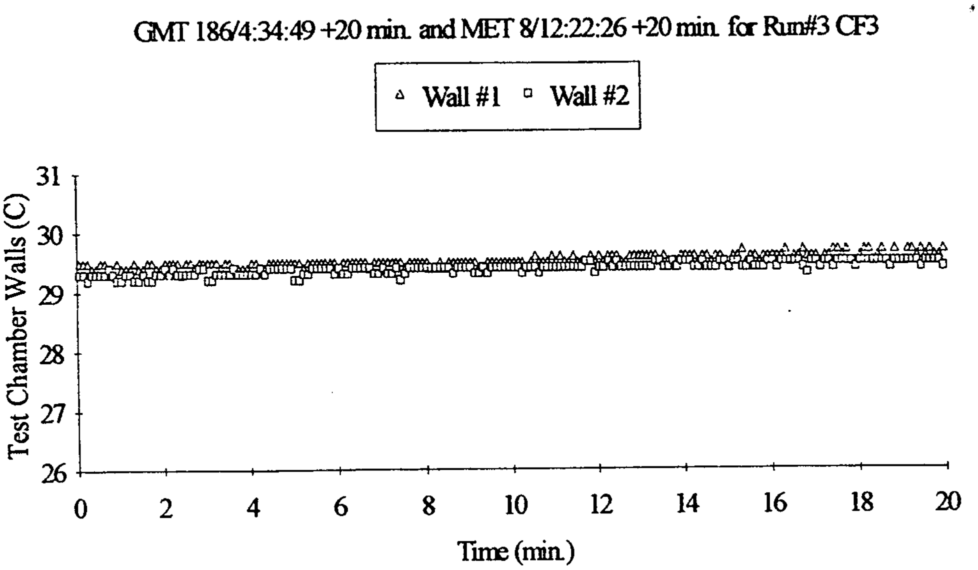

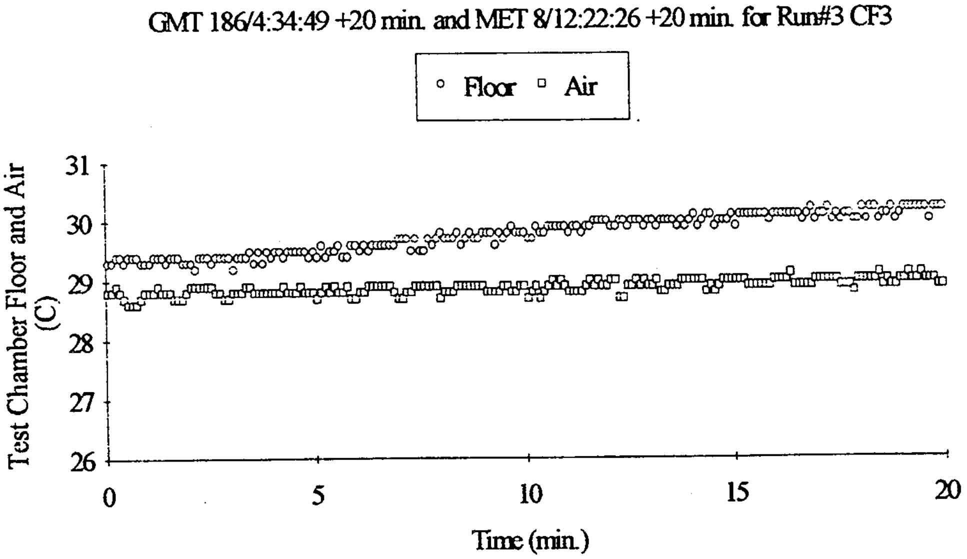

Figure E32 Thermistor data

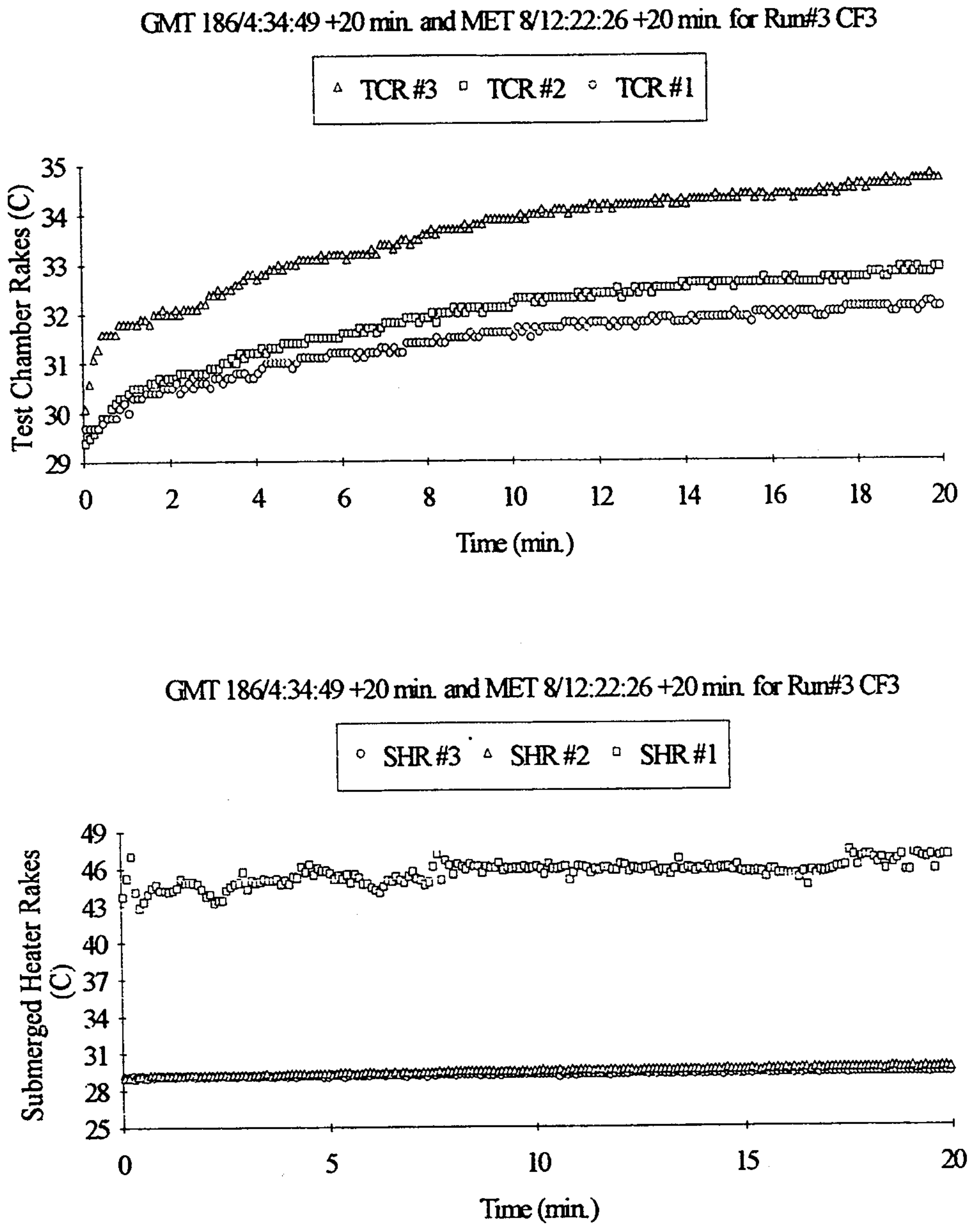

Figure E33 Thermistor data

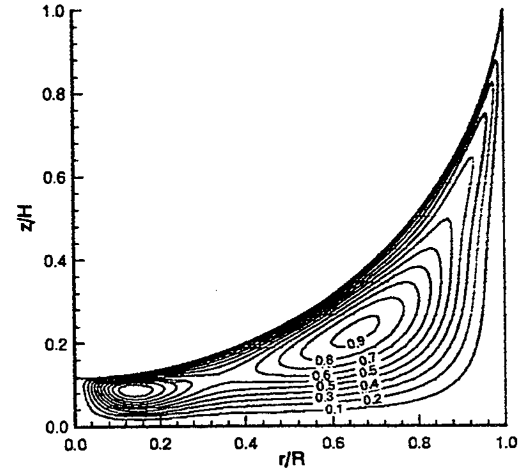

Streamlines for Run#3 Test CF3

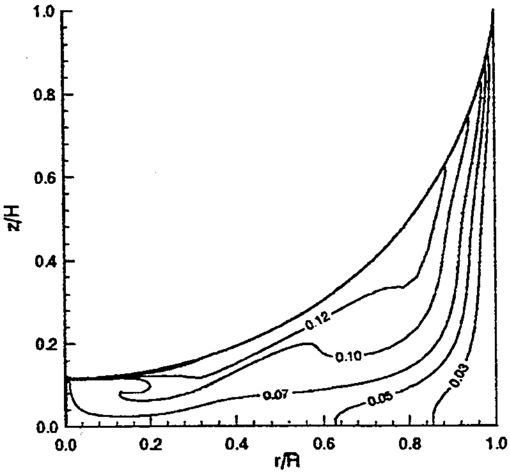

Isotherms for Run#3 Test CF3

Figure E34 Computed streamlines and isotherms

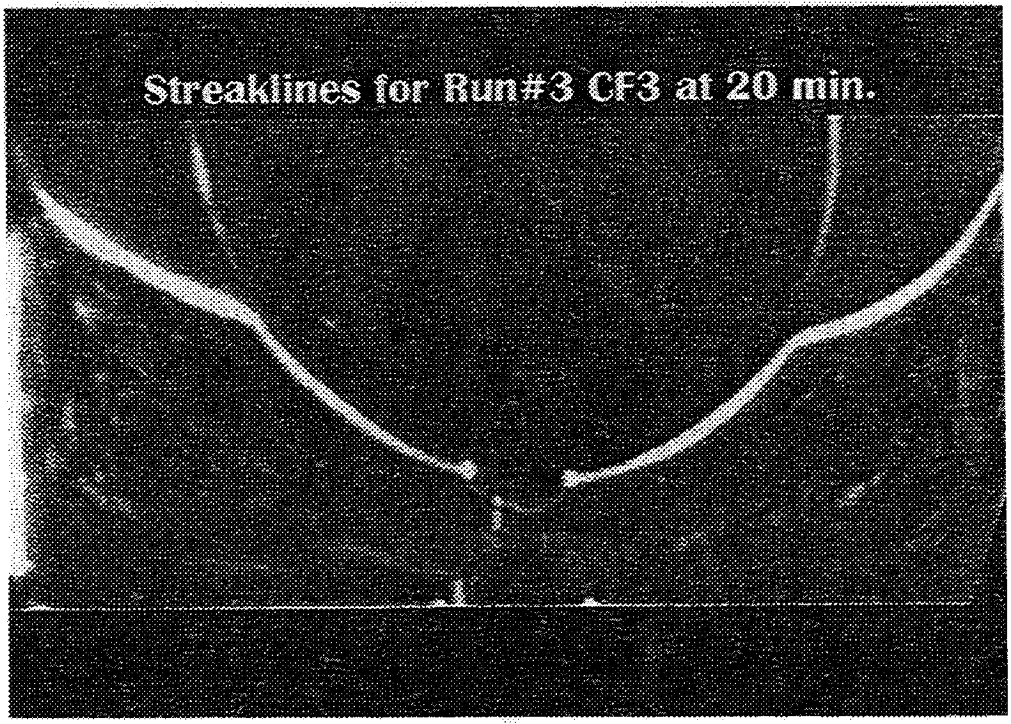

Figure E35 Experimental pathlines

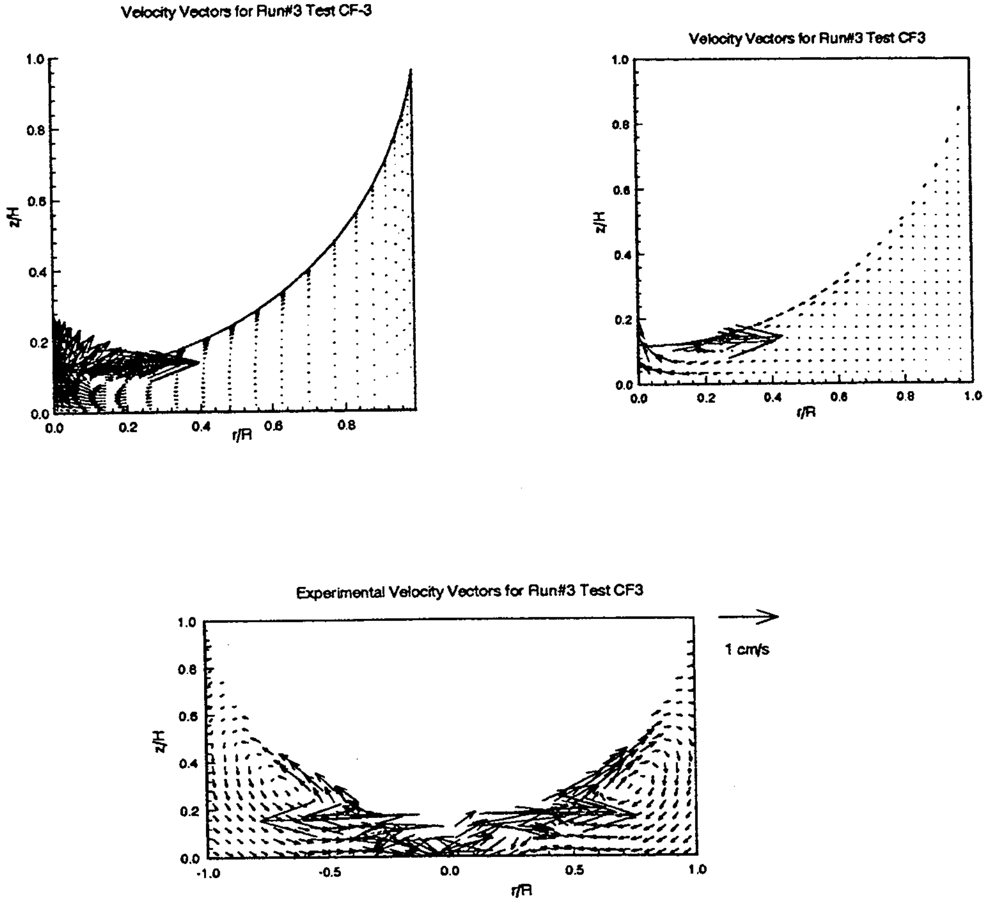
Velocity Vectors for Run#3 Test CF-3

Velocity Vectors for Run#3 Test CF3

Experimental Velocity Vectors for Run#3 Test CF3

Figure E36 Computed and measured velocity vectors

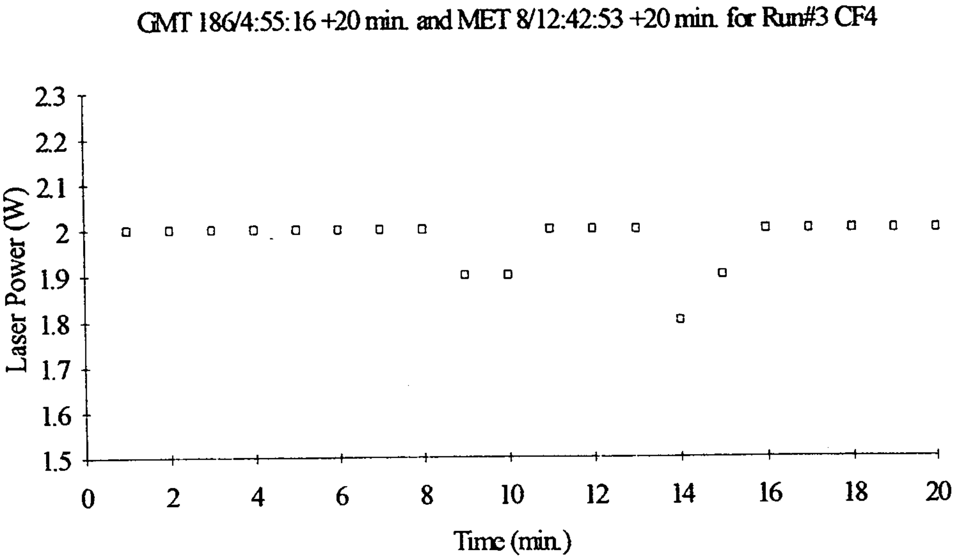

Figure E37 Laser power

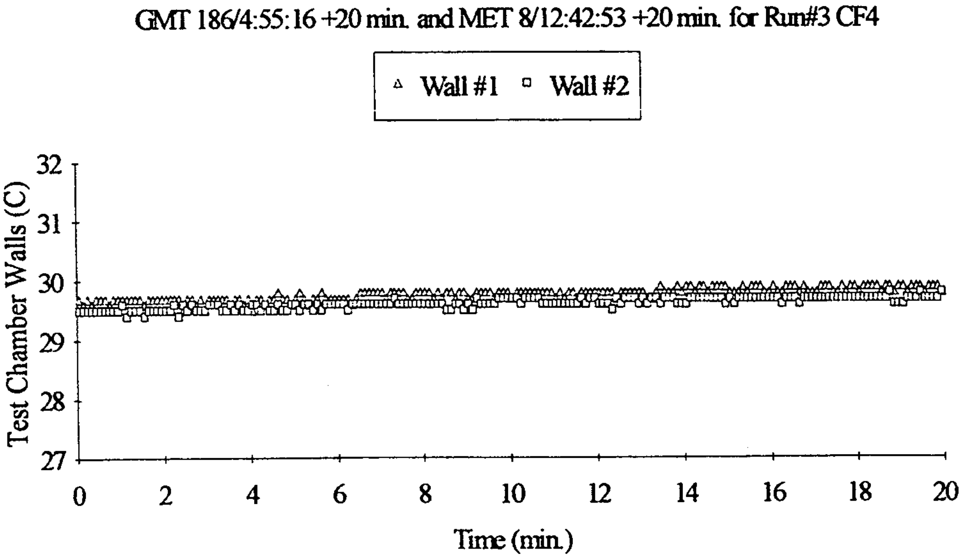

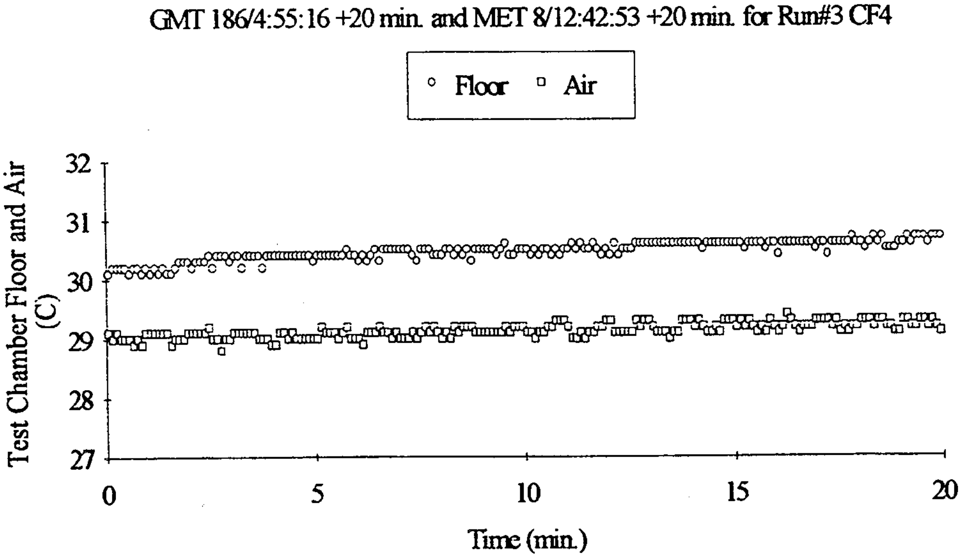

Figure E38 Thermistor data

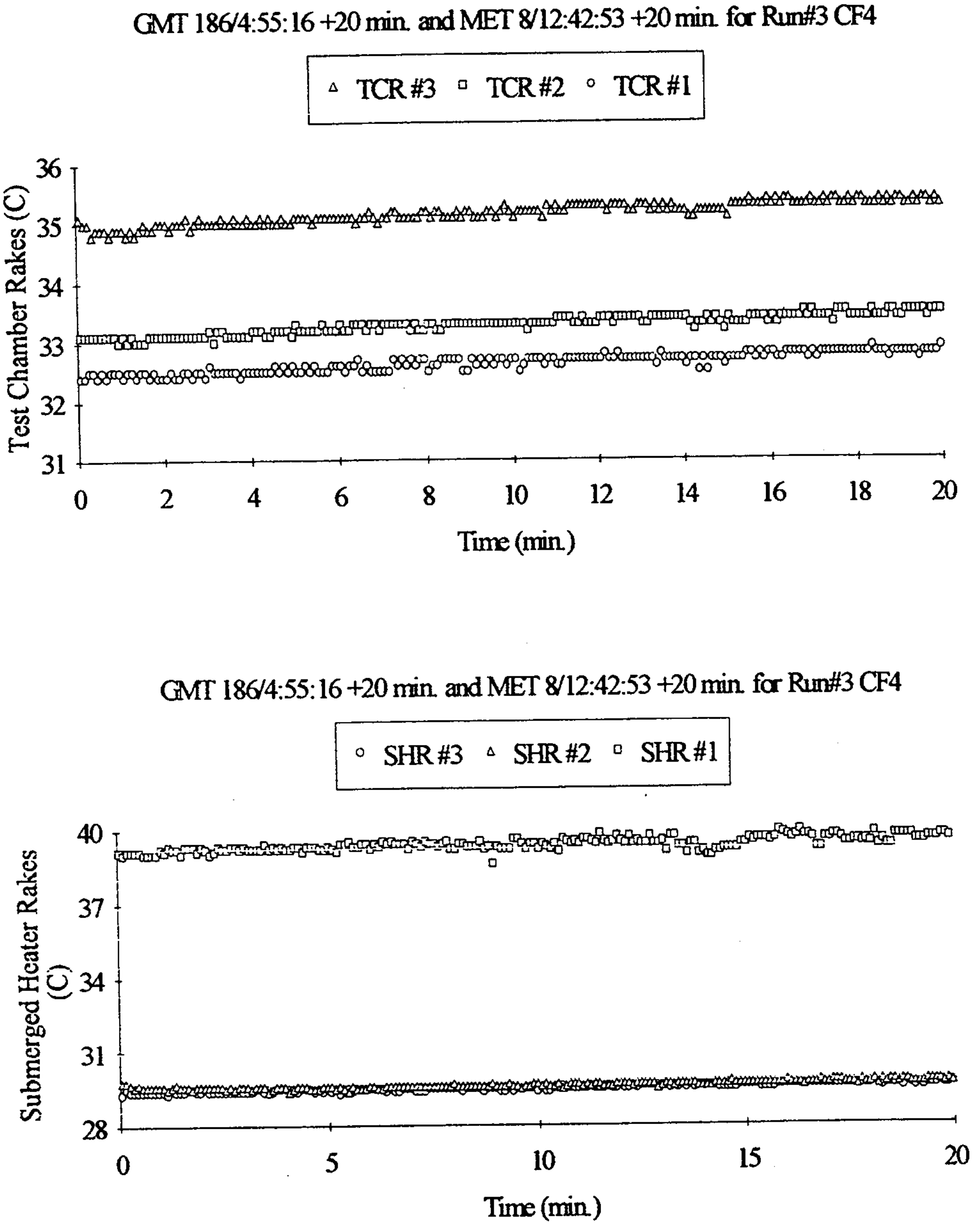

Figure E39 Thermistor data

Streamlines for Run#3 Test CF4

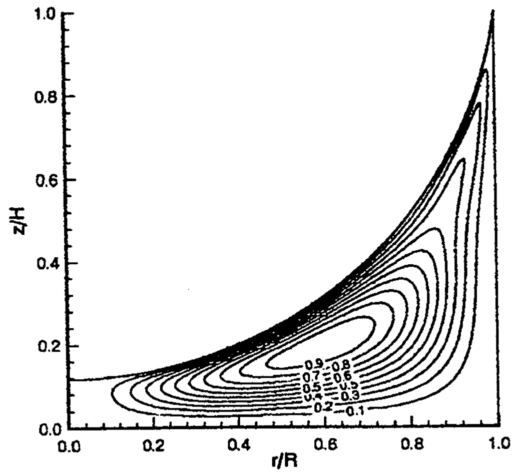

Isotherms for Run#3 Test CF4

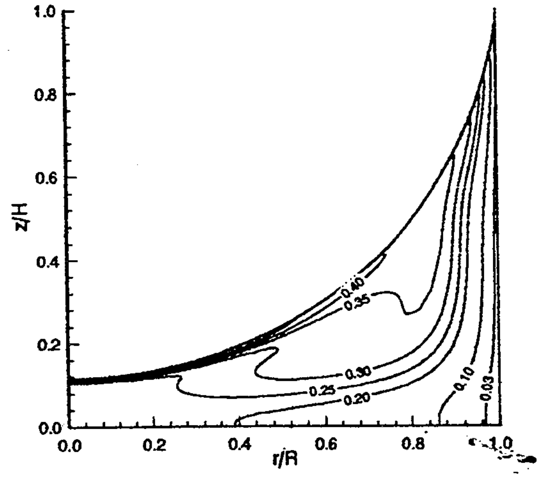

Figure E40 Computed streamlines and isotherms

Figure E41 Experimental pathlines

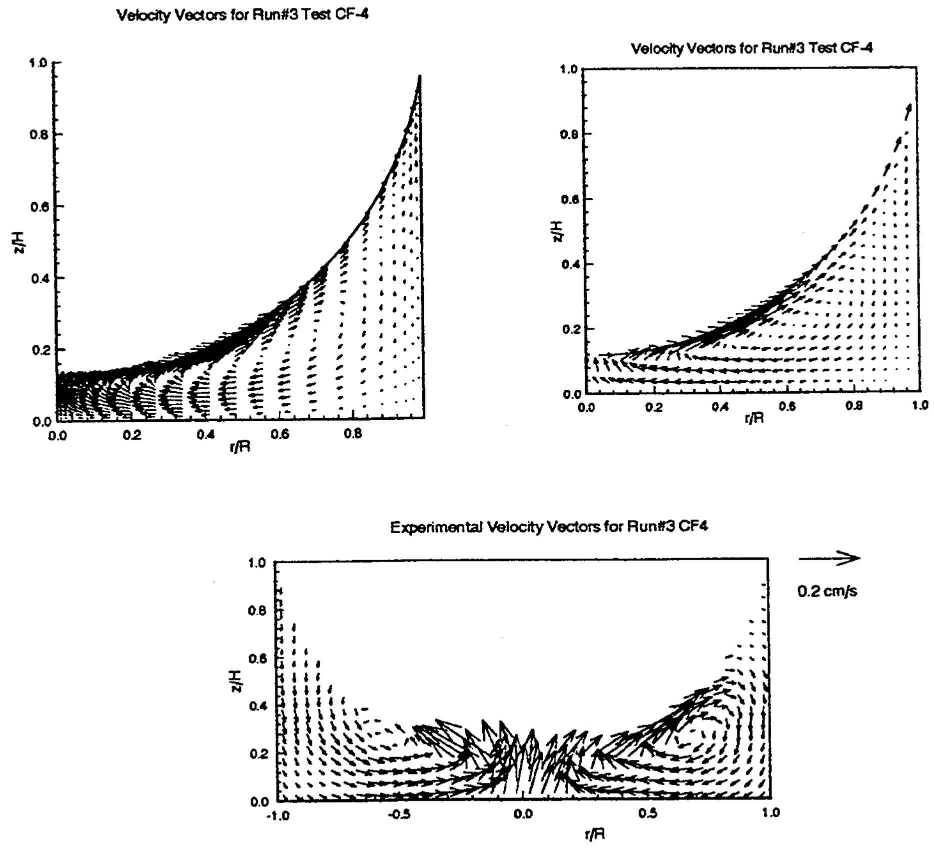

Figure E42 Computed and measured velocity vectors

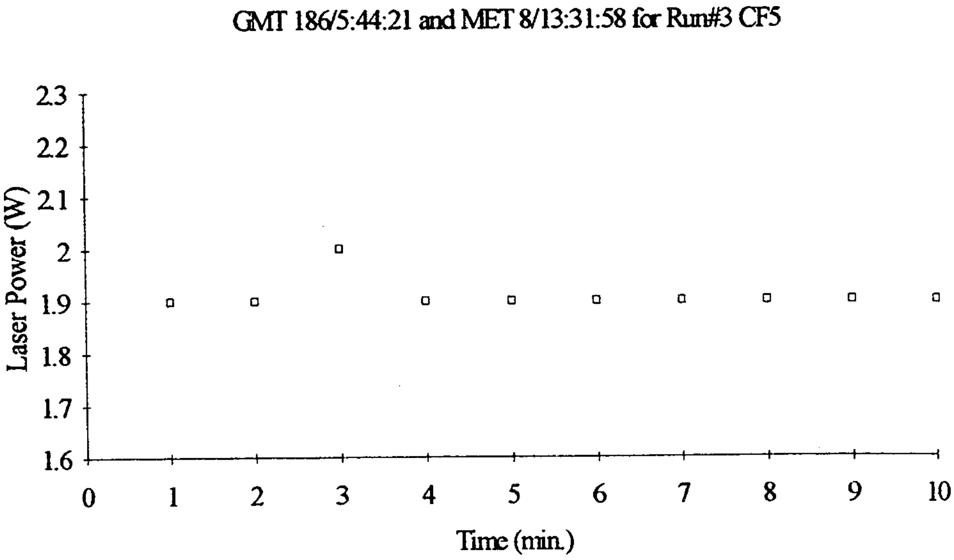

Figure E43 Laser power

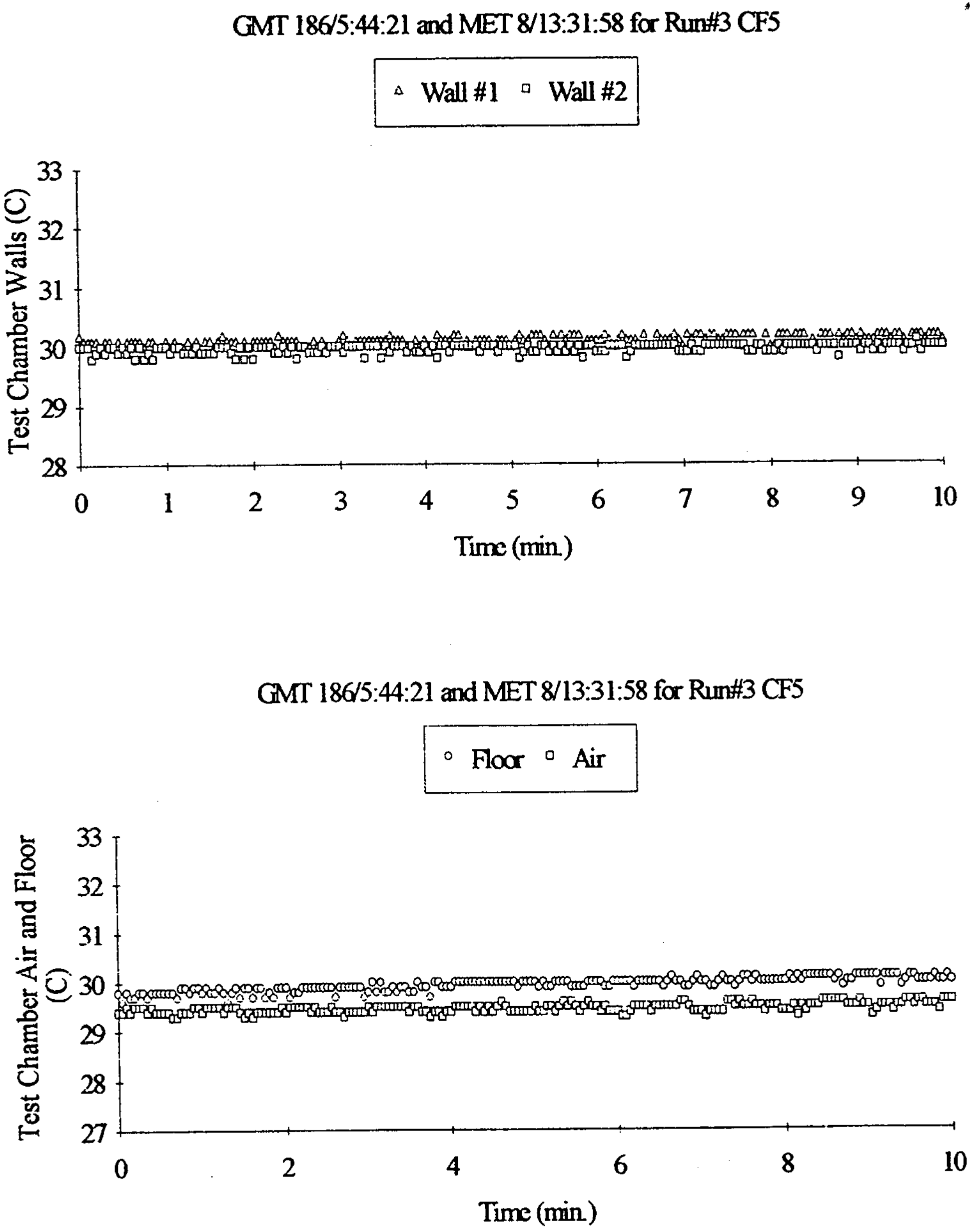

Figure E44 Thermistor data

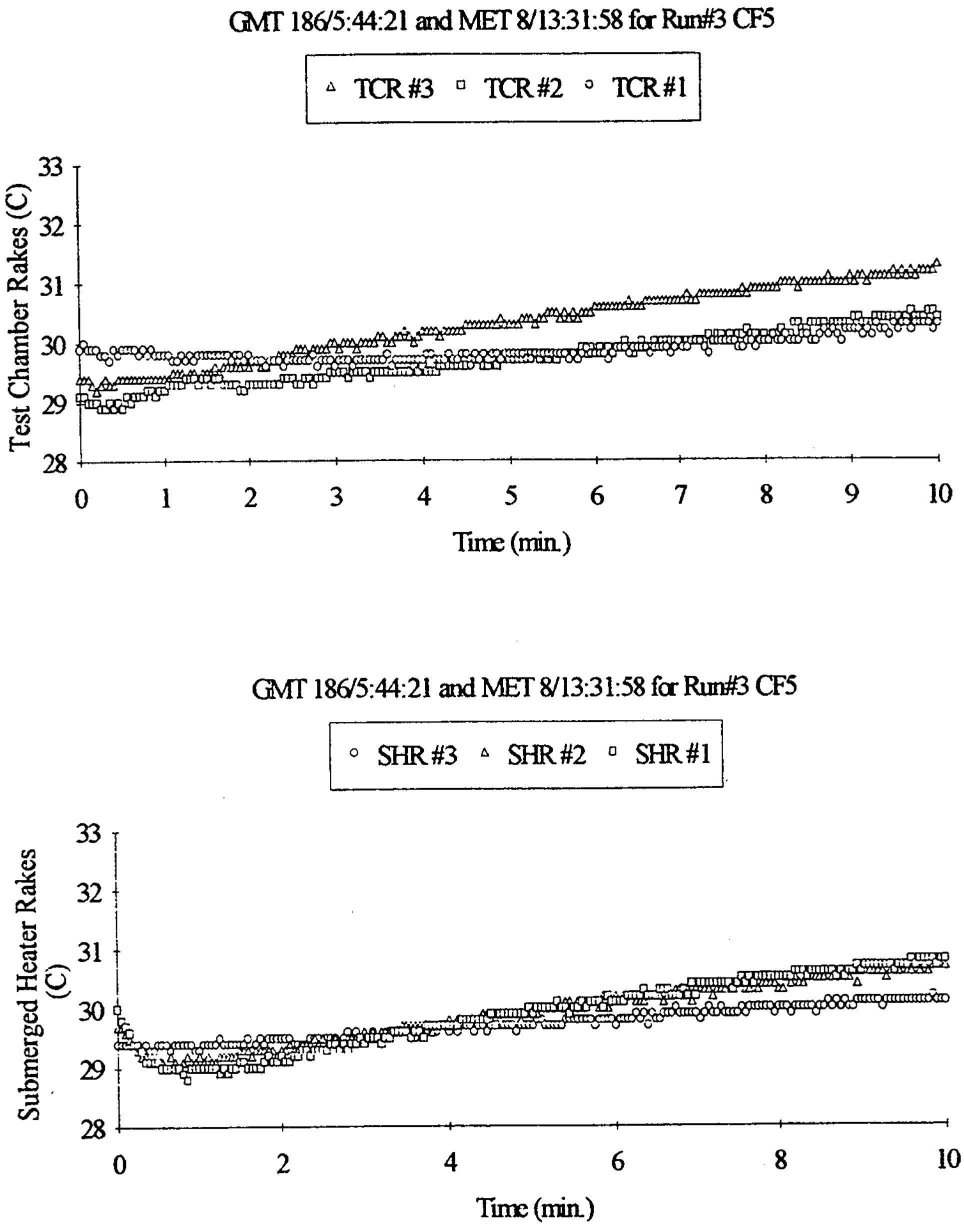

Figure E45 Thermistor data

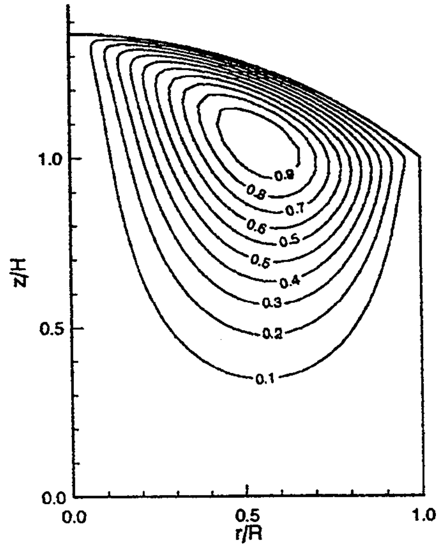

StreamLines for Run#3 Test CF5

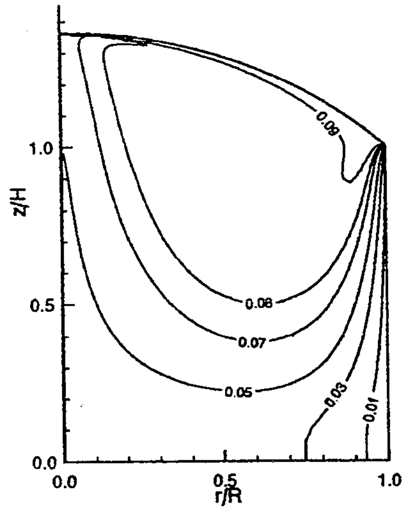

Isotherms for Run#3 Test CF5

Figure E46 Computed streamlines and isotherms

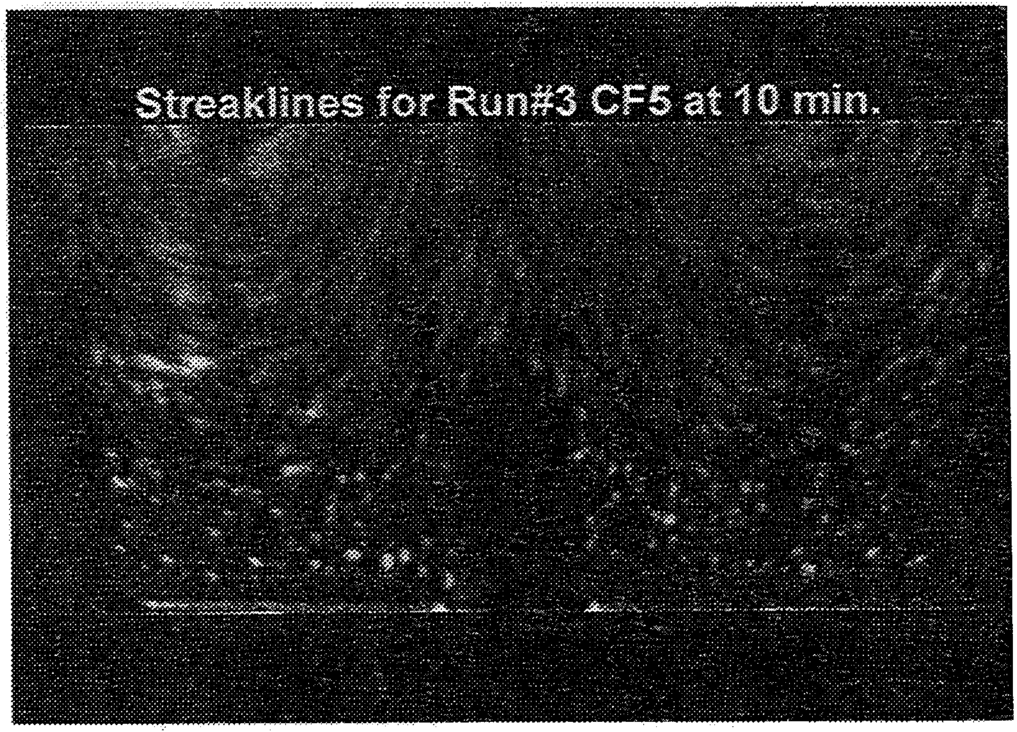

Figure E47 Experimental pathlines

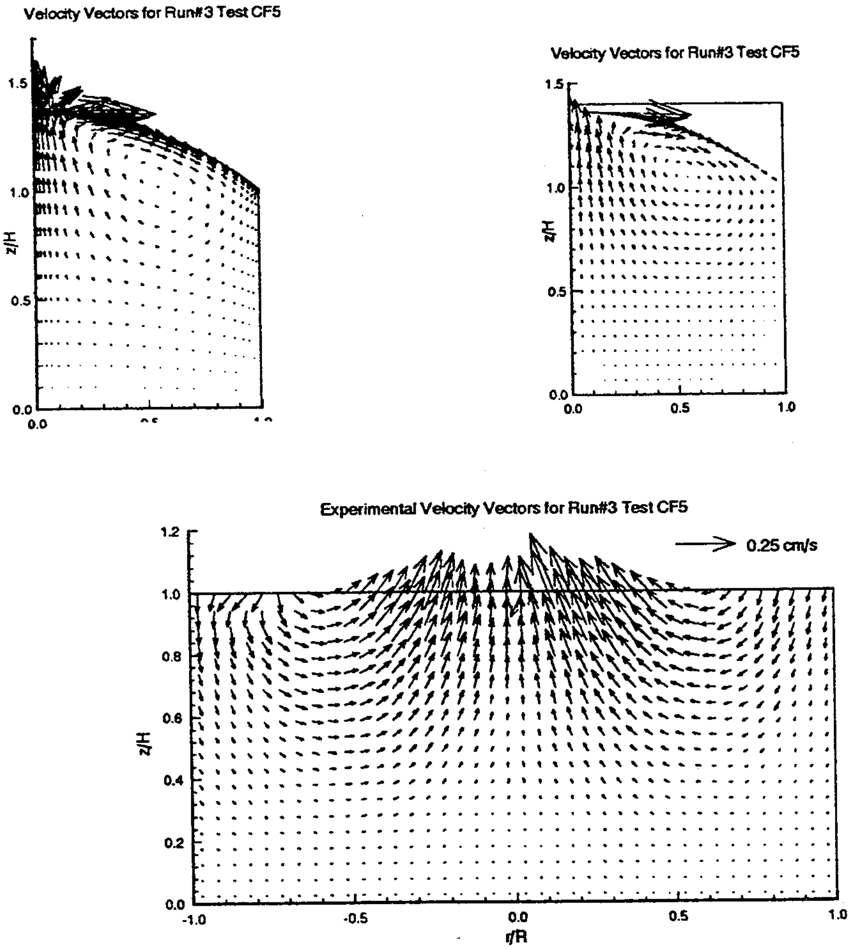

Figure E48 Computed and measured velocity vectors

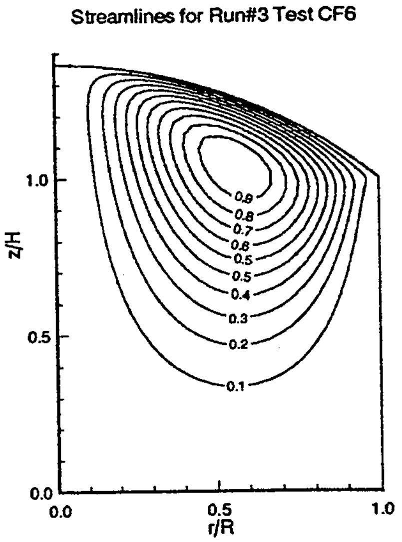
Streamlines for Run#3 Test CF6

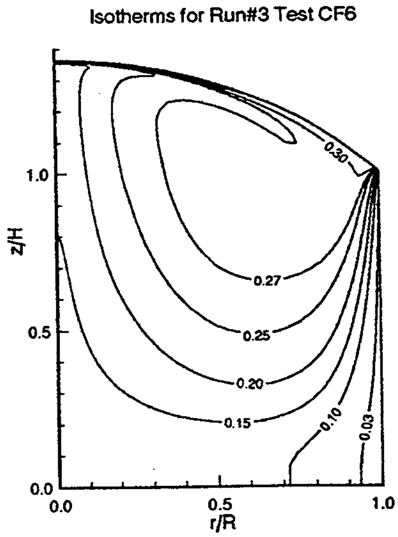
Isotherms for Run#3 Test CF6

Figure E49 Computed streamlines and isotherms

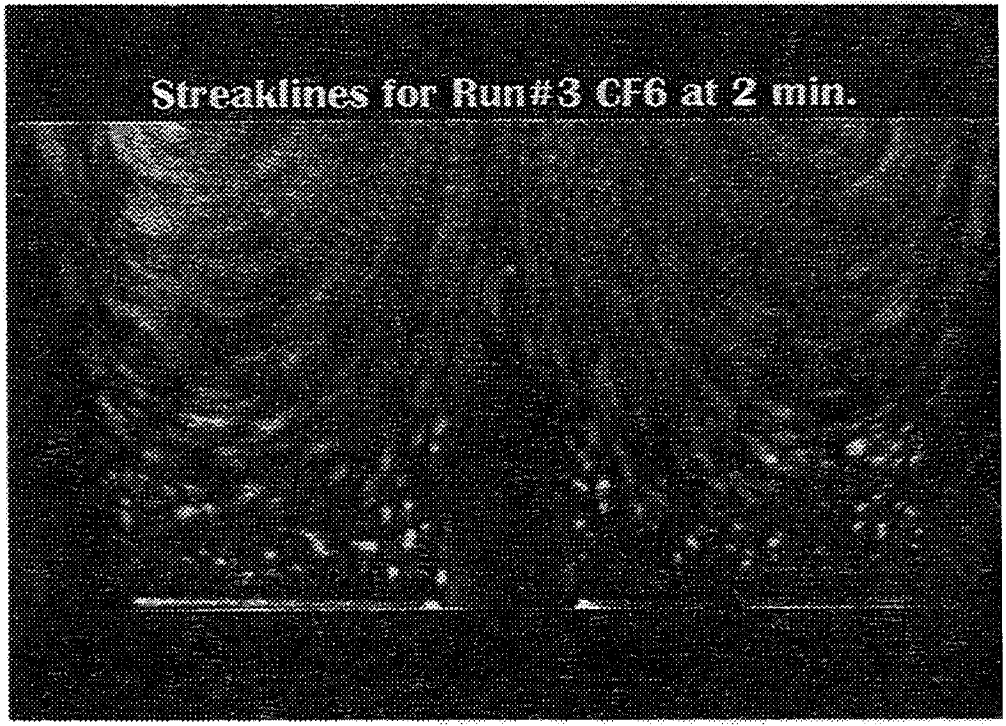

Figure E50 Experimental pathlines

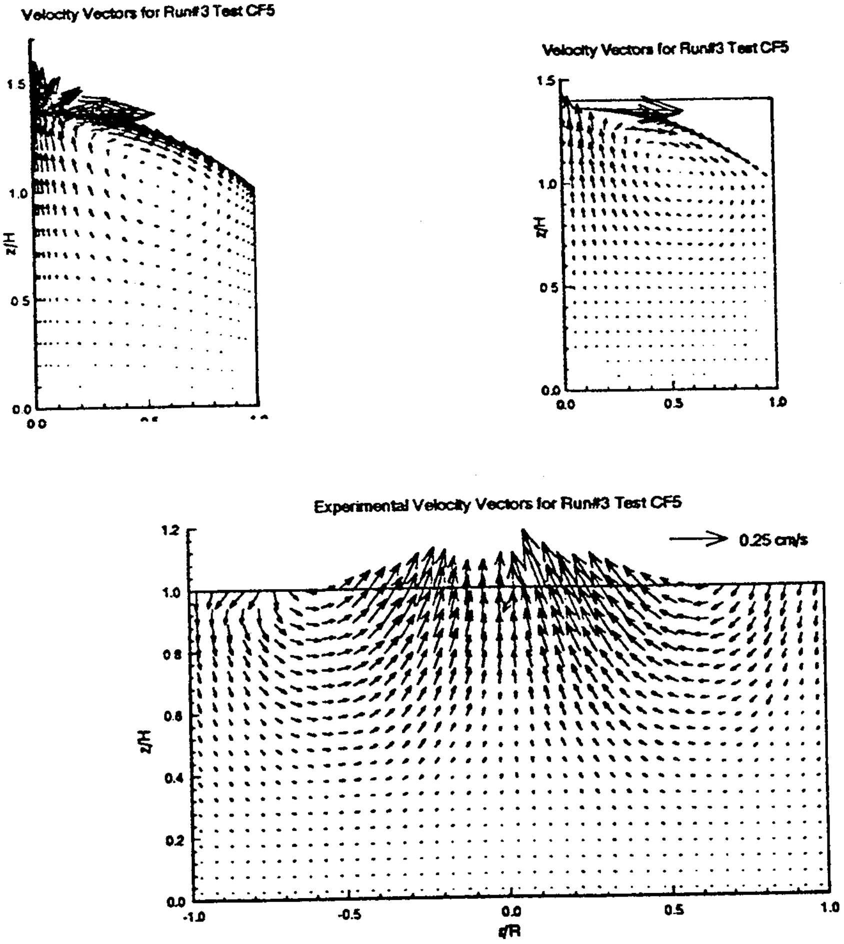

Velocity Vectors for Run#3 Test CF5

Velocity Vectors for Run#3 Test CF5

Experimental Velocity Vectors for Run#3 Test CF5

Figure E51 Computed and measured velocity vectors

APPENDIX F

CT CURVED SHORTER TESTS

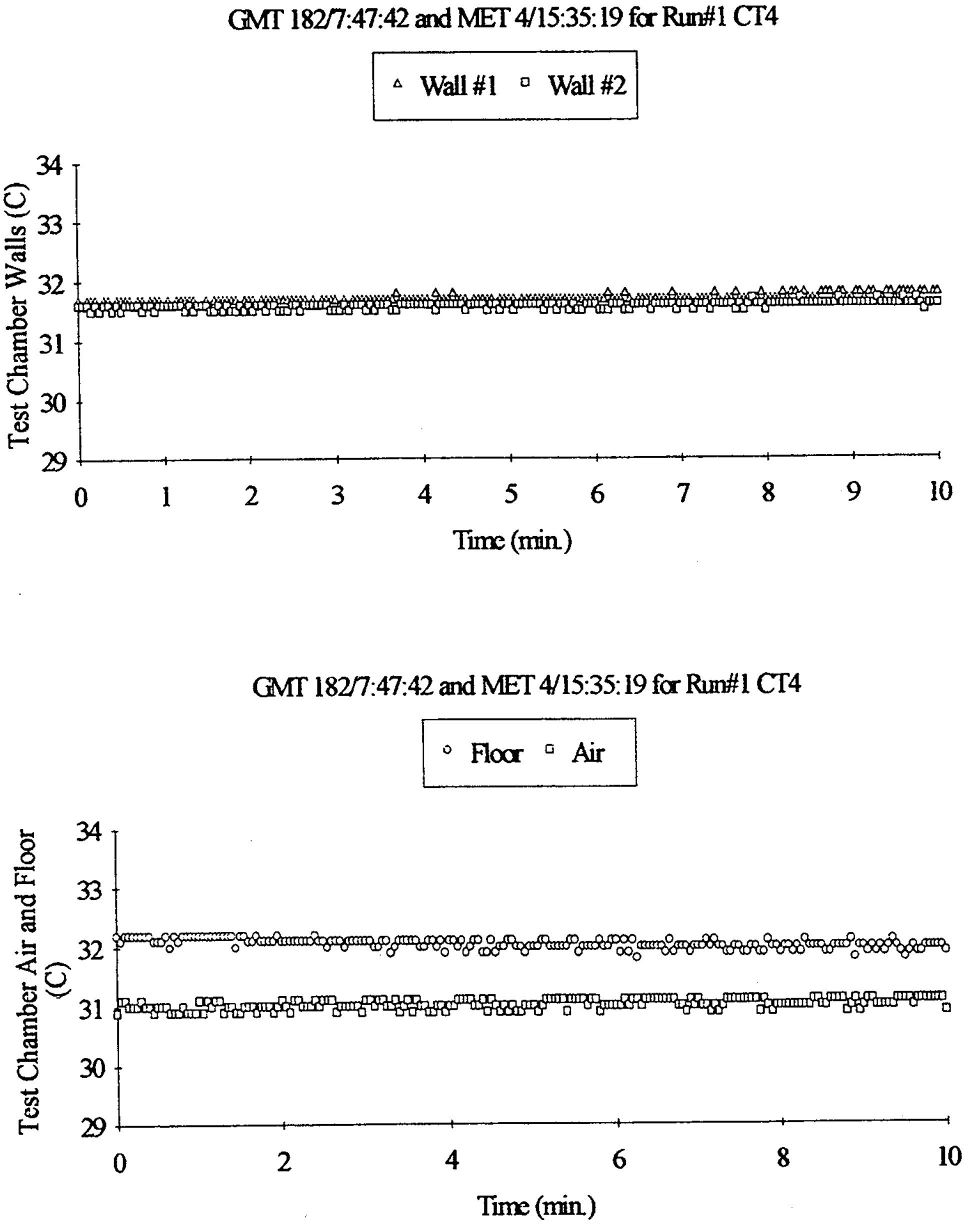

Figure F1 Thermistor data

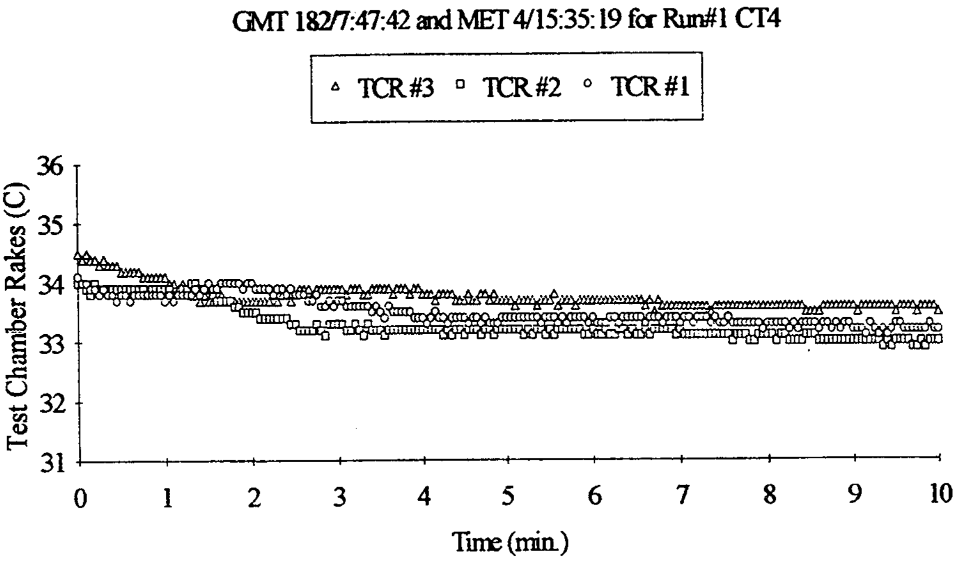

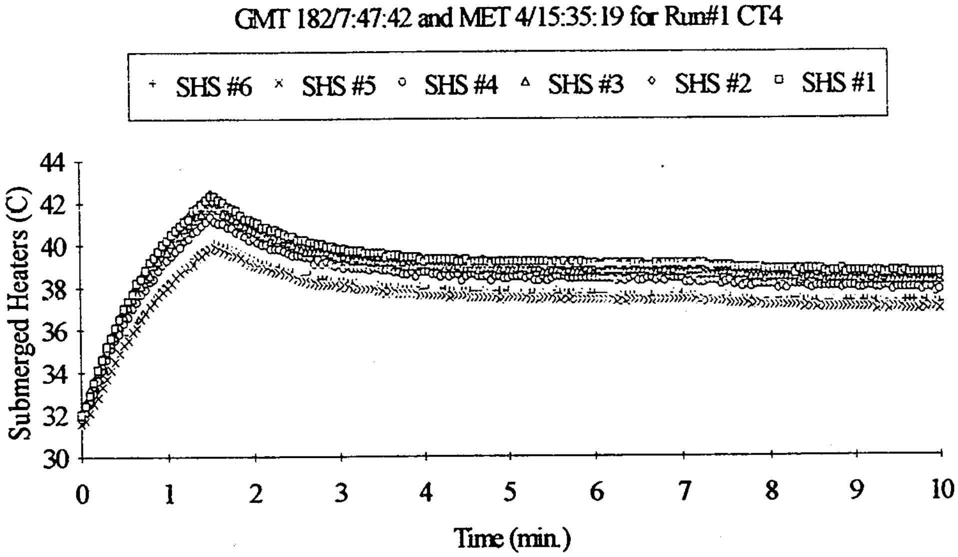

Figure F2 Thermistor data

Streamlines for Run#1 Test CT4

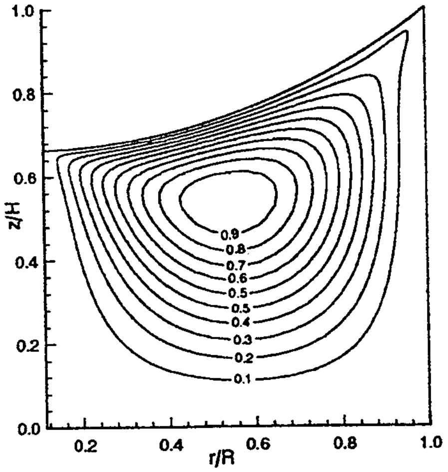

Isotherms for Run#1 Test CT4

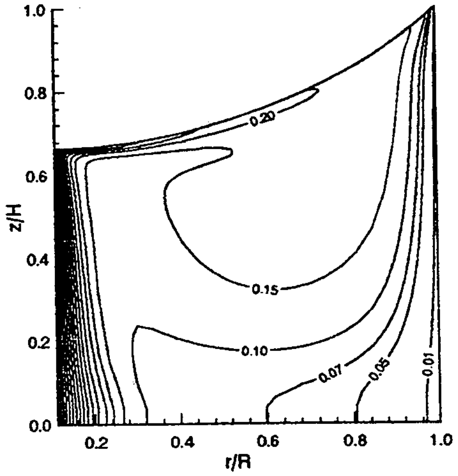

Figure F3 Computed streamlines and isotherms

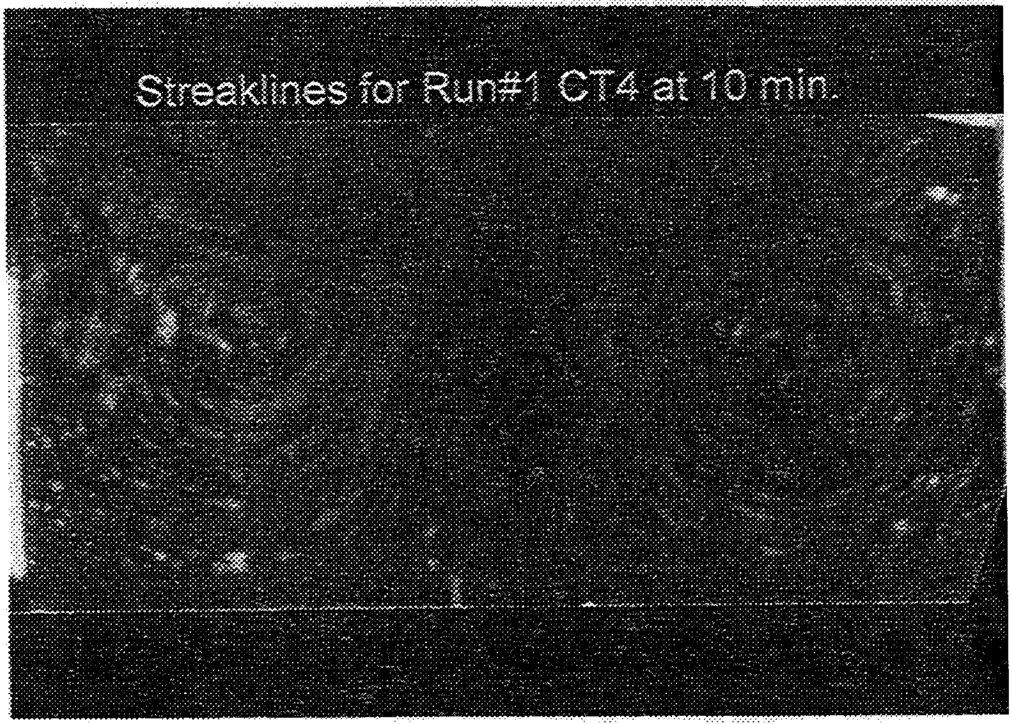

Figure F4 Experimental pathlines

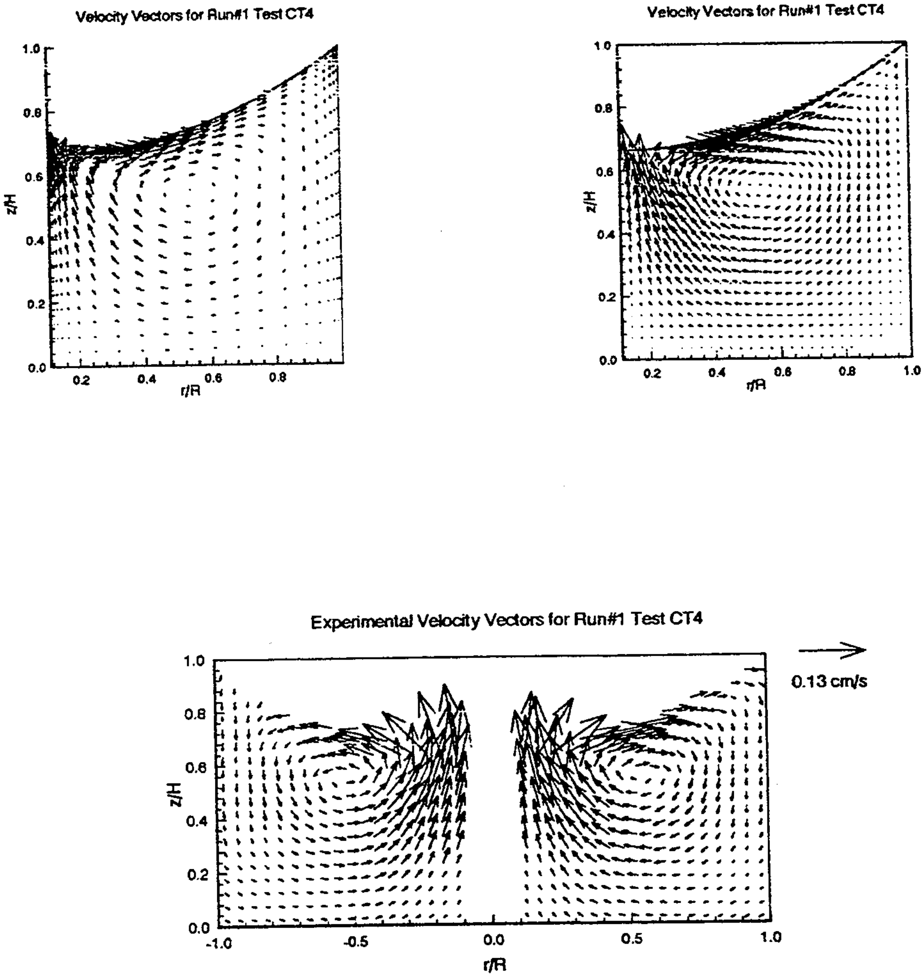

Figure F5 Computed and measured velocity vectors

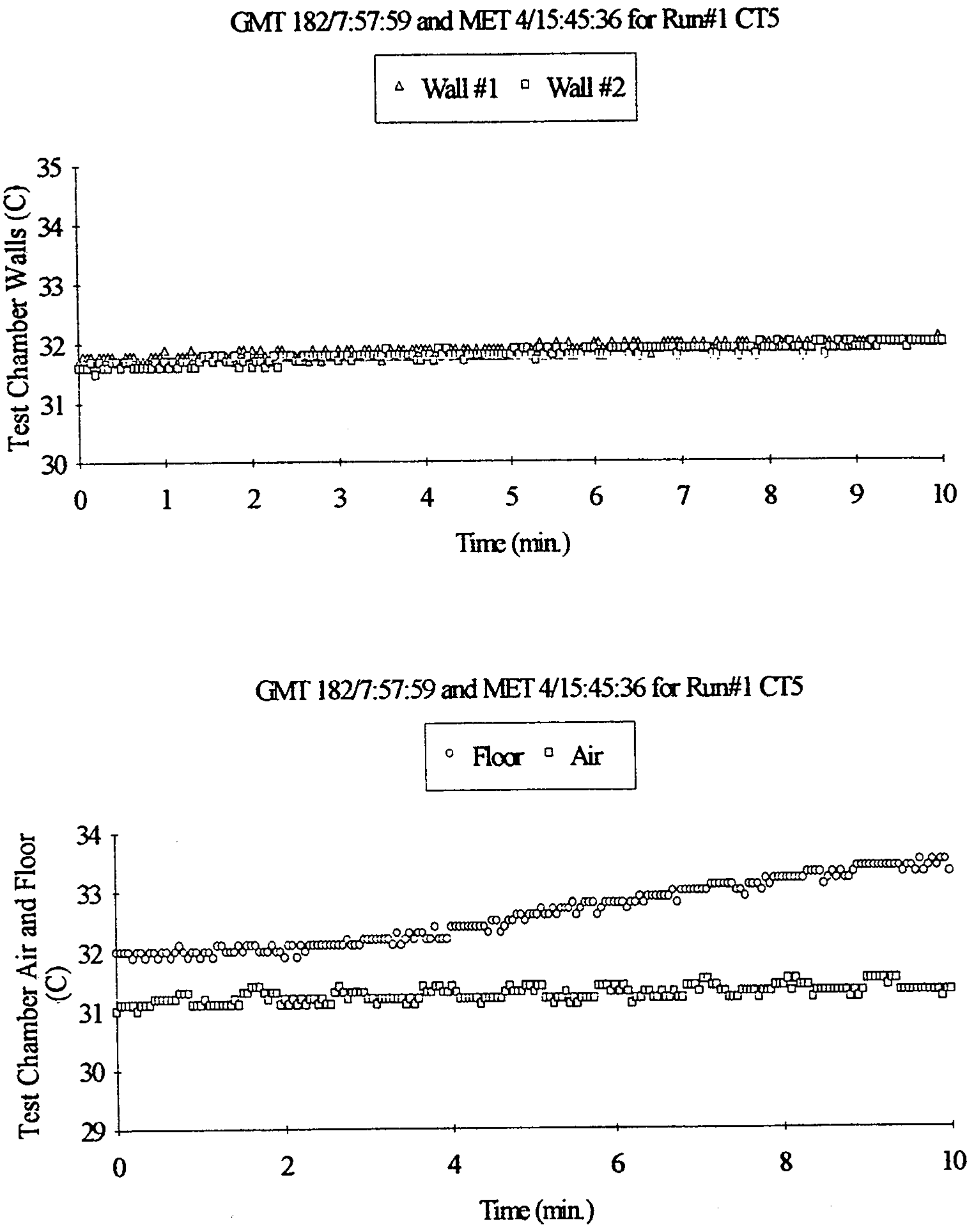

Figure F6 Thermistor data

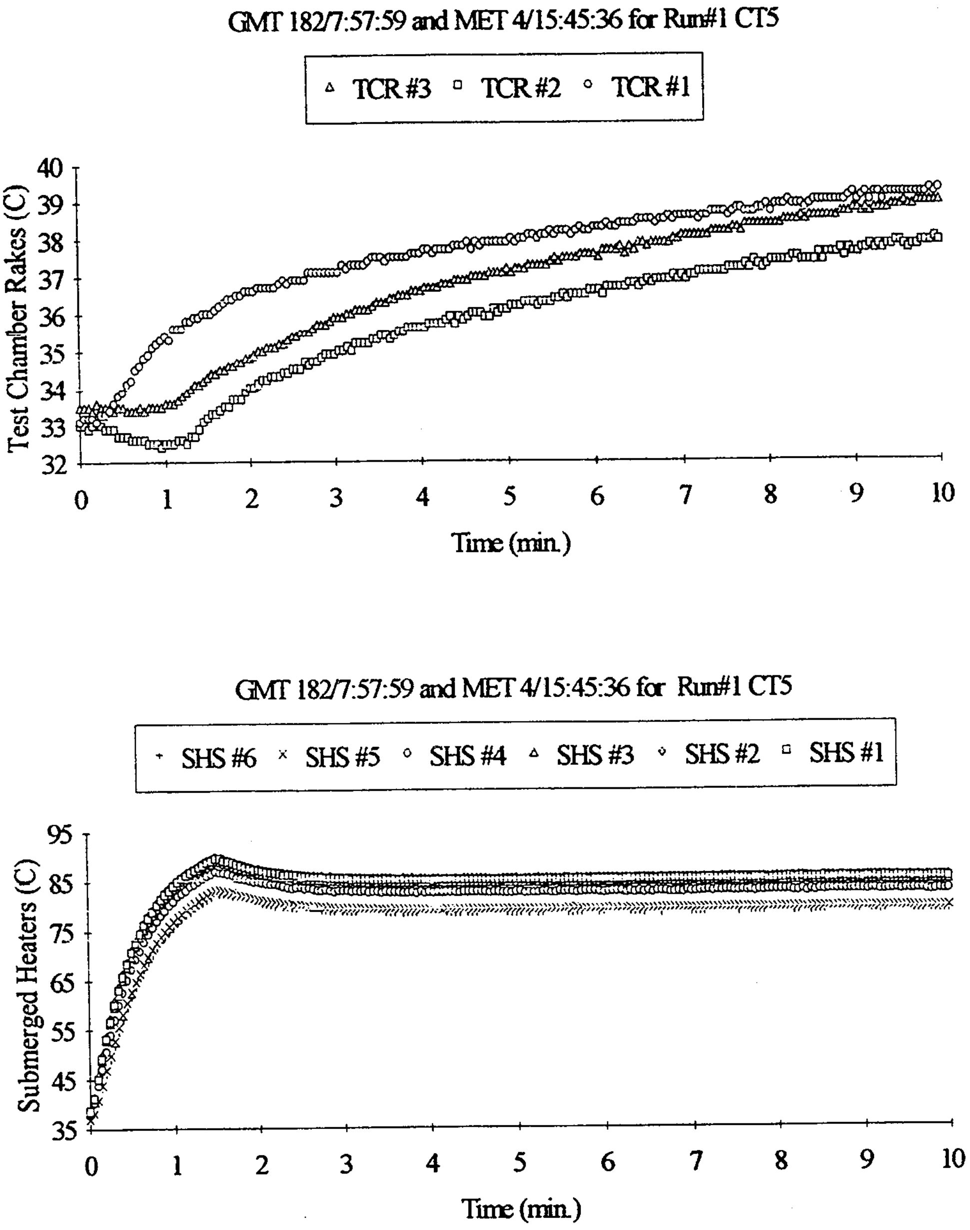

Figure F7 Thermistor data

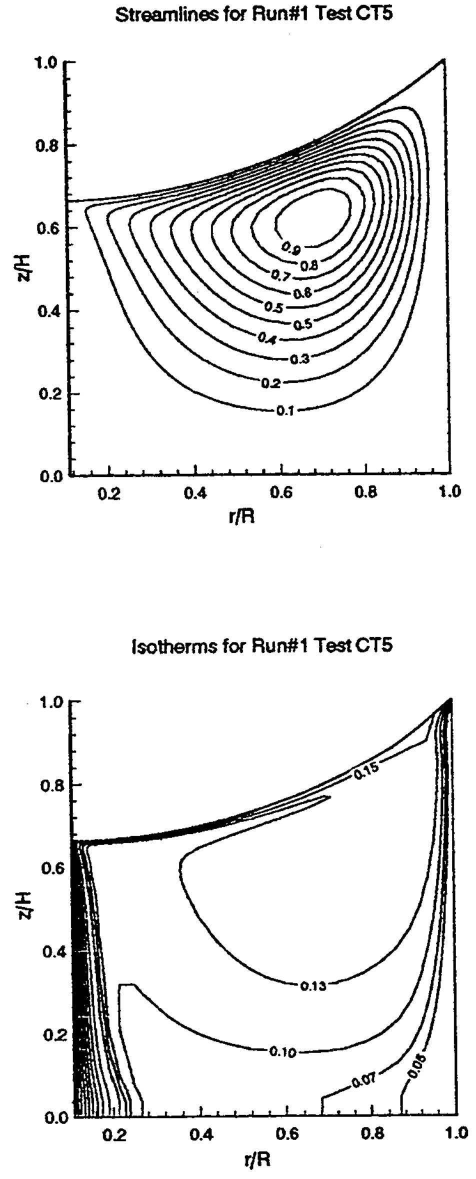

Figure F8 Computed streamlines and isotherms

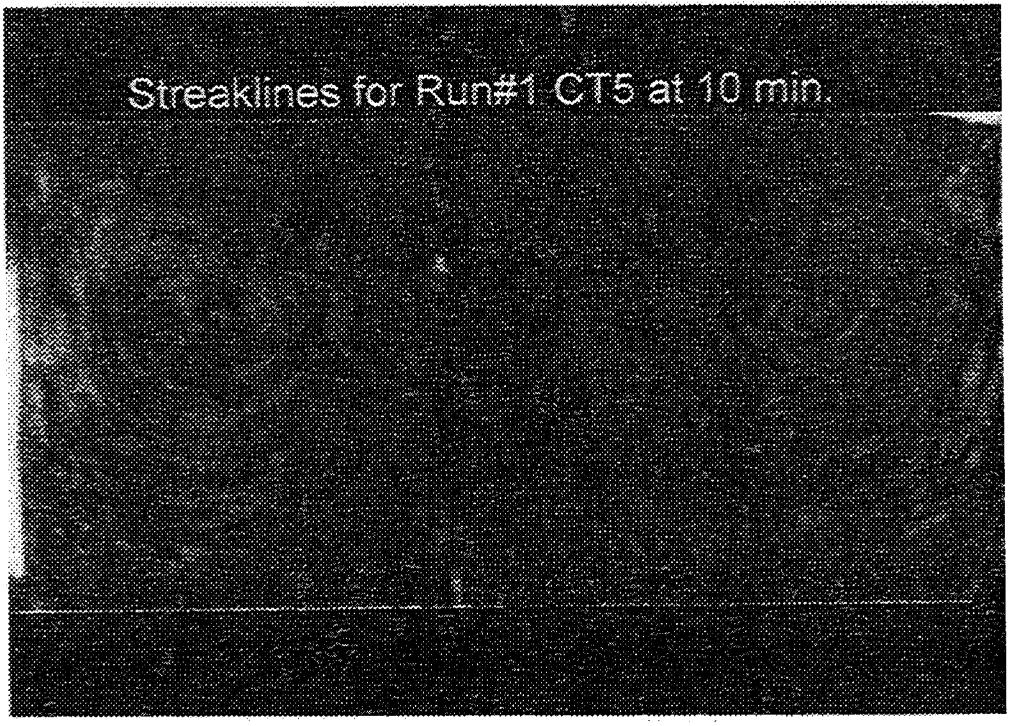

Figure F9 Experimental pathlines

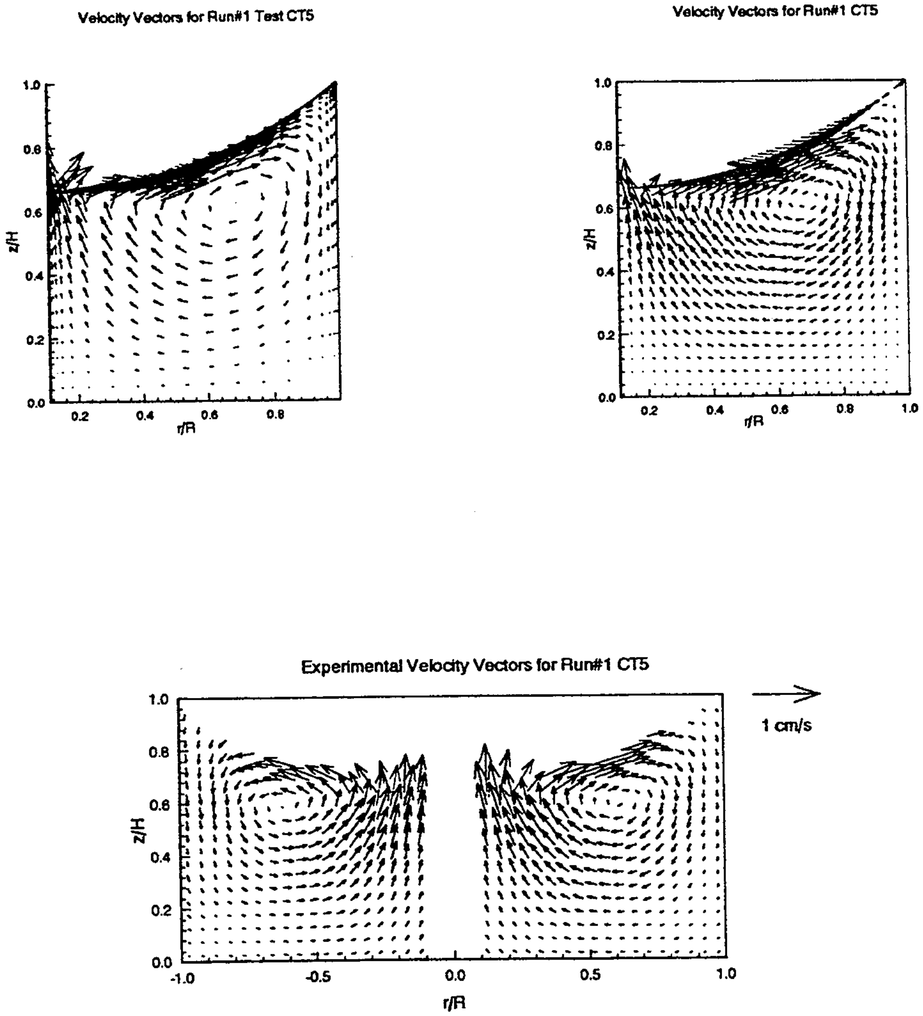

Figure F10 Computed and measured velocity vectors

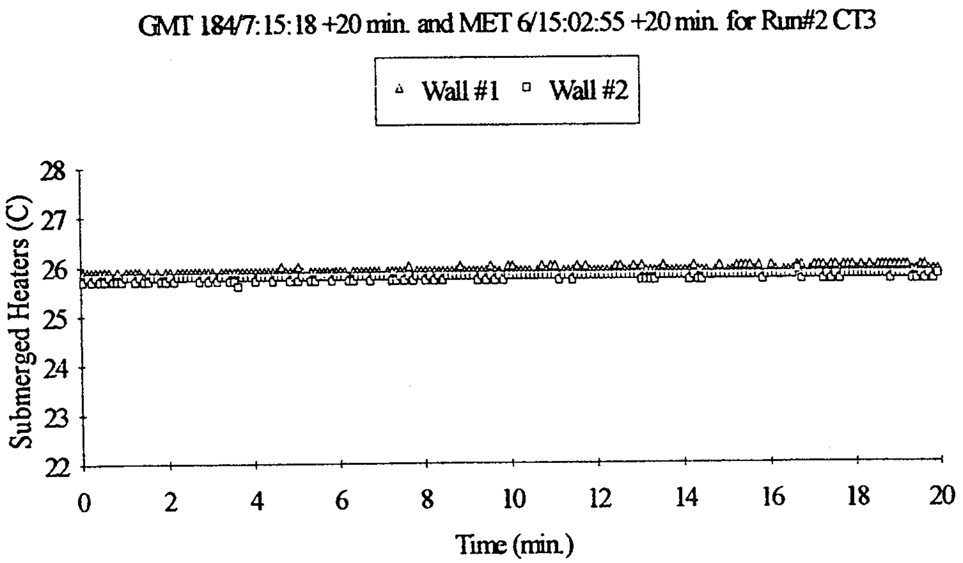

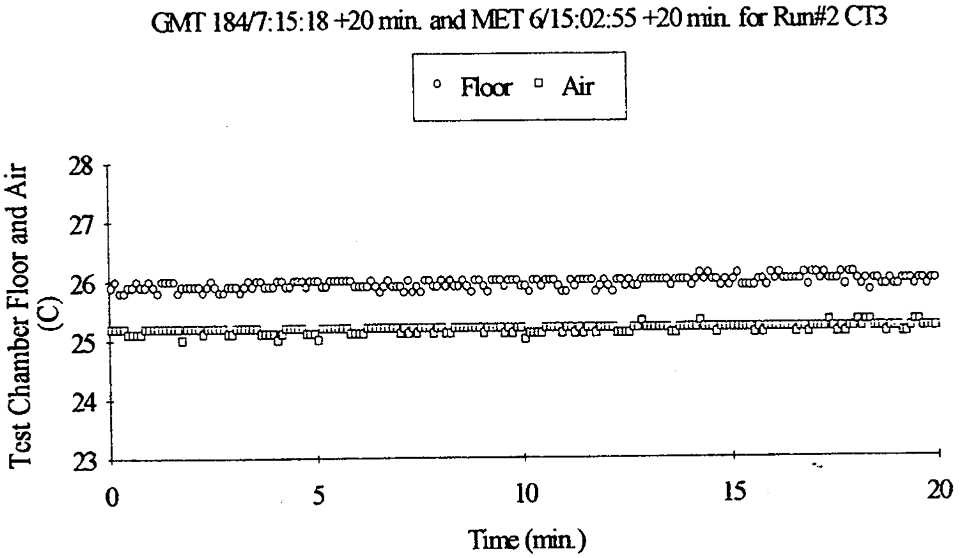

Figure F11 Thermistor data

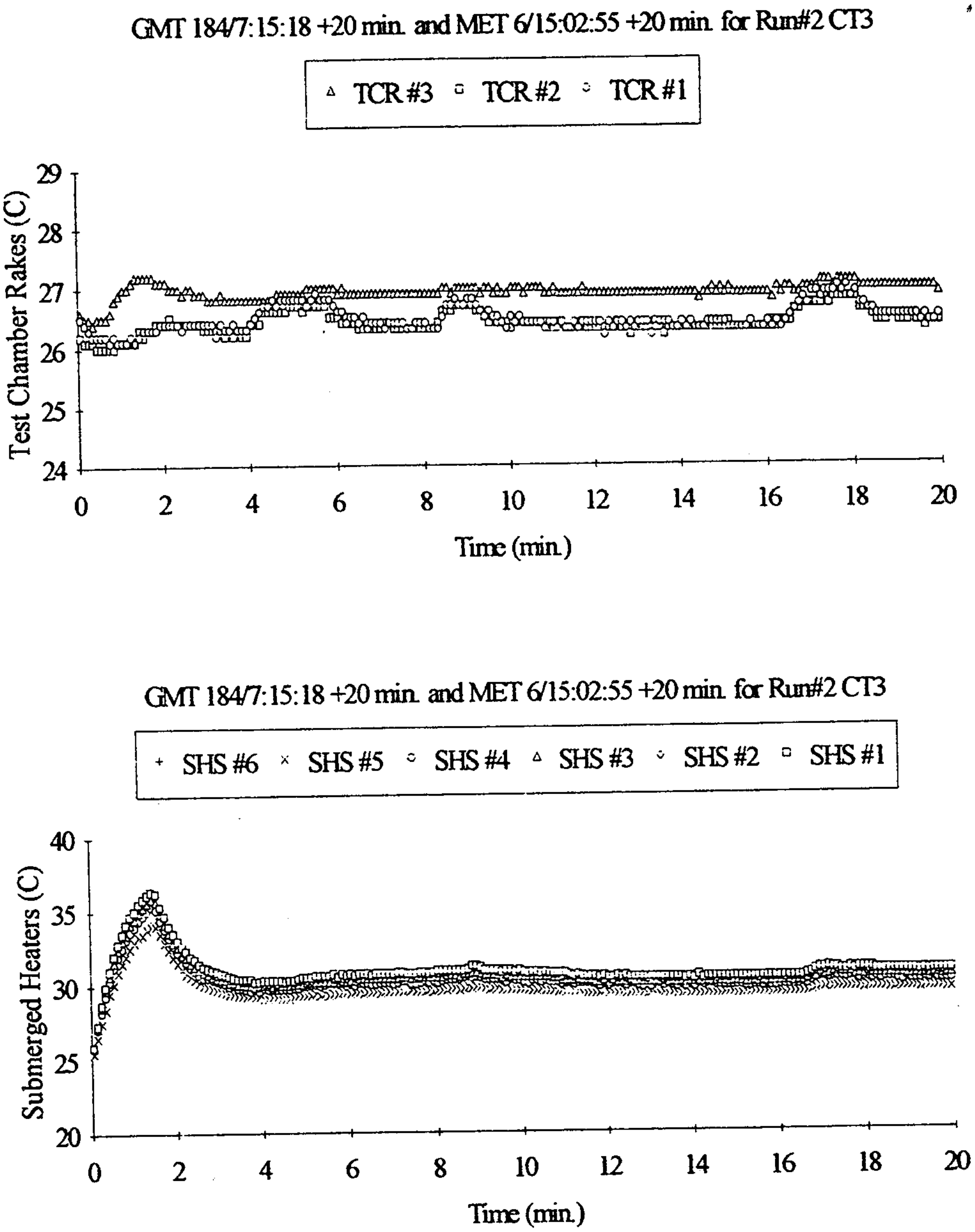

Figure F12 Thermistor data

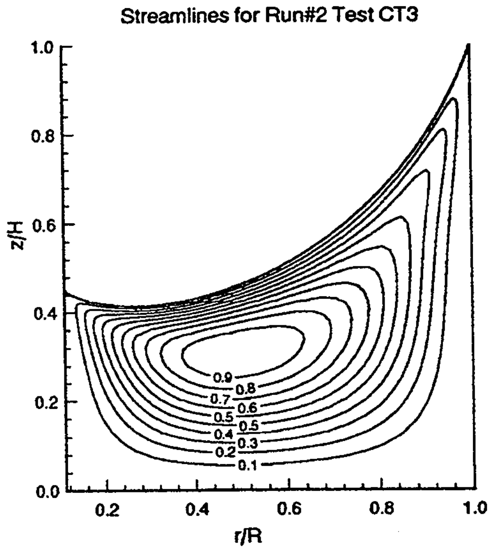

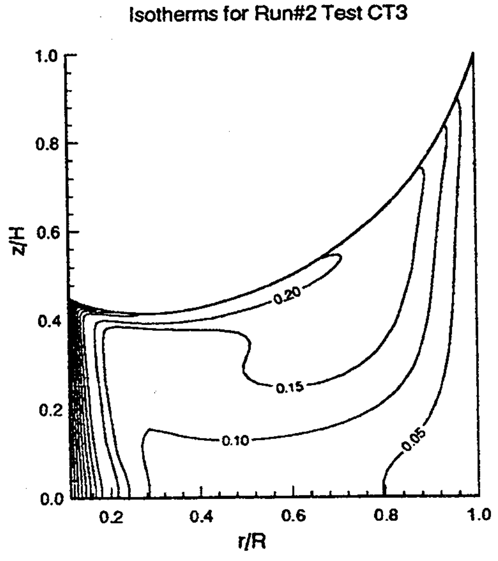

Figure F13 Computed streamlines and isotherms

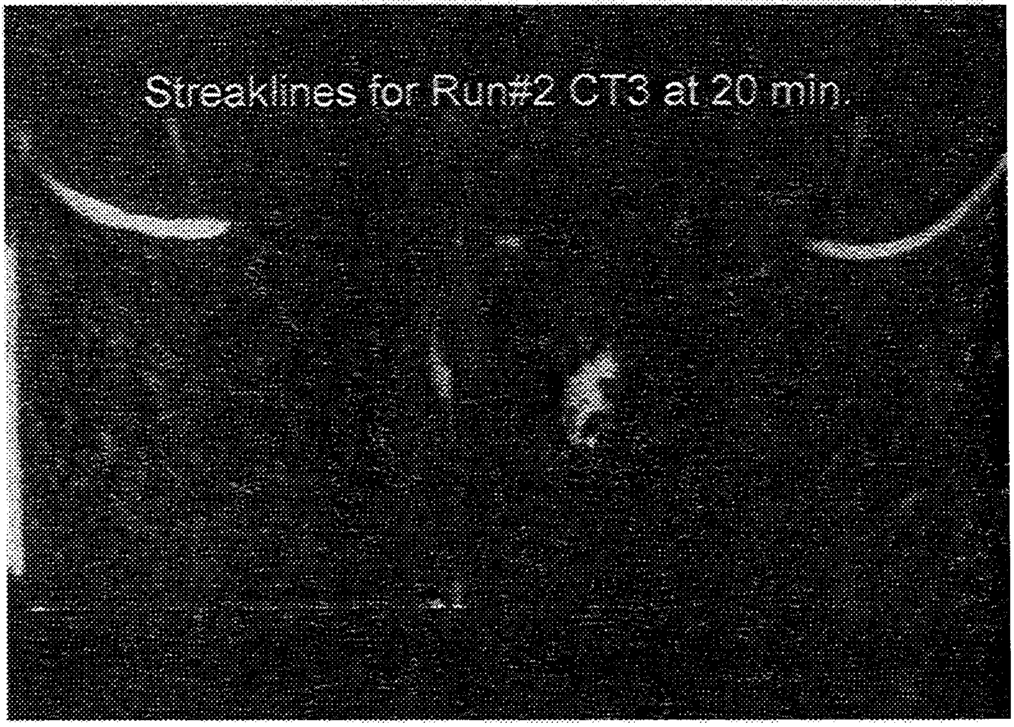

Figure F14 Experimental pathlines

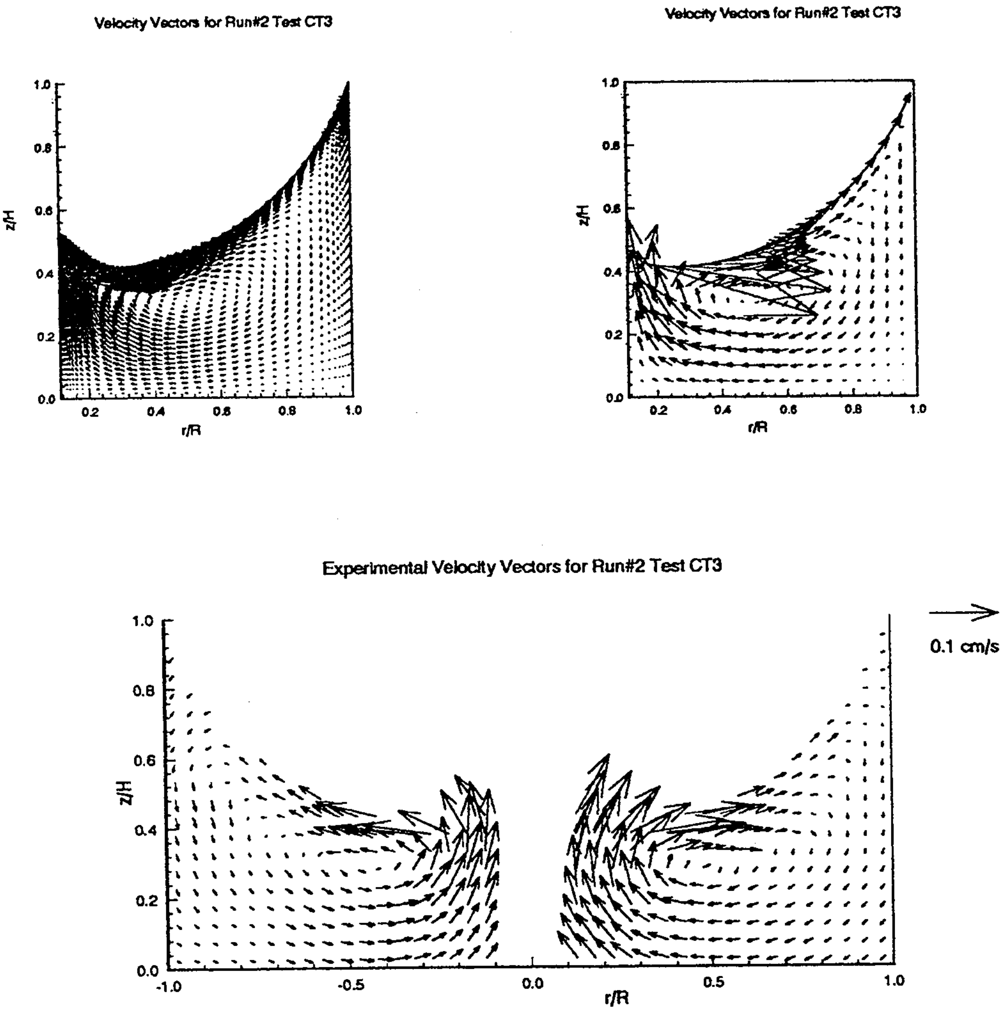

Figure F15 Computed and measured velocity vectors

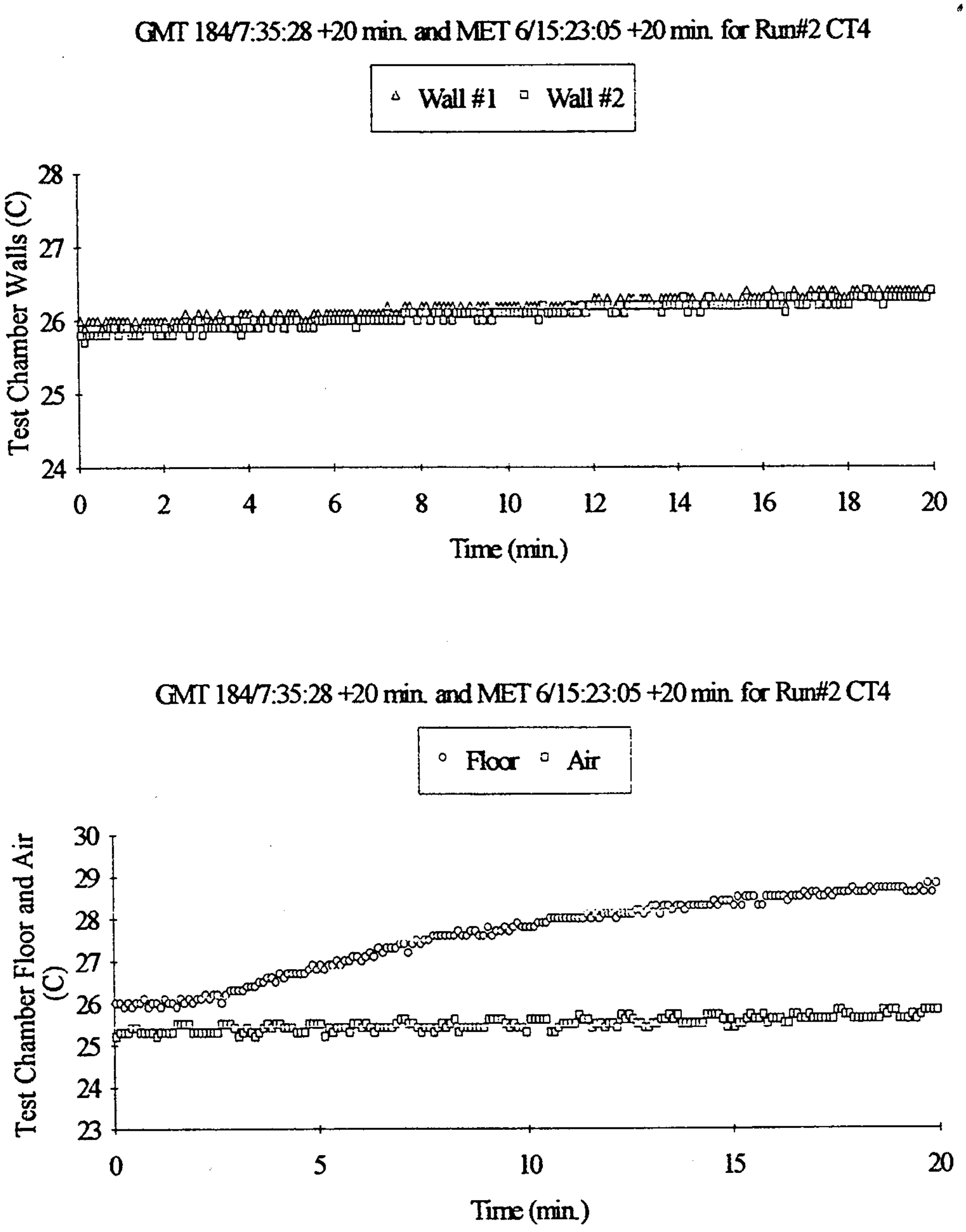

Figure F16 Thermistor data

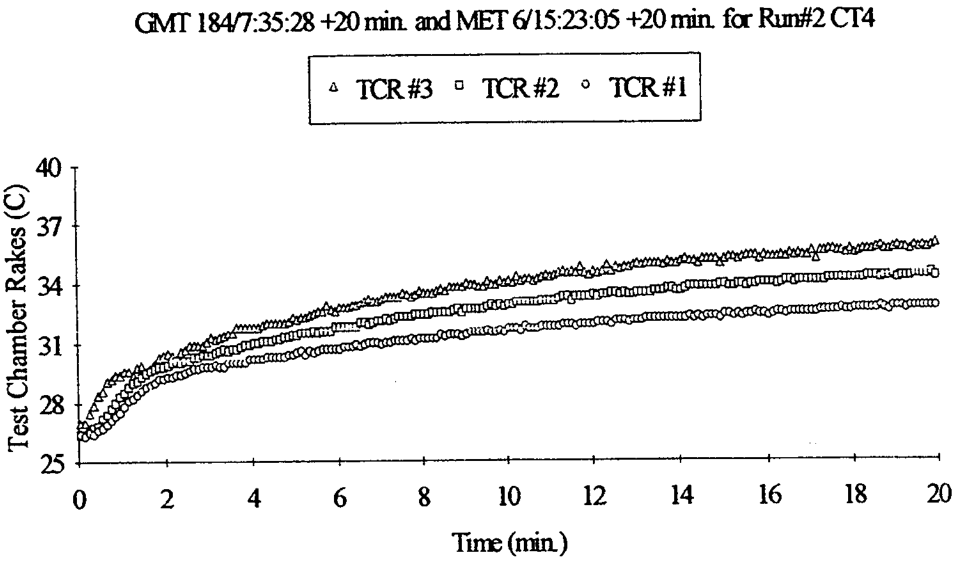

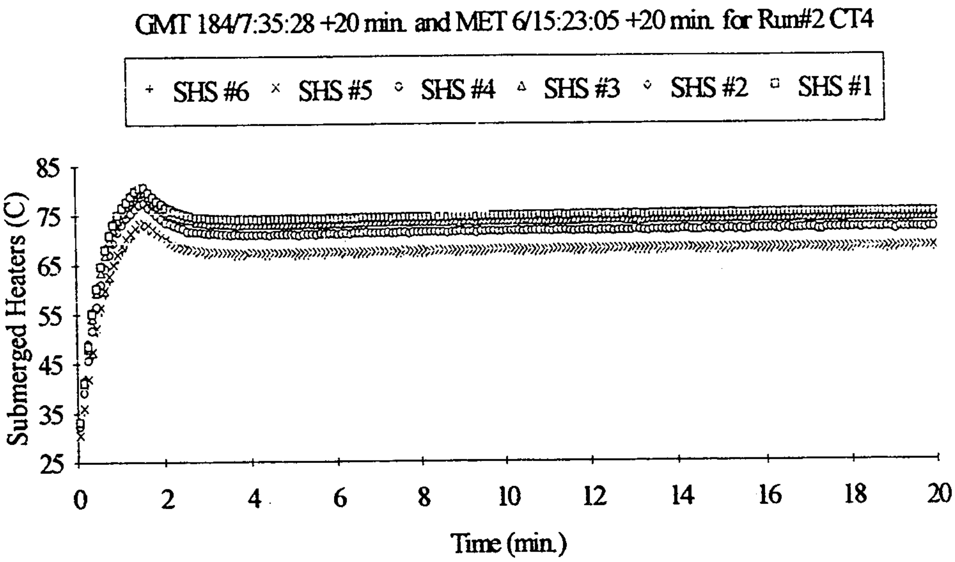

Figure F17 Thermistor data

Streamlines for Run#2 Test CT4

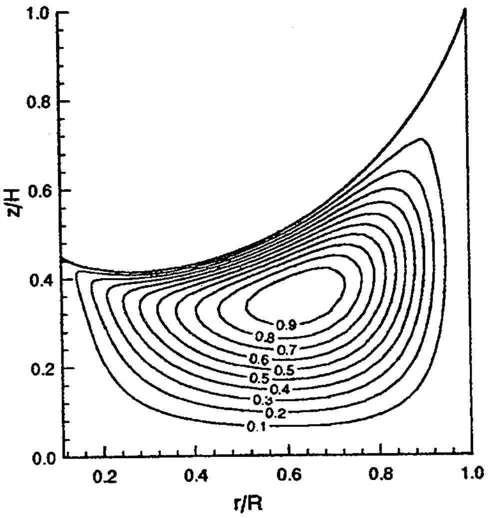

Isotherms for Run#2 Test CT4

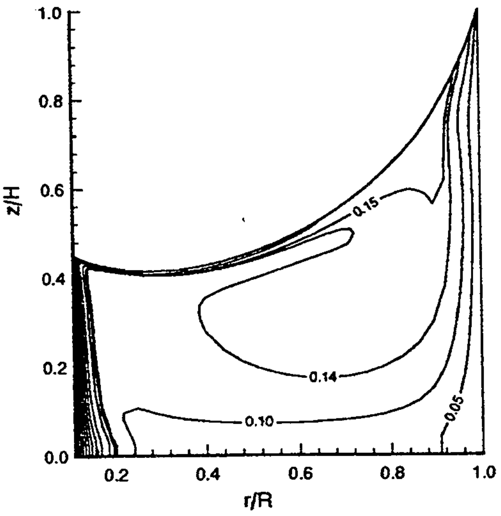

Figure F18 Computed streamlines and isotherms

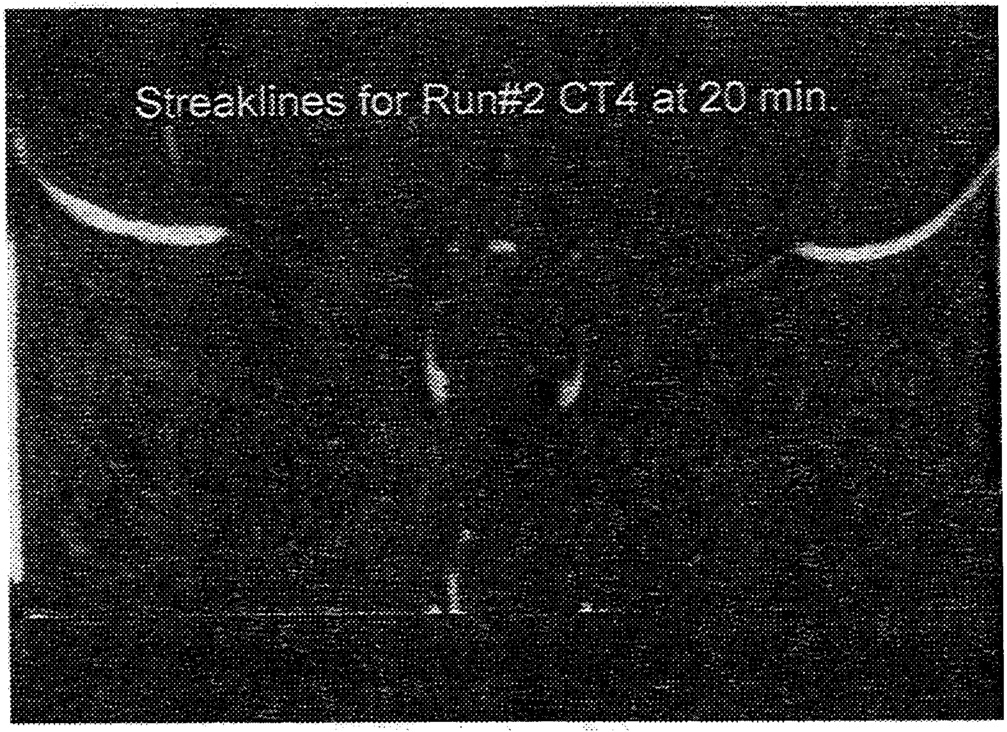

Figure F19 Experimental pathlines

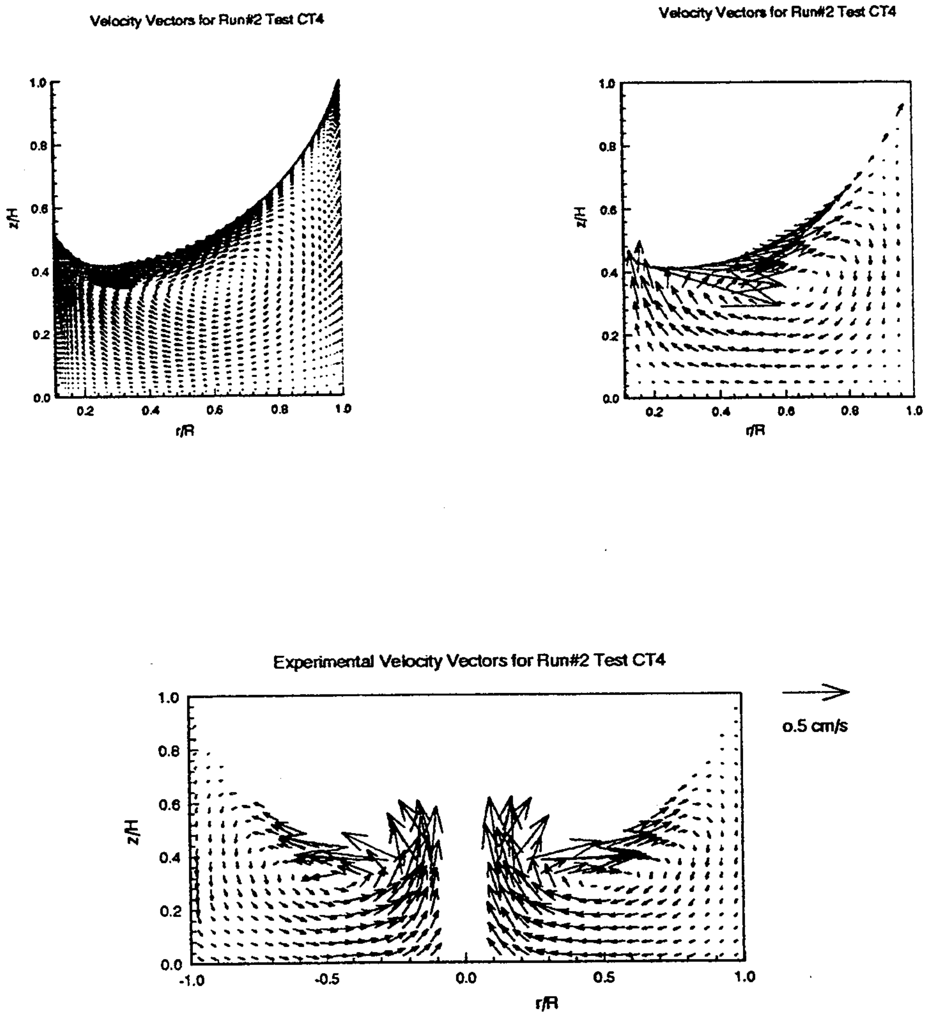

Figure F20 Computed and measured velocity vectors

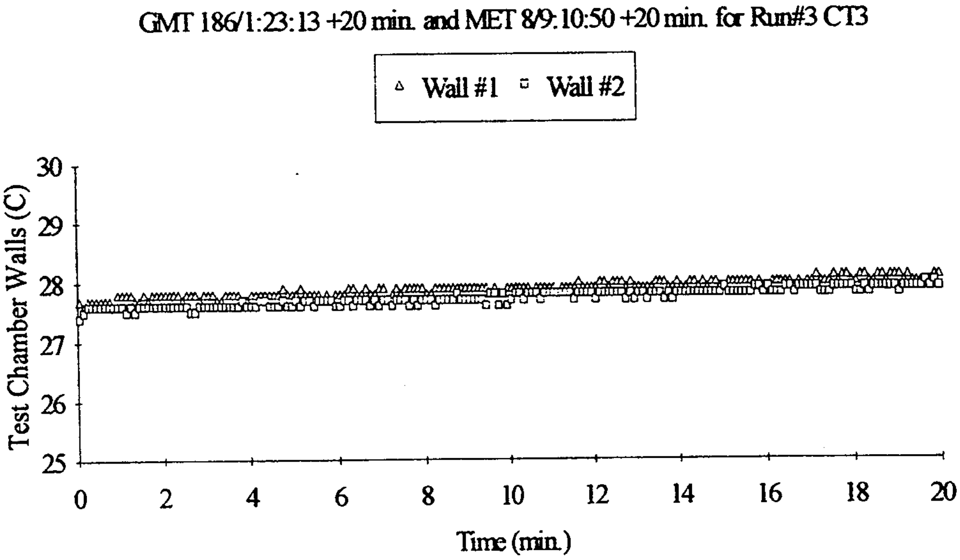

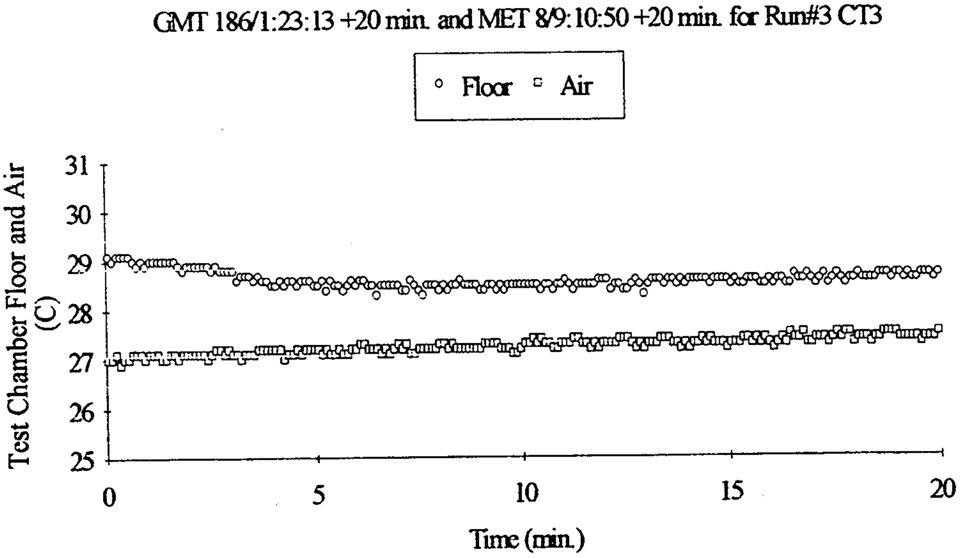

Figure F21 Thermistor data

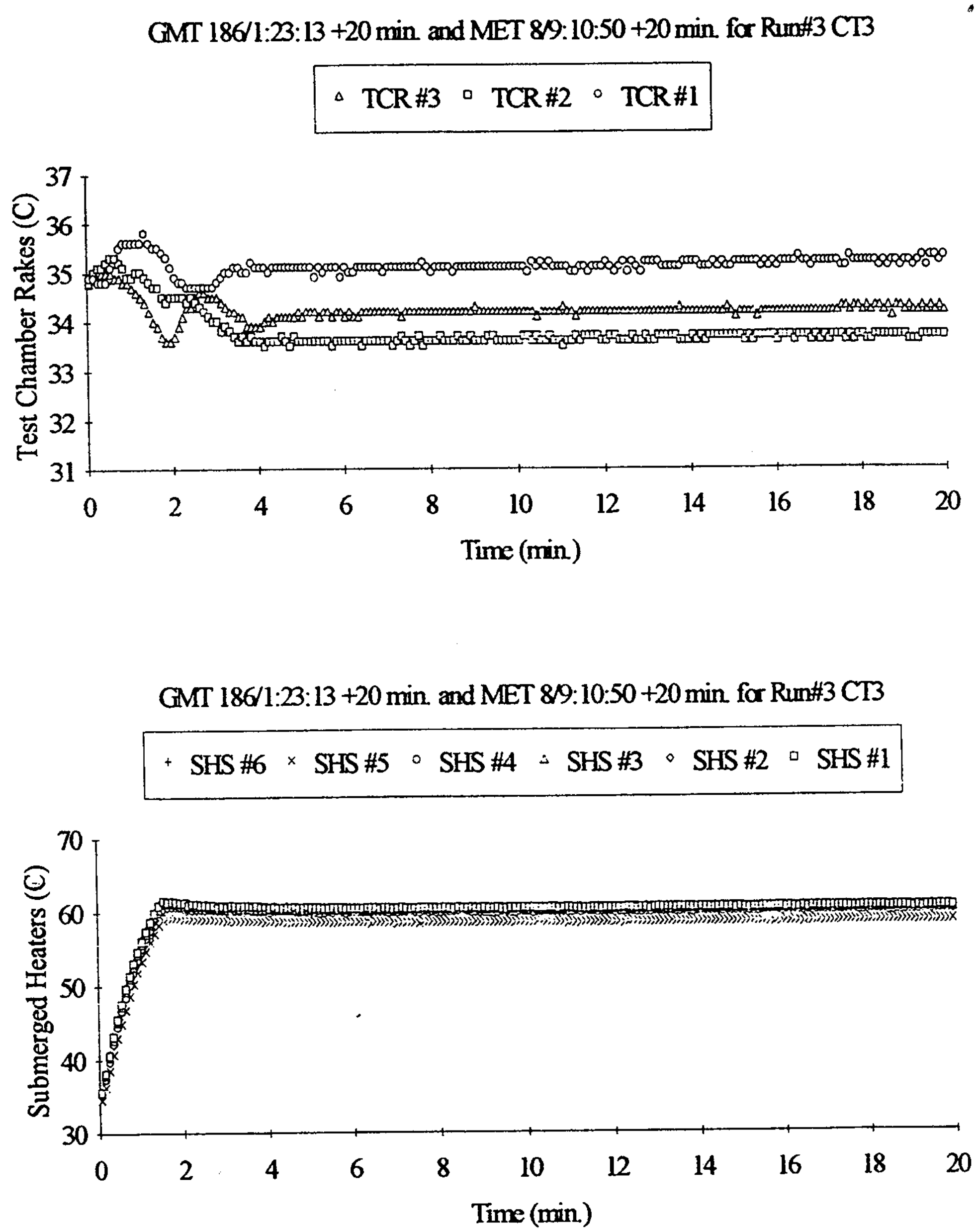

Figure F22 Thermistor data

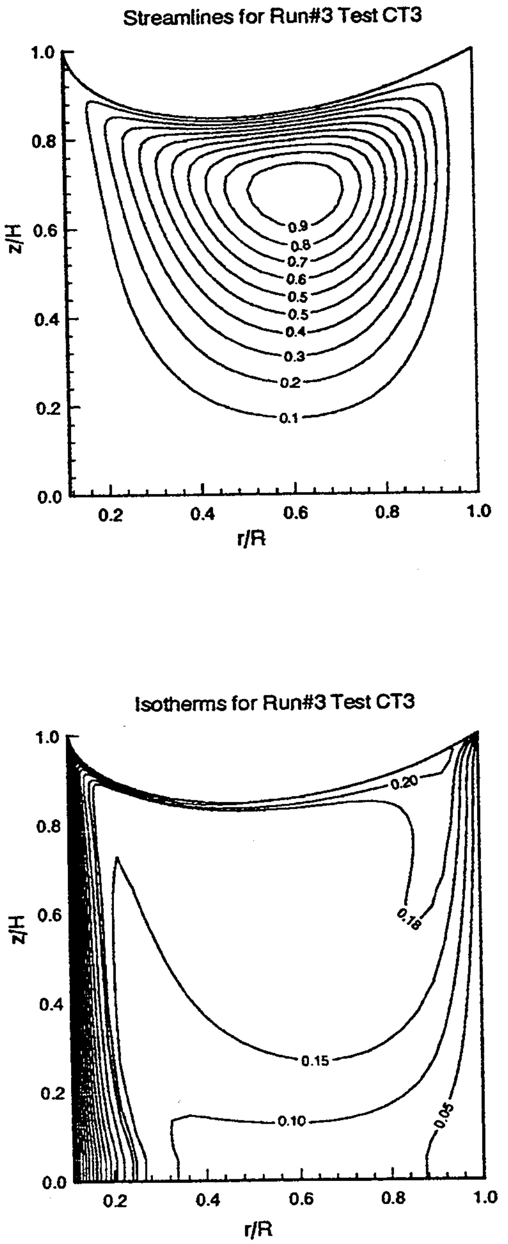
Streamlines for Run#3 Test CT3

Isotherms for Run#3 Test CT3

Figure F23 Computed streamlines and isotherms

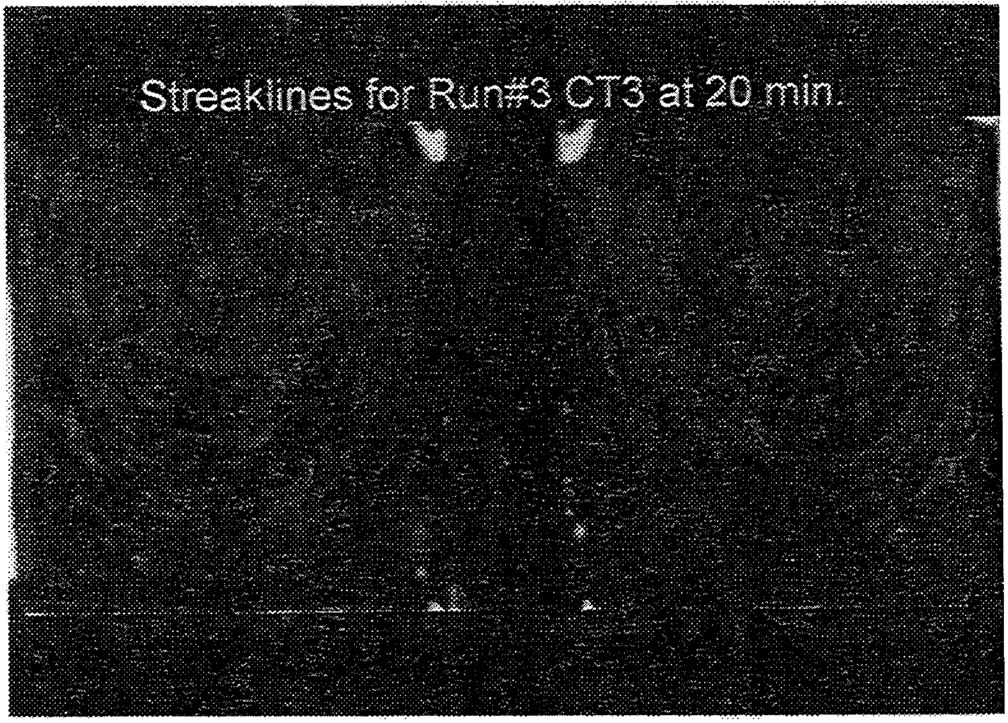

Figure F24 Experimental pathlines

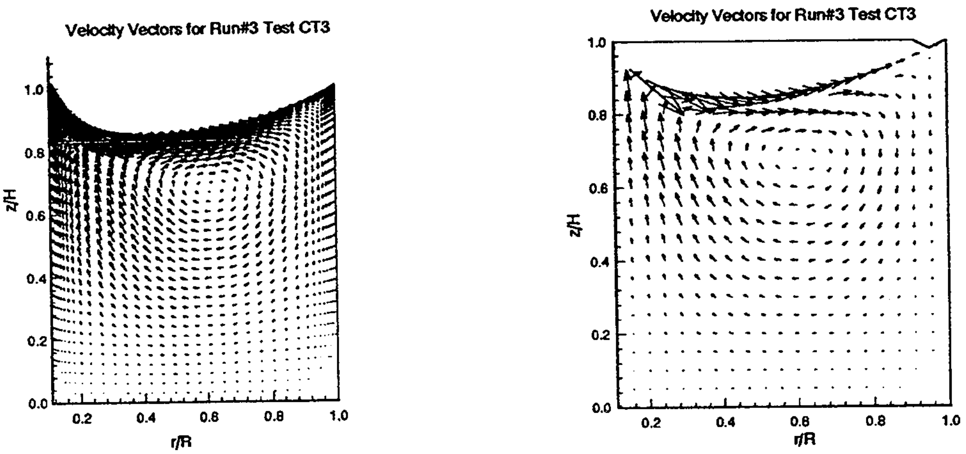

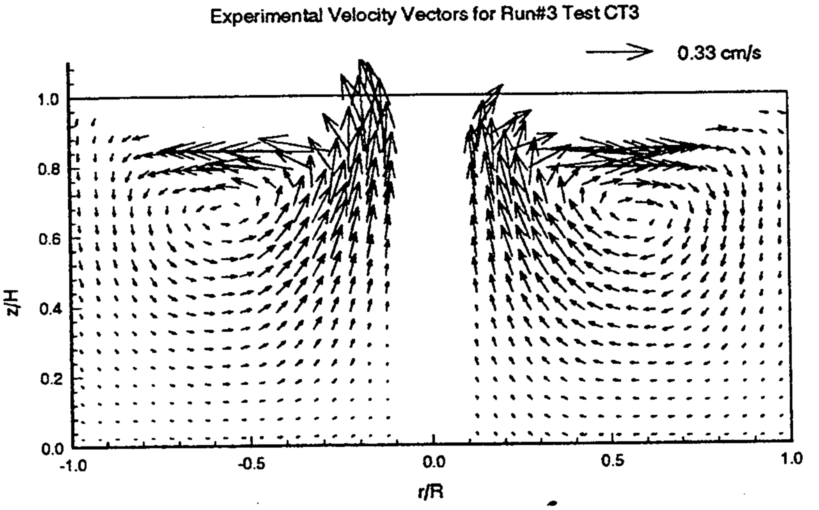

Figure F25 Computed and measured velocity vectors

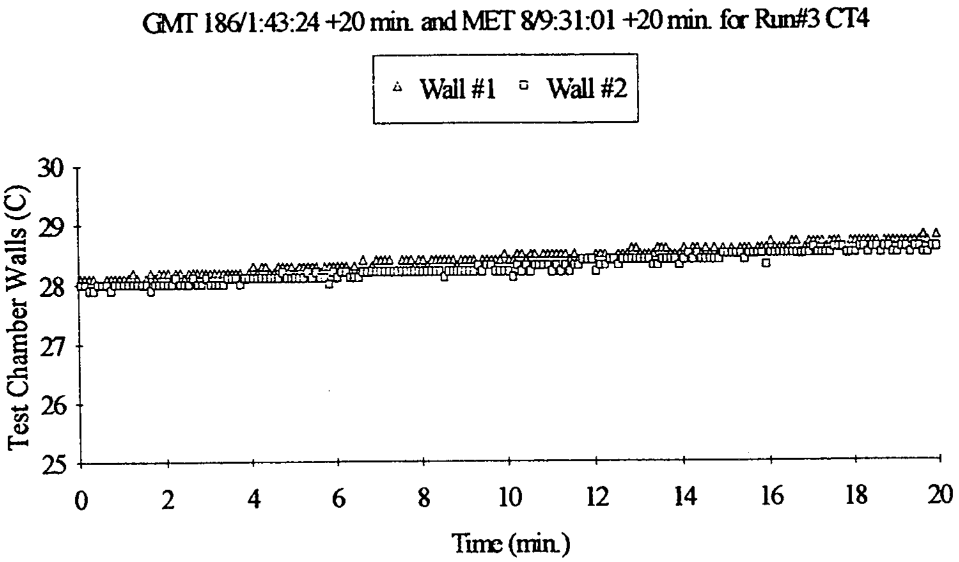

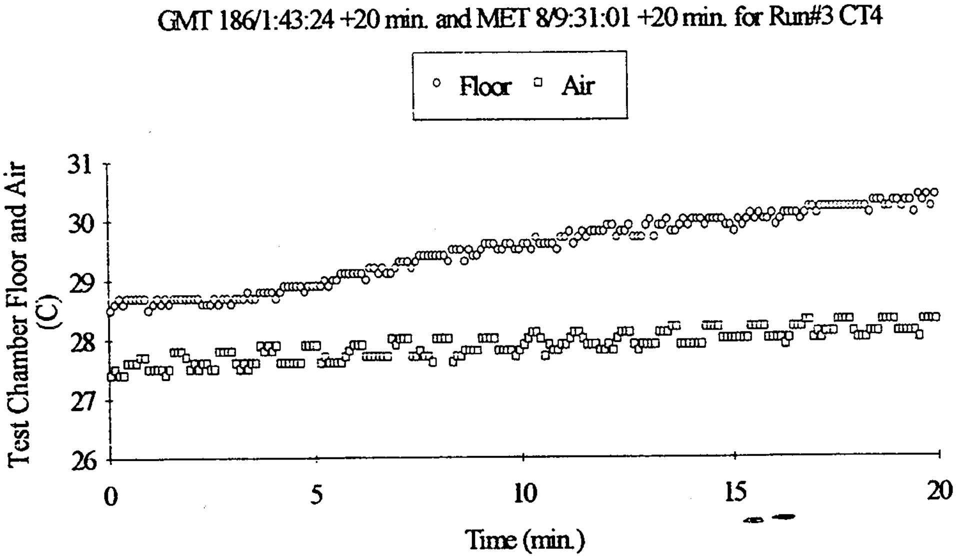

Figure F26 Thermistor data

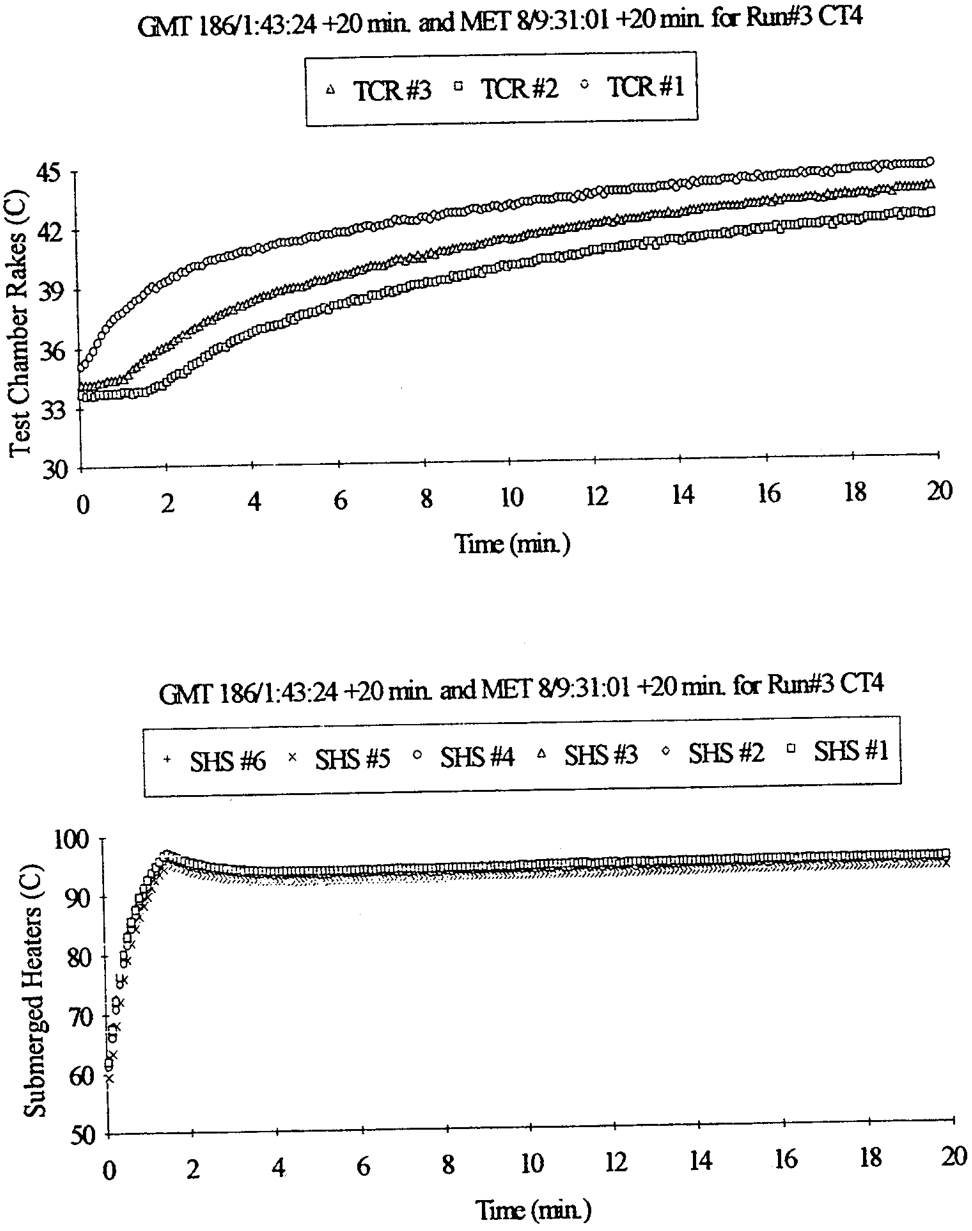

Figure F27 Thermistor data

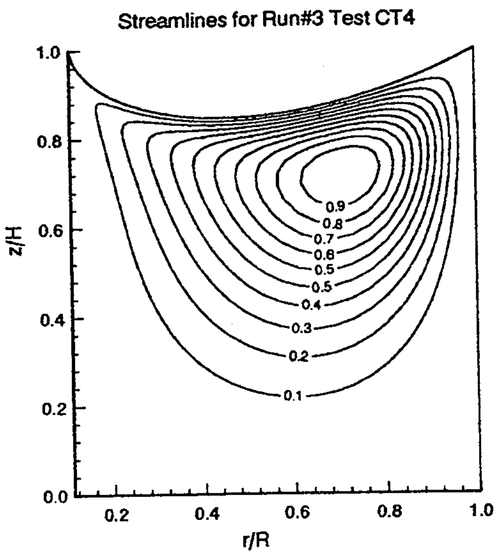

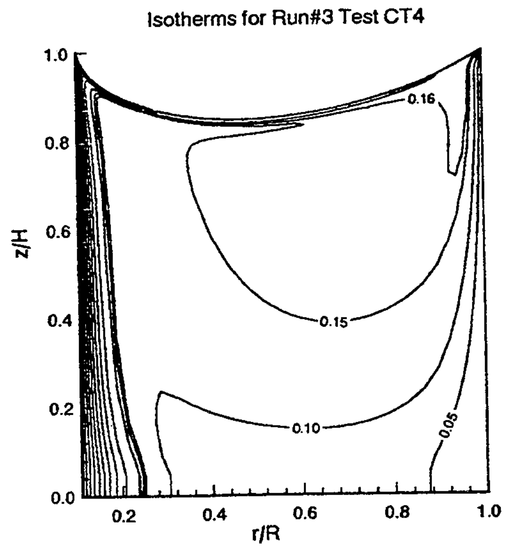

Figure F28 Computed streamlines and isotherms

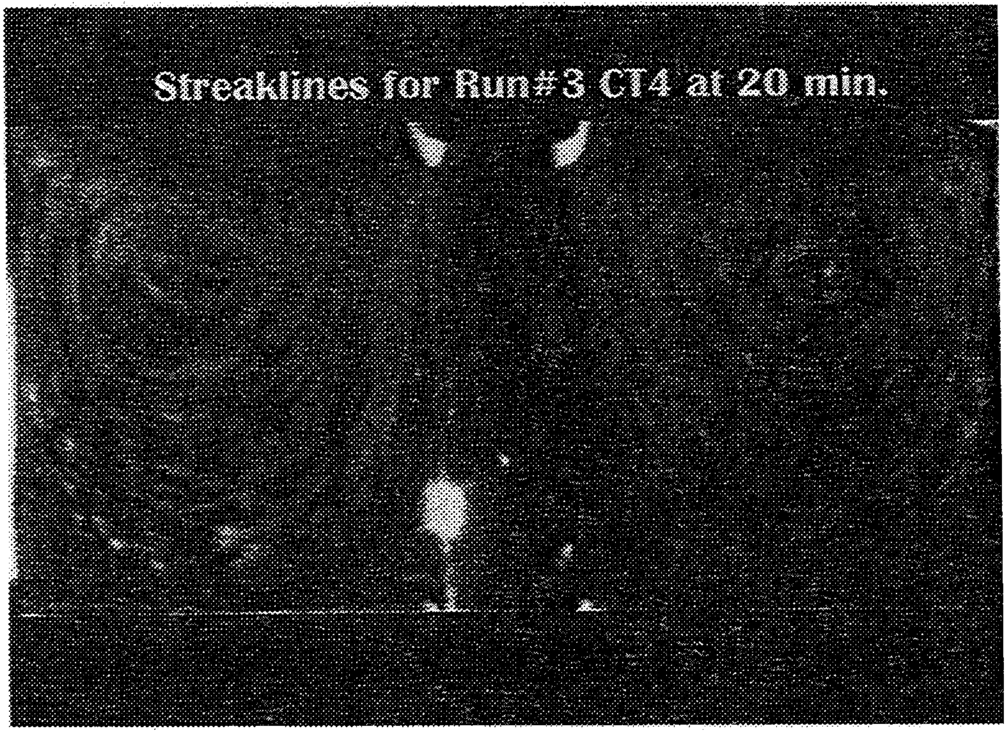

Figure F29 Experimental pathlines

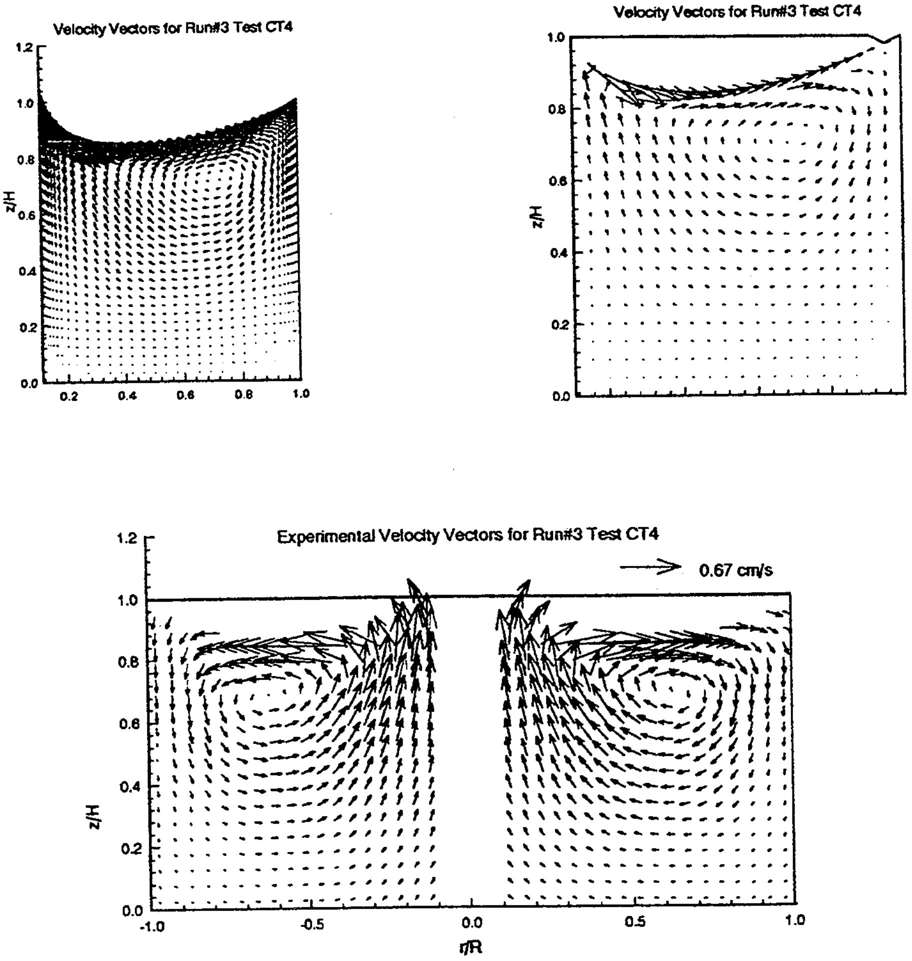

Figure F30 Computed and measured velocity vectors

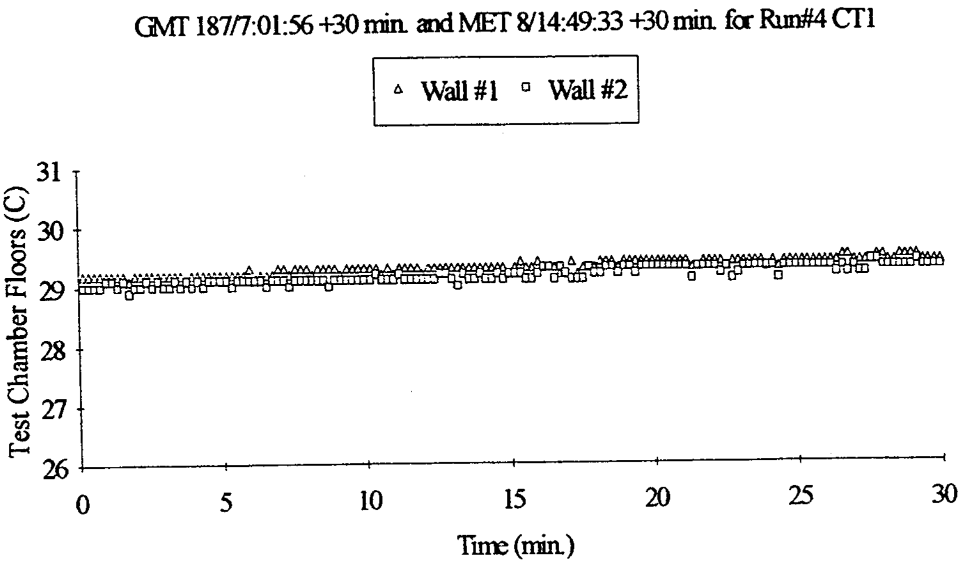

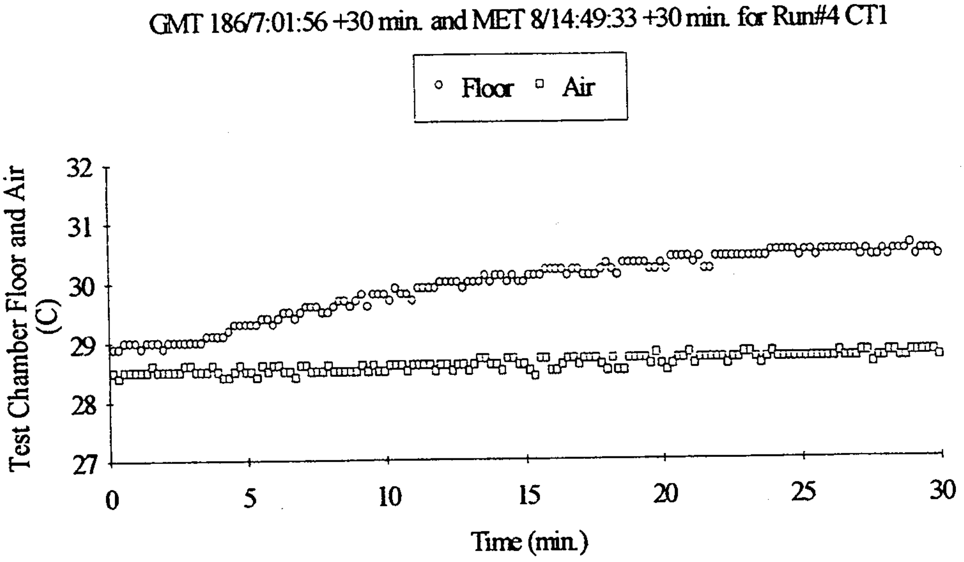

Figure F31 Thermistor data

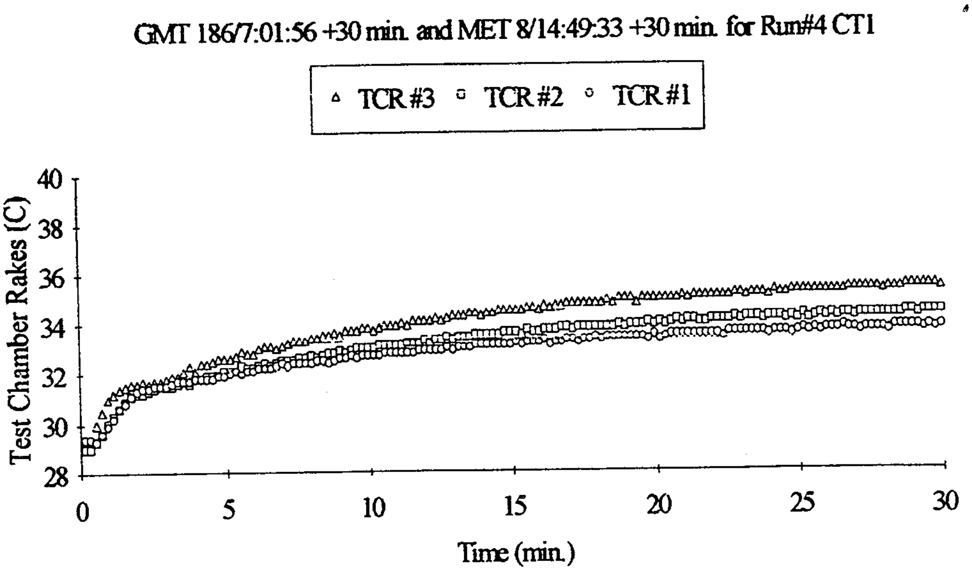

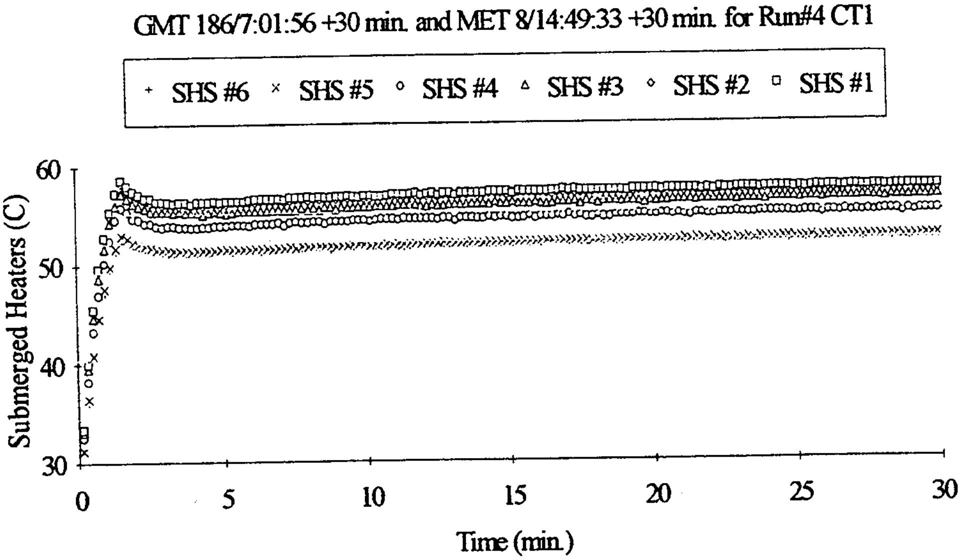

Figure F32 Thermistor data

Streamlines for Run#4 Test CT1

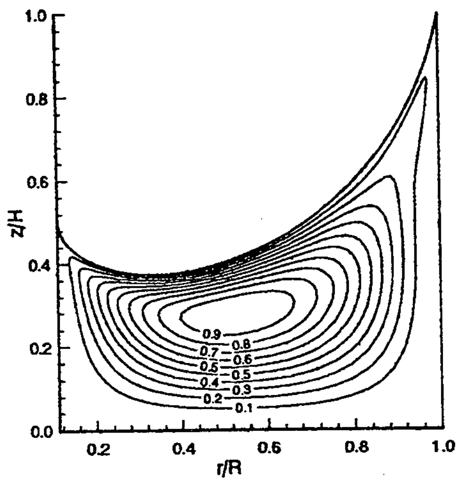

Isotherms for Run#4 Test CT1

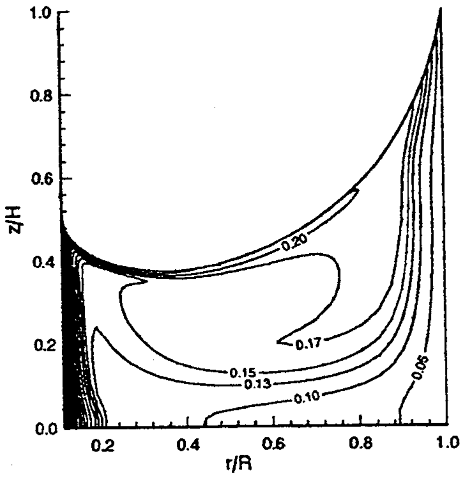

Figure F33 Computed streamlines and isotherms

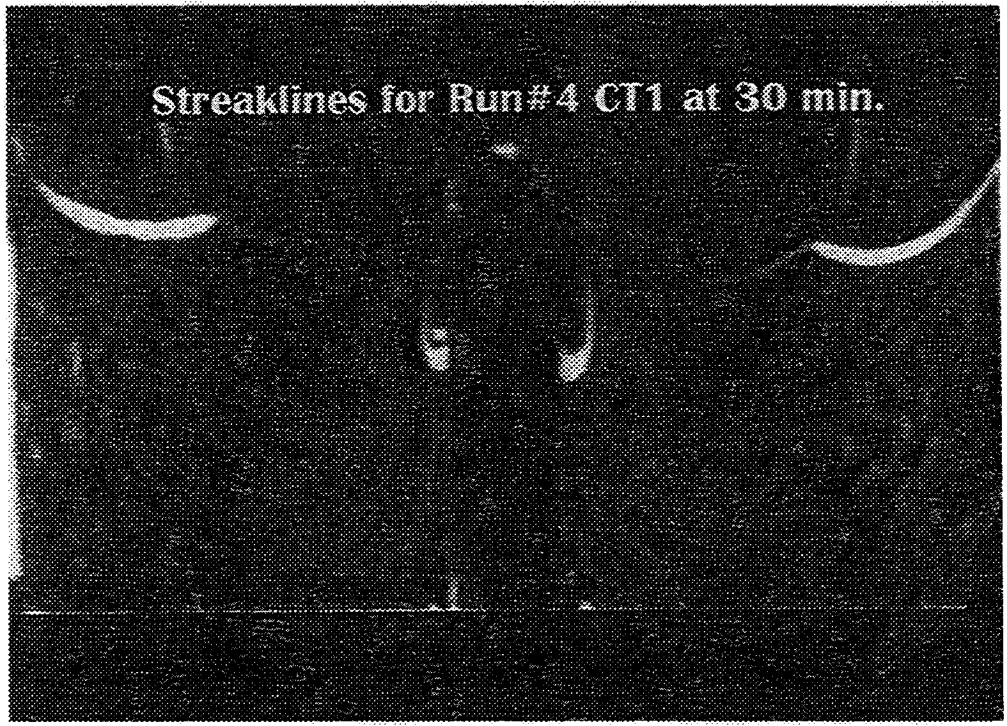

Figure F34 Experimental pathlines

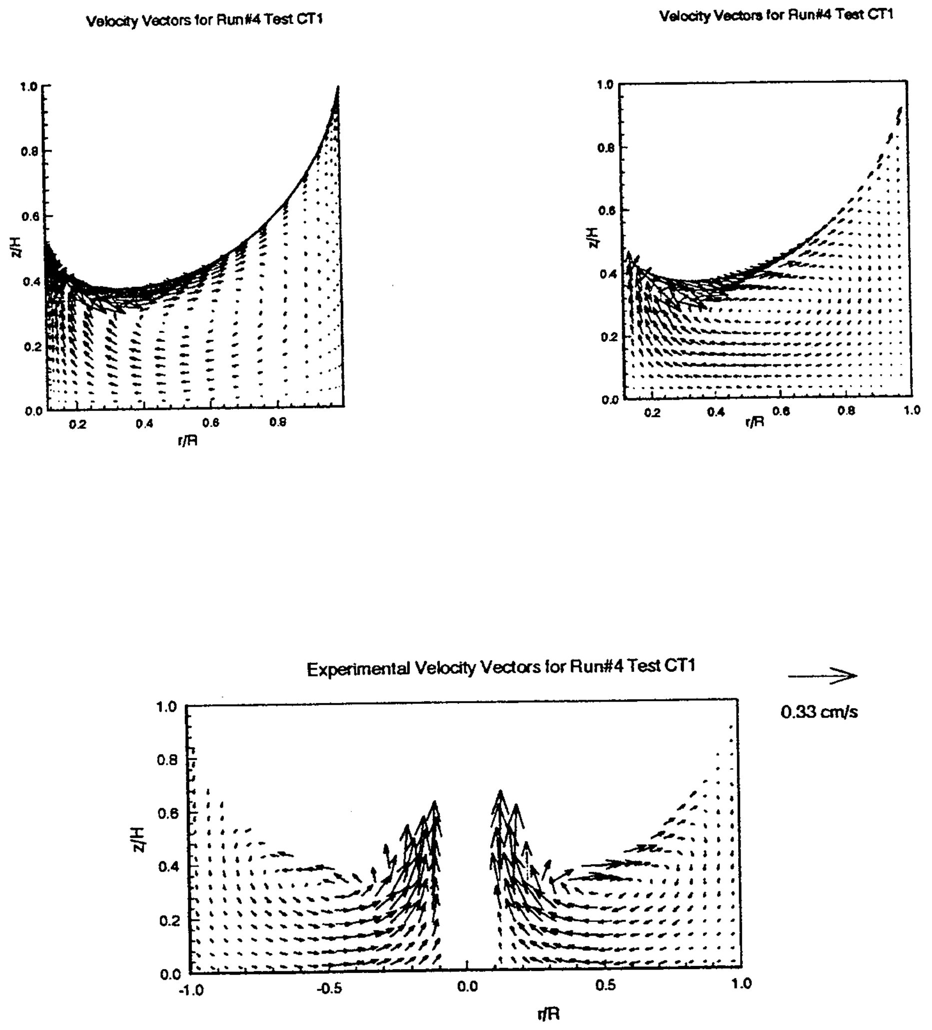

Velocity Vectors for Run#4 Test CT1

Velocity Vectors for Run#4 Test CT1

Experimental Velocity Vectors for Run#4 Test CT1

Figure F35 Computed and measured velocity vectors

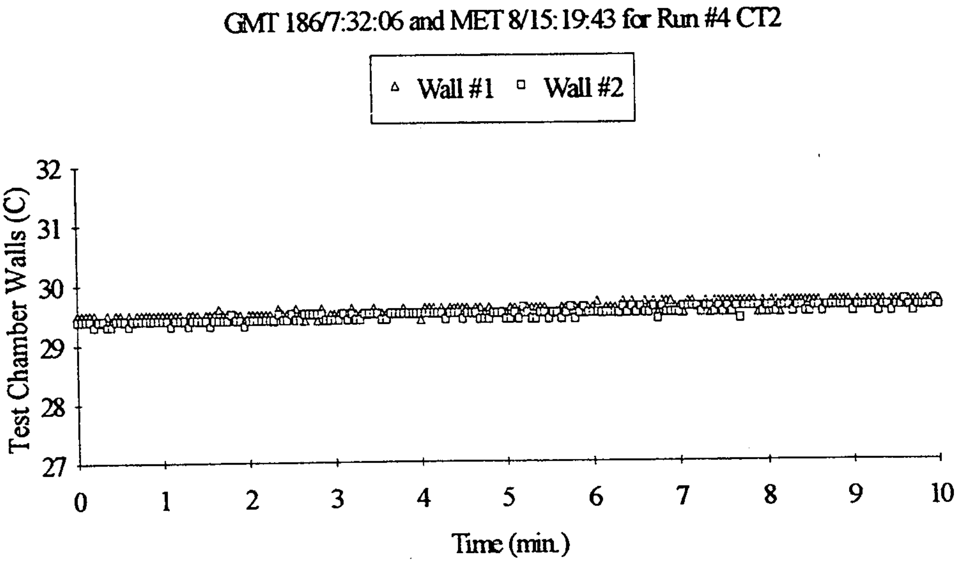

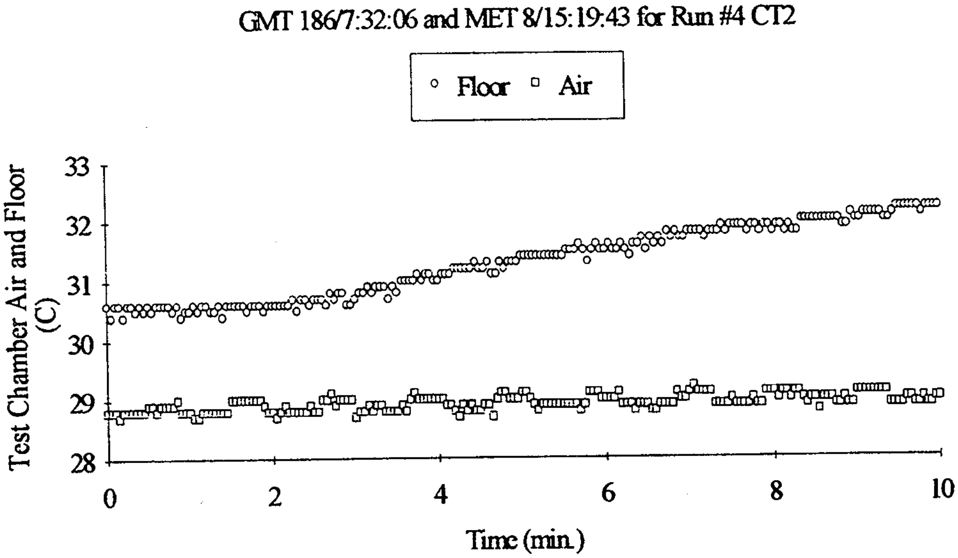

Figure F36 Thermistor data

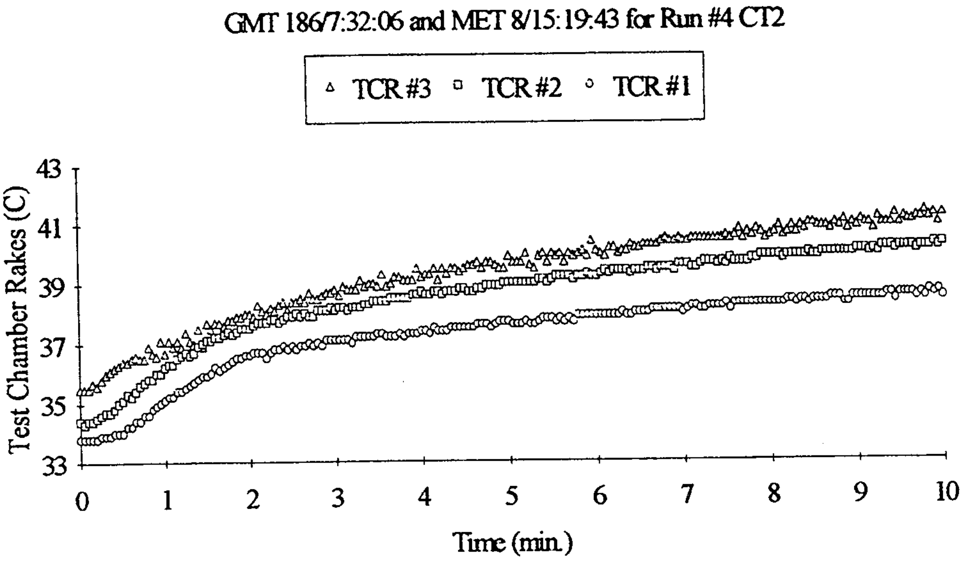

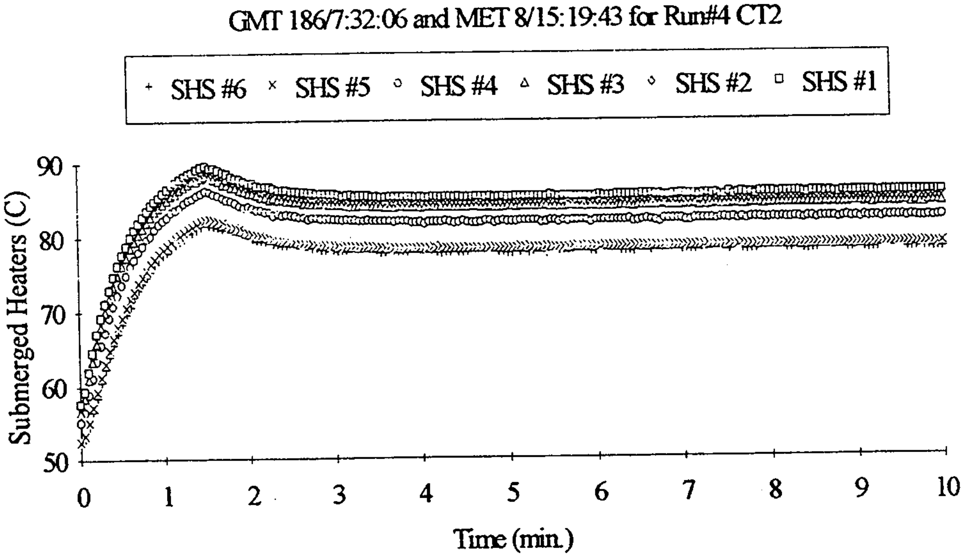

Figure F37 Thermistor data

Streamlines for Run#4 Test CT2

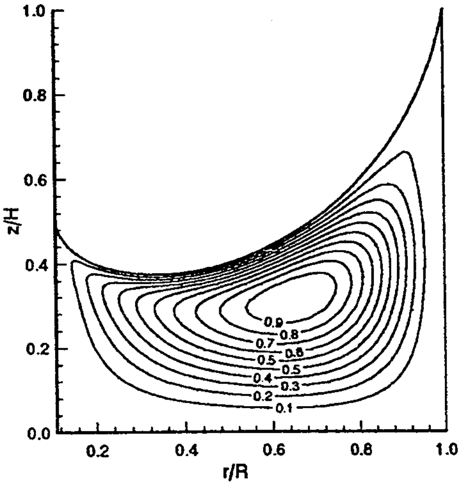

Isotherms for Run#4 Test CT2

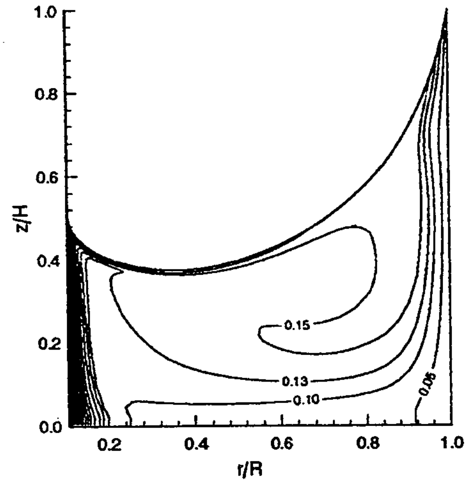

Figure F38 Computed streamlines and isotherms

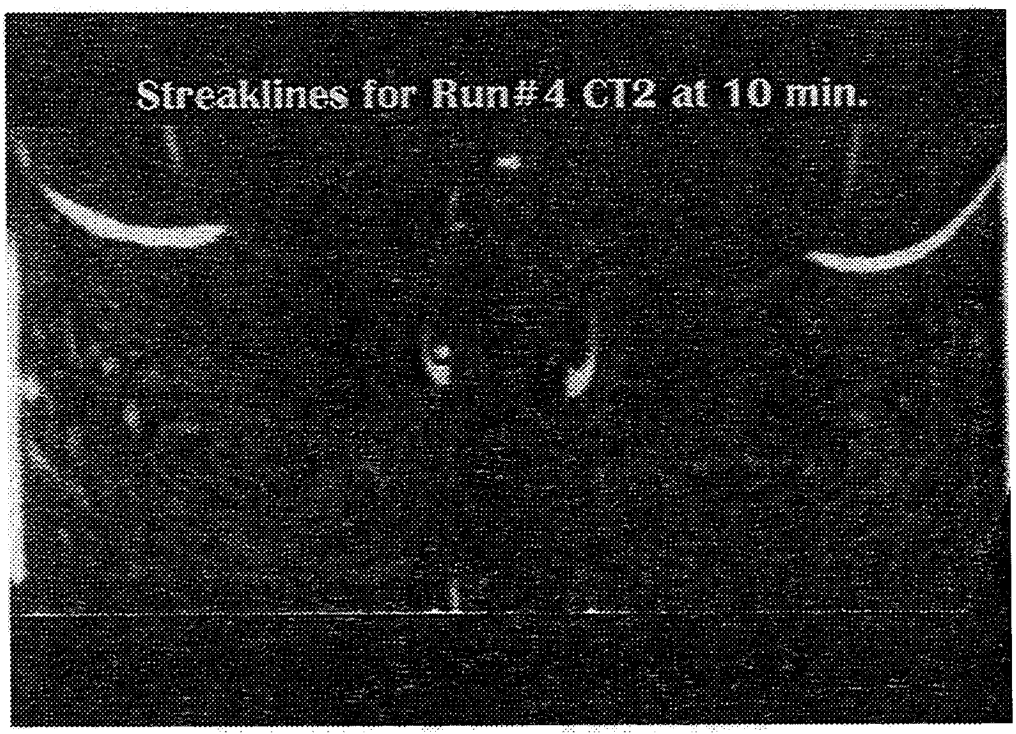

Figure F39 Experimental pathlines

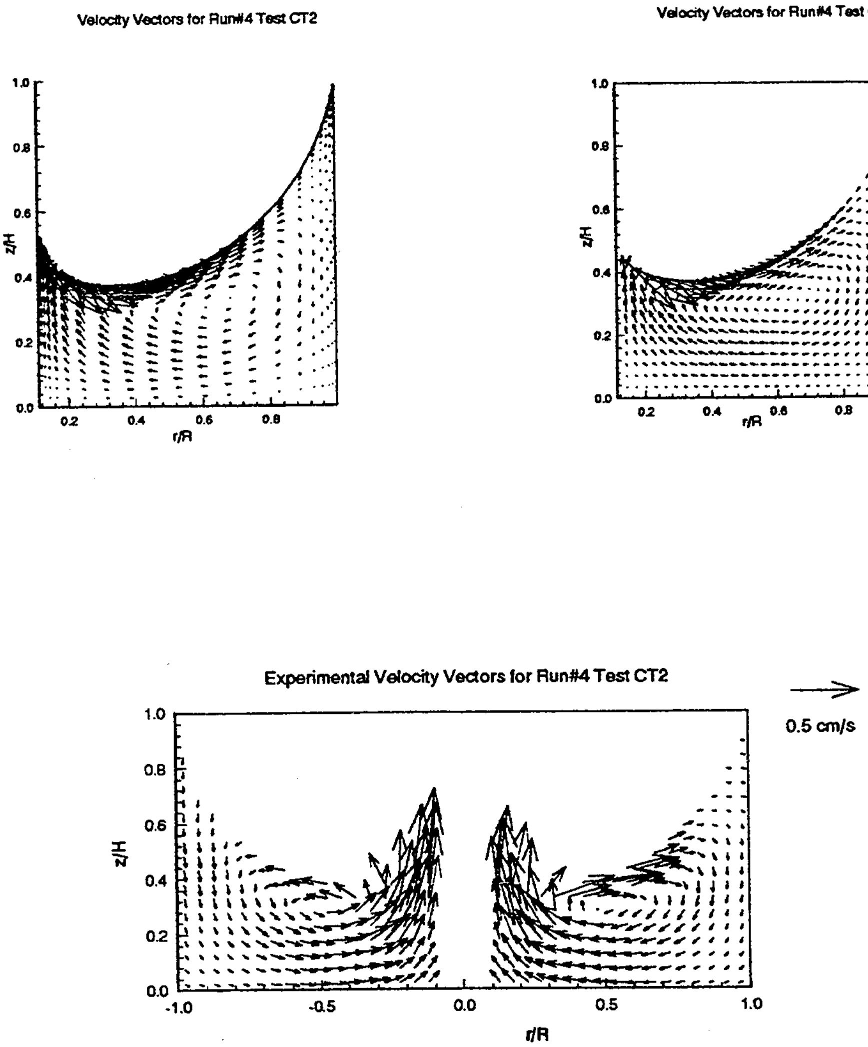

Figure F40 Computed and measured velocity vectors

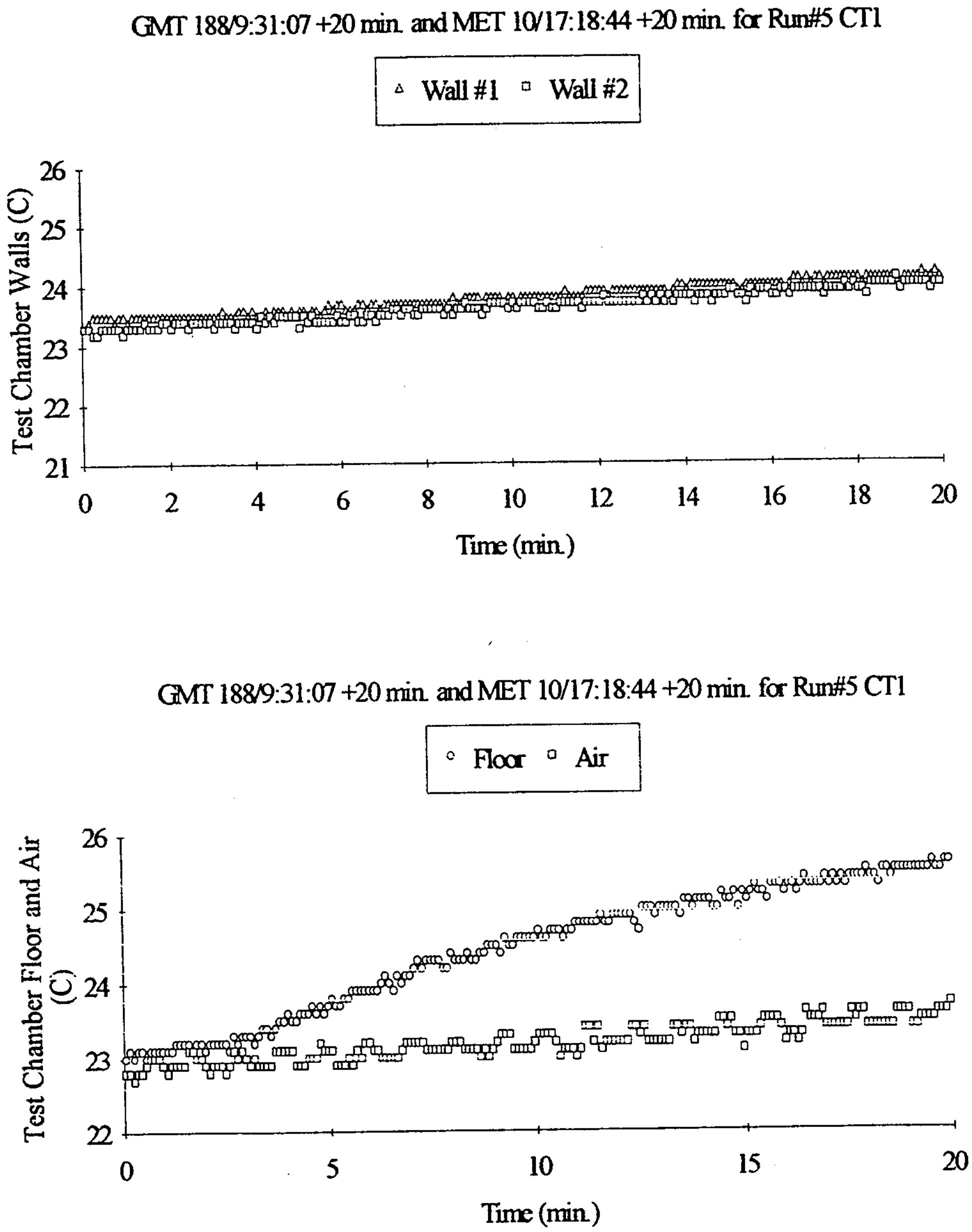

Figure F41 Thermistor data

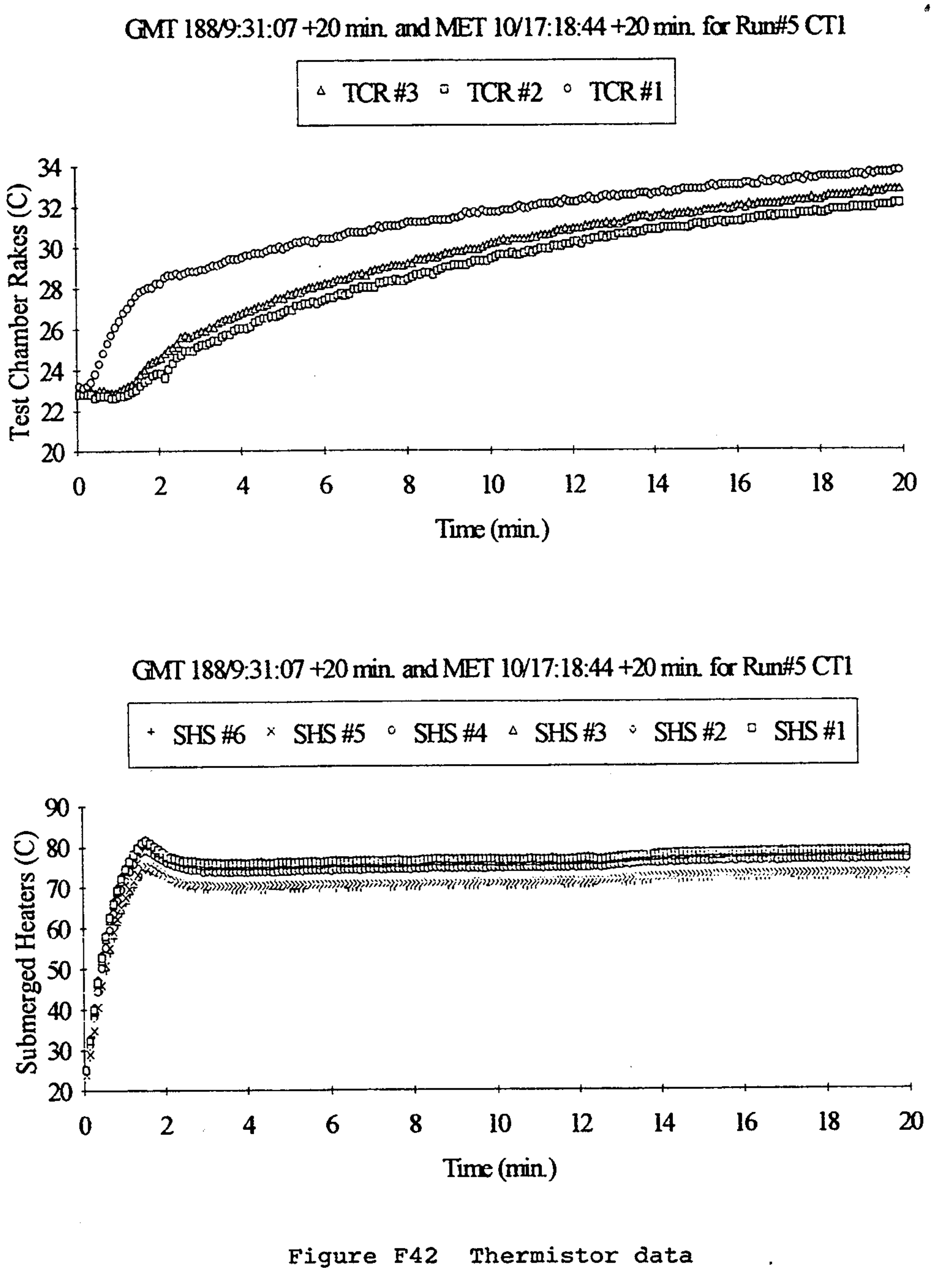

Figure F42 Thermistor data

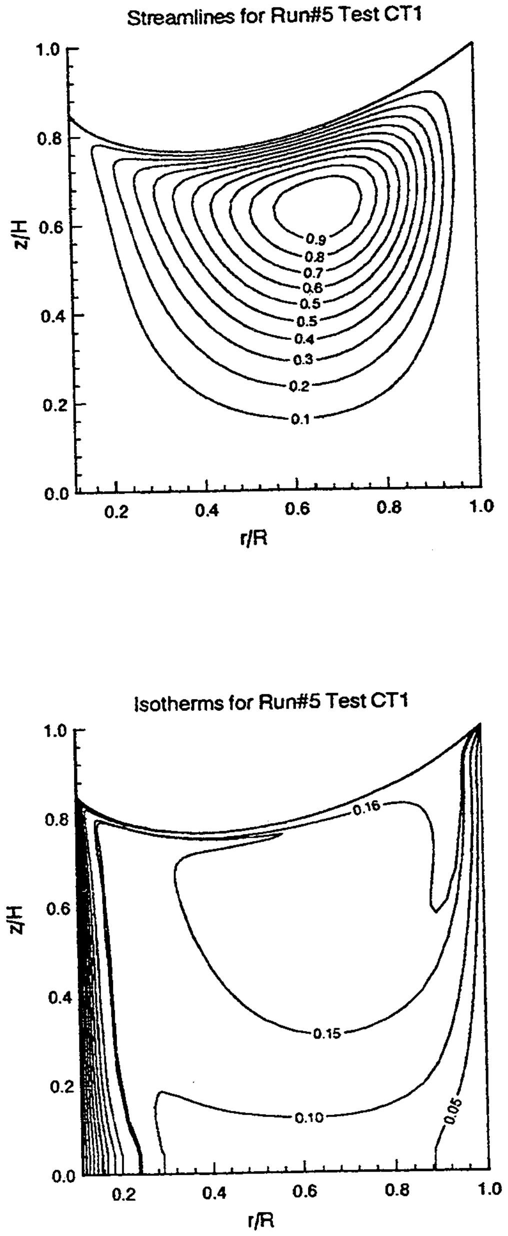

Figure F43 Computed streamlines and isotherms

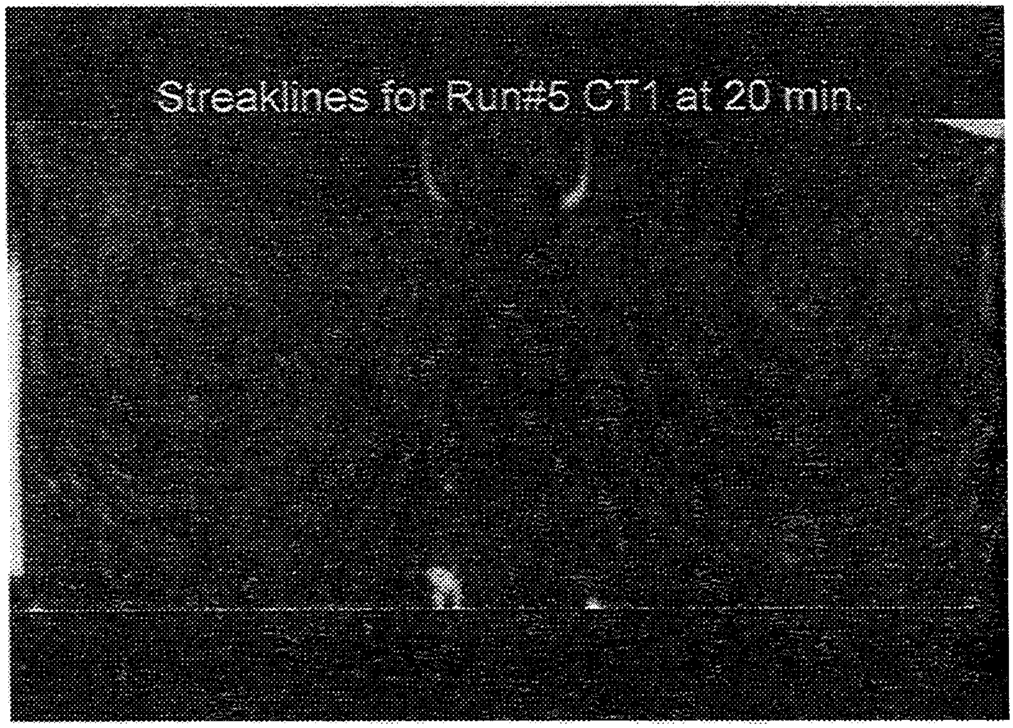

Figure F44 Experimental pathlines

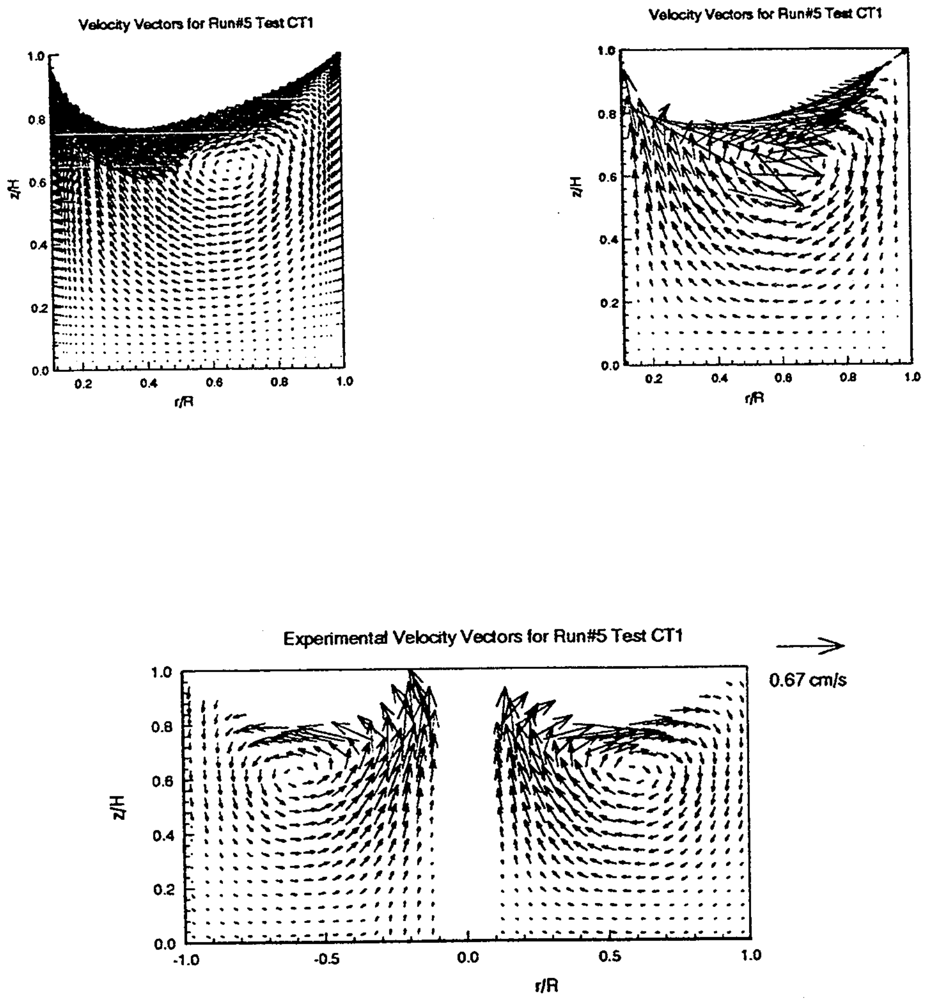

Figure F45 Computed and measured velocity vectors

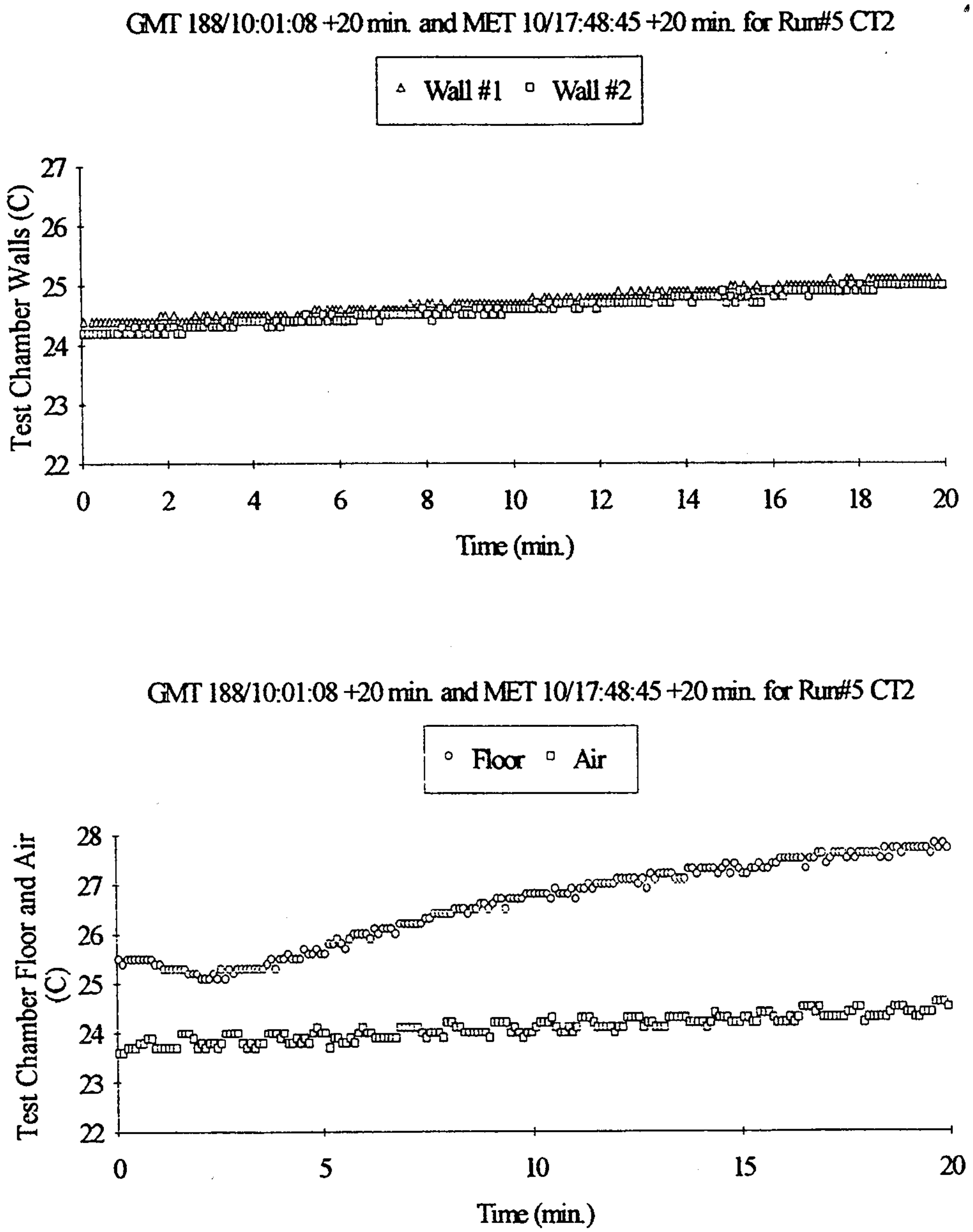

GMT 188/10:01:08 +20 min. and MET 10/17:48:45 +20 min. for Run#5 CT2

GMT 188/10:01:08 +20 min. and MET 10/17:48:45 +20 min. for Run#5 CT2

Figure F46 Thermistor data

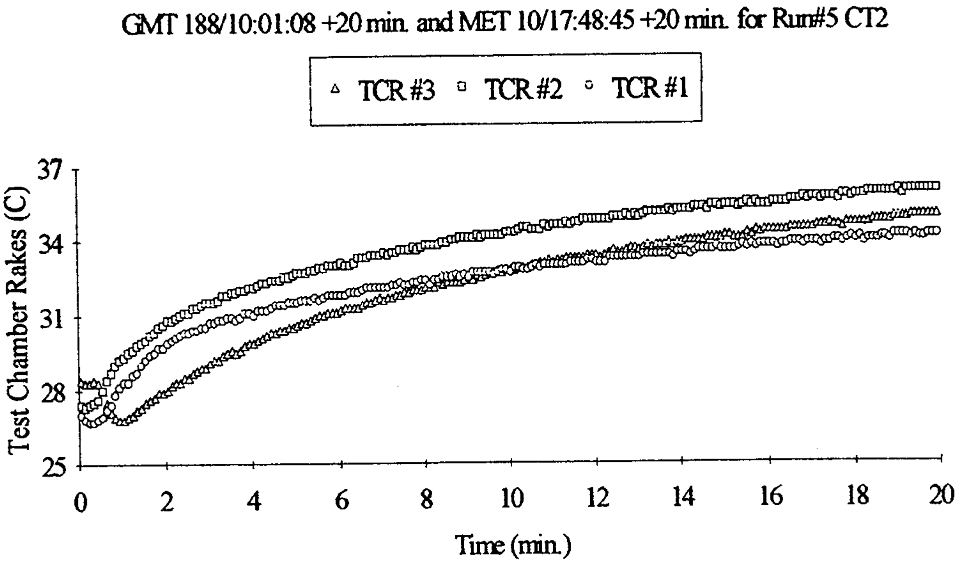

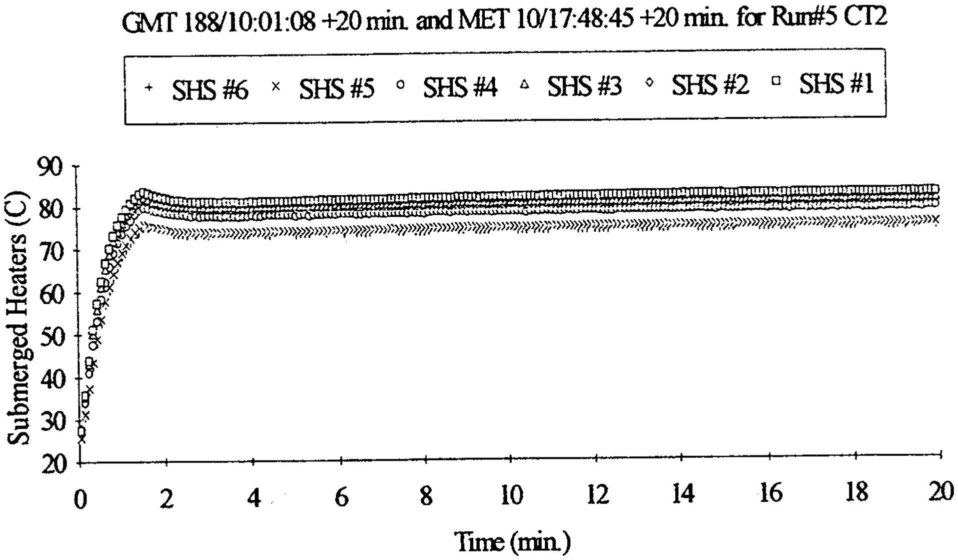

Figure F47 Thermistor data

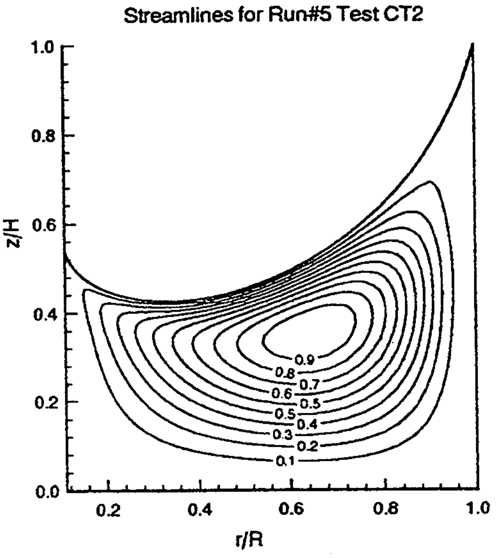

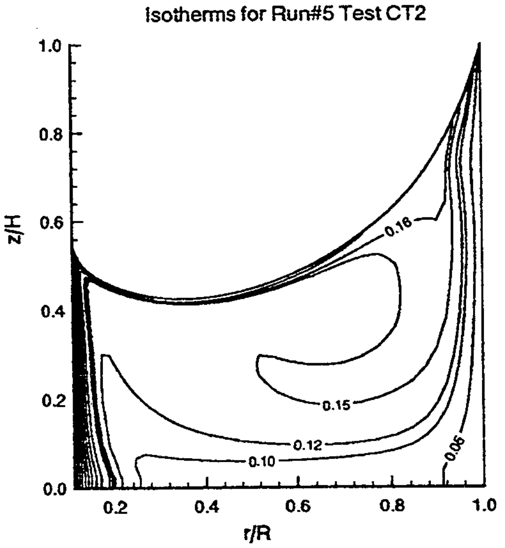

Figure F48 Computed streamlines and isotherms

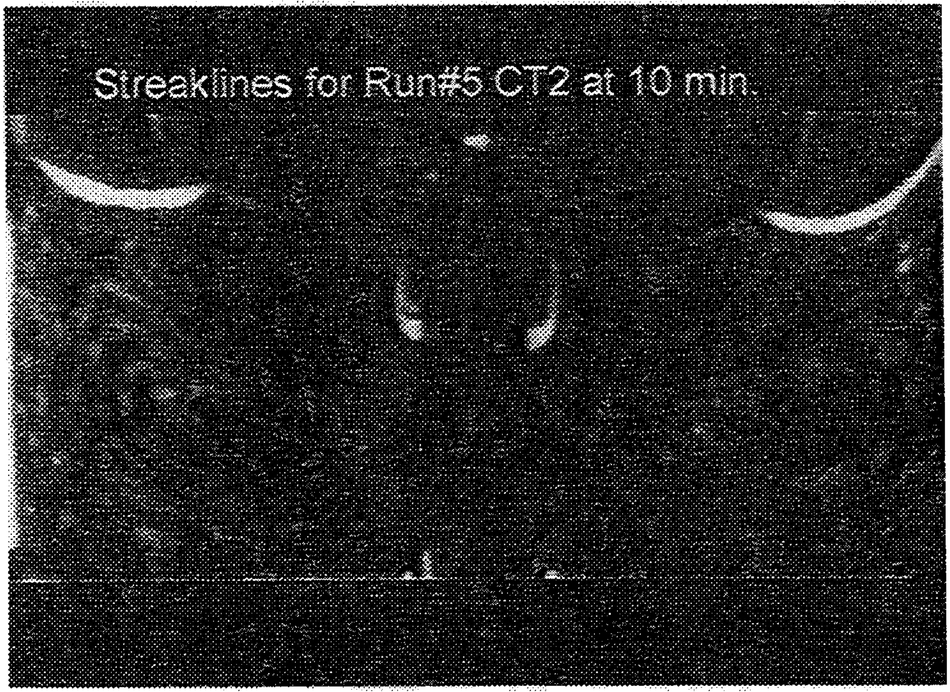

Figure F49 Experimental pathlines

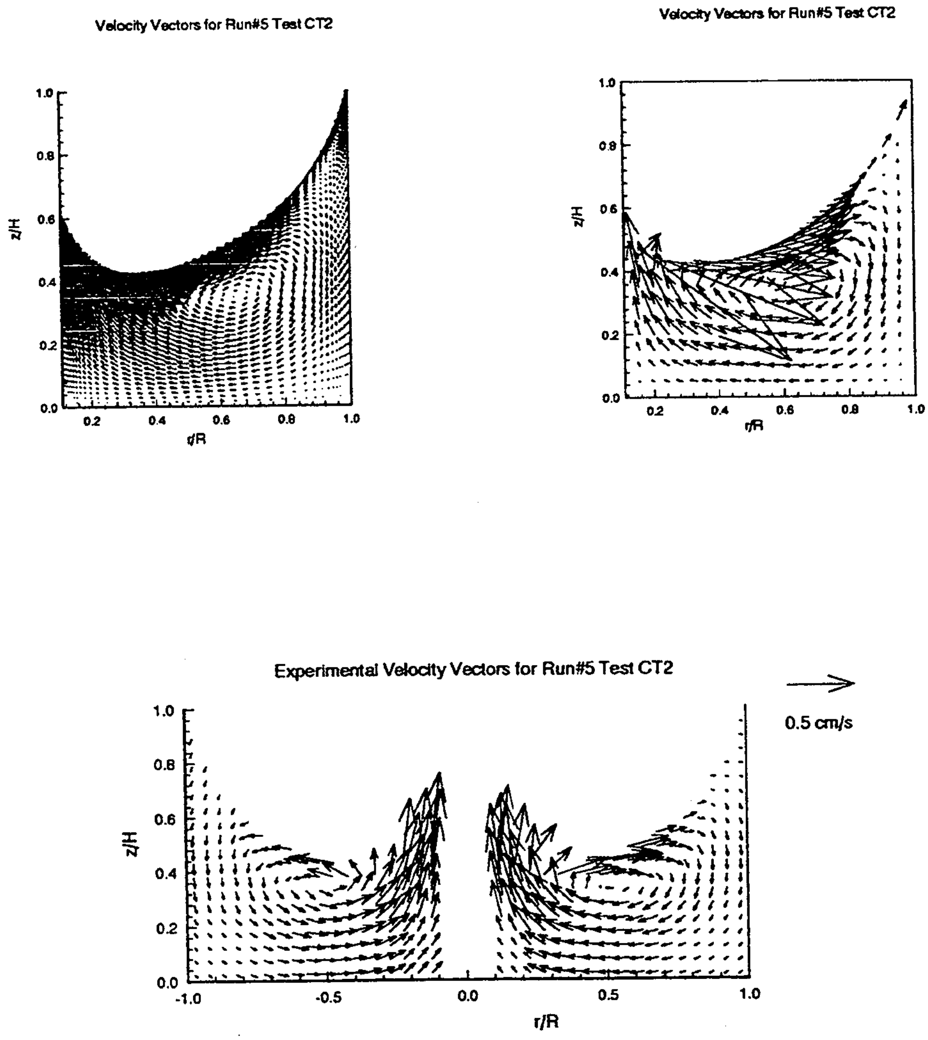

Figure F50 Computed and measured velocity vectors

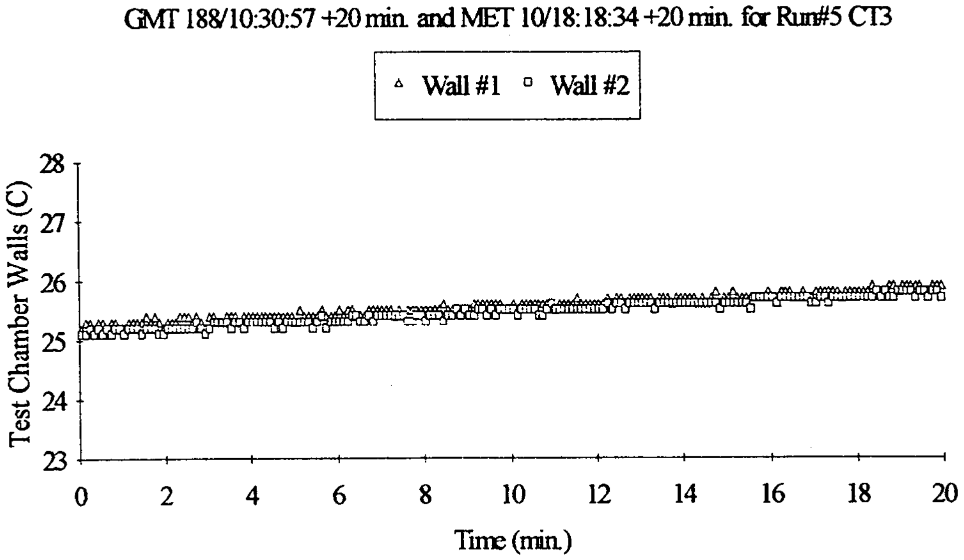

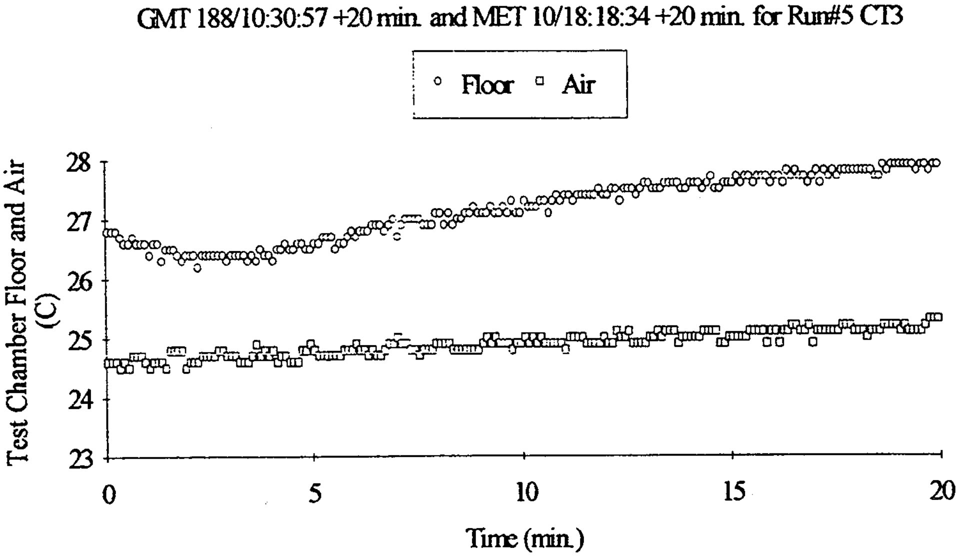

Figure F51 Thermistor data

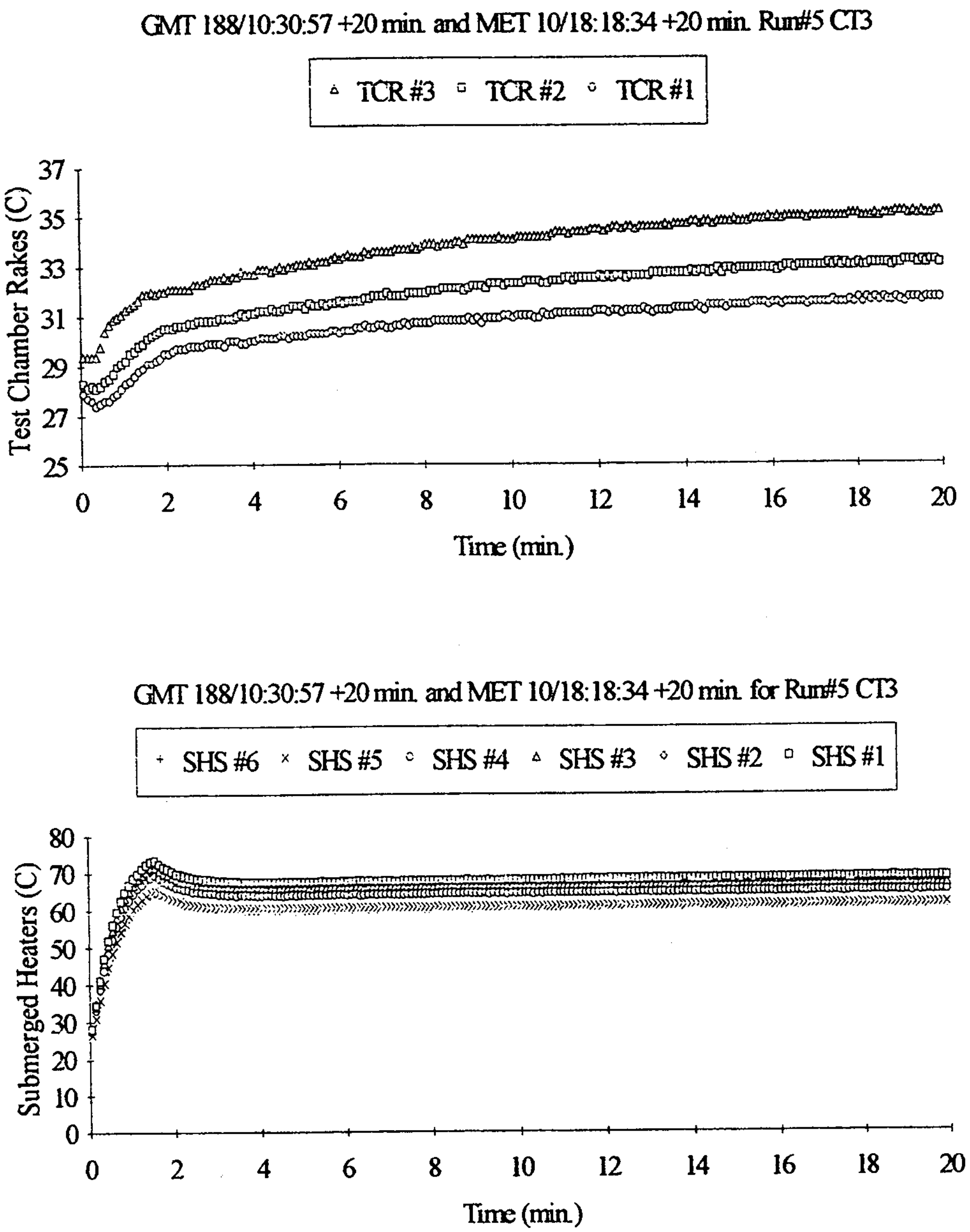

Figure F52 Thermistor data

Streamlines for Run#5 Test CT3

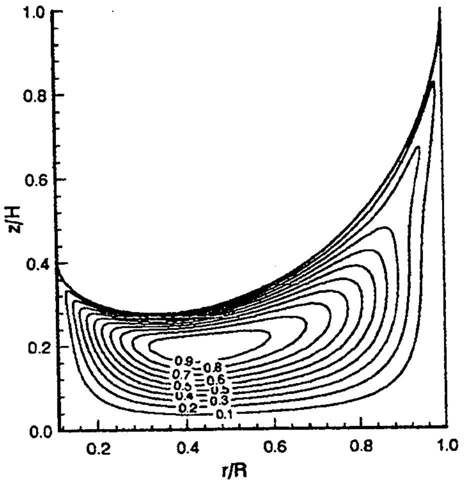

Isotherms for Run#5 Test CT3

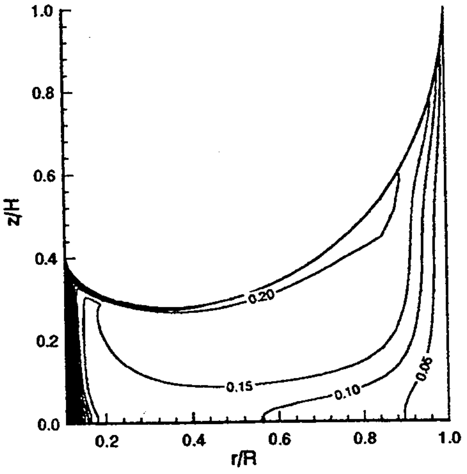

Figure F53 Computed streamlines and isotherms

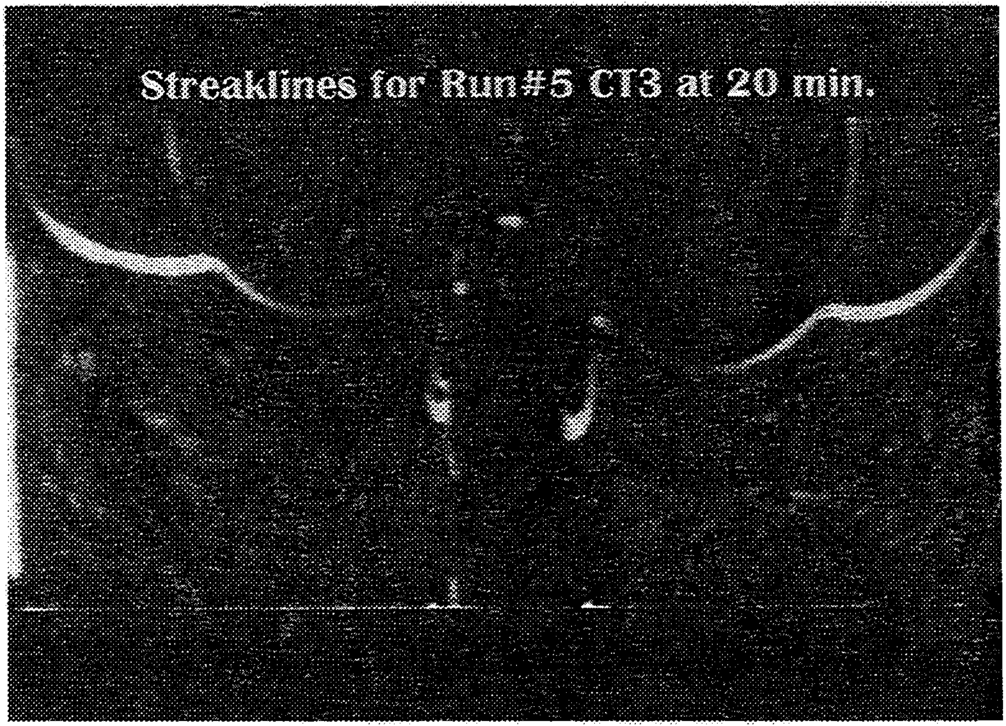

Figure F54 Experimental pathlines

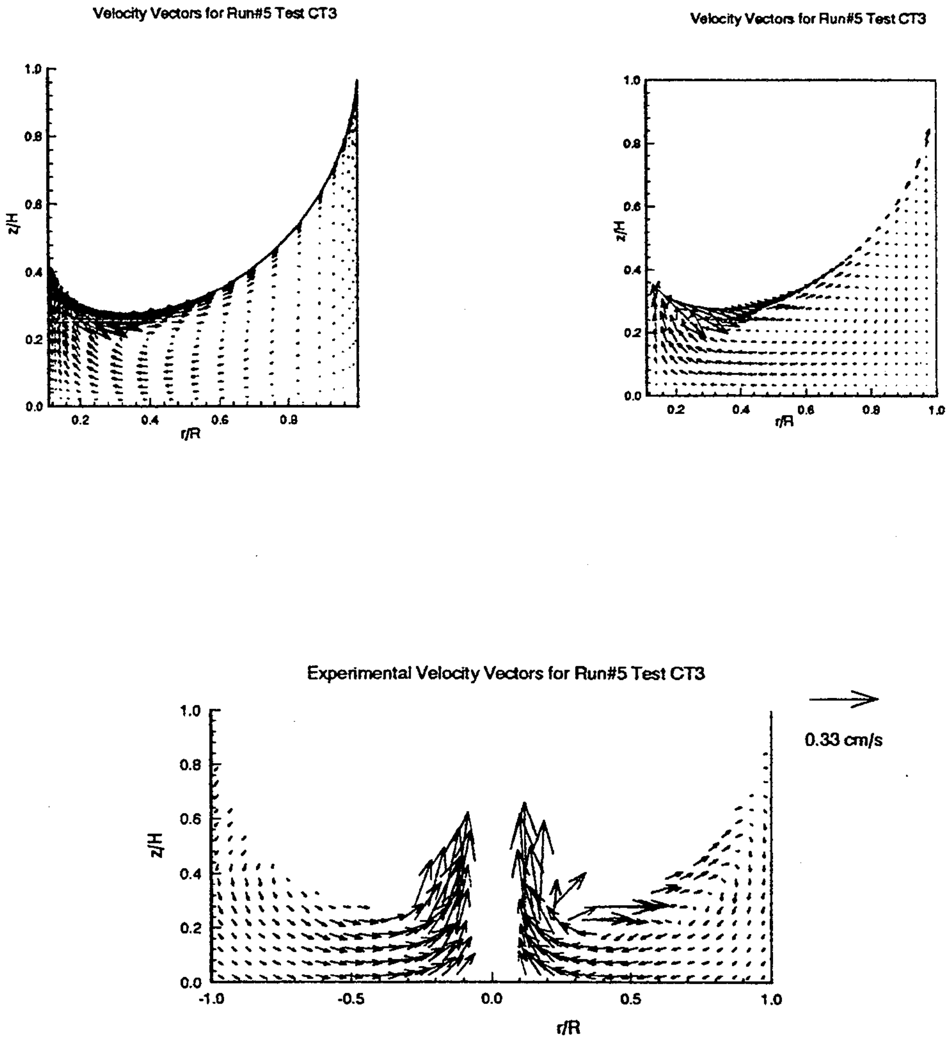

Velocity Vectors for Run#5 Test CT3

Velocity Vectors for Run#5 Test CT3

Experimental Velocity Vectors for Run#5 Test CT3

Figure F55 Computed and measured velocity vectors

National Aeronautics and
Space Administration
Lewis Research Center
21000 Brookpark Rd.
Cleveland, OH 44135-3191